

**Structural Studies of Peptides that Influence the Pathogenicity of Bacterial Infections, and  
Investigation of Structure-Activity-Relationships of Antimicrobial Peptides with  
Application to Cancer Therapy.**

by

Kaitlyn Marie Towle

A thesis submitted in partial fulfilment of the requirements for the degree of

Doctor of Philosophy

Department of Chemistry

University of Alberta

© Kaitlyn Marie Towle, 2017

## Abstract

Enterocin 7 is a two-component, leaderless bacteriocin comprised of an A and B peptide and produced by *Enterococcus faecalis* 710C. The secondary structure of enterocin 7B was investigated through circular dichroism. A high degree of  $\alpha$ -helicity was discovered by circular dichroism, regardless of solvent. The solution structure of enterocin 7B was solved based on NMR spectroscopic data. The peptide was found to consist of three amphipathic  $\alpha$ -helices, confirming the high degree of helicity predicted by circular dichroism. The overall structural fold in enterocin 7B was identified in other leaderless and circular bacteriocins and is a privileged motif in these classes of antimicrobial peptides.

Subtilosin A is a circular, sactibiotic bacteriocin isolated from *Bacillus subtilus* JH642. This highly hydrophobic peptide of 34 amino acid residues contains three thioether bonds between the sulphur of cysteine side chains, at position 4, 7, and 13, and the  $\alpha$ -carbon of partnering amino acids (Phe31, Thr28, and Phe22, respectively). A previous study of the solution structure of subtilosin A determined the stereochemistry of each  $\alpha$ -carbon of Phe31, Thr28, and Phe22 to be D, D, and L, respectively. The all D energy minimization calculation was very close in energy to the reported D,D,L isomer, and therefore the crystal structure of this peptide is desirable. The solubility of subtilosin A was investigated; cyclodextrins were used as additives to increase the solubility of subtilosin A. A biotin bioconjugate of subtilosin A was synthesized to use as a non-covalent co-crystallization partner with streptavidin. A Meldrum's acid derivative was synthesized to conjugate subtilosin A with carbonic anhydrase for use as a covalent co-

crystallization partner. Efforts are underway to optimize the linkage between subtilisin A and carbonic anhydrase using the Meldrum's acid derivative.

Phenol-soluble modulins are virulence factors produced by a wide variety of staphylococcus bacteria. Of particular interest are the phenol-soluble modulins produced by the multi-drug resistant *Staphylococcus aureus*. Phenol-soluble modulins  $\alpha 1$ , and  $\alpha 3$  were synthesized by solid phase peptide synthesis and phenol-soluble modulin  $\beta 2$  was isolated as a fusion protein with the small-ubiquitin like modifier protein that was subsequently cleaved. The secondary structure of these peptides was investigated using circular dichroism. Each peptide was found to be  $\alpha$ -helical in a solution of 50 % trifluoroethanol: water. The solution structure of each peptide was solved using NMR spectroscopic data. Phenol-soluble modulins  $\alpha 1$ , and  $\alpha 3$  were each found to be a single amphipathic  $\alpha$ -helix and phenol-soluble modulin  $\beta 2$  was found to be comprised of three amphipathic  $\alpha$ -helices that pack in such a way as to give a hydrophobic core and hydrophilic surface. The structure of phenol-soluble modulin  $\alpha 1$  differed slightly from a predicted structure previously reported. Phenol-soluble modulin  $\beta 2$  was found to be primarily  $\alpha$ -helical, despite the low values of  $\alpha$ -helicity predicted by circular dichroism.

Neopetrosiamide A and B are tricyclic peptides isolated from the marine sponge *Neopetrosia* spp. These peptides are potent metastasis inhibitors and they differ from one another only in the stereochemistry of the sulfoxide moiety of the oxidized methionine at position 24. Analogues of these peptides in which the methionine sulfoxide is replaced with various non-canonical and canonical amino acids revealed reduced or abolished activity, suggesting a mechanistic 'hot-spot' of this peptide. Efforts to reduce the synthetic steps required to form the

three disulfide bridges by substituting the cysteine residues with hydrophobic residues were unsuccessful, indicating that the native neopetrosiamide is held tightly together by the three disulfides. Attempts to isolate and identify the biological receptor of neopetrosiamides through fluorescent labeling were unsuccessful. New folding studies using structure inducing solvents did not greatly improve the global oxidation of the cysteine residues to the correct disulfide connectivity. However, the use of chaotropic salts improved the global oxidation, resulting in a 1:1 mixture of desired neopetrosiamide with correct disulfide connectivity to undesired neopetrosiamide with incorrect disulfide connectivity.

## Preface

Parts of Chapter 2 of this thesis have been published as Lohans et al. *Biochemistry* **2013**, 52, 3987-3994. I isolated enterocin 7B, ran circular dichroism experiments and acquired the NMR spectroscopic data for this peptide. I interpreted the NMR data and through the use of CYANA, I performed the structure calculations for enterocin 7B. Dr. Chris Lohans performed similar experiments for the partner peptide enterocin 7A. Additionally, Dr. Chris Lohans performed antimicrobial activity tests and prepared the manuscript for publication. I assisted with editing and providing supplementary information for enterocin 7B for this paper. Overall I was responsible for 45 % of the work on this manuscript. Subsequent studies and attempts to identify the biological receptor through genome sequencing have been done in collaboration with Dr. Marco van Belkum and myself.

Chapter 4 has been published as Towle et al. *Biochemistry* **2016**, 55, 4798–4806. I synthesized PSM $\alpha$ 1, PSM $\alpha$ 3 and attempted to synthesize PSM $\beta$ 2. When the biological approach for isolating PSM $\beta$ 2 was adopted I worked in collaboration with Dr. Marco van Belkum to obtain the required genes for the SUMO fusion protein. Dr. van Belkum assisted with the molecular biology aspect of this project. I was responsible for the initial protein isolation and purification of PSM $\beta$ 2 from the heterologous expression. Jeella Acedo isolated and purified additional PSM $\beta$ 2 while I was on maternity leave. I performed the circular dichroism experiments and acquired NMR spectroscopic data for all three peptides. I interpreted the NMR data and performed the structure calculation experiments for PSM $\alpha$ 3 and PSM $\beta$ 2. The NMR data for PSM $\alpha$ 1 was sent to Dr. Chris Lohans. He solved the structure of PSM $\alpha$ 1. Jeella Acedo

acquired additional NMR data for PSM $\beta$ 2 while I was on maternity leave. I performed approximately 80 % of the work on this project, and wrote the manuscript with help from Dr. Marco van Belkum and edits from Dr. Chris Lohans and Ms. Jeella Acedo.

Part of Chapter 5 has been published as Towle et. al *Org. Biomol. Chem.*, **2013**, *11*, 1476-1481. I synthesized the analogues of neopetrosiamide in conjunction with Dr. Jennifer Chaytor. Of the 9 methionine 24 analogues I synthesized and purified 7. Dr. Jennifer Chaytor synthesized the 3 leucine disulfide replacement analogues and Dr. Hongqiang Liu synthesized the 3 phenylalanine disulfide replacement analogues. I re-synthesized the 3 phenylalanine disulfide analogues when we required more material and I purified all of Dr. Jennifer Chaytor's analogues. All biological testing of the analogues was performed by myself or in collaboration with Pamela Austin at UBC. I was responsible for writing the neopetrosiamide manuscript and Dr. Chaytor, Pamela Austin, Dr. Roberge, and Dr. Vederas provided edits to the manuscript.

## **Dedication**

*For my family and friends who have stood by me through all my schooling, I could not have accomplished this without you.*

*“Our greatest weakness lies in giving up. The most certain way to succeed is always to try just one more time” - Thomas A. Edison*

## Acknowledgements

First and foremost I must thank my supervisor, Dr. John C. Vederas, for his unending support. You have imparted to me a deep respect for learning. You have fostered in me a sense of curiosity about the world and a thirst for knowledge for which I will be forever grateful.

I must next thank the support staff in the Department of Chemistry. To the NMR, mass spec, biological services, and analytical services staff, it has been a privilege to learn from you all. In particular, a very special thank you goes out to Mark Miskolzie. Mark, you have taken endless hours out of your days to show me something new or explain something old, thank you.

There are too many memorable and important Vederas group members, past and present, to name them all. Thank you all for your friendship and mentorship. To Sorina Chiorean, Christian Förster, and Marco van Belkum, thank you for reading and editing this thesis. A special thank you to Shaun McKinnie for your continual encouragement; you are truly a great friend. Justin Thus, you have given the lab so many hours of laughter, your humour and outlook on life brighten the world around you. Stephen Cochrane, your pranks may have driven me crazy, but I am thankful for your friendship and advice. Dr. Marco van Belkum, your patience is incredible, you have been a great mentor and friend. Jeella Acedo your heart is kind, and your soul is gentle, it is a privilege to work alongside you. Amy Norquay, I am grateful to have taken this journey with you, I am so proud of how far we have come since that first year. Chris Lohans, I never knew what an honour it would be to move into the desk beside you. Your mentorship has taught me more than I can describe. I am forever grateful for the opportunity to work with you. It has been my greatest pleasure to call you my friend. Rachel Cochrane, words cannot express what

your friendship has meant to me. You have shown me infinite grace and support. Your tenacity leaves me in awe. You have taught me what it means to sacrifice for your children. Witnessing your honesty and abundant love has given me a model for motherhood, and for that, I cannot thank you enough.

To Amy Dupuis, there are no words. You are one of my best friends; you have been my solid support through all of my schooling. You have taught me what it looks like to walk in faith. Janene Hoetmer, I am so lucky to have a childhood friend that I can continue to call my best friend. No one knows me and supports me quite like you do. Jamie Malimban, thank you for always understanding the life of a student. Lauren Kelly, you have always been like a sister to me, thank you for loving me the way you do. To my husband Curtis, this journey would never have been possible without your support. You have shown an unbelievable amount of dedication to my dreams. What an incredible gift of love you have given me. Corbin, you have radically changed my world for the better. I can only hope to encourage you to follow your dreams the way all these people have encouraged me.

I would like to take a special moment to thank my dad, Brynne Towle. You have encouraged, supported and loved me throughout everything and I am eternally grateful.

Thank you all from the bottom of my heart, for walking through this life with me and for pushing me through the difficult times. Most importantly, thank you for providing me with friendships that will endure the test of time.

*“Kindred spirits are not so scarce as I used to think. It is splendid to think that there are so many of them in the world.” – Anne of Green Gables*

## Table of Contents

Abstract.....	ii
Preface.....	v
Dedication.....	vii
Acknowledgements.....	viii
Table of Contents.....	x
List of Tables.....	xvii
List of Figures and Illustrations.....	xix
List of Schemes.....	xxiii
List of Symbols, Abbreviations and Nomenclature.....	xxiv
CHAPTER ONE: INTRODUCTION.....	1
1.1 Introduction.....	1
1.2 Leaderless Bacteriocins.....	5
1.2.1 Introduction.....	5
1.2.2 Biosynthesis.....	7
1.2.3 Mode of Action.....	8
1.3 Sactibiotics.....	11
1.3.1 Introduction.....	11
1.3.2 Biosynthesis.....	11
1.3.3 Mode of Action.....	14
1.4 Phenol-soluble Modulins.....	16
1.4.1 Introduction.....	16
1.4.2 Biosynthesis.....	18
1.4.3 Mode of Action.....	19
1.5 Neopetrosiamides.....	20
1.5.1 Introduction.....	20
1.5.2 Biosynthesis.....	21
1.5.3 Chemical Synthesis.....	21
1.5.4 Mode of Action.....	23
1.6 Applications of Antimicrobial Peptides.....	24
1.6.1 Food Preservation.....	24
1.6.2 Antibiotic Therapeutics.....	25
1.6.3 Anti-tumor Therapeutics.....	26
1.7 Overview of Projects.....	27
CHAPTER TWO: STRUCTURE ELUCIDATION OF ENTEROCIN 7B.....	29
2.1 Background.....	29
2.1.1 Biological Significance of Enterocin 7.....	29

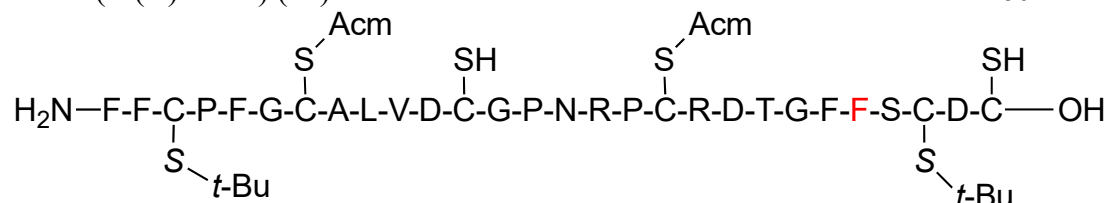
2.2 Results and discussion .....	30
2.2.1 Isolation and Characterization of Enterocin 7B .....	30
2.2.2 Circular Dichroism .....	30
2.2.3 NMR Spectroscopy of Enterocin 7B .....	31
2.2.4 Structure Calculation of Enterocin 7B .....	32
2.2.5 Structural Features of Enterocin 7B .....	34
2.2.6 Comparison of Enterocin 7B to Enterocin 7A .....	37
2.2.7 Comparison of Enterocin 7B to Other Leaderless and Circular Bacteriocins .....	38
2.2.8 Efforts Towards the Identification of a Biological Receptor of Enterocin 7B .....	41
2.3 Conclusions and Future Work .....	42
CHAPTER THREE: SUBTILOSIN A .....	45
3.1 Introduction .....	45
3.1.1 Biological Significance of Subtilosin A .....	45
3.1.2 Elucidation of NMR Solution Structure of Subtilosin A .....	45
3.1.3 Potential Approaches to Recrystallization of Small Peptides. ....	49
3.1.3.1 Racemic Mixture .....	49
3.1.3.2 Co-crystallization of Proteins and Peptides .....	50
3.1.4 Previous Co-crystallization Attempts with Subtilosin A .....	51
3.2 Results and Discussion .....	52
3.2.1 Isolation of subtilosin A .....	52
3.2.2 Investigation Into New Co-Crystallization Protein Targets .....	52
3.2.2.1 Capping Hydrophobic Residues with Cyclodextrins .....	53
3.2.2.2 Investigation of Streptavidin Stability in Organic Solvents. ....	54
3.2.2.3 Linking Subtilosin A Through a Covalent Bond to a Readily Crystallizable Protein. ....	59
3.3 Discussion and Conclusions .....	65
CHAPTER FOUR: PHENOL-SOLUBLE MODULINS. ....	70
4.1 Introduction .....	70
4.1.1 Biological Significance .....	70
4.2 Results and Discussion .....	70
4.2.1 Synthesis and Isolation of Phenol-soluble Modulins. ....	70
4.2.2 Heterologous Expression and Isolation of SUMO-PSM $\beta$ 2 Fusion Protein ....	71
4.2.3 Circular Dichroism of Phenol-soluble Modulins. ....	72
4.2.4 PSM NMR Spectroscopy .....	73
4.2.5 Structure Calculation of PSM $\alpha$ 1, PSM $\alpha$ 3 and PSM $\beta$ 2 .....	74
4.2.6 Description of the Overall Structure of PSM $\alpha$ 1 .....	75
4.2.7 Description of the Overall Structure of PSM $\alpha$ 3 .....	75
4.2.8 Description of the Overall Structure of PSM $\beta$ 2 .....	76
4.2.9 Comparison of PSM $\alpha$ 1 to PSM $\alpha$ 3 .....	78
4.2.10 Tertiary Structure and its Influence on Biological Activity .....	79

4.2.11 Comparison of PSM $\beta$ 2 Structure to Leaderless Bacteriocins .....	81
4.3 Conclusions and Future Outlook .....	83
CHAPTER FIVE: NEOPETROSIAMIDE A AND B .....	86
5.1 Introduction.....	86
5.1.1 Biological Significance .....	87
5.2 Results and Discussion .....	88
5.2.1 Synthesis of residue 24 analogues of Neopetrosiamides A and B .....	88
5.2.2 Synthesis of neopetrosiamide analogues with disulfide bonds substituted with hydrophobic pairs.....	92
5.2.3 Activity Testing of the M(O)24 Neopetrosiamide Analogues and the Disulfide Replacement Analogues.....	93
5.2.4 Synthesis of Fluorescently Labeled Neopetrosiamide .....	97
5.2.5 Synthesis of Modified Aspartic Acid Derivative .....	103
5.2.6 Synthesis of a Photoaffinity Label. ....	105
5.2.7 Plasma Stability Assay of Neopetrosiamide.....	111
5.2.8 Folding studies on Neopetrosiamide .....	112
CHAPTER SIX: OVERVIEW AND SUMMARY OF THESIS WORK .....	115
CHAPTER SEVEN: METHODS AND MATERIALS .....	118
7.1 General Experimental Details .....	118
7.1.1 Reagents and Solvents.....	118
7.1.2 General Techniques for Microbiological Work .....	118
7.1.2.1 Preparation of Media .....	118
7.1.2.2 Glycerol Stocks.....	119
7.1.2.3 Antimicrobial Testing through Spot-on-Lawn Assays .....	119
7.1.2.4 Cell Lysis .....	120
7.1.3 General Chromatographic Purification of Peptides and Proteins.....	120
7.1.3.1 Amberlite XAD-16 Hydrophobic Interactions Chromatography .....	120
7.1.3.2 C18 Solid-Phase Extraction Cartridges .....	120
7.1.3.3 C8 Solid-Phase Extraction Cartridges .....	121
7.1.3.4 HPLC .....	121
7.1.3.5 Fluorescence Experiments .....	121
7.1.4 Characterization of Proteins, Peptides and Small Molecules .....	122
7.1.4.1 MALDI-TOF MS.....	122
7.1.4.2 LC- ESI MS .....	122
7.1.4.3 HR-ESI MS.....	122
7.1.4.4 EI MS .....	122
7.1.4.5 NMR Spectroscopy.....	123
7.1.4.6 SDS-PAGE Gel Characterization .....	123
7.1.4.7 Native PAGE Gel Characterization .....	123

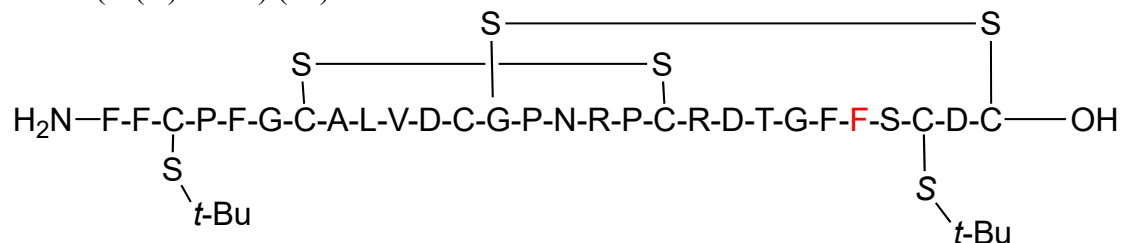
7.1.5 General Solid Phase Peptide Synthesis Conditions.....	124
7.1.5.1 General Procedure for Automated Solid Phase Peptide Synthesis (SPPS) using ABI 433A .....	124
7.2 Experimental Procedures for the Structural Characterization of Enterocin 7B, a Leaderless Bacteriocin.....	125
7.2.1 Isolation of Enterocin 7B (4) .....	125
7.2.2 Circular Dichroism .....	126
7.2.3 NMR Spectroscopy .....	127
7.2.4 Structure Calculations .....	130
7.3 Experimental Procedures for Subtilosin A .....	130
7.3.1 General HPLC Method for Subtilosin A .....	130
7.3.1.1 Isolation of Subtilosin A (5) .....	131
7.3.1.2 Capping with Cyclodextrin.....	132
7.3.1.3 Stability of Streptavidin to Various Organic Solvents.....	132
7.3.1.4 Linkage of Subtilosin A with Biotin (7) .....	133
7.3.1.5 Bioconjugation of Subtilosin A with Streptavidin.....	133
7.3.1.6 Purification of Subtilosin A Streptavidin Complex with HPLC.....	133
7.3.1.7 Purification of Subtilosin A using Amicon Tubes.....	134
7.3.1.8 Synthesis of Meldrum's Acid Derivative (8).....	134
7.3.1.9 Linkage of Meldrums Acid Derivative to Subtilosin A and Carbonic Anhydrase (12).....	135
7.3.1.10 Coupling of 5- Azido-2,5,-dioxo-1pyrrolidinyl Ester Linker to Subtilosin A (13).....	135
7.3.1.11 Synthesis of 5- azido-2,5,-dioxo-1pyrrolidinyl ester (14). .....	135
7.4 Experimental Procedures for the Synthesis and Isolation of Phenol-soluble Modulins .....	136
7.4.1 Synthesis of PSM $\alpha$ 1 and PSM $\alpha$ 3. ....	136
7.4.1.1 Manual Solid-phase Peptide synthesis of PSM $\alpha$ 1 and PSM $\alpha$ 3 .....	136
7.4.1.2 Purification of PSM $\alpha$ 1 and PSM $\alpha$ 3 .....	137
7.4.1.3 Construction of Expression Vectors. ....	138
7.4.1.4 Expression of His-Tagged SUMO-PSM $\beta$ 2. ....	138
7.4.1.5 Purification of Fusion Protein.....	139
7.4.1.6 Cleavage of Fusion Protein.....	139
7.4.1.7 NMR Spectroscopy.....	140
7.4.1.8 Circular Dichroism Spectroscopy. ....	144
7.4.1.9 Structure Calculations.....	145
7.5 Experimental Procedures for the Synthesis of Neopetrosiamide Analogues .....	145
7.5.1 General Procedure for Stepwise Disulfide Formation.....	145
7.5.1.1 Formation of Bis-disulfide Bond Method A.....	145
7.5.1.2 Formation of Bis-disulfide Bond Method B .....	146
7.5.1.3 Formation of Tris-disulfide Peptide.....	146

7.5.1.4 General Method for the [2+3] Cycloaddition of Fluorescent Organic Dyes to the Azide Functionalized peptide.....	147
7.5.1.5 General Method for Purification of Peptides by HPLC.....	147
7.5.1.6 General Cell Culture Protocols.....	147
7.5.1.7 General Procedure for Invasion Assay of Analogues Against MDA-MB-231 Cells .....	148
7.5.1.8 Linear Peptide Formation of Residue 24 Substitution with <i>O</i> -Methyl Homoserine (M(O)24O-methyl HSE) (17).....	148
7.5.1.9 Bis-disulfide Formation Residue 24 Substitution with <i>O</i> -Methyl Homoserine (M(O)24O-methyl HSE) (18).....	149
7.5.1.10 Tris-disulfide Formation of Residue 24 Substitution with <i>O</i> -Methyl Homoserine (M(O)24O-methyl HSE) (19).....	149
7.5.1.11 Linear Peptide Formation of Residue 24 Substitution with Glutamine (M(O)24Gln) (20) .....	150
7.5.1.12 Bis-disulfide Formation of Residue 24 Substitution with Glutamine (M(O)24Gln) (21) .....	150
7.5.1.13 Tris-disulfide Formation of Residue 24 Substitution with Glutamine (M(O)24Gln) (22) .....	151
7.5.1.14 Linear Peptide Formation of 24 Substitution with Glutamic Acid (M(O)24Glu) (23) .....	151
7.5.1.15 Bis-disulfide Formation of Residue 24 Substitution with Glutamic Acid (M(O)24Glu) (24) .....	152
7.5.1.16 Tris-disulfide Formation of Residue 24 Substitution with Glutamic Acid (M(O)24Glu) (25) .....	152
7.5.1.17 Linear Peptide Formation of Residue Asparagine (M(O)24Asn) (26).....	153
7.5.1.18 Bis-disulfide formation of Residue 24 Substitution with Asparagine (M(O)24Asn) (27).....	153
7.5.1.19 Tris-disulfide Formation of Residue 24 Substitution with Asparagine (M(O)24Asn) (28).....	154
7.5.1.20 Linear Peptide Formation of Residue 24 Substitution with Alanine (M(O)24Ala) (29) .....	154
7.5.1.21 Bis-disulfide Formation of Residue 24 Substitution with Alanine (M(O)24Ala) (30) .....	155
7.5.1.22 Tris-disulfide Formation of Residue 24 Substitution with Alanine (M(O)24Ala) (31) .....	155
7.5.1.23 Linear Peptide Formation of Residue 24 Substitution with Leucine (M(O)24Leu) (32).....	156
7.5.1.24 Bis-disulfide Formation of Residue 24 Substitution with Leucine (M(O)24Leu) (33).....	156
7.5.1.25 Tris-disulfide Formation of Residue 24 Substitution with Leucine (M(O)24Leu) (34).....	157

7.5.1.26 Linear Peptide Formation of Residue 24 Substitution with Isoleucine (M(O)24Ile) (35).....	157
7.5.1.27 Bis-disulfide Formation of Residue 24 Substitution with Isoleucine (M(O)24Ile) (36).....	158
7.5.1.28 Tris-disulfide Formation of Residue 24 Substitution with Isoleucine (M(O)24Ile) (37).....	158
7.5.1.29 Linear Peptide Formation of Residue 24 Substitution with Histidine (M(O)24His) (38).....	159
7.5.1.30 Bis-disulfide Formation of Residue 24 Substitution with Histidine (M(O)24His) (39).....	159
7.5.1.31 Tris-disulfide Formation of Residue 24 Substitution with Histidine (M(O)24His) (40).....	160
7.5.1.32 Linear Peptide Formation of Residue 24 Substitution with Phenylalanine (M(O)24Phe) (41).....	160



.....	160
7.5.1.33 Bis-disulfide Formation of Residue 24 Substitution with Phenylalanine (M(O)24Phe) (42).....	161



.....	161
7.5.1.34 Tris-disulfide Formation of Residue 24 Substitution with Phenylalanine (M(O)24Phe) (43).....	161
7.5.1.35 Linear Peptide Formation of C3L, C26L (44).....	162
7.5.1.36 Bis-disulfide Peptide Formation of C3L, C26L (45).....	162
7.5.1.37 Linear Peptide Formation of C7L, C18L (46).....	162
7.5.1.38 Bis-disulfide Peptide Formation of C7L, C18L (47).....	163
7.5.1.39 Linear Peptide Formation of C12L, C28L (48).....	163
7.5.1.40 Bis-disulfide Peptide Formation of C12L, C28L (49).....	164
7.5.1.41 Linear Peptide Formation of C3F, C26F (50).....	164
7.5.1.42 Bis-disulfide Peptide Formation of C3F, C26F (51).....	164
7.5.1.43 Linear Peptide Formation of C7F, C18F (52).....	165

7.5.1.44 Bis-disulfide peptide formation of C7F, C18F (53) .....	165
7.5.1.45 Linear peptide formation of C12F, C28F (54).....	166
7.5.1.46 Bis-disulfide peptide formation of C12F, C28F (55) .....	166
7.5.1.47 Linear Peptide formation of Asp20-PEG-3-Azide-linear (56) .....	166
7.5.1.48 Bis-disulfide formation of Asp20-PEG-3-Azide-Bisdisulfide (57)...	167
7.5.1.49 Tris-disulfide formation of Asp20-PEG-3-Azide-trisdisulfide (58)..	167
7.5.1.50 Synthesis of PEG <sub>3</sub> Aspartic acid: (S)-15-(((9H-Fluoren-9-yl)methoxy)carbonylamino)-1-azido-13-oxo-3,6,9-trioxa-12-azahexadecan-16-oic acid (60) .....	168
7.5.1.51 Formation of the alkyne functionalized Rhodamine B (65) .....	169
7.5.1.52 Formation of the Alkyne Functionalized Coumarin: N-(Prop-2-ynyl)-2-oxo-2H-chromene-3-carboxamide (68) .....	170
7.5.1.53 Synthesis of 4,4-difluoro-8-(hept-6-yne)-1,3,5,7-tetramethyl-4-bora-3a,4a-diaza-s-indacene, the alkyne functionalized BODIPY (73).....	170
7.5.1.54 Formation of Asp20-PEG-3-Rhodamine (74) .....	172
7.5.1.55 Formation of Asp20-PEG-3-Coumarin (75).....	172
7.5.1.56 Formation of Asp20-PEG-3-BODIPY (76).....	173
7.5.1.57 Synthesis of PEG <sub>6</sub> Linker (79).....	174
7.5.1.58 Linear Peptide Formation of Asp20-PEG-6-Azide-Linear (80).....	175
7.5.1.59 Bis-disulfide Formation of Asp20-PEG-6-Azide-bisdisulfide (81)...	175
7.5.1.60 Tris-disulfide Formation of Asp20-PEG-6-Azide-trisdisulfide (82) .	176
7.5.1.61 4-Bromobenzyl Alcohol- <i>O</i> -( <i>tert</i> -Butyldimethylsilyl) Ether (84).....	176
7.5.1.62 4-[( <i>tert</i> -Butyldimethylsiloxy)methyl]-2,2,2-trifluoroacetophenone (85)	177
7.5.1.63 4-[( <i>tert</i> -Butyldimethylsiloxy)methyl]-2,2,2-trifluoroacetophenone oxime (86).....	178
7.5.1.64 4-[( <i>tert</i> -Butyldimethylsiloxy)methyl]-2,2,2-trifluoroacetophenone- <i>O</i> -(4-toluenesulphonyl) oxime (87) .....	179
7.5.1.65 3-[ $\alpha$ -( <i>tert</i> -Butyldimethylsiloxy)-4-tolyl]-3-(trifluoromethyl)diaziridine (88).....	180
7.5.1.66 3-[ $\alpha$ -( <i>tert</i> -Butyldimethylsiloxy)-4-tolyl]-3-(trifluoromethyl)diazirine (89) .....	181
7.5.1.67 4-[3-Trifluoromethyl-3 <i>H</i> -diazirin-3-yl]benzyl alcohol (90).....	182
7.5.1.68 3-( $\alpha$ -Iodo-4-tolyl)-3-(trifluoromethyl)-3 <i>H</i> -diazirine (91).....	182
7.5.1.69 Nickel Complexation of ( <i>S</i> )-2-[ <i>N</i> -( <i>N'</i> -benzylpropyl)amino]benzophenone and glycine (92) .....	183
7.5.1.70 Alkylation of Nickel Complex with 3-( $\alpha$ -iodo-4-tolyl)-3-(trifluoromethyl)-3 <i>H</i> -diazirine (93).....	184
7.5.1.71 ( <i>S</i> )-3-[4-[3-(Trifluoromethyl)-3 <i>H</i> -diazirin-3-yl]phenyl]alanine (94)	186
7.5.1.72 ( <i>S</i> )- <i>N</i> -(9-Fluorenylmethoxycarbonyl)-[4-[3-(trifluoromethyl)-3 <i>H</i> -diazirin-3-yl]phenyl]alanine (95) .....	187
7.5.1.73 Linear Peptide Formation of F1PA (96) .....	188
7.5.1.74 Bis-disulfide Formation of F1PA (97).....	188

7.5.1.75 Tris-disulfide Formation of Residue 1 Substitution with Phenylazide F1PA (98).....	189
7.5.1.76 Linear Peptide Formation of F1BA (99).....	189
7.5.1.77 Bis-disulfide Formation of F1BA (100) .....	190
7.5.1.78 Tris-disulfide Formation of Residue 1 Substitution with Benzylamine F1BA (101) .....	190
7.5.1.79 Linear Peptide Formation of F2PA (102).....	191
7.5.1.80 Bis-disulfide Formation of F2PA (103).....	191
7.5.1.81 Tris-disulfide Formation of Residue 1 Substitution with Phenylazide F2PA (104).....	192
7.5.1.82 Linear Peptide Formation of F2BA (105).....	192
7.5.1.83 Bis-disulfide Formation of F2BA (106) .....	193
7.5.1.84 Tris-disulfide Formation of Residue 1 Substitution with Phenylazide F2BA (107) .....	193
7.5.1.85 Linear Formation of Phenylalanine 23 Substitute with Photophenylalanine (PP) (F23PP) (108).....	194
REFERENCES .....	195

### List of Tables

Table 1.1- NMR structure statistic of enterocin 7B .....	33
Table 2.1-Summary of NMR Solution Structure Calculations of PSM $\alpha$ 1, PSM $\alpha$ 3, and PSM $\beta$ 2.....	75
Table 3.1- Activity Against the Invasion of MDA-MB-231 Cells through Matrigel.....	96
Table 6.1- Experiment Parameters of NMR Spectroscopic Data for Enterocin 7B.....	127
Table 6.2- Chemical Shift Assignment of Enterocin 7B.....	128
Table 6.3- NMR Experimental Parameters for PSM $\alpha$ 1, PSM $\alpha$ 3, and PSM $\beta$ 2.....	141
Table 6.4- Chemical Shift Assignments of PSM $\alpha$ 1.....	142
Table 6.5- Chemical Shift Assignments of PSM $\alpha$ 3.....	142
Table 6.6- Chemical Shift Assignment of PSM $\beta$ 2 .....	143



## List of Figures and Illustrations

Figure 1- Examples of antimicrobial compounds isolated from fungi and bacteria.....	2
Figure 2- Examples of derivitization of common backbone scaffolds to give new antibiotic drug compounds.....	3
Figure 3- Clustal Omega sequence alignment of the different families of leaderless bacteriocins. <sup>33</sup> Asterisks (*) indicate identical amino acids, colon (:) indicate amino acids which are highly similar and periods (.) indicate amino acids that are similar. ....	7
Figure 4- Proposed mechanism of thioether formation by radical SAM enzyme between a cysteine thiol and the $\alpha$ -carbon of a neighbouring amino acid. ....	12
Figure 5- PyMOL representations of A) corrected NMR structure of neopetrosiamides and B) originally proposed NMR structure of neopetrosiamide. Color-coding is as follows: green; represents hydrophobic residues, blue; positive charge, red; negative charge, yellow; disulfide bonds, and grey; neutral in the space filling surface structure.....	22
Figure 6- Sequence alignment of enterocin 7A and 7B. Asterisks (*) indicate identical amino acids, semi-colons (;) indicate highly similar amino acids and periods (.) indicate similar amino acids. ....	30
Figure 7- Circular dichroism data for enterocin 7B. Blue: water; red: phosphate buffer; and black: 50 % trifluoroethanol. ....	31
Figure 8- Overlap of the 20 lowest energy conformers of enterocin 7B as calculated by CYANA 2.1. N-terminus indicated by arrow. ....	33
Figure 9- Ribbon diagram of enterocin 7B showing the saposin-like fold. N-terminus is indicated with an arrow.....	34
Figure 10- PyMOL representation of $\pi$ -hydrogen interactions in enterocin 7B. Amino acid side chains are depicted in green with nitrogen, oxygen, sulfur, and hydrogen shown explicitly in blue, red, yellow, and grey, respectively. ....	35
Figure 11- Surface structure of enterocin 7B depicting A) hydrophobicity, and B) electrostatic potential. ....	37
Figure 12- Side-by-side comparison of enterocin 7A; blue, and enterocin 7B; teal. N- termini are indicated by an 'N.' .....	38

Figure 13- Various peptides that contain a saposin-like fold. Each distinct helix is colored a different color to exemplify directionality. Starting with the N-terminus, red; $\alpha$ -helix 1, yellow; $\alpha$ -helix 2, green; $\alpha$ -helix 3 and orange; $\alpha$ -helix 4. In the case that there is a 5 <sup>th</sup> $\alpha$ -helix it is colored blue. ....	39
Figure 14- Hydrophobic surface maps of various circular and leaderless bacteriocins. Common to all of these peptides is a predominately hydrophobic face and on the opposite side, a hydrophobic patch sandwiched between two hydrophilic patches. ....	40
Figure 15- Pictogram of method used to identify biological receptors through whole-genome sequencing. Resistant colonies are picked, genomic DNA isolated and sequenced. The genomes of the resistant colonies are compared to the genomes of wild-type colonies, sensitive to the bacteriocin of interest, and SNPs are identified. ....	42
Figure 16- Compounds synthesized to model the chemical shift effect of an adjacent sulfur to the $\alpha$ -carbon of phenylalanine or threonine as proposed for subtilisin A. ....	46
Figure 17- Complete amino acid sequence of subtilisin A with post-translational modifications. ....	47
Figure 18- NMR solution structure of subtilisin A. Residues involved in thioether bridges are shown explicitly. The blue color represent nitrogen; red; oxygen, and yellow; sulfur. ....	49
Figure 19- Cone-like structure of $\alpha$ - and $\beta$ - cyclodextrin. The cyclodextrins cap hydrophobic residues like phenylalanine, leucine and isoleucine. Locations that may be capped are indicated with arrows. Blue indicate capping with $\alpha$ -clycodextrin and black indicate capping with and $\beta$ -cyclodextrin. ....	54
Figure 20- Graphical representation of fluorecence intensity of streptavidin in various organic solvents. Solid lines represent fluorecence of streptavidin solution prior to incubation with biotin. Dashed lines represent fluorecence of streptavidin solution after incubation with biotin-coated 96-well plate. ....	57
Figure 21- Crystal structure of carbonic anhydrase. A model compound is docked depicting the orientation of the lysine side chain in subtilisin A with the Meldrum's acid derivative (8) covalently linked to the cysteine side chain in carbonic anhydrase. ....	62
Figure 22- Crystal structure of carbonic anhydrase with a model ligand, compound 11, attached to a representative lysine residue and the cysteine residue on carbonic anhydrase. ....	63
Figure 23- CD spectra of A) PSM $\alpha$ 1 and PSM $\alpha$ 3 and B) PSM $\beta$ 2. Spectra were acquired in 50 % trifluoroethanol at 25, 37, and 40 °C, respectively. ....	73

Figure 24- NMR solution structures depicting amphipathic helices of A) PSM $\alpha$ 1 D) PSM $\alpha$ 3 and G) PSM $\beta$ 2. Hydrophobic surface maps indicate a hydrophobic face and hydrophilic face in B) PSM $\alpha$ 1 and E) PSM $\alpha$ 3. The amphipathic helices in PSM $\beta$ 2 pack to give a hydrophobic core and hydrophilic outside as shown by the hydrophobicity surface map of H) PSM $\beta$ 2. The formylmethionines of PSM $\alpha$ 1 and PSM $\alpha$ 3 are depicted in traditional coloring: nitrogen, blue; carboxyl, red; and sulfur, yellow. Hydrophobicity surface map representations of the PSMs were generated using PyMOL.<sup>156</sup> Electrostatic potential surface maps of C) PSM $\alpha$ 1, F) PSM $\alpha$ 3, and I) PSM $\beta$ 2. Electrostatic potential surface maps were generated using the APBS function of the PDB2PQR online pipeline.<sup>157</sup> ..... 77

Figure 25- PyMOL<sup>156</sup> cartoon representation of (A) PSM $\alpha$ 1, (B) PSM $\alpha$ 3, and (C) PSM $\beta$ 2. Side chains that may be participating in salt bridges ..... 78

Figure 26- Location of amino acids in PSM $\alpha$ 3 responsible for enacting a biological response, determined by Cheung and co-workers through an alanine scan. The top row reflects the hydrophilic side of PSM $\alpha$ 3, and the bottom row reflects the hydrophobic side. Amino acids not enacting any biological response are colored green. Amino acids contributing to biofilm formation and detachment are colored orange, those contributing to antimicrobial activity light blue, those contributing to pro-inflammatory response red, and those contributing to cytolytic activity dark blue. .... 80

Figure 27- Cartoon representation of amphipathic helices in leaderless bacteriocin enterocin 7B and peptide toxin PSM $\beta$ 2. Both peptides contain three  $\alpha$ -helices, two of which form a “v-shape” and a third perpendicular helix. In enterocin 7B, helix 1 and helix 2 form the “v- shape” and helix 3 is perpendicular to the curved helix 2. In PSM $\beta$ 2, helix 2 and helix 3 form the “v-shape” and helix 1 is perpendicular to the curved helix 3. .... 82

Figure 28- Extended amyloid structure of A) PSM $\alpha$ 3 and B) a 42-residue  $\beta$ -amyloid formed in Alzheimer’s disease. The fibril structure formed in the case of PSM $\alpha$ 3 is an atypical  $\alpha$ -cross amyloid structure whereas, the structure of the  $\beta$ -amyloid is a  $\beta$ -cross structure usually observed in fibril formation. .... 85

Figure 29- A) Cartoon representation of methionine sulfoxide substitution with various amino acids at position 24. B) Cartoon representation of the disulfide replacement of cysteine 3 and cysteine 26. C) Cartoon representation of disulfide replacement of cysteine 7 and cysteine 18. D) Cartoon representation of disulfide replacement of cysteine 12 and cysteine 28. .... 89

Figure 30- Images of MDA-MB-231 breast cancer cells upon treatment with neopetrosiamide analogues. Scale bars on the bottom right corner of the pictures indicate 100  $\mu$ m. A) Example of MDA-MB-231 cells treated with an active neopetrosiamide analogue. Cells have rounded and detached from surface of matrigel. B) Representative picture of cells

<p>treated with a partially active analogue of neopetrosiamide. C) Picture of MDA-MB-231 cells that have been treated with an inactive neopetrosiamide analogue. Cells have invaded the matrigel and maintain their oblong shape. ....</p>	95
<p>Figure 31- Hydrophobic surface map of neopetrosiamide. One face of the peptide is hydrophilic and the other face of the peptide is hydrophobic. ....</p>	97
<p>Figure 32- Neopetrosiamide analogue containing a modified PEG<sub>6</sub> linker at the aspartic acid residue at position 20. ....</p>	104
<p>Figure 33- PyMOL surface structure of neopetrosiamide. Aspartic acid 20 is shown in pink and methionine 24 is shown in blue. All other amino acid are colored grey. Aspartic acid 20 is located on the hydrophilic face and methionine 24 is located on the hydrophobic face. A 90 degree rotation of the peptide reveals the close spatial proximity of Asp20 to Met24. ....</p>	105
<p>Figure 34- Phenylalanine 1 and phenylalanine 2 analogues that provide a synthetic handle for fluorescent labeling of neopetrosiamide. ....</p>	109
<p>Figure 35- Spatial orientation of A) Phe1, Met(O)24, and Phe23 and B) Phe2, Met(O)24, and Phe23. The backbone residues are color coded grey, amino acids of particular interest are colored explicitly as follows: A) Phe1, magenta; B) Phe2, magenta; Me(O)24, blue; and Phe23, teal. ....</p>	110
<p>Figure 36- Fragments observed by LC-MS of neopetrosiamide after incubation with mouse blood plasma. ....</p>	111

## List of Schemes

Scheme 1- Conjugation of subtilosin A to biotin through an amide bond.....	58
Scheme 2- Synthetic scheme of "click" chemistry between an amine and a thiol using a Meldrum's acid derivative.....	60
Scheme 3- Synthesis of Meldrum's acid derivative.....	61
Scheme 4-Retrosynthetic analysis of subtilosin A derivative containing a five-carbon linker bound to the Meldrum's acid derivative able to undergo a 'click' reaction with a free thiol on a cysteine side chain.....	65
Scheme 5- Synthetic scheme of the sequential formation of disulfide bonds utilizing an orthogonal protection/deprotection strategy.....	92
Scheme 6- Synthesis of fluorescently labeled neopetrosiamide.....	99
Scheme 7- Functionalization of Rhodamine B with propargyl amine to form alkynal functionalized Rhodamine B.....	100
Scheme 8- Formation of the alkyne functionalized coumarin dye through acylation and amide bond formation.....	101
Scheme 9- Synthesis of alkyne functionalized BODIPY dye.....	101
Scheme 10- Copper catalyzed 'click' reaction to afford fluorescently labeled neopetrosiamide analogues, 74, 75, and 76.....	102
Scheme 11- Synthesis of Pegylated Aspartic Acid Residue.....	103
Scheme 12- Synthetic scheme of the synthesis of the diazotized derivative of phenylalanine....	107

## List of Symbols, Abbreviations and Nomenclature

Abbreviation	Definition
ABC	ATP-binding Cassette
ACM	Acetamidomethyl
Ac <sub>2</sub> O	Acetic Anhydride
Ala or A	Alanine
APBS	Adaptive Poisson-Boltzmann Solver
APT	All-purpose Tween
Aq.	Aqueous
Arg or R	Arginine
Asn or N	Asparagine
Asp or D	Aspartic acid
BLAST	Basic Local Alignment Search Tool
Bn	Benzyl
Boc	<i>tert</i> -butoxycarbonyl
Bp	Base Pairs
<i>t</i> Bu	<i>tert</i> -Butyl
<i>t</i> BuOH	<i>tert</i> -Butanol
<sup>13</sup> C-HSCQ	Carbon 13, Heteronuclear Single Coherence Correlation Experiment
CD	Circular dichroism

COSY	Homonuclear Correlation Spectroscopy
CYANA	Combined assignment and dynamics algorithm for NMR applications
Cys or C	Cysteine
$\delta$	Chemical shift
d	Doublet
DCC	1, 3-Dicyclohexylcarbodiimide
DCM	Dichloromethane
DIPEA	Diisopropylethylamine
DMAP	4-Dimethylaminopyridine
DMF	Dimethylformamide
DMSO	Dimethylsulfoxide
DNA	Deoxyribonucleic acid
DPC	Dodecylphosphocholine
DSS	4,4-Dimethyl-4-silapentane-1-sulfonic acid
DTT	Dithiothreitol
EDT	1, 2-Ethanedithiol
EDC	1-Ethyl-3-(3-dimethylaminopropyl)carbodiimide
EI-MS	Electron Impact Mass Spectrometry
equiv	Equivalents
ESI	Electrospray Ionization

Et	Ethyl
Et <sub>2</sub> O	Diethyl Ether
Et <sub>3</sub> N or TEA	Triethylamine
EtOAc	Ethyl Acetate
FDA	Food and Drug Administration
Gly or G	Glycine
Gln or Q	Glutamine
Glu or E	Glutamic Acid
GRAS	Generally Regarded as Safe
HATU	1-[Bis(dimethylamino)methylene]-1 <i>H</i> -1,2,3-triazolo[4,5- <i>b</i> ]pyridinium 3-oxid hexafluorophosphate
HBTU	2- (1 <i>H</i> -benzotriazole-1-yl)-1,1,3-tetramethyluronium hexafluorophosphate
HCCA	$\alpha$ -Cyano-4-hydroxycinnamic acid
HOBt	1-Hydroxybenzotriazole
HPLC	High Performance Liquid Chromatography
HR-ESI MS	High Resolution Electrospray Ionization Mass Spectrometry
Ile or I	Isoleucine
IPTG	Isopropyl $\beta$ -D-1-thiogalactopyranoside
<i>J</i>	Coupling Constant

Kan	Kanamycin
LAB	Lactic Acid Bacteria
LB Broth	Luria-Bertani Broth
LC	Liquid Chromatography
LC-MS/MS	Liquid Chromatography Tandem Mass Spectrometry/Mass Spectrometry
Leu or L	Leucine
Lys or K	Lysine
m	Multiplet
MALDI-TOF MS	Matrix Assisted Laser Desorption Ionization Time of Flight Mass Spectrometry
Me	Methyl
MeCN or ACN	Acetonitrile
MeOH	Methanol
MHz	Megahertz
MHB	Mueller Hinton Broth
MIC	Minimum Inhibitory Concentration
MRSA	Multidrug Resistant <i>Staphylococcus aureus</i>
MS	Mass Spectrometry
MS/MS	Tandem Mass Spectrometry
MW	Molecular weight
N-HSQC	Nitrogen-15 Heteronuclear Single Coherence Correlation Experiment

NHS	<i>N</i> -Hydroxysuccinimide
Ni-NTA	Nickel affinity
NMM	<i>N</i> -Methylmorpholine
NMP	<i>N</i> -Methyl-2-pyrrolidone
NMR	Nuclear Magnetic Resonance
NOE	Nuclear Overhauser Effect
NOESY	Nuclear Overhauser Spectroscopy
OD <sub>600</sub>	Optical Density at 600 nm
ORF	Open Reading Frame
Ph	Phenyl
Phe or F	Phenylalanine
ppm	Parts Per Million
q	Quartet
RP	Reverse Phase
rpm	Rotations Per Minute
RMSD	Root Mean Square Deviation
s	Singlet
SAM	<i>S</i> -Adenosylmethionine
SAR	Structure Activity Relationship Studies
SDS-PAGE	Sodium Dodecyl Sulphate-Polyacrylamide Gel Electrophoresis
Ser or S	Serine

sp.	Species
Spp.	All Species
SPE	Solid Phase Extraction
SubA	Subtilosin A
Subsp.	Sub-species
t	Triplet
TCEP	Tris(2-carboxyethyl)phosphine
TFA	Trifluoroacetic Acid
TFE	Trifluoroethanol
TFFH	Fluoro- <i>N,N,N',N'</i> -tetramethylformamidinium hexafluorophosphate
THF	Tetrahydrofuran
Thr or T	Theronine
TLC	Thin Layer Chromatography
t <sub>R</sub>	Retention Time
TOCSY	Total Correlation Spectroscopy
UV-Vis	Ultraviolet-Visible

## **Chapter One: Introduction**

### **1.1 Introduction**

Secondary metabolites produced by bacteria are highly diverse in structure and function.<sup>1,2</sup> In fact, the natural products biosynthesized by bacteria have been the cornerstone of the pharmaceutical industry over the past 60 years.<sup>2</sup> There has been a golden age of drug discovery upon the realization that bacteria produced a plethora of biologically active compounds.<sup>1,3</sup> These compounds are known for their wide variety of medicinal applications, but perhaps the most noteworthy property of these metabolites has been their evolution as antibiotics.<sup>3,4</sup> The discovery and use of penicillin arguably transformed human existence, enabling many medical procedures by preventing and treating bacterial infections. From the discovery of penicillin, many more antibiotics followed including vancomycin, erythromycin, and tetracycline (Figure 1).<sup>4</sup> Through the continued use and overuse of antibiotics, our global community has observed an overall increase in the number of bacterial infections resistant to our current drug therapies. Ongoing development of new antibiotics is primarily limited to the elaboration of scaffolds derived from antibiotics already on market (Figure 2).<sup>5</sup> While this has led to more potent antibiotics, bacterial resistance remains a problem due to targeting the same pathways as before.<sup>6</sup> By the year 2050, an estimated 10 million people will die prematurely due to drug-resistant bacterial infections, costing the global economy approximately 100 trillion USD in medical fees and lost production.<sup>7</sup> There is an urgent need to further expand our repertoire of novel antibiotics with alternative modes-of-action. Along with new drug-discovery, it is

necessary to form a more complete understanding of bacterial pathogenicity and emergence of resistance through investigation of cellular mechanisms.

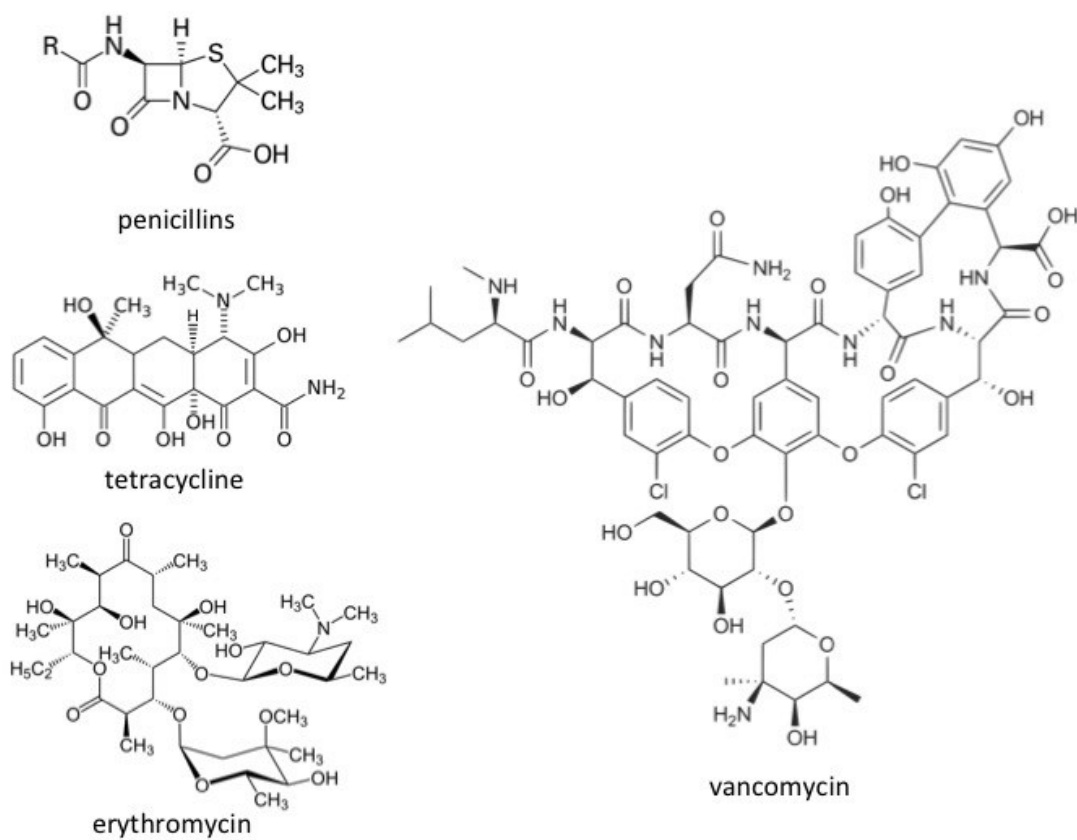


**Figure 1- Examples of antimicrobial compounds isolated from fungi and bacteria.**

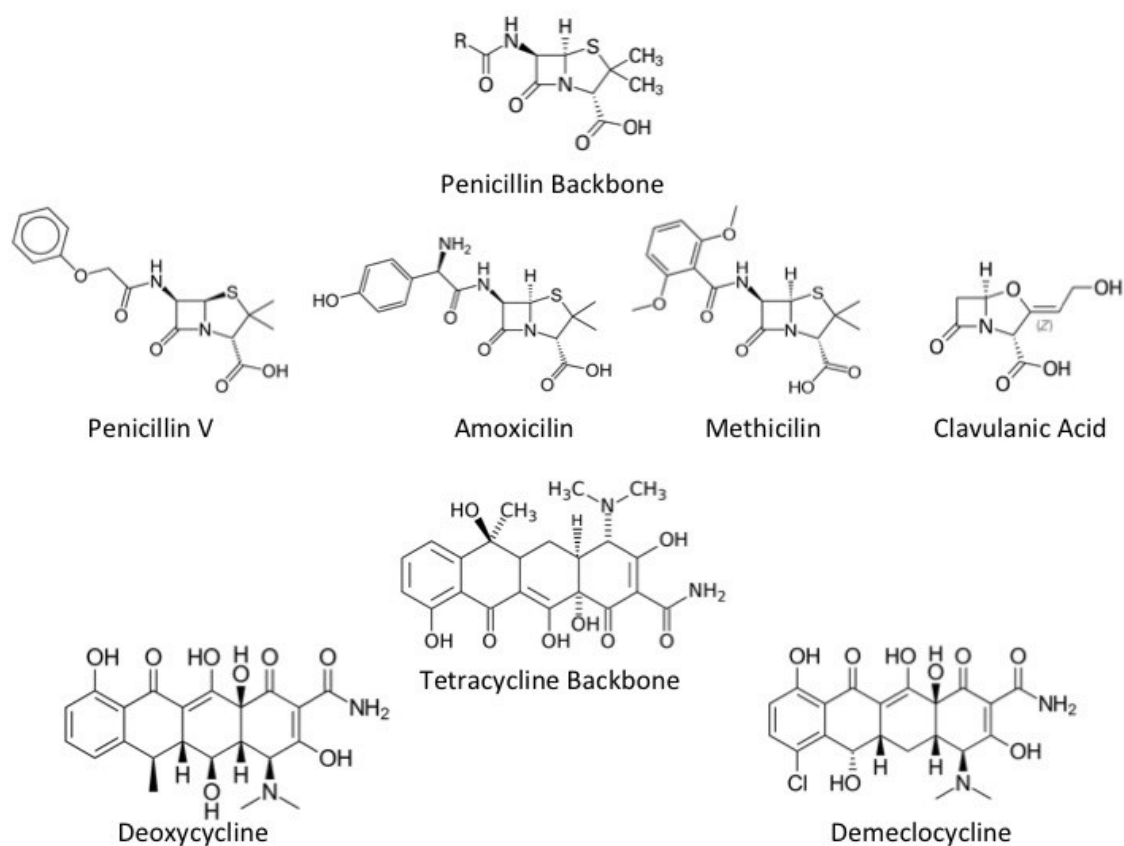


**Figure 2- Examples of derivitization of common backbone scaffolds to give new antibiotic drug compounds.**

Many bacteria produce ribosomally synthesized antibiotic peptides called bacteriocins.<sup>8-</sup>  
<sup>10</sup> These peptides offer an advantage over traditional antibiotics due to their highly diverse structures and more recently revealed, differing modes-of-action.<sup>3,5,11</sup> Bacteriocins have traditionally been thought to be produced by bacteria as a way of providing the producing organism with an evolutionary edge over other bacteria in their respective environments.<sup>8</sup> Many foodborne pathogens are Gram-positive bacteria, and for this reason, the bacteriocins produced by Gram-positive bacteria are of particular interest.<sup>12-14</sup> More recently, many bacteriocins have

displayed a broad-spectrum of activity against many different species of bacteria, garnering attention from not only the pharmaceutical industry, but also the food preservation industry.<sup>11,12,15</sup>

The structural diversity of bacteriocins, particularly those isolated from Gram-positive bacteria, has led to a rudimentary classification system.<sup>16</sup> As more bacteriocins are discovered and reported, it is apparent that this classification system is imperfect, and is primarily based on bacteriocins produced by lactic acid bacteria. These antimicrobial peptides are grouped as follows. Class I bacteriocins are called lantibiotics.<sup>16,17</sup> Peptides of this class contain post-translational modifications and have at least one lanthionine (Lan) or a methyllanthionine (MeLan) ring.<sup>16,17</sup> Class II bacteriocins are small (<10 kDa) heat-stable peptides; many subclasses of bacteriocins are included under this umbrella, such as leaderless and circular bacteriocins.<sup>16,17</sup> Crossover exists between the subclasses of Class II bacteriocins and many fit within the definition of two or more subclasses. Bacteriolysins are the Class III bacteriocins and they are large heat-labile, antimicrobial proteins.<sup>11,16,17</sup> The last class of bacteriocins are Class IV, these antimicrobial peptides include post-translational modification to attach lipid or sugar moieties.<sup>10,11</sup>

Development of new antibiotics from bacterial fermentations suffers from several drawbacks. There is a high rate of re-discovery of known biologically active compounds, and newly discovered bacteriocins are typically difficult to synthesize chemically.<sup>17-19</sup> Problems with low-yielding fermentations, toxic side effects, and chemical instability of the desired antimicrobial peptides are all setbacks in the development of therapeutic bacteriocins.<sup>12,15,17</sup>

Many pharmaceutical companies have abandoned natural product discovery in favour of the more efficient modification of existing scaffolds, which suffer from the same pitfalls of bacterial resistance as their predecessors.<sup>1,2,5,20</sup> As a global community, we are facing a post-antibiotic era where common medical procedures may no longer be available, and ordinary bacterial infections may become fatal.<sup>7</sup> We must expand the selection of antibiotics we have in our arsenal and we must work towards understanding the nuances of antibiotic resistance.

## **1.2 Leaderless Bacteriocins**

### ***1.2.1 Introduction***

Leaderless bacteriocins are a subclass of Class II bacteriocins.<sup>17</sup> Unique from other bacteriocins in that they are produced without a leader sequence, these peptides contain no post-translational modifications.<sup>21</sup> Typically, recognition of the leader sequence by enzymes is required to install post-translational modifications such as lanthionine and methyllanthionine rings or the creation of thioether bonds, as in the case of sactibiotics. The leader sequence is also thought to potentially be important in the cyclization of the C- and N-termini.<sup>22-24</sup> Transport proteins also recognize the leader sequence, facilitating the export of the bacteriocin from the host cell with cleavage of the leader peptide to form the mature, biologically active compound.<sup>23,25</sup> Furthermore, observation of biological activity can be reduced until this proteolytic cleavage occurs, suggesting the leader peptide imparts self-immunity to the producing organism.<sup>23</sup> The production of bacteriocins without this leader sequence represents a growing group of Class II bacteriocins that display potent antibacterial activity against a wide variety of organisms.<sup>26</sup>

The first leaderless bacteriocins reported were isolated from *Enterococcus faecium* L50.<sup>21</sup> A two-component bacteriocin, enterocin L50A and enterocin L50B (EntL50A and EntL50B) display individual activity and additional synergistic activity. Since this first report, there been many other leaderless bacteriocins discovered, including enterocin 7 (Ent7), weisellicin M (WeiM), aureocin A53 (AurA53), lactacin Q (LqnQ), lactacin Z (LcnZ), mutacin BhtB (BhtB), and epidermicin N (EN101), LsbB, enterocin K1 (EntK1) and enterocin EJ97 (EntEJ97).<sup>27</sup>

Grouped further, three families of leaderless bacteriocins exist based on sequence similarity (Figure 3).<sup>28</sup> Those containing a conserved C-terminal K-XXX-G-XX-PWE motif are consolidated into the LsbB family, whereas those that contain around 44 amino acids are part of the EntL50 family.<sup>29</sup> The largest class, the AurA53 family, characterized by sequences of approximately 50 amino acids. The scope of activity of these leaderless bacteriocins varies greatly, and more recently there have been considerable advances in the structural studies and mode of action studies for each class of these leaderless bacteriocins.<sup>30-32</sup>

### EntL50A Family

```
WeiM      MVSAAKVALKVGWGLVKKYYTKVMQFIGEGWSVDQIADWLKRH-
EntL50A   MGAIAKLVAKFGWPIVKKYYKQIMQFIGEGWAINKIIEWIKKHI
Ent7A     MGAIAKLVAKFGWPIVKKYYKQIMQFIGEGWAINKIIDWIKKHI
EntL50B   MGAIAKLVTKFGWPLIKKFYKQIMQFIGQGWTDQIEKWLRH-
Ent7B     MGAIAKLVAKFGWPFIKKFYKQIMQFIGQGWTDQIEKWLRH-
* : **: . *.** :***:*.::*****:**:::* .*:**
```

### AurA53 Family

```
BhtB      --MWGRILAFVAKYGTKAVQWAWKNKWFLSLG-----EAVFDYIRSIWGG-
AurA53    -MSWLNFLKYIAKYGKKAVSAAWKYKGVLEWLVNVPPTLEWVWQKLKKIAGL-
EN101     MAAFMKLIQFLATKGQKYVSLAWKHKGITLKWLNAGQSFWEIYKQIKLWA--
LcnQ      MAGFLKVVQLLAKYGSKAVQWAWANKGKILDWLNAGQAIDWVVKIKQILGIK
LcnZ      MAGFLKVVQILAKYGSKAVQWAWANKGKILDWLNAGQAIDWVVEKIKQILGIK
          : ..: :*. * * *.** * :*.          : : . :.: .
```

### LsbB Family

```
LsbB      -----MKTILRFVAGYDIASHKKKTGGYPWERGKA
EntEJ97   SLAKIKAMIKKFPNPYTLAAKLTTYEINWYKQYGRYPWERPVA
EntK      -----MKFKFNPTGTIVKKLQYEIAWFKNKHGYYPWEIPRC
          *:   :: ** .*: : * **** .
```

**Figure 3- Clustal Omega sequence alignment of the different families of leaderless bacteriocins.<sup>33</sup> Asterisks (\*) indicate identical amino acids, colon (: ) indicate amino acids which are highly similar and periods (.) indicate amino acids that are similar.**

## 1.2.2 Biosynthesis

The biosynthesis of leaderless bacteriocins is not well understood in comparison to other groups of bacteriocins. Annotated gene clusters are available for several leaderless bacteriocins including enterocin L50, aureocin A53, lacticin Q, lacticin Z, epidermicin N101, mutacin BhtB, and LsbB; however, only a few of these have been studied extensively.<sup>21,34-39</sup>

Enterocin L50 was the first reported leaderless bacteriocin, and yet, the specific genes that code for immunity and transport of this peptide are still unknown. Despite the simplicity of

the locus containing the Enterocin L50 structural genes, none of the neighboring open reading frames exhibit homology with known transport or immunity proteins.<sup>21</sup>

Gene clusters of leaderless bacteriocins belonging to the AurA53 family are better understood. Unlike many other classes of bacteriocins, the locus encoding for AurA53 contains genes for two immunity proteins. Similarly, the gene cluster of BhtB, LqnQ, and LcnZ each contain genes encoding for three immunity proteins. Also unique to this family of bacteriocins is the presence of a multicomponent ABC transport protein. AurA53 has a three-component ABC transporter whereas the loci encoding for BhtB, LqnQ, and LcnZ contain a two-component ABC transporters.<sup>34-37</sup> Of this family of bacteriocins, the genes of LqnQ are the most studied.<sup>36,40</sup> Heterologous expression of six genes in the LqnQ locus is sufficient for full production and immunity of LqnQ.<sup>40</sup> Genes that encode for the transport of LqnQ, *lnqEF* are also able to impart partial immunity.<sup>40</sup> However, three additional genes, *lnqBCD*, are required for full immunity of the producer to LqnQ.<sup>40</sup>

### ***1.2.3 Mode of Action***

Historically, bacteriocins were thought to elicit a bactericidal response through non-specific interactions with the cell membrane of organisms.<sup>41</sup> Many types of interactions were postulated to play a role in the antimicrobial behaviour exhibited by these bacteriocins. Ionic interactions between the cationic peptides and the anionic phospholipid cell membrane were considered dominant in the initial attraction of these antimicrobial agents to the cell surface.<sup>41</sup> Upon contact between the peptide and cell membrane, hydrophobic interactions were considered to take over, specifically, anchoring of the peptide into the membrane by the surface-exposed

aromatic residues.<sup>42,43</sup> Regardless of the initial mode of attraction, these bacteriocins appear to form pores within the cell membrane leading to leakage of small and large molecules.<sup>41</sup> Lacticin Q and aureocin A53 are perhaps the most well studied regarding mode of action and pore formation.<sup>44-46</sup> Lacticin Q has been reported to form torroidal pores, at micromolar concentrations, in liposomes containing L- $\alpha$ -phosphatidylcholine and L- $\alpha$ -phosphatidyl-DL-glycerol, suggesting that no docking molecule is needed.<sup>44,45</sup> The pores formed when lacticin Q interacts with membranes has been reported to be as large as 4.6 nm, which allows for leakage of both small and large molecules.<sup>45</sup>

Similarly, aureocin A53 has been shown to interact with liposomes in the low micromolar range. However, aureocin A53 does not form discrete pores, but rather, causes general permeation of the cell membrane to elicit a bactericidal response.<sup>46</sup> Interestingly, aureocin A53 was found to interact more strongly with neutral membranes over anionic membrane surfaces, contrary to the hypothesis that ionic interactions initially dominate the electrostatic attraction between the cationic antimicrobial peptides and the cell membranes.<sup>46</sup>

With the advent of readily available and affordable whole genome sequencing (WGS), mutation of bacterial strains sensitive to bacteriocins that results in resistant colonies can be investigated and the resulting genomes are being sequenced.<sup>31,47-49</sup> In many cases the comparison between the mutated and parent genomes has revealed single nucleotide polymorphisms (SNPs) that result in mutations in specific membrane bound proteins, suggesting the mode of action of bacteriocins may be more complex than originally proposed. The first reported case of using genome comparisons to identify a receptor or docking molecule for a bacteriocin is in the case of

garvicin ML.<sup>47</sup> In this study, it was found that all mutant strains of bacteria contained large mutations in the chromosomal region that encodes for maltose breakdown and uptake. This 13.5 kb deletion encodes 12 different proteins including 3 that are involved in the maltose ABC transport protein. To confirm the maltose ABC transporter as a receptor to the garvicin ML bacteriocin, carbohydrate fermentation assays were studied. The wild type *L. Lactis* IL1403 ferments starch and maltose while the resistant *L. lactis* mutants did not grow in the presence of either carbohydrate, indicating that the resistant mutants had lost the ability to utilize maltose.<sup>47,48</sup> Similar studies have been conducted for the leaderless bacteriocins LsbB, EntEJ97, and EntK1.<sup>31</sup> For each of these leaderless bacteriocins, a frameshift mutation has been identified in either the *YvjB* or *rseP* gene, genes that are important in the stress response of bacteria.<sup>31</sup> While RseP has been identified as a receptor for the EntJ97 and Entk1 leaderless bacteriocins, there remains some question as to the specific interactions responsible for eliciting a bactericidal response. The RseP protein is highly conserved among different species of bacteria, and yet each of these leaderless bacteriocins has differing spectrums of activity. It is also unknown whether leaderless bacteriocins of the EntL50 and AurA53 families share a similar receptor. Considering the differences in secondary structures and the lack of the K-XXX-G-XX-PWE motif, it seems unlikely that the leaderless bacteriocins of the latter families share the same receptor as the LsbB family of bacteriocins.

Despite the fact that the receptor-bacteriocin interactions are not well understood, it is becoming clear that the interaction between these antimicrobial peptides and the cell membrane is no longer as simple as it was once proposed. It appears that there is accumulating evidence

that, at low concentrations, these peptides do indeed have a receptor or docking molecule, though it remains unclear if the presence of a receptor governs the initial attraction of the bacteriocin to the cell membrane.<sup>31,47-49</sup> It may be that the cationic surface dominates the initial attraction, but that the docking molecule is required to orient the antimicrobial peptide on the cell membrane surface in such a way that allows for hydrophobic insertion and pore formation.<sup>31,47-49</sup>

## **1.3 Sactibiotics**

### ***1.3.1 Introduction***

Sactibiotics are a subclass of bacteriocins that contain a relatively rare sulfur to  $\alpha$ -carbon linkage. These ribosomally synthesized peptides are post-translationally modified to insert a thioether bond between the sulfur atom on the cysteine side chain and the  $\alpha$ -carbon atom of another amino acid. Sactibiotics exhibit a relatively narrow scope of activity relative to many other bacteriocins. The first sactibiotic to be discovered was subtilisin A (SubA) though this class of peptides has been expanded to include thuricin CD, thurincin H, sporulation killing factor, and a T6I variant of subtilisin A.<sup>50-53</sup>

### ***1.3.2 Biosynthesis***

The gene clusters involved for sactibiotics are similar to other bacteriocins in that they include structural genes and genes encoding for transport, immunity, and post-translational modifications. Unique to the sactibiotic gene clusters is the presence of genes encoding one or more *S*-adenosylmethionine (SAM) proteins.<sup>54</sup> Radical SAM proteins contain iron-sulfur clusters and participate in the cleavage of *S*-adenosylmethionine, resulting in the formation of a *S*-adenosyl radical that can lead to a variety of biological reactions.<sup>54</sup> These enzymes have been

found to participate in isomerizations, aerobic oxidations, and, in the case of sactibiotics, ring formation (Figure 4).<sup>55,56</sup>

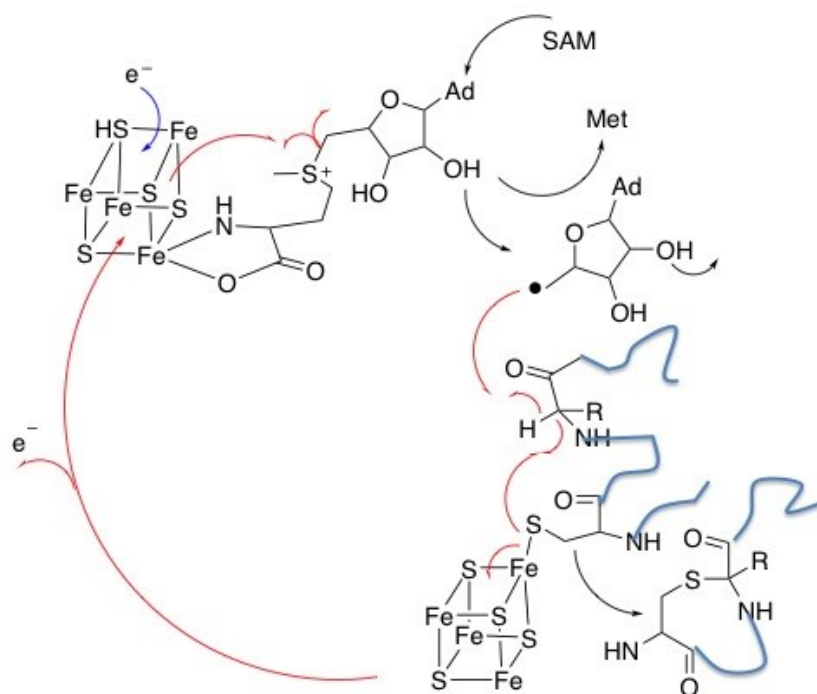


**Figure 4- Proposed mechanism of thioether formation by radical SAM enzyme between a cysteine thiol and the  $\alpha$ -carbon of a neighbouring amino acid.**

The individual gene loci of the different sactibiotics are quite interesting. In the case of thuricin CD, two genes, *trnC* and *trnD*, encode for two separate radical SAM enzymes. Most likely, the resulting proteins TrnC and TrnD each modify one peptide, TrnA or TrnB, respectively.<sup>51</sup> Each peptide in Thurincin CD contains three thioether bonds. Interestingly, while both TrnC and TrnD contain the signature amino acid motif found in most SAM enzymes, C-XXX-C-XX-C, TrnC has been shown to have sequence homology with an oxidoreductase aryl

sulfatase regulatory protein, whereas TrnD has been shown exhibit sequence homology with a family of molybdenum cofactor enzymes.<sup>51</sup> The significance of this is not yet known.

The biosynthesis of subtilosin A is particularly complex. There is an operon that contains seven genes (*albA- albG*), encoding for proteins which modify the precursor peptide of subtilosin A, encoded by the structural gene *sboA*.<sup>57,58</sup> Subtilosin A contains three thioether bonds in addition to being cyclized through the N- and C-termini. Located upstream of the modifying peptides, *sboA* is overlapping with a second structural gene, *sboX*.<sup>58</sup> A single nucleotide reading frameshift from *sboA*, *sboX* encodes a putative class II bacteriocin.<sup>57</sup> The leader sequence of SboX contains the typical Gly-Gly motif indicative of a prebacteriocin cleavage site.<sup>57</sup> However, the resulting peptide product from the gene *sboX* has never been detected, nor has disruption of the gene itself affected the biosynthesis of subtilosin A.<sup>57</sup> Remarkably, a single promoter has been found to be responsible for the transcription of the *sbo- alb* genes. Mutagenesis studies on each of the *sbo- alb* genes has revealed that non-polar mutations in *albBCD* resulted in reduced antimicrobial activity, whereas non-polar mutations in *sboA*, *albA*, and *albF* resulted in abolishment of antimicrobial activity indicating the respective genes are essential for subtilosin A biosynthesis.<sup>57</sup> AlbA has been found to contain two C-XXX-C-XX-C motifs characteristic of the iron-sulfur clusters present in SAM enzymes.<sup>24</sup> Furthermore, this study was the first published account of an active radical SAM sactibiotic enzyme reconstituted *in vitro*.<sup>24</sup> This study also suggests that the leader peptide is essential for maturation of the subtilosin A precursor and that the formation of the three thioethers is performed during the first step in the maturation process.<sup>24</sup> AlbBCD are required for subtilosin A

immunity, and AlbC has additionally been shown to be homologous with ABC transport proteins, suggesting it is responsible for the extracellular transport of subtilisin A.<sup>24</sup> AlbE and AlbF are putative proteases, presumably needed for the cleavage of the leader peptide and macrocyclization.<sup>24</sup> The exact role of each protein involved in each proteolytic step remains unclear. Additionally, it is unknown what function AlbG plays in the biosynthesis of subtilisin A.<sup>24</sup>

Relatively little information has been revealed regarding the synthetic gene cluster of Thuricin H. Thuricin H is unique in that the gene locus contains three identical structural genes in tandem.<sup>52</sup> This is thought to allow for increased production of bacteriocin but may also point to an evolutionary origin involving gene duplication.<sup>52</sup> In addition, it is the only sactibiotic that contains four thioether bridges.<sup>59</sup> Interestingly, the gene cluster of thuricin H is the only example of a sactibiotic gene cluster successfully expressed in a heterologous host to date.<sup>60</sup> Notably, the host was immune to the bacteriocin upon introduction of the entire gene cluster, suggesting that immunity genes are present in the loci, though which exact gene is responsible for immunity remains unknown.

### ***1.3.3 Mode of Action***

The mode of action of sactibiotics remains largely a mystery. In contrast to what is known about the lantibiotics and many class II bacteriocins. Only a few studies exist that look at the mechanism of action of sactibiotics. Unlike many other bacteriocins, sactibiotics are not believed to form pores in bacterial cell membranes. Thuricin CD has been found to trigger a relatively slow release of the intracellular enzyme acetate kinase from *Clostridium difficile* cells,

but it has been postulated that this is not the same pore forming mode of action as it is in the case of the lantibiotic lactacin 3147.<sup>61</sup> Lactacin 3147 induces rapid release of acetate kinase, whereas thuricin CD slowly releases acetate kinase.<sup>51,61</sup> The slow liberation rate of acetate kinase observed upon treatment of thuricin CD suggests that it is unlikely that discrete membrane pores are formed.<sup>51</sup>

When *B. cereus* F4552, sensitive to thurincin H, was exposed to thurincin H the cell membrane integrity was maintained.<sup>62</sup> The rod-like structure of the cells was intact at concentrations of 32 x the MIC. Concentrations of 256 x the MIC caused changes in the morphology of the cells.<sup>62</sup> This is in contrast to nisin, in which concentrations as little as 2 x the MIC affects membrane permeability through sequestering lipid II and inhibiting peptidoglycan formation resulting in pore formation.<sup>62</sup> The high concentrations of bacteriocin required to disrupt membranes indicate that thurincin H is most likely not involved in pore formation.<sup>62,63</sup>

Subtilosin A is perhaps the most well studied bacteriocin, and yet its exact mode of action remains elusive. One study suggests that subtilosin A does indeed form pores, as the addition of this bacteriocin to *G. vaginalis* cells resulted in immediate depletion of the transmembrane pH gradient even though there was no effect on the transmembrane electric potential.<sup>64</sup> This study also observed efflux of intracellular ATP and the authors propose that subtilosin A forms transient pores which allow for the efflux of ions and intracellular ATP, ultimately resulting in cell death.<sup>65</sup>

A second study focused on the mode of action of subtilosin A proposed general membrane permeabilization through interaction with the phospholipid head group.<sup>66</sup> Through the

use of solid-state NMR, fluorescence studies and differential scanning calorimetry, subtilisin A was found to be partially buried in the lipid bilayers.<sup>66</sup> As the concentration of peptide increases, the portion of the peptide embedded in the lipid bilayer results in a conformational change in the lipid head group and disruption of the hydrophobic component of lipid membranes leading to general permeabilization, leading to cell death.<sup>66</sup>

It is still unknown as to whether or not sactibiotics require a receptor molecule on the surface of the cell membrane. The high concentrations of peptide required to elicit a bactericidal response suggests that these peptides act in a general detergent manner. However, the specificity and narrow-spectrum of activity contradicts this hypothesis. The use of genome sequencing holds promise for unraveling the specific mode of action of many of these sactibiotics. Whole-genome sequencing of wild type and resistant strains offers the advantage of locating single nucleotide polymorphisms (SNPs) in genes that encode for membrane bound proteins. As in the case of lactococcin G, LsbB, garvacin ML and others, application of this genetic technique to sactibiotics could further illuminate exactly how these sactibiotics elicit antimicrobial responses.

31,47-49

## **1.4 Phenol-soluble Modulins**

### ***1.4.1 Introduction***

Bacteria have evolved to produce many secondary metabolites that create a competitive edge to aid in their survival. While the production of antimicrobial peptides in bacteria has garnered much attention due to potential therapeutic applications, this represents only one half of the story in regards to the evolution of bacterial survival in hostile environments. Production of

virulence factors by bacteria represent a second method in which bacteria can manipulate their environment to make it more hospitable to the organism's own growth and survival.<sup>67</sup>

Traditionally, our therapeutic approach for the treatment of bacterial infections has been limited to treatment with antibiotics. With the emergence of antibiotic resistance, the global community has addressed the need to develop new antimicrobials. There are several inherent problems with this strategy, namely that new resistance is likely to always occur in receptor-dependent antibiotics.<sup>68</sup> An alternative to this traditional strategy is to look at the virulence factors produced by bacteria, and potentially “disarm” the pathogenic bacteria, enabling the host immune system to eliminate the infection.<sup>67</sup> There are many contributing factors to virulence in bacteria, but anti-virulence research typically focuses on toxin production, quorum sensing, and biofilm formation.<sup>67</sup>

Methicillin-resistant *Staphylococcus aureus* (MRSA) leads to a bacterial infection with wide-reaching global implications. Typical *S. aureus* infections affect the respiratory tract as well as skin and soft tissue infections.<sup>69,70</sup> Left untreated, *S. aureus* can lead to endocarditis, osteomyelitis and septicaemia.<sup>69,70</sup> MRSA is particularly pathogenic due to the large number of virulence factors produced.<sup>71</sup> Phenol-soluble modulins (PSMs) are thought to be some of the predominantly produced virulence factors; in fact, up to 60% of the protein mass excreted by some strains of staphylococci is due to these peptides.<sup>72-76</sup> Additionally, the wide-ranging functions of these virulence factors make them an attractive target in attempts to circumvent the pathogenicity of staphylococcal infections.<sup>72,74-78</sup>

### 1.4.2 Biosynthesis

Phenol-soluble modulins gene clusters are located in three distinct locations of the genome.<sup>79</sup> Interestingly, the loci encoding for all PSMs are located in the core genome or in highly conserved genomic islands of the genome, meaning that they are present throughout all species of Staphylococci.<sup>75</sup> An important distinction is that while PSMs from different species may share the same name, the amino acid sequence is often different. For that reason, when referring to PSMs, one must refer to the specific organism in which the PSM was isolated (e.g. *S. aureus* PSM $\alpha$ 1).<sup>75</sup> In the case of MRSA, the shorter,  $\alpha$ -type PSMs are encoded by the *psm- $\alpha$*  locus, and the longer,  $\beta$ -type PSMs are encoded in the *psm- $\beta$*  locus.<sup>79</sup> Notably, the last PSM produced by MRSA,  $\delta$ -toxin, is encoded by the *agr locus*, which also encodes for RNAIII, an effector molecule of the Agr quorum sensing system.<sup>80</sup>

Like antimicrobial peptides produced by bacteria, these virulence factors are exported from the host cell through the use of an ABC transporter, termed the phenol-soluble modulins transporter (Pmt).<sup>81</sup> The locus encoding for this transport system contains four genes (*pmtA-D*), of these *pmtA* and *pmtC* encode ATPases. Two membrane associated proteins are encoded by *pmtB* and *pmtD*.<sup>81</sup> Remarkably, this transport system is responsible for the extracellular transport of all PSMs regardless of size or structure. Also worthy of notice, is the fact that the *pmt* locus is highly conserved throughout all species of staphylococci and absent from non-staphylococcal genomes as is the production of PSMs.<sup>75,81</sup> Recent studies have shown that deletion or mutation of the *pmt* locus results in cell death. Without the Pmt transporter, the PSMs

accumulate in the cytoplasm leading to cellular deficiencies and defects.<sup>81</sup> In addition, the Pmt transporter has been found to contribute to self-immunity of the producing organism.<sup>81</sup>

### ***1.4.3 Mode of Action***

PSMs have been reported to have a wide variety of functions, with differing functions attributed to  $\alpha$ -type and  $\beta$ -type peptides. Common to all of the PSM peptides are the attributes that aid the staphylococcus species for survival in their environmental niche, namely, the epithelial surfaces of mammals.<sup>72</sup> The detergent-like characteristics of all PSM peptides have been shown to be important in the spreading of staphylococci on solid surfaces and, not yet proven, are thought to be important in the emulsification of nutrients from solid surfaces.<sup>72</sup> The structuring of biofilms also seems to be a common characteristic of all PSM peptides.<sup>82–84</sup> Biofilms are important to the pathogenic bacteria for many reasons. These surface-attached agglomerations protect the bacterial cell from the host's immune response and, in some cases, can help safeguard the organism from antibiotics.<sup>82,85</sup> Biofilm formation is well studied. In particular, the components which make up the extracellular matrix are well characterized and include a mixture of poly N-acetylglucosamine, extracellular DNA, teichonic acids and a variety of proteins.<sup>86</sup> PSMs are unique in their biofilm function as they play a key role in the structuring of these agglomerations.<sup>72,83</sup> PSMs, specifically the  $\beta$ -type PSMs, have been shown to form channels within the biofilm; important for nutrient delivery throughout the biofilm.<sup>83</sup> The  $\beta$ -type PSMs also play a crucial role in the detachment of cells from the biofilm and spread of the cells to other locations.<sup>83</sup>

The shorter,  $\alpha$ -type PSMs have been found to have additional deleterious characteristics, such as cytolysis of many eukaryotic cells.<sup>79</sup> PSMs of the  $\alpha$ -type elicit cytolysis through membrane perturbation.<sup>78</sup> Membrane disruption is proposed to result from a non-specific interaction between the PSMs and the cell membrane. Much of our understanding of the cytolytic nature of the PSMs has been through studies with PSM  $\delta$ -toxin, which has been shown to form transient pores within phosphatidylcholine lipid vesicles.<sup>87</sup> Recent reports have shown that even the  $\beta$ -type PSMs, which are not cytolytic *in vitro*, display pore formation in these artificial membranes.<sup>88</sup> These observations, along with the new developments in the discovery of receptors for various antimicrobial peptides, may suggest that the pore formation of these virulence factors may be due to more than their detergent-like natures and that there may be more complex, receptor-based interactions taking place at the cell membranes.

## **1.5 Neopetrosiamides**

### ***1.5.1 Introduction***

Bacteria and cancer cells share a commonality in that the surface of their membranes are more negatively charged than the normal mammalian cell.<sup>89</sup> This physical attribute lead to the hypothesis that anticancer peptides (ACPs) and AMPs may share similar determinates of selectivity and activity. However, many AMPs do not exhibit anti-cancer characteristics and the specific cellular targets and interactions between anti-cancer peptides and antimicrobial peptides are not well understood.<sup>90</sup>

Anti-cancer peptides are generally sub-divided into two distinct groups. The first group of ACPs exhibit activity against bacterial cells and human cancerous cells but do not show

activity against healthy mammalian cells.<sup>89,90</sup> The second group of ACPs exhibits activity against both cancerous and non-cancerous cells. Certain anti-cancer peptides are thought to elicit a membranolytic response in a similar manner to antimicrobial peptides, specifically through membrane permeabilization.<sup>89,90</sup>

Neopetrosiamides A and B are interesting anti-cancer peptides in that they are active against cancer cells and inactive against healthy mammalian cells.<sup>91</sup> These peptides do not cause cell death through membrane permeation, rather they inhibit the growth and spread of the cancer cells in a reversible fashion.<sup>91</sup> Neopetrosiamide A and B share the same amino acid sequence and differ only in the stereochemistry of the sulfoxide moiety at the oxidized methionine at position 24.<sup>92,93</sup> Each diastereomer displays equal activity in vitro, herein the combination of neopetrosiamide A and B is referred to as simply neopetrosiamide.<sup>92</sup>

### ***1.5.2 Biosynthesis***

The biosynthesis of neopetrosiamides is currently unknown. Isolated from a sponge in Papua New Guinea, it is unknown as to whether the sponge produces the peptide or if a symbiotic bacterium is responsible its formation. Attempts to sequence the genome of the sponge were unsuccessful simply because we were unable to obtain a sample of the original sponge.

### ***1.5.3 Chemical Synthesis***

Chemical synthesis of neopetrosiamides requires selective oxidation of the cysteine residues to form the three disulfide bonds sequentially. Our group previously developed an orthogonal protection/deprotection strategy to control disulfide formation between the cysteine residues.<sup>93</sup> This complex synthesis is required as the global oxidation of the neopetrosiamide

peptides resulted in biologically inactive peptides. Disulfide mapping through partial reduction, alkylation of disulfide bonds, and MS/MS sequencing revealed incorrect disulfide connectivity lead to inactive peptides, despite the NMR structures being virtually identical (Figure 5).

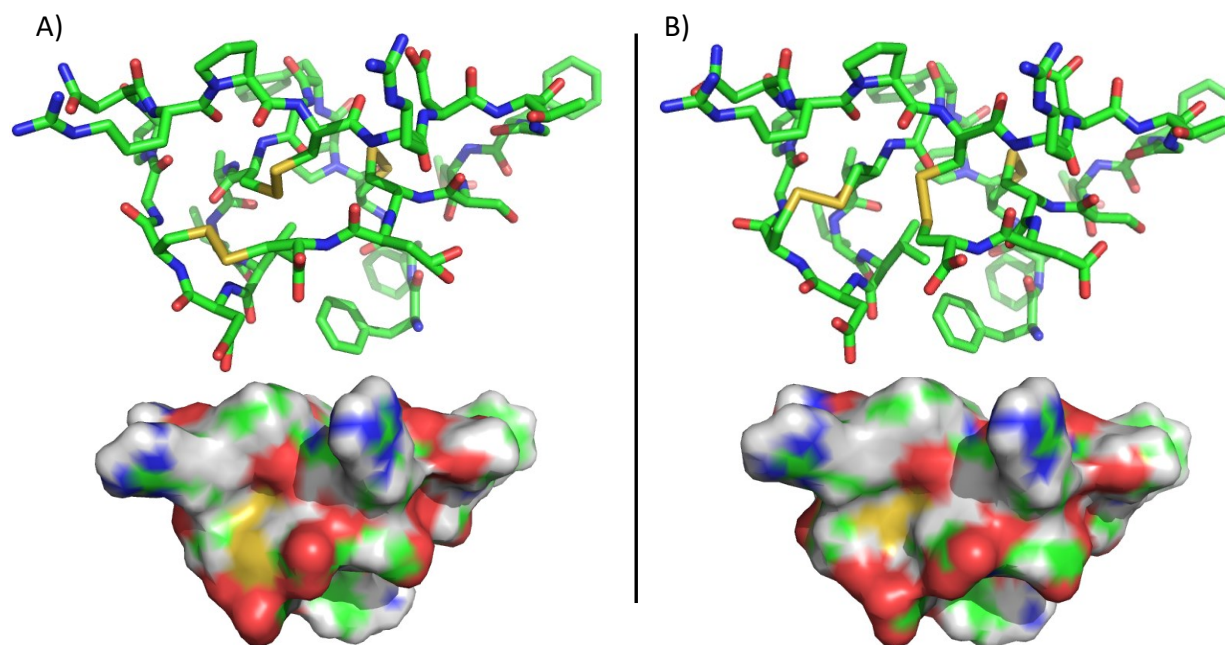


**Figure 5- PyMOL representations of A) corrected NMR structure of neopetrosiamides and B) originally proposed NMR structure of neopetrosiamide. Color-coding is as follows: green; represents hydrophobic residues, blue; positive charge, red; negative charge, yellow; disulfide bonds, and grey; neutral in the space filling surface structure.**

Fmoc-solid phase peptide synthesis, with orthogonal protecting groups with respect to the cysteine side chains, afforded the linear peptide.<sup>93</sup> Cleavage of the peptide from the resin with trifluoroacetic acid lead to the linear amino acid chain with all acid labile groups removed, including the two cysteines protected with the trityl protecting group.<sup>93</sup> The crude peptide is

dissolved in acetic acid and the first disulfide is formed through the oxidation of the free thiols with iodine. Upon formation of the first disulfide bond, the second pair of protecting groups are removed *in-situ* by the addition of water.<sup>93</sup> The second disulfide is formed by excess iodine still in solution. The desired bis-disulfide peptide is separated from mono-disulfide peptides and incorrectly folded bis-disulfides by HPLC.<sup>93</sup> Trifluoroacetic acid was used to dissolve the purified bis-disulfide peptide which leads to the removal of the final cysteine protecting group, *t*-butyl. Oxidation of the last disulfide bond was achieved through oxidation with DMSO and the resulting *t*-butyl cations were quenched with anisole.<sup>93</sup> Final purification of the desired tris-disulfide is accomplished by HPLC.

#### ***1.5.4 Mode of Action***

There is little known about the exact mode of action of the neopetrosiamide peptides. They have been shown to inhibit the amoeboid migration, a crawling-like movement where the cytoplasm slides and a pseudopodium is formed to move the cell forward, of LS147T colon carcinoma.<sup>94</sup> Neopetrosiamides have also been shown to inhibit mesenchymal migration, cell motility characterized by cell polarization and proteolytic degradation of the extracellular matrix (ECM), of MDA-MB-231 breast carcinoma and HT-1080 fibrosarcoma cells.<sup>91,92,95</sup> Previous studies have shown that the inhibition of cancer cell migration is a result of reduced cellular adhesion to the ECM. Pre-attached cells became round and retract from the underlying layer of ECM. Retraction of the cells from the substratum is characteristic of reduced cell-surface  $\beta$ -integrins. Indeed, many other anti-tumor peptides have been developed which block integrins from binding with their cognate ECM ligands.<sup>96</sup> Unlike other anti-tumor peptides, which contain

the RGD amino acid motif, neopetrosiamide does not include a known binding domain to the integrins.<sup>96,97</sup> Importantly, neopetrosiamides cause membrane protrusions on the cell surface which trigger the release of membrane vesicles containing high concentrations of integrin subunits, growth-factor receptors, and other proteins associated with surface adhesion.<sup>91</sup> The effects of neopetrosiamides are reversible upon removal of the peptide, and do not affect non-cancerous cells. While the effects of neopetrosiamides are well characterized, it is not well understood how these peptides elicit these biological responses.

## **1.6 Applications of Antimicrobial Peptides**

### ***1.6.1 Food Preservation***

Lactic acid bacteria (LAB) are a unique class of bacteria in the sense that they are designated as “generally regarded as safe” (GRAS). This classification has afforded their use in the food preservation industry. Commonly found in fermented foods, LAB produce a wide variety of bacteriocins. The antimicrobial peptides produced by the LAB are active against a broad-range of Gram-positive bacteria that cause food spoilage and that are food pathogens such as *Listeria monocytogenes*, *Clostridium botulinum*, and *Bacillus cereus*. Though chemical food preservatives are effective in preventing the growth of most food borne pathogens, they compromise the quality of the food, and detract from the food’s freshness.<sup>15</sup> The drawbacks of using chemical preservatives has lead to an opening in the food preservation industry for the use of bacteriocins produced by LAB.<sup>15</sup>

Despite the plethora of bacteriocins produced by LAB, only two are currently utilized by the industry, Nisin A and Pediocin PA-1.<sup>98</sup> Nisin A, a lantibiotic, has been in use since 1969 and

is used in over 50 different countries.<sup>15</sup> It is active against a wide variety of important food pathogens including *L. monocytogenes*, *S. aureus*, *Clostridium* spp., and *B. cereus*.<sup>15,99</sup> Pediocin PA-1 is commercially available as a powdered fermentate and is used against the Gram-positive bacteria, *L. monocytogenes*, *Clostridium perfringens*, and *Enterococcus faecalis*.<sup>100</sup>

### **1.6.2 Antibiotic Therapeutics**

Bacteriocins exhibit key characteristics that make them attractive alternatives for use as antibiotics. Specifically, the low toxicity, high potency, wide availability, broad- or narrow-spectrum of activity, and their ability to be bioengineered are features of these peptides that have lead to a renewed interest in their application as antibiotic therapeutics.<sup>11</sup> Many bacteriocins have been shown to have *in vitro* activity. Lantibiotics, such as nisin, lacticin 3147, and actagardine have all been shown to be active against notable pathogens such as vancomycin-resistant enterococci, *Streptomyces pneumonia*, and MRSA.<sup>101</sup> Sactibiotics, namely thuricin CD and subtilosin A, have been shown to have selective activity against *C. difficile* and *L. monocytogenes*, respectively.<sup>51</sup> Furthermore, class II bacteriocins have been shown to have broad-spectrum activity against a wide variety of Gram-positive bacteria including *L. monocytogenes*.<sup>38,102–104</sup>

Regardless of *in vitro* studies demonstrating the potential of bacteriocins against many pathogens, the clinical relevance of these antimicrobial peptides is still quite limited. Lantibiotics have been the most widely studied. Nisin has been shown to inhibit *S. pneumonia* and, when administered intravenously, is 8-16 times more effective than vancomycin.<sup>105</sup> A naturally occurring variant of nisin, nisin F, has been shown to be effective against *S. aureus* infections in

the respiratory tract of rats.<sup>106,107</sup> Furthermore, mercacidin is active against this same pathogen in the nasal cavity of mice.<sup>108</sup> The thiopeptide LFF571 is currently in phase II clinical trials for the treatment of *C. difficile* and vancomycin-resistant enterococci.<sup>109</sup> Notably, class IIa pediocin-like bacteriocin, E50-52, has been shown to inhibit growth of *Mycobacterium tuberculosis*.<sup>110</sup>

Clinical trials of purified bacteriocins are quite rare, despite the plethora of biodiversity in this class of antimicrobials. With the rise in antibiotic resistance there is renewed interest in the application of these bioactive peptides as therapeutics.

### ***1.6.3 Anti-tumor Therapeutics***

With the growing interest in peptide therapeutics, there has been an increased interest in the use of antimicrobial peptides as potential anti-cancer agents.<sup>111</sup> Application of bacteriocins as anti-cancer therapeutics offers an attractive alternative to the highly toxic chemotherapeutics currently used. Due to being fairly small peptides, they are reasonably non-immunogenic in nature, and they are easily hydrolyzed to individual amino acids.<sup>111,112</sup> Colicins, microcins, pyocins, pediocins and nisin are just a few bacteriocins that have displayed potent activity against cancer cell lines.<sup>111-118</sup> Laboratory studies have shown these peptides display activity against a wide variety of cancer cell lines through differing modes-of-action. The cell surface targets on differing cancer cell lines appear to greatly affect the activity of the different bacteriocins.<sup>119,120</sup> The interactions between bacteriocins and their cellular targets is not well understood and requires further investigation. Despite the overwhelming evidence of effectiveness *in vitro* there are no studies looking at the efficacy of using bacteriocins in cancer patients.<sup>111</sup>

## 1.7 Overview of Projects

From a scientific perspective, much is still unknown about the wide variety of peptides produced by bacteria. Wide-ranging in function, many of these peptides have evolved to optimize bacterial colonization. Some peptides have evolved to have antimicrobial activity against related organisms, providing an evolutionary edge; others have evolved to increase the pathogenicity of the bacteria, further enhancing the bacteria's chance of survival in hostile environments. Certain peptides have been found to have beneficial attributes such as anti-tumor characteristics. Herein, the projects describe structural elucidation of peptide antimicrobials and virulence factors, as well as investigation of structure activity relationships of an anti-tumor peptide. Furthermore, efforts towards the identification of the biological receptor of various antimicrobial and anti-metastatic peptides will be discussed.

Chapter 2 describes the structure elucidation of Enterocin 7B, one component of a two-component, leaderless bacteriocin.<sup>32</sup> As one of the first structures of this class of bacteriocin, determined by NMR spectroscopy, an interesting comparison to circular bacteriocins was discovered.<sup>27</sup> Efforts towards the elucidation of a biological receptor is discussed.

Chapter 3 focuses on the development of a methodology that will allow for the crystallization of small peptides. Using subtilisin A as a sample substrate, this chapter will examine the advantages and disadvantages of using a readily crystallizable peptide to form a co-crystal structure of subtilisin A. The use of co-crystallization is desirable in peptides, when the enantiomer is not readily synthesized. In the case of subtilisin A, the enantiomer is synthetically unavailable due to the presence of three sulfur-to- $\alpha$ -carbon linkages, which are

without synthetic precedent. Specifically, bioconjugation of subtilosin A with streptavidin and carbonic anhydrase will be discussed.

Chapter 4 concentrates on the synthesis, isolation and characterization of phenol-soluble modulins, virulence factors produced by MRSA.<sup>121</sup> As the first time these structures have been reported, their NMR solution structure provides insight into the relationship between their structure and function. A comparison between previous structural models is discussed.<sup>78,121</sup>

Chapter 5 focuses primarily on the synthesis of analogues of the natural neopetrosiamide A and B analogues.<sup>122</sup> The analogues emphasize the importance of key residues within the peptides. Efforts towards the identification of its biological receptor are discussed.

## Chapter Two: Structure Elucidation of Enterocin 7B

### 2.1 Background

Leaderless bacteriocins represent a class of bacteriocins that remains relatively unexplored. With no leader sequence present, and thus no post-translational modifications made to this class of peptides, the genetic simplicity might be attractive in its potential for heterologous expression or synthetic apprehension, and thus its expanded use in the therapeutic or food preservative industry.

#### 2.1.1 Biological Significance of Enterocin 7

*Enterococcus faecalis* 710C was first reported to exhibit broad-spectrum activity against a number of Gram-positive bacteria including the noteworthy MRSA, *L. monocytogenes*, and multiple *Clostridium* spp.<sup>123</sup> The observed antimicrobial activity is traced to the production of two bacteriocins, enterocin 7A and 7B. Due to their synergistic behaviour, these two bacteriocins are part of a synergistic two-component bacteriocin system, though it should be noted that individually the peptides also display antimicrobial activity.<sup>123</sup> Enterocin 7, comprised of an A and B peptide, is produced as a leaderless bacteriocin. Typical of other leaderless bacteriocins, enterocin 7 has formylated N-termini.<sup>21,121</sup> MS/MS sequencing revealed identical amino acid sequences to the already known, enterocin MR10A and MR10B respectively. The A and B component of enterocin 7 were found to have a highly conserved primary structure, with 74% of the amino acids being identical (Figure 6).



water, phosphate buffer, and 50 % TFE, respectively.<sup>125</sup> The extent of the estimated  $\alpha$ -helicity was somewhat unexpected as many small peptides, particularly unmodified small peptides, may remain unstructured until contact with a receptor or membrane is made.

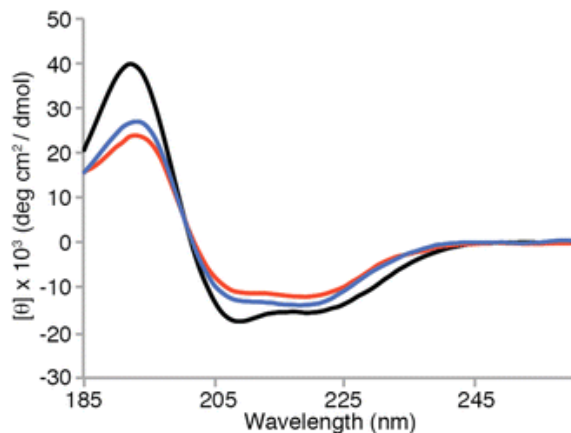


**Figure 7- Circular dichroism data for enterocin 7B. Blue: water; red: phosphate buffer; and black: 50 % trifluoroethanol.**

### **2.2.3 NMR Spectroscopy of Enterocin 7B**

One-dimensional NMR spectroscopy was obtained for enterocin 7B in 10 % D<sub>2</sub>O. Little to no overlap of the amide proton signals indicated a highly structured peptide in aqueous conditions. Other indications of peptide structuring were present, such as the uncharacteristically low hydrogen chemical shifts (e.g., 0.53 ppm, 0.65 ppm and 0.82 ppm), and degenerate signals for many of the  $\beta$ - and  $\gamma$ -protons. Due to the large number of structural indicators in the one-dimensional proton NMR, and poor preliminary experimental results in attempts of double labeling the peptide with <sup>15</sup>N and <sup>13</sup>C, the NMR experiments were carried forward with the naturally produced, unlabeled peptide.

Homonuclear NMR experiments, TOCSY, COSY, and NOESY of the unlabeled peptide and a heteronuclear, natural abundance  $^{15}\text{N}$ -HSQC were conducted. Analysis of the  $^{15}\text{N}$ -HSQC data revealed that there was minimal overlap of signals and in fact, there was no overlap of signals in the amide backbone of enterocin 7B. Similarly there was no overlap of signals in the TOCSY spectrum, allowing for full chemical assignment of the amino acid side chains. Chemical shifts of the amino acid side chains were assigned in accordance with signals observed in the TOCSY and COSY spectra. Amino acids were ordered using the standard pattern of NOESY signals present in  $\alpha$ -helical structures, specifically the NH-NH( $i$ ,  $i+1$ ) and  $\alpha\text{H}$ -NH ( $i$ ,  $i+1$ ) NOESY crosspeaks. The presence of multiple  $\alpha\text{H}$ -NH( $i$ ,  $i+3$ ) NOESY signals is in agreement with the CD analysis of a primarily  $\alpha$ -helical structure.

#### ***2.2.4 Structure Calculation of Enterocin 7B***

The structure of enterocin 7B was determined using the automated structure calculation program, CYANA 2.1.<sup>126</sup> Utilizing the chemical shift assignments along with a peaklist containing all NOESY crosspeaks (majority unassigned), the CYANA program generated 20 lowest energy structures of enterocin 7B (Figure 8). The backbone of the 20 lowest energy structures overlapped well and had an overall root mean square deviation (RMSD) of 0.74 Å. A summary of the structure calculation statistics can be found in Table 1.1.

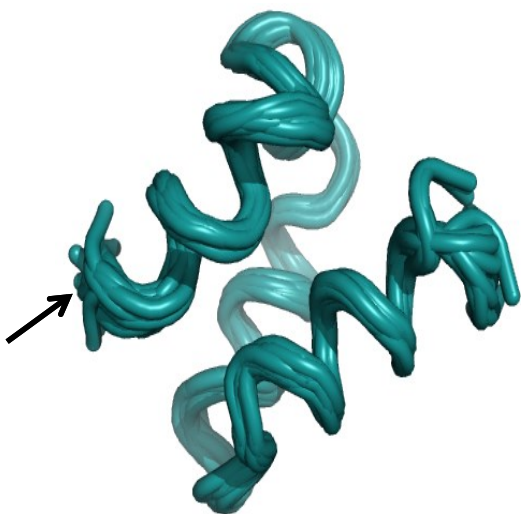


**Figure 8- Overlap of the 20 lowest energy conformers of eneterocin 7B as calculated by CYANA 2.1. N-terminus indicated by arrow.**

**Table 1.1- NMR structure statistic of eneterocin 7B**

	Ent. 7B
Total NOE's	1005
Short ( $ i-j  \leq 1$ )	355
Medium ( $1 <  i-j  \leq 5$ )	173
Long ( $ i-j  \geq 5$ )	107
Average Target Function value	0.64
RMSD for full peptide	
Backbone Atoms (Å)	$0.74 \pm 0.20$
Heavy Atoms (Å)	$1.39 \pm 0.31$

### ***2.2.5 Structural Features of Enterocin 7B***

Enterocin 7B is comprised of three  $\alpha$ -helices, spanning from residues 4-10, 14-29, and 33-43 (Figure 9). The second  $\alpha$ -helix contains a kink at residue 19, where a glycine is located. All  $\alpha$ -helices are amphipathic, creating a hydrophobic core and a hydrophilic outer surface. Within the hydrophobic core there are aromatic residues participating in  $\pi$ -hydrogen interactions, explaining the upfield chemical shift of the  $\beta$ -,  $\gamma$ -, and  $\delta$ -protons for Lys10, Lys18 and Leu40, respectively (Figure 10). The numerous long range NOEs are consistent with a highly compact structure. Multiple NOE signals are observed between residues between all three  $\alpha$ -helices in the structure calculated using the CYANA program.

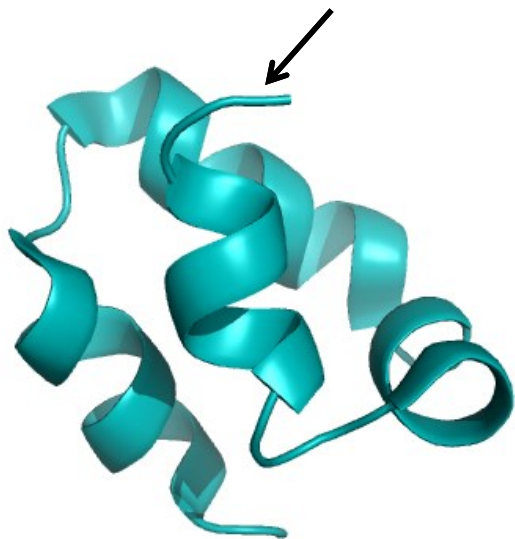


**Figure 9- Ribbon diagram of enterocin 7B showing the saposin-like fold. N-terminus is indicated with an arrow.**

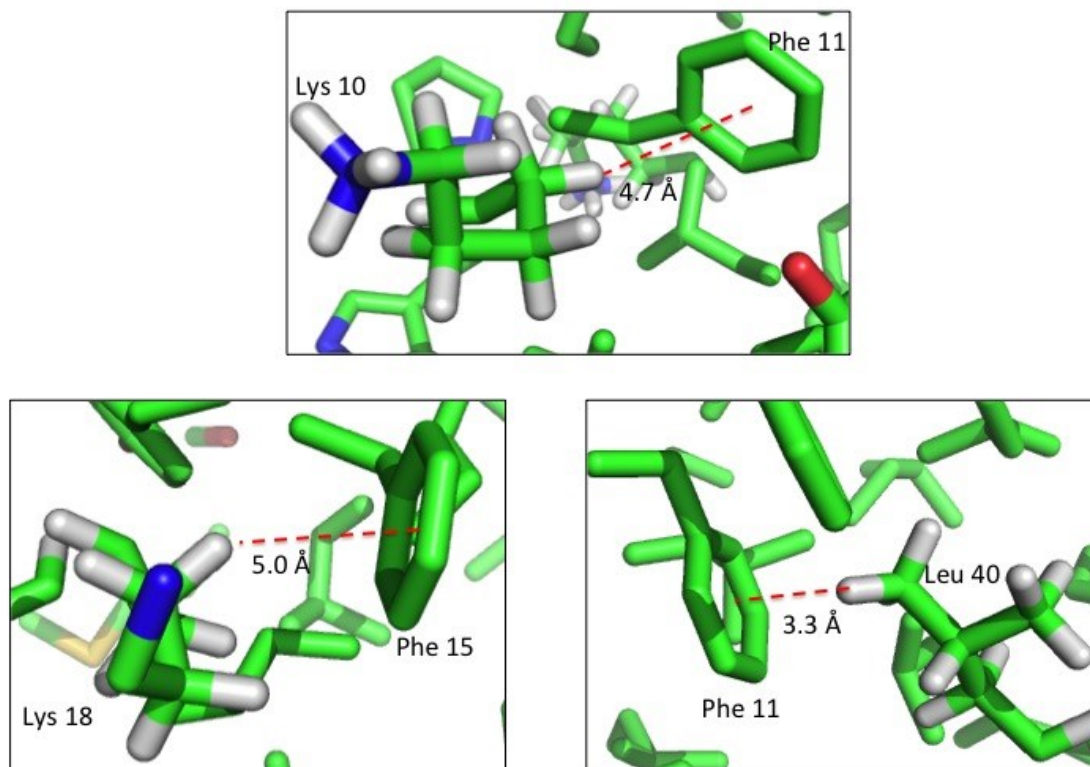


**Figure 10- PyMOL representation of  $\pi$ -hydrogen interactions in enterocin 7B. Amino acid side chains are depicted in green with nitrogen, oxygen, sulfur, and hydrogen shown explicitly in blue, red, yellow, and grey, respectively.**

As expected from the compact structure of the three-amphipathic helices arranged to create a hydrophobic core, the hydrophobic surface map reveals a largely hydrophilic surface. The presence of the hydrophilic surface is consistent with the observation that enterocin 7B is highly soluble in water. Interestingly, one side of the peptide has an extended region of hydrophobicity, however, the exact function of this hydrophobic patch is still not well understood (Figure 11A). The hydrophobic face may initially form a dimeric structure as in the

case with the circular bacteriocin AS-48.<sup>127</sup> Alternatively, the hydrophobic patch may interact with the lipid membrane leading to membrane permeabilization. Additionally, there are solvent exposed aromatic tryptophan residues within this hydrophobic patch. Recent studies have shown that aromatic residues, particularly tryptophan, are responsible for anchoring the peptides in lipid membranes.<sup>42,43</sup> On the opposite face of this peptide there is a smaller hydrophobic patch sandwiched between two hydrophilic regions. Again, the presence of this motif is not well understood. It may be that this hydrophobic patch may be essential for binding to a hydrophobic receptor, though there is no evidence to support this.

Considering the high pI (10.95) of enterocin 7B, it is not surprising that the electrostatic potential surface map reveals a predominately cationic surface of this peptide (Figure 11B). The high number of lysine residues in the sequence of peptide is predominately responsible for this cationic surface. Historically, the cationic surfaces of antimicrobial peptides were proposed to be an important factor in the mode of action of these peptides.<sup>128</sup> A positively charged surface on antimicrobial peptides is believed to draw the peptide toward the anionic phospholipid membrane through electrostatic interactions. This explanation fell short upon the observation that aureocin A53, a highly cationic leaderless bacteriocin, binds more strongly to neutral lipid membranes than anionic lipid membranes.<sup>46</sup> Additionally, whole-genome sequencing was used to compare sensitive wild-type bacterial strains against resistant counter parts. This has led to the discovery that many bacteriocins act in a receptor-dependent mechanism.<sup>29,47-49,129</sup>

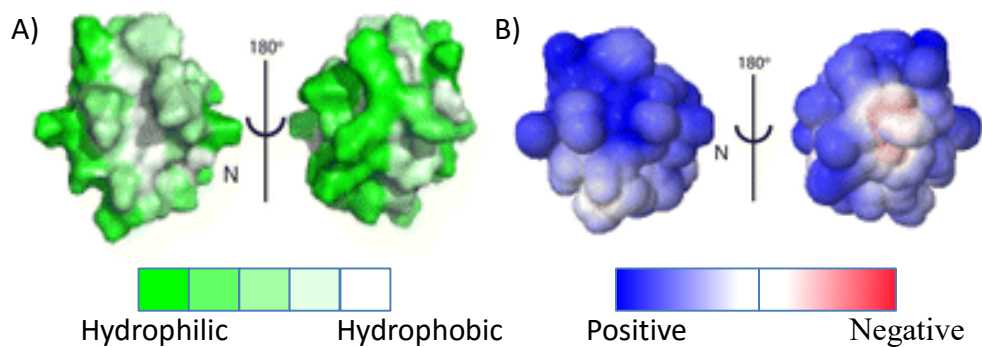


**Figure 11- Surface structure of enterocin 7B depicting A) hydrophobicity, and B) electrostatic potential.**

### ***2.2.6 Comparison of Enterocin 7B to Enterocin 7A***

Former graduate student, Dr. Chris Lohans, solved the structure of enterocin 7A. The structure of enterocin 7A was comparable to that of enterocin 7B (Figure 12). Similar structures were expected due to the high sequence similarity between these two peptides. Both peptides have an overall hydrophilic surface, with one face more hydrophobic than the other face. Each of these peptides are cationic, and enterocin 7A appears to have two slightly larger anionic patches on opposite sides of the peptide due to the anionic residues Glu29 and Asp38.

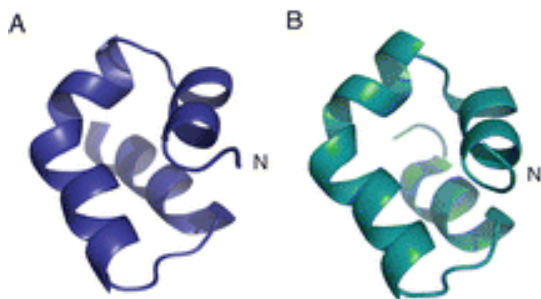


**Figure 12- Side-by-side comparison of enterocin 7A; blue, and enterocin 7B; teal. N-termini are indicated by an ‘N.’**

Enterocin 7A was observed to have a slightly stronger antimicrobial response than enterocin 7B, and when mixed together these peptides had a slight synergistic effect.<sup>130</sup> Interestingly, the synergism observed between these two peptides does not arise from these peptides interacting exclusively with one another as no binding interactions were observed during isothermal calorimetry studies and there were no changes in the chemical shift of the amide protons in the <sup>15</sup>N-HSQC when the peptides were mixed in solution.<sup>32</sup> These results further suggest the presence of a receptor molecule for these bacteriocins.

### ***2.2.7 Comparison of Enterocin 7B to Other Leaderless and Circular Bacteriocins***

A conserved structural motif is identified in a number of leaderless and circular bacteriocins and is also present in enterocin 7B. The similarity between these classes of bacteriocins was first discovered in our lab upon solving the structures of the two enterocin 7 peptides, and was later confirmed in the solution structures of aureocin A53 and lactacin Q.<sup>27,30,32,131</sup> The common structural fold was coined as “the saposin-like” fold, due to its similarity to the fold found in saposin-like peptides (Figure 13).<sup>27,30,32,131</sup> Our group showed that

the saposin-like fold, comprised of three  $\alpha$ -helices, two of which are oriented in a “v-shape” and a third that is nearly perpendicular to the helices participating in the “v-shape,” is conserved in some leaderless and circular bacteriocins.<sup>27</sup> The common fold of the amphipathic helices results in similar features in the hydrophobic surface maps. Namely, the presence of a pocket of hydrophobicity sandwiched between two hydrophilic surfaces and one face of the peptide displaying a larger hydrophobic patch (Figure 14).<sup>27</sup> Speculation about the function of these hydrophobic patches were made above, however, there is no experimental evidence as to whether or not these theories are correct.

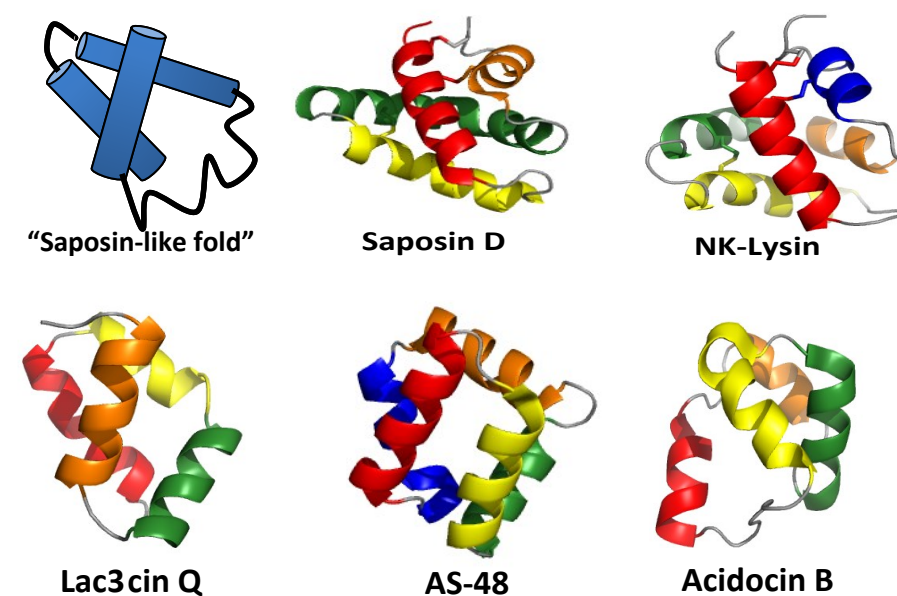


**Figure 13- Various peptides that contain a saposin-like fold. Each distinct helix is colored a different color to exemplify directionality. Starting with the N-terminus, red;  $\alpha$ -helix 1,**

yellow;  $\alpha$ -helix 2, green;  $\alpha$ -helix 3 and orange;  $\alpha$ -helix 4. In the case that there is a 5<sup>th</sup>  $\alpha$ -helix it is colored blue.

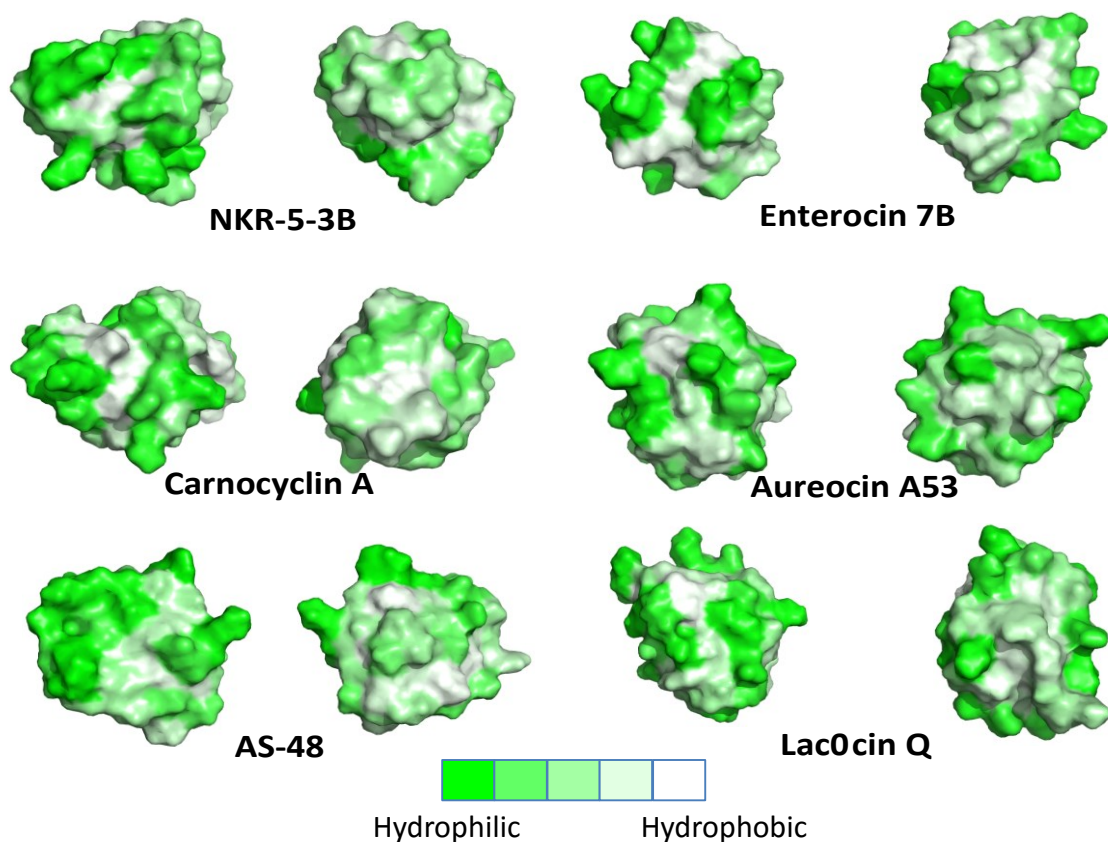


**Figure 14- Hydrophobic surface maps of various circular and leaderless bacteriocins. Common to all of these peptides is a predominately hydrophobic face and on the opposite side, a hydrophobic patch sandwiched between two hydrophilic patches.**

With respect to the mode of action of these peptides, many of these bacteriocins have been extensively studied. All of these bacteriocins share commonalities with the saposin-like peptides, that share the same structural fold.<sup>27</sup> For these peptides, previous work has shown that

many form pores in the cell membrane. Variation exists in the type of pores formed by these peptides. In the case of the leaderless bacteriocin lactacin Q, it has been shown that it forms toroidal pores in cell membranes whereas the circular bacteriocin, carnocyclin A forms anion specific channels.<sup>45,132</sup> Recent studies have shown that the circular bacteriocin, garvacin ML, interacts with a membrane bound maltose ABC transporter to elicit a bactericidal effect.<sup>47</sup> More and more studies are revealing the presence of receptors for a variety of bacteriocins and current theories suggest that the mode of action of bacteriocins may be a combination of initial electrostatic interaction, followed by receptor recognition and hydrophobic insertion and finally membrane permeabilization.<sup>31,47-49</sup>

### ***2.2.8 Efforts Towards the Identification of a Biological Receptor of Enterocin 7***

Whole-genome sequencing has opened the doors to understanding the exact mode of action of antimicrobial peptides (Figure 15). Examination of single nucleotide polymorphisms (SNPs) between the wild-type sensitive bacterial strains and mutant resistant strains of bacteria can provide valuable insight into a potential biological receptor for a specific bacteriocin. Indeed, there have been several studies that have shown that heterologous expression of the wild-type gene, which contained SNPs in the resistant strain, can sensitize bacteria to a specific bacteriocin.<sup>31</sup> This represents a major step forward in our understanding and development of new potential therapeutics.

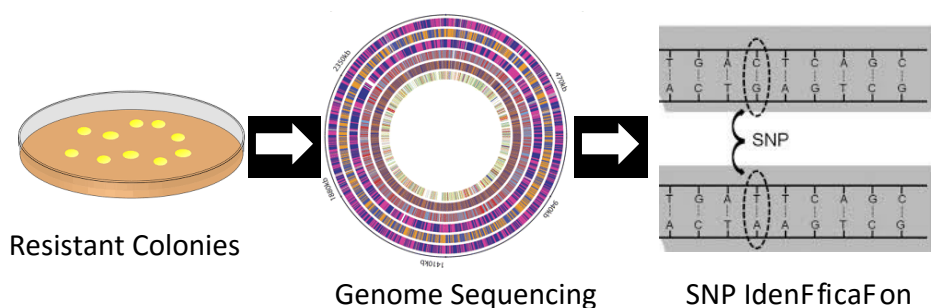


**Figure 15- Pictogram of method used to identify biological receptors through whole-genome sequencing. Resistant colonies are picked, genomic DNA isolated and sequenced. The genomes of the resistant colonies are compared to the genomes of wild-type colonies, sensitive to the bacteriocin of interest, and SNPs are identified.**

There have been several methods reported for the generation of bacterial colonies resistant to antimicrobial of interest.<sup>47-49</sup> In our first attempt at generating mutants, whole-genome sequencing revealed a bacterial contamination was present, leading to isolation of genomic DNA from an undesired bacterial species. Currently, exploration of new methods to produce bacterial mutants of enterocin 7 and carnocyclin A are underway.

### 2.3 Conclusions and Future Work

Two-dimensional NMR spectroscopy was used to characterize the structure of enterocin 7B. The structure of enterocin 7B was solved using CYANA 2.1 programming with distance constraints generated by NOESY signals.<sup>126</sup> Highly structured in water, as determined by circular dichroism, enterocin 7B forms a compact globular peptide containing a saposin-like fold. Three amphipathic  $\alpha$ -helices are arranged to give a hydrophobic core and a mainly hydrophilic surface. Synergism is observed in the spot-on-lawn tests of enterocin 7A and 7B but there seems to be no

physical interaction between the two peptides, as indicated by ITC and  $^{15}\text{N}$ -HSQC.<sup>130</sup> The overall structure bears a resemblance to a large number of other circular and leaderless bacteriocins, such as carnocyclin A. No experimental evidence has been gathered for the mode of action of enterocin 7. It is likely that it has a similar mode of action to the leaderless and circular bacteriocins that share the same structural motif.

Enterocin 7, unlike other small peptides, are highly structured without the use of structure inducing solvents or lipid micelles. Solving the structures of these leaderless bacteriocins represent a tremendous step forward as a previously unknown relationship between circular bacteriocins and leaderless bacteriocins was discovered. This realization has led to the discovery of a larger structural motif common throughout many peptides in nature. The function of this structural motif is still unclear, namely whether or not bacteriocins possessing this fold descend from the same branch of the phylogenetic tree or if nature is simply reusing an energetically favourable fold. Regardless, the similarities that exist in structure and mode of action, not only in bacteriocins but also in saposin-like peptides is quite striking.

Many circular, leaderless and saposin-like peptides are known to form pores. It appears likely that enterocin 7 would have a similar mode of action, however, the nature of pore-formation seems to be dependent on primary structure of the peptides. The differences between the formation of a huge toroidal pore (lactacin Q), and the formation of anion specific channels (carnocyclin A) is dependent on amino acid sequence. Recent studies have shown that many bacteriocins do indeed have a biological receptor.<sup>31,47-49</sup> Receptors have been determined for a number of different classes of bacteriocins. Shorter, leaderless bacteriocins of the LsbB family

bind to the RseP protein. Members of the two-component bacteriocin family, like lactococcin G and enterocin 1071, have been found to exploit the UppP protein where as another two-component bacteriocin, plantaricin J/K, has been found to bind to an amino transferase.<sup>31,48,49</sup> Furthermore, the circular bacteriocin garvicin ML has been found to interact with the maltose ABC transporter.<sup>47</sup> The interaction of these bacteriocins and their receptors is not well understood. For example, despite the high level of homology between in RseP proteins across bacteria, the LsbB family of bacteriocins still seems to be highly specific in the scope of activity against different bacteria.<sup>31</sup> Additionally, enterocin 7, a two-component and leaderless bacteriocin, has a much different structure than either lactococcin G or LsbB. Its structure is more similar to the structure that is proposed for garvicin ML and the implication of this, in terms of receptor recognition, is unknown. Specifically, it is unclear as to whether similar secondary structures translate to similar biological receptors. Perhaps the comparable secondary structure is more important than the similar genetic characteristics and its receptor will be related to the receptor of garvicin ML. Additional experimentation is required to explore the presence of a specific enterocin 7 receptor.

Identification of a receptor could lead to additional studies focusing on conformational changes upon interaction of enterocin 7 with the receptor. Identification of the receptor may even shed light on the synergistic activity between enterocin 7A and enterocin 7B. Additionally, it may be interesting to look at mechanistic studies of enterocin 7A and enterocin 7B individually with lipid membranes, followed by combined mechanistic studies. It would be advantageous to understand the nature of the membrane permeabilization caused by enterocin 7.

## Chapter Three: Subtilosin A

### 3.1 Introduction

#### 3.1.1 Biological Significance of Subtilosin A

Subtilosin A has garnered much attention due to its potent antimicrobial activity against a broad-spectrum of Gram-positive and some Gram-negative bacteria when combined with EDTA treatment.<sup>14,133</sup> Of particular interest are its anti-listerial activity and its application as a spermicidal peptide.<sup>14,134</sup>

#### 3.1.2 Elucidation of NMR Solution Structure of Subtilosin A.

Initial isolation of subtilosin A led to an incomplete amino acid sequence analysis due to the blocked N- and C-termini.<sup>50</sup> It was not until genetic studies identified the structural gene of subtilosin A that a complete and correct amino acid sequence was published.<sup>57,58</sup> The exact nature of the linkages between the sulfur and  $\alpha$ -carbon remained unknown, as did the source of N- and C-terminal blocking.

Early NMR studies proposed a cyclic peptide, where the N- and C-termini were covalently connected via an amide bond and the linkages between cysteine residues 4, 7, and 13 and Phe31, Thr28, Phe22, respectively. These studies were not able to elucidate the nature of the linkages between the cysteine, phenylalanine and threonine residues.<sup>135</sup> The authors hypothesized that the linkages may be sulfur to carbon or sulfur to oxygen linkages.

Concurrently, subtilosin A was isotopically labeled in our lab.<sup>136</sup> In a labeling method developed by our group, subtilosin A was grown in [<sup>13</sup>C, <sup>15</sup>N] labeled peptone, derived from a cyanobacterium, *Anabaena* sp. grown in <sup>13</sup>C labeled sodium bicarbonate and <sup>15</sup>N labeled sodium

nitrate.<sup>136</sup> A suite of three-dimensional, triple-resonance NMR experiments were obtained leading to complete assignment of all proton, carbon, and nitrogen chemical shifts. The chemical shift assignments revealed that there were absent,  $\alpha$ -proton signals on Phe22, Phe31, Thr28.<sup>136</sup> Accompanying the missing proton signals were deshielded  $\alpha$ -carbon signals. A hypothetical cysteine sulfur to  $\alpha$ -carbon linkage was proposed.<sup>136</sup> To confirm this unique modification, a culture of *B. subtilis* JH642 was fermented in the presence of [<sup>13</sup>C, <sup>15</sup>N] threonine and phenylalanine, resulting in subtilisin A, containing <sup>13</sup>C and <sup>15</sup>N labels at these key residues. Investigation of the  $\alpha$ -carbon signals in questions revealed a chemical shift of 10 ppm higher than expected, in agreement with the chemical shifts observed in the fully labeled peptide.<sup>136</sup> Due to the unprecedented nature of the linkage, model compounds (**1-3**) were chemically synthesized to confirm the downfield shift of carbon when attached to sulfur (Figure 16). Finding agreement with the chemical shifts of the model compounds and that of the carbon chemical shift in the labeled peptide, the presence of the thioether linkage between cysteine and the  $\alpha$ -carbons was reported for subtilisin A (**4**) (Figure 17).<sup>136</sup>

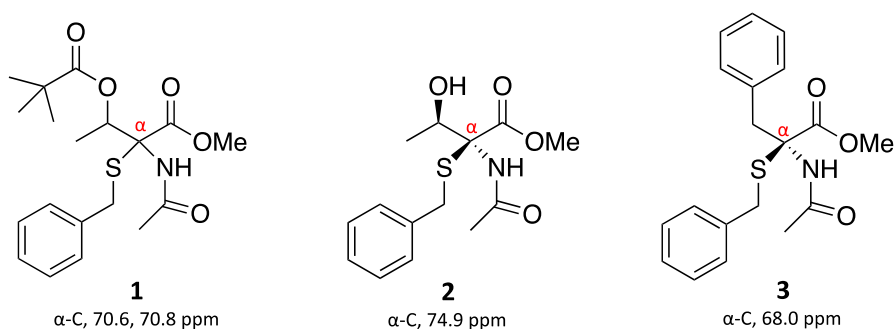


**Figure 16- Compounds synthesized to model the chemical shift effect of an adjacent sulfur to the  $\alpha$ -carbon of phenylalanine or threonine as proposed for subtilisin A.**

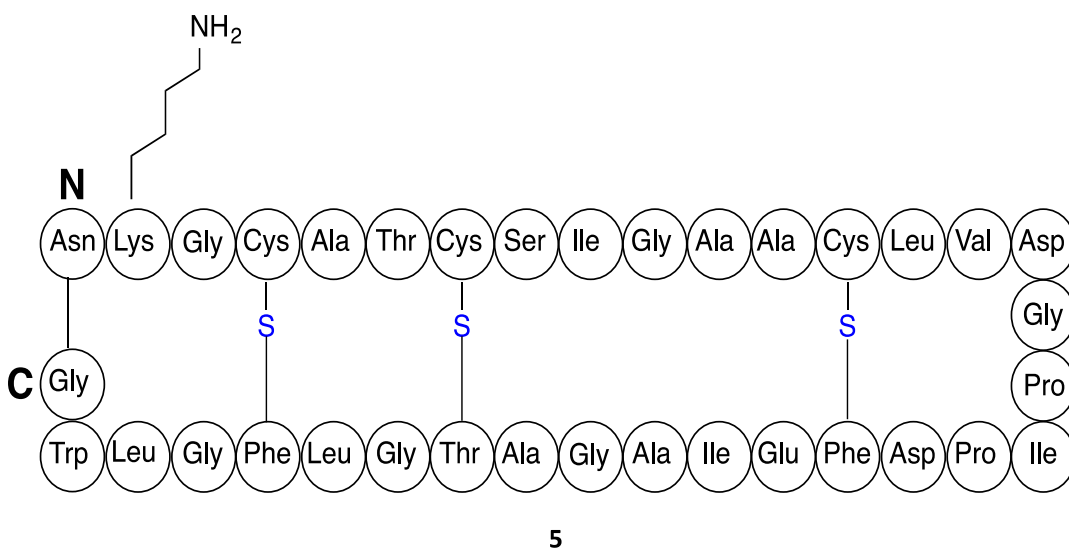


**Figure 17- Complete amino acid sequence of subtilisin A with post-translational modifications.**

Since subtilisin A, there have been additional bacteriocins discovered with this linkage.<sup>51,52</sup> The term, sactibiotics, was coined for this group of bacteriocins. Subtilisin A remains unique within this class of bacteriocins due to the cyclization of the N- and C-termini, which is not found in any other sactibiotic.<sup>63</sup>

The stereochemical nature of each thioether bond was explored next, specifically, the stereochemistry at the quaternary carbon centers formed by the cysteine thiolate adding to the  $\alpha$ -carbon. Nickel borohydride reduction of the thioether bonds and subsequent acid hydrolysis gave individual amino acids, which were subsequently functionalized with pentafluoropropanamide anhydrides to give the corresponding ester.<sup>137</sup> The resulting amino acid esters were analyzed by

chiral GC-MS. However, the stereochemistry of the phenylalanine at position 31 was inconclusive.<sup>124</sup>

Multi-dimensional NMR spectroscopy was used to determine the stereochemical centers of the modified residues in subtilisin A. Specifically, energy minimization calculations were performed for all potential sulfur to  $\alpha$ -carbon isomers.<sup>137</sup> Ultimately, the stereochemistry was proposed to be L-Phe22, D-Thr28 and D-Phe31. This resulting lowest energy isomer is only slightly lower in energy than the all D-isomer (Figure 18).<sup>137</sup> NMR solution structures are reported of other sactibiotics, and the stereochemistry of the modified residues has been determined in a similar manner. The stereochemistry of the cysteine to  $\alpha$ -carbon linkage is varied in other sactibiotics. The calculated lowest energy isomer for thurincin H is the all D-isomer, whereas the LLD-isomer is the calculated lowest energy isomer in the case of the  $\alpha$ -Trn and  $\beta$ -Trn of Thuricin CD.<sup>59,138</sup> Due to the ambiguity in the NMR structure of subtilisin A, it is an attractive target for peptide crystallization to confirm the stereochemistry of the modified residues.

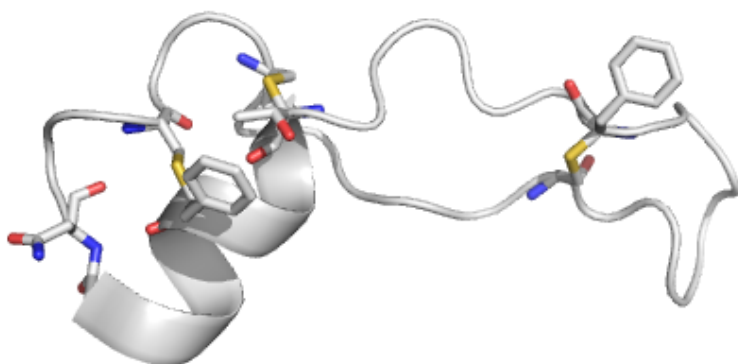


**Figure 18- NMR solution structure of subtilisin A. Residues involved in thioether bridges are shown explicitly. The blue color represent nitrogen; red; oxygen, and yellow; sulfur.**

### ***3.1.3 Potential Approaches to Recrystallization of Small Peptides.***

#### **3.1.3.1 Racemic Mixture**

The recrystallization of small peptides suffers from the inherent disadvantage that chiral substrates have a limited number of space groups in which they can crystallize. Of the 230 space groups observed, only 65 are accessible to chiral molecules.<sup>139</sup> This is due to the fact that the remaining 165 achiral space groups contain symmetry operations, such as mirror planes or centers of inversion, inherently impossible in a chiral molecule.<sup>139</sup> Of the remaining 65 space groups, one specific space group,  $P2_12_12_1$ , is empirically determined to be the most common for proteins and peptides, accounting for nearly 1/3 of the crystal structures known.<sup>139</sup> In fact, approximately 80 % of all protein and peptide crystal structures pack in ten different space groups.<sup>139</sup> Well defined crystals are formed when there is a network of molecules that are arranged in such a way that there are contacts between each molecule. When the network of interactions is sufficiently large, a crystal is formed. The contacts between the molecules can be

arranged in such a way that symmetry exists within the crystal structure. Each space group is a description of specific symmetries present between molecules making up the crystal structure, meaning each space group has restrictions on the orientation of molecules relative to one another within the crystal structure.<sup>139</sup> Not surprisingly, some types of symmetry are harder to achieve than others. The most commonly observed space groups are those that allow molecules to be oriented in numerous ways to achieve the desired symmetry. Mathematically, this phenomenon is described as the rigid body degrees-of-freedom (DOF) or dimensionality.<sup>139</sup> The larger the number of degrees-of-freedom the more readily proteins and peptides will crystallize in a particular space group.<sup>139</sup> When dimensionality is applied to achiral space groups, one specific achiral space group has a predicted DOF greater than any other space group, P1( $\bar{1}$ ).<sup>139</sup> This led scientists to believe that chiral substrates could crystallize more readily if made into an achiral substrate, achievable by making a racemic mixture.<sup>139</sup> Additionally, two more achiral space groups, P2<sub>1</sub>/c and C<sub>2</sub>/c, have the same number of degrees-of-freedom as the most common chiral space group. Extension of the available chiral crystal packing motifs with these three achiral space groups increases the likelihood of recrystallization of proteins and peptides by three-fold, representing a significant step forward in the efforts to make proteins and peptide crystallography a more accessible mode of structure determination.<sup>139</sup>

### **3.1.3.2 Co-crystallization of Proteins and Peptides**

Co-crystallization of proteins and peptides offers one major advantage over racemic crystallization; the enantiomer is not needed.<sup>140</sup> Synthesis of enantiomeric proteins requires substantial amounts of D- amino acids, which is expensive. The synthesis itself poses problems

as the proteins and peptides of interest are large. In addition, some peptides and proteins have post-translational modifications that are synthetically inaccessible, as is the case with subtilisin A. Co-crystallization hinges on connecting a readily crystallizable substrate to a target that is difficult to crystallize. The easily crystallizable substrate will force the target of interest into an ordered conformation that is crystallizable. There is excellent success with this approach.<sup>140</sup> This method typically relies on the presence of an inhibitor that will link the target to the readily crystallizable enzyme. Bioconjugation of a small peptide, such as subtilisin A, to an inhibitor of a readily crystallizable enzyme is an attractive approach to structure determination where the NMR solution structure provided inconclusive results.

#### ***3.1.4 Previous Co-crystallization Attempts with Subtilisin A.***

Two co-crystallization substrates, lysozyme and carbonic anhydrase, were identified as potential partners for subtilisin A crystallization. Lysozyme was one of the earliest enzymes crystallized with two potential inhibitors, N-acetylglucosamine, and chitotriose.<sup>141</sup> Subtilisin A was linked to these inhibitors through by copper-catalyzed click chemistry.<sup>142</sup> Crystallization attempts of this bioconjugate with lysozyme resulted in crystals of lysozyme without the inhibitor-subtilisin A conjugate present.<sup>142</sup> A bioconjugate of carbonic anhydrase and subtilisin A was attempted through inhibition of carbonic anhydrase with a sulfonamide derivative. Linkage of subtilisin A to benzenesulfonamide was achieved through an amide linkage.<sup>142</sup> Subsequent crystallization studies with this conjugate also resulted in carbonic anhydrase crystals with no benzenesulfonamide-subtilisin A inhibitor present.

## **3.2 Results and Discussion**

### ***3.2.1 Isolation of subtilisin A***

Subtilisin A was isolated using a *n*-butanol extraction from the cell supernatant of a culture of *Bacillus subtilis* JH642. Upon concentration of the butanol layer, the residue was resuspended in water and run through a solid phase extraction column (Phenomenex strata). The SPE column was washed with increasing amounts of isopropanol, specifically, 20 %, 40 %, 60%, and 80% IPA with 0.1 % trifluoroacetic acid. Subtilisin A was eluted in the 80 % fraction and further purified to homogeneity by RP-HPLC.

### ***3.2.2 Investigation Into New Co-Crystallization Protein Targets***

Two major factors have hindered our previous attempts at obtaining a co-crystal structure of subtilisin A. First, subtilisin A is highly sensitive to basic pH. Degradation of the peptide occurs at pH > 5. Matrix-assisted laser desorption ionization time-of-flight (MALDI-TOF) mass spectrometry of the degradation product reveals a net increase of +6 in the mass (M+6H). At first glance, the mass increase suggests that the thioether bridges may potentially be broken resulting in free thiols of natural cysteines and reduction of an N-acyl imine. However, there is no structural evidence for this and the exact degradation product is unknown at this time. Second, subtilisin A is highly hydrophobic; the hydrophobicity is problematic in the sense that robotic crystallization screens are usually compatible with aqueous solvents. In addition, many typical co-crystallization proteins are water-soluble. Our intent was that following bioconjugation to a highly water-soluble protein, subtilisin A would become water-soluble also. Due to the failed attempts to bring subtilisin A and its analogues containing co-crystallization linkers into water-

soluble environments in previous studies, strategies to improve the solubility of subtilisin A in water or to explore a linking strategy compatible with organic solvents were investigated.<sup>142</sup>

### **3.2.2.1 Capping Hydrophobic Residues with Cyclodextrins**

Cyclodextrins are cyclic oligosaccharides consisting of 5, 6 or 7  $\alpha$ -D-glucoopyranoside sugars linked in a 1,4 manner, similar to amylose. These ring structures create a cone-like structure that has a hydrophobic core and a hydrophilic outside.<sup>143</sup> Cyclodextrins have found widespread application as drug-delivery agents.<sup>144</sup> Previous studies have demonstrated increased stability of peptides when in the presence of cyclodextrins.<sup>145</sup> Specifically, the hydrophobic cavity may interact with surface-exposed hydrophobic residues, effectively enhancing the solubility of a hydrophobic peptide in aqueous solutions.<sup>143,145</sup> Equimolar amounts of  $\alpha$ -cyclodextrin, and  $\beta$ -cyclodextrin were dissolved in a 1:1 mixture of acetonitrile: water, to which, subtilisin A was added, such that there was 5x excess of the cyclodextrins in relation to subtilisin A. The mixture was stirred overnight and NMR analysis of the aqueous layer indicated that only cyclodextrin was present, suggesting that application of this technique to subtilisin A did not lead to any noticeable increase in peptide solubility (Figure 19).

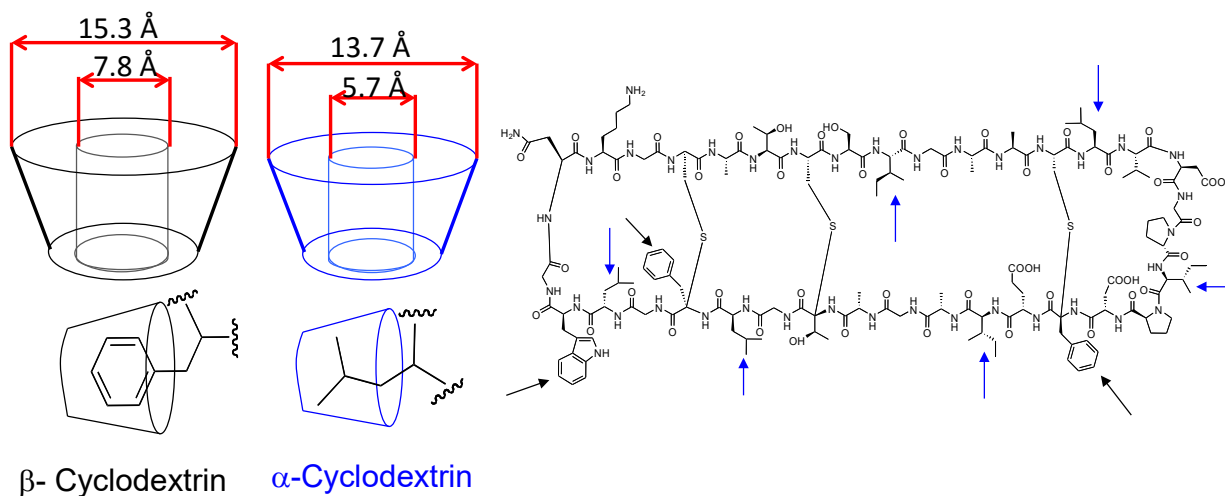


**Figure 19- Cone-like structure of  $\alpha$ - and  $\beta$ - cyclodextrin. The cyclodextrins cap hydrophobic residues like phenylalanine, leucine and isoleucine. Locations that may be capped are indicated with arrows. Blue indicate capping with  $\alpha$ -cyclodextrin and black indicate capping with  $\beta$ -cyclodextrin.**

### 3.2.2.2 Investigation of Streptavidin Stability in Organic Solvents.

Extensive efforts have gone into making subtilisin A more water soluble, none of which have been successful. Rather than continue efforts towards increasing the water solubility of this peptide by linking the peptide to a water-soluble protein, the focus was shifted to investigate proteins that are water soluble, but that maintain their conformational integrity in organic solvents. By finding a protein stable to organic solvents, the linkage reaction between the protein and subtilisin A conjugate could be performed in a single solvent rather than a biphasic mixture, increasing the rate and chance of success. Further restrictions were placed on the prospective

protein; namely, the interaction between the protein and ligand had a strong dissociation constant.

Streptavidin was the first protein to be investigated under this new approach. Various literature sources report that the binding interaction of biotin to streptavidin is unperturbed in organic solvent.<sup>146</sup> However, it was not clear as to whether streptavidin was stable in organic solvents prior to biotin binding. A fluorescent assay was used to assess the stability of streptavidin in organic solvents. Fluorescently labeled streptavidin was dissolved in a variety of organic solvents in the presence of an organic acid or an organic base. The fluorescence of each solution was measured. Each solution was inserted into a well of a 96-well plate coated with biotin. After incubation, the solution was removed from the 96-well plate, and the fluorescence is measured for the second time. Low fluorescence is indicative of an intact biotin binding pocket, and therefore the fluorescently labeled streptavidin is removed from the solution and bound to the 96-well plate. Solvents that disrupted the structure of streptavidin exhibited high fluorescence signals after incubation, indicating that the binding pocket was no longer able to bind biotin.

At the lowest pH, *t*-BuOH, EtOH, and MeOH all maintained high levels of fluorescence after incubation with a biotin coated 96-well plate, indicating that the fluorescein labelled streptavidin did not bind to biotin and removed from the solution. In contrast, DMSO, MeCN, and *i*-PrOH all displayed lower fluorescence after incubation with the biotin coated plate signifying removal of the fluorescently labelled streptavidin through binding with biotin. At a pH of 5, *i*-PrOH showed the most pronounced difference in fluorescence, followed by MeCN and EtOH. In this assay, *t*-BuOH, MeOH and DMSO all displayed relatively similar levels of

fluorescence before and after exposure to the biotin coated 96-well plate. In the least acidic solutions tested, pH = 7.5, all solvents had a favourable trend of lowered fluorescence after exposure with the biotin coated plate. The extent of the decrease in fluorescence was not the same however, and the most pronounced effect was observed with DMSO and MeCN. The commercially available source of streptavidin is a lyophilized powder from 10 mM phosphate buffer. Upon dissolving the streptavidin, the pH of the solution is 7.8 and for this reason, solvent selection was restricted to the solvents run at pH 7.5. DMSO and MeCN were the only two solvents in which the fluorescently labelled streptavidin had moderate to high fluorescence before exposure to biotin and close to no observed fluorescence after exposure to biotin. Of these, MeCN has a much lower boiling point in comparison to DMSO, theoretically making removal of the solvent more facile. Acetonitrile was found to be an acceptable organic solvent to dissolve subtilisin A while maintaining the structural integrity of streptavidin (Figure 20).

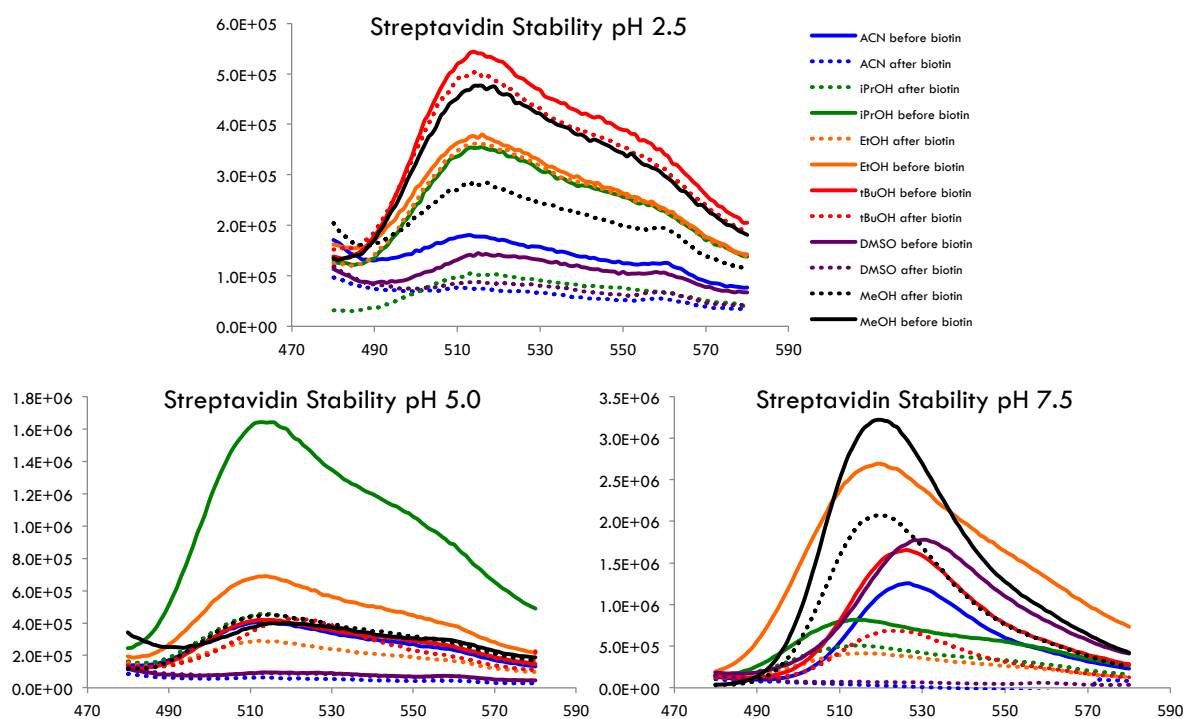


**Figure 20- Graphical representation of fluorescence intensity of streptavidin in various organic solvents. Solid lines represent fluorescence of streptavidin solution prior to incubation with biotin. Dashed lines represent fluorescence of streptavidin solution after incubation with biotin-coated 96-well plate.**

A single lysine at position 2 of subtilisin A provides a convenient handle for synthetic modification of the peptide. Linkage of biotin to subtilisin A is achieved through an amide bond between the aforementioned lysine and an activated ester of biotin. Subtilisin A was dissolved in a mixture of 50% acetonitrile: phosphate buffered saline solution. Importantly, degradation of subtilisin A at pH=7-8 could be slowed and even eliminated using an aqueous solution containing high salt concentrations. To the solution of subtilisin A, the *N*-hydroxysuccinimide

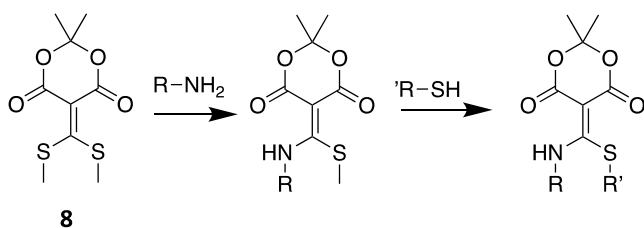


Crystallization attempts of the subtilisin A-biotin-streptavidin complex resulted in small crystals that were determined to be phosphate buffer. Buffer exchange into water did not lead to any crystals of a desirable size or shape. Even though the biotin-streptavidin interaction is among the strongest non-covalent bonds known ( $k_d=10^{-15}$ ), the presence of subtilisin A conjugated to biotin may disrupt the ligand-protein interaction thereby decreasing the dissociation constant. This was somewhat unexpected for the interaction of the subtilisin A-biotin-streptavidin conjugate due to the strong binding constant recorded for the biotin-streptavidin interaction. When bound, the biotin-streptavidin interaction is reportedly as strong as a covalent bond. It has been demonstrated that a loop on streptavidin undergoes a conformational change from open to closed upon binding of biotin.<sup>150</sup> It is the loop which forms a 'lid' on the binding pocket of streptavidin and may account for the exceptionally strong binding constant for this interaction.<sup>150</sup> It may be that attaching subtilisin A to biotin disrupts the ability of the loop to close, making the interaction of biotin-streptavidin weaker when subtilisin A is attached.

### **3.2.2.3 Linking Subtilisin A Through a Covalent Bond to a Readily Crystallizable Protein.**

The combined work of Dr. Fan and myself resulted in either a lack of crystals or the presence of crystals of the readily crystallizable protein without the desired subtilisin A linked ligand. This suggests that the non-covalent interaction between the ligand and its receptor may not be strong enough to promote solubility of with this highly hydrophobic bacteriocin in water, and thus co-crystallization attempts in aqueous solvents are unsuccessful. For this reason, our efforts turned towards a crystallization strategy involving the covalent linkage of subtilisin A to a readily crystallizable protein.

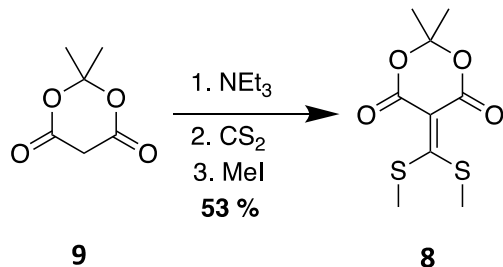
Click chemistry, a term that refers to reactions that are high yielding, have a broad substrate scope, are bioorthogonal, and create byproducts that are easily removable, has been used widely in bioconjugate chemistry. Traditionally introduced as the reaction between alkynes and azides, many more types of reactions have been developed as click reactions.<sup>151</sup> Recently, amine-containing peptides have been “clicked” to thiol-containing peptides in a reversible click reaction involving a derivative of Meldrum's acid (**8**) (Scheme 2).<sup>151</sup>



**Scheme 2- Synthetic scheme of "click" chemistry between an amine and a thiol using a Meldrum's acid derivative.**

Application of this methodology towards the efforts of crystallization of subtilisin A suffers from one main restriction with respect to substrate selection. The desired partner protein for subtilisin A requires that only one surface exposed cysteine is present. Multiple cysteine residues would lead to a mixture of conjugate products with one or more subtilisin molecules linked creating inhomogeneity in the crystallization sample, hindering crystallization attempts.

Synthesis of the Meldrum's acid derivative was performed in accordance to literature procedure.<sup>151,152</sup> An enolate was formed by deprotonating Meldrum's acid (**9**) with triethylamine. Following an enolate addition of carbon disulfide to the deprotonated **9**, an SN<sub>2</sub> with methyl iodide affords compound **8** in a 53 % yield (Scheme 3).



**Scheme 3- Synthesis of Meldrum's acid derivative.**

Attempts to link subtilisin A to compound **8** through an aza 1,4 Michael addition in buffered solution containing carbonic anhydrase were ineffective. Subtilisin A (**4**), compound **8**, and carbonic anhydrase were dissolved in a 50 % acetonitrile: phosphate buffered saline solution (PBS). The mixture is stirred for 72 h with continuous argon bubbling. Reaction progress is monitored with MALDI-TOF spectroscopy and RP-HPLC. After 72 h no reaction had taken place as there was no change in the mass of subtilisin A and no shift in retention time of the peak due to subtilisin A in the RP-HPLC. A more detailed inspection of the structure of carbonic anhydrase suggests that a linker may be necessary to connect subtilisin A with carbonic anhydrase using compound **8** (Figure 21).

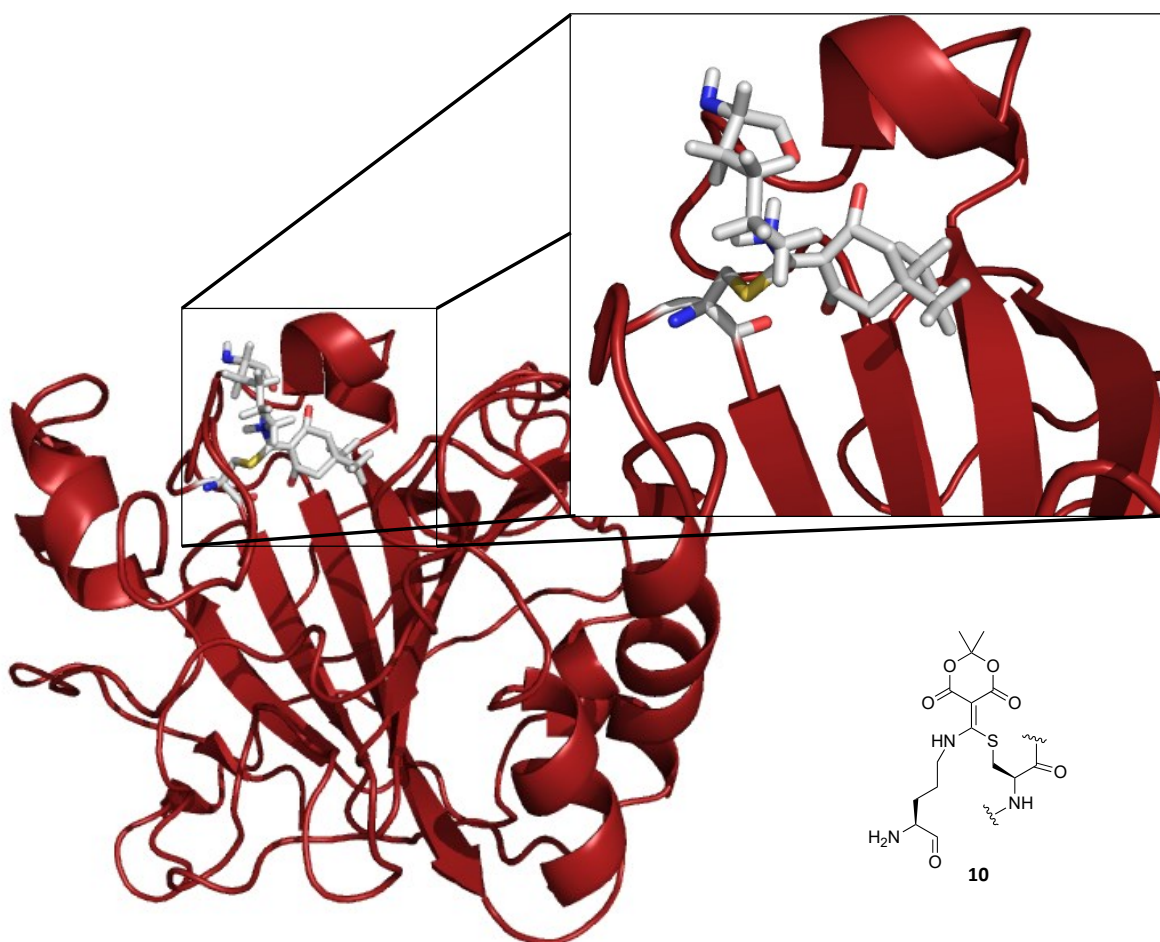


**Figure 21- Crystal structure of carbonic anhydrase. A model compound is docked depicting the orientation of the lysine side chain in subtilisin A with the Meldrum's acid derivative (8) covalently linked to the cysteine side chain in carbonic anhydrase.**

A theoretical, model compound was docked into the crystal structure of carbonic anhydrase to depict the linkage between the lysine side chain of subtilisin A, the Meldrum's acid derivative, and the cysteine side chain of carbonic anhydrase. From this docked structure, it is apparent that the full subtilisin A peptide backbone is too bulky to allow for linkage between itself and carbonic anhydrase by the synthesized Meldrum's acid derivative. A linker was

designed to circumvent the predicted steric hindrance of linking subtilisin A to carbonic anhydrase through compound **8**. Using molecular modeling, it was determined that a carbon chain of 5 carbons would be sufficiently long to alleviate the detrimental steric hindrance that presumably impedes subtilisin A from binding to carbonic anhydrase (Figure 22).

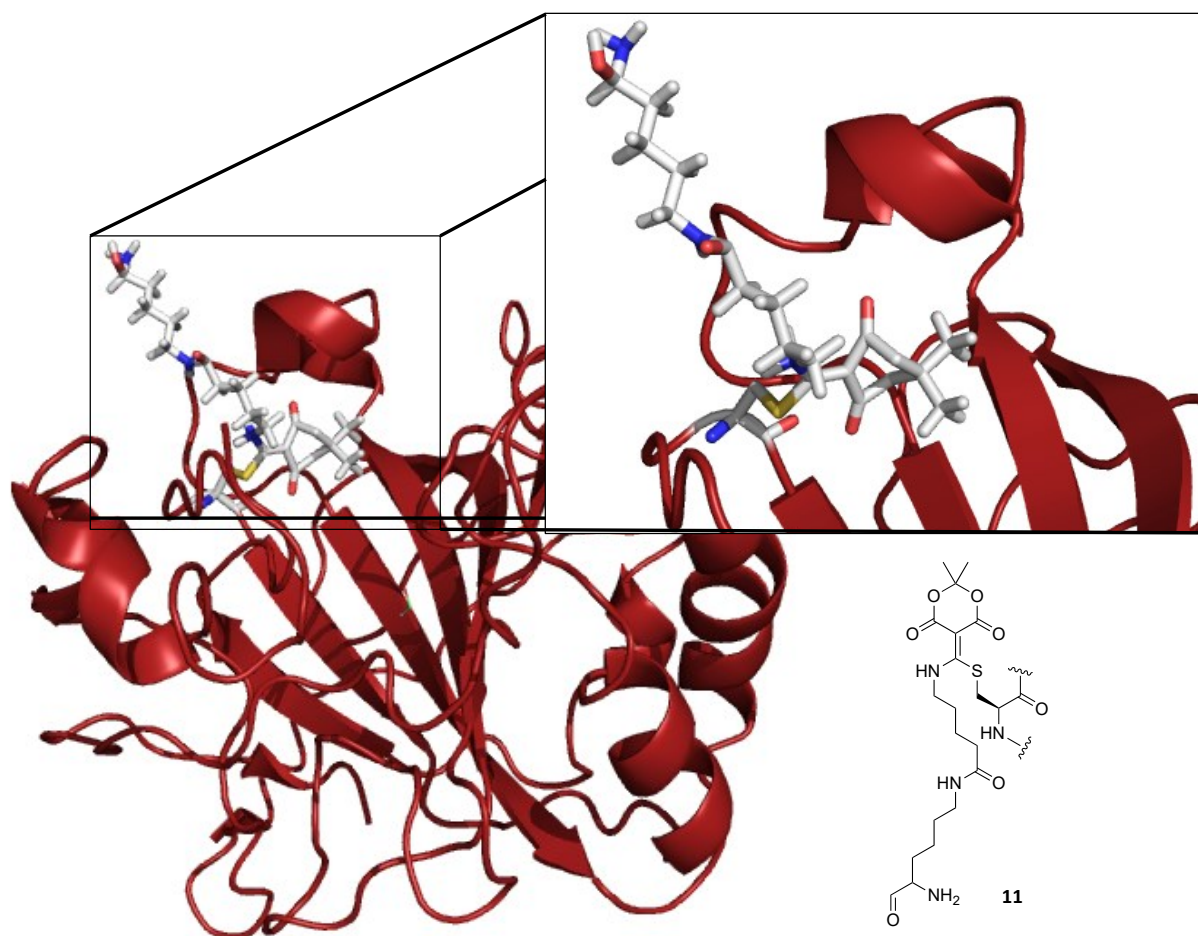
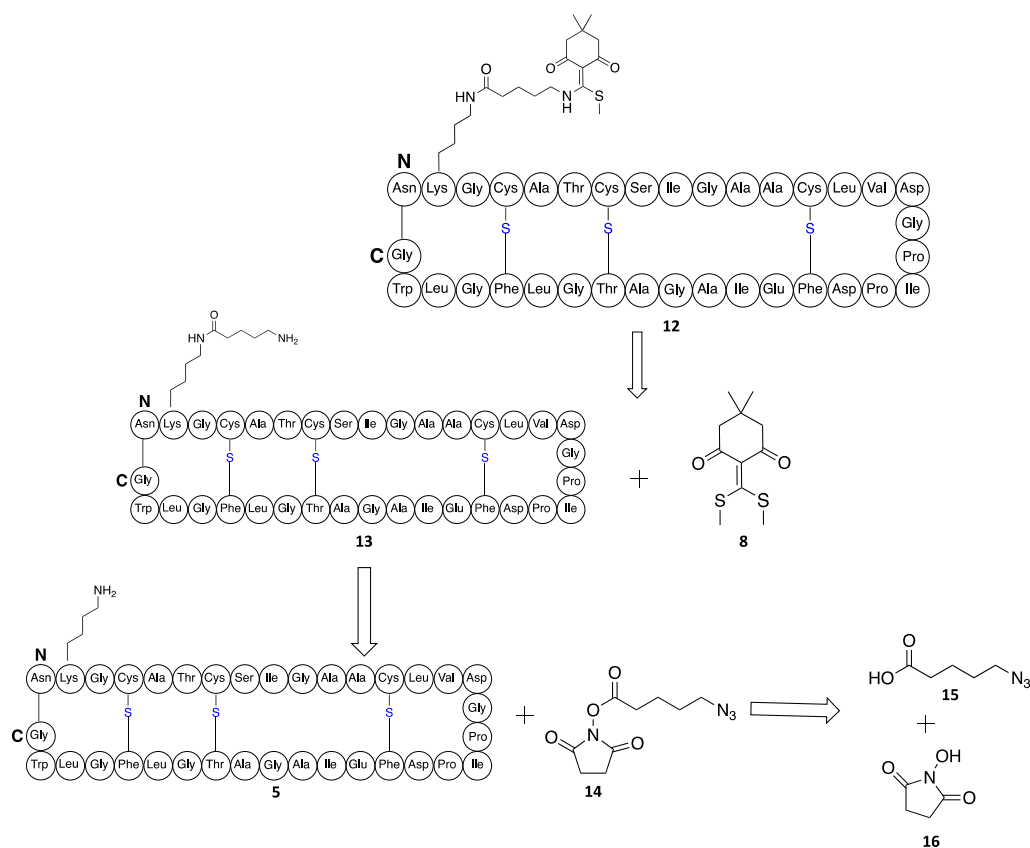


**Figure 22-** Crystal structure of carbonic anhydrase with a model ligand, compound **11**, attached to a representative lysine residue and the cysteine residue on carbonic anhydrase.

To circumvent the steric hindrance, a strategy to incorporate a linker between subtilisin A and compound **8** was adopted (Scheme 3). The retrosynthetic analysis was as follows: subtilisin A, functionalized with a five carbon linker and the Meldrum's acid derivative (**8**), can be obtained from the click reaction of subtilisin A derivatized with an extra five carbons at the lysine (**13**) and compound **8**. Compound **13** is made from subtilisin A (**4**) and an NHS-ester of the desired linker (**14**). Synthesis of the NHS-ester (**14**) is achieved through a coupling reaction between azidopentanoic acid (**15**) and *N*-hydroxysuccinamide (**16**). To prevent homodimerization of the pentanoic linker during the synthesis of the NHS-ester between the carboxylic acid and *N*-hydroxysuccinamide, the free amine is protected as an azide, which can later be removed using a TCEP reduction.

*N,N'*-Dicyclohexylcarbodiimide was used to activate the azidopentanoic acid and facilitate the formation of the NHS-ester. Upon coupling, the resultant compound (**14**) is dissolved in minimal DMSO and added to a solution of 50 % acetonitrile: PBS (pH 7.5, 0.2 M) containing subtilisin A. No conjugation was observed between subtilisin A and compound **14**.

In attempt to force the reaction forward 10 % NaOH was added to ensure the lysine of subtilisin A was nucleophilic enough to add to the NHS-ester of compound **14**. No functionalization of the subtilisin A is observed and the MALDI-TOF spectrum indicates a mass increase of +6, indicative of the degraded subtilisin A.



**Scheme 4-Retrosynthetic analysis of subtilisin A derivative containing a five-carbon linker bound to the Meldrum's acid derivative able to undergo a 'click' reaction with a free thiol on a cysteine side chain.**

### 3.3 Discussion and Conclusions

Subtilisin A was successfully linked to biotin through an amide bond. Importantly, degradation of subtilisin A was found to be minimized in the presence of a high concentrations of salt, specifically phosphate buffered saline solutions inhibited the degradation of subtilisin A over the course of 48 h at pH= 7. The biotin linked subtilisin A was successfully incorporated

into a solution of streptavidin, though the exact number of biotins bound to a single streptavidin molecule could not be assessed due to degradation during ionization methods of mass spectrometry. A crude, native gel revealed a shift from the natural streptavidin and the streptavidin bound to a biotin-subtilosin A conjugate. Purification of this complex revealed that streptavidin was unstable under HPLC conditions and therefore spin filtration with Amicon tubes were applied to purify this reaction. The absence of successful crystallization conditions suggests that the streptavidin-biotin-subtilosin A complex was unable to pack in a favourable, repeatable way. This could be due to a number of factors including inhomogenous sample (variable number of biotin-subtilosin A molecules for every molecule of streptavidin), the network of streptavidin molecules could have been interrupted by attaching bulky subtilosin A molecules, and unfavourable crystallization conditions. Linkage of subtilosin A to carbonic anhydrase through the use of a small molecule linker proved to be unsuccessful. Investigation of the surface structure of carbonic anhydrase and subtilosin suggests that steric hindrance may be the culprit of preventing linkage. To overcome steric hindrance, a linking strategy was adopted to allow for additional space between subtilosin A and carbonic anhydrase. This approach is currently in progress.

Efforts towards the crystallization of subtilosin A have, thus far, been unsuccessful. Important realizations have been uncovered, providing insight towards future attempts of crystallization. Solubility, stability, and strength of non-covalent interactions appear to be the major hurdles encountered in linking subtilosin A to a crystallizable protein partner.

New approaches may be needed to gain a crystal structure of subtilisin A. Recognizing that the non-covalent interactions between the crystallization partners and the ligands linked to subtilisin A may not be strong enough, efforts to create a covalent bond between the ligand and protein of interest are being pursued. Lysozyme is still considered to be an attractive crystallization partner due to its propensity to form well-ordered crystals. Previous studies show that lysozyme's enzymatic activity can be inhibited with chitotriose and chitobiose.<sup>141</sup> It is possible that activation of these molecules with biologically reactive functional group, like an epoxide, could afford a covalent linkage between lysozyme and the ligand-subtilisin A conjugate. Irreversible inhibitors of lysozyme have been extensively studied, and many inhibition methodologies have been developed. Sugars containing a diazirine ring have been shown to be only modest inhibitors of lysozyme though they strongly resemble natural lysozyme substrates.<sup>148</sup> Further exploration of photoaffinity tags has had greater success using photoaffinity tag that resembles the transition state rather than the substrate.<sup>153</sup> These irreversible inhibitors would be difficult to synthesize with subtilisin A attached due to the instability of chemical reaction conditions needed to synthesize the inhibitors. A more attractive approach would be the use of an epoxide containing substrate. Previous work has shown that 2',3', epoxypropyl  $\beta$ -glycosides are irreversible inhibitors of lysozyme and these inhibitors could be modified to allow for attachment of subtilisin A.<sup>141,153</sup>

The synthetic challenges of working with subtilisin A presents a major hurdle in the attachment of subtilisin A to a crystallizable protein. A more biological approach could be envisioned using a fusion protein. Heterologous expression of a gene encoding for lysozyme

fused to the propeptide of subtilisin A could be a novel strategy to access this peptides crystal structure. The major drawback of this technique is the number of post-translational modifications that are required to convert the propeptide into subtilisin A. As discussed in the introduction, the gene cluster of subtilisin A is not well understood. AlbA has been found to catalyze the thioether bond formation, but it is still unclear the exact function of AlbBCDEFG. Previous work has suggested that formation of the thioether bonds by AlbA requires recognition of the leader sequence and is the probable first step in a series of post-translational modifications.<sup>24</sup> Theoretically, expression of a lysozyme fusion to the subtilisin A propeptide could lead to a substrate in which recombinant AlbA could form the thioether bonds. What is unclear in this methodology is whether the lysozyme and poly-gly linker would interfere with the recognition of the leader sequence by AlbA.

A second biological approach to the crystallization of subtilisin A is to crystallize the peptide in the presence of its receptor. It is common for small peptides to become more structured upon binding to its biological substrate. Identification of the receptor of subtilisin A is now possible using the aforementioned whole-genome sequencing techniques. It is likely that the subtilisin A receptor is a membrane bound protein or a membrane bound lipid as in the case of class II bacteriocins and lantibiotics respectively. If this is the case, this method would require the crystallization of membrane proteins or membrane lipids. Crystallization of these types of complexes would present significant challenges of their own. It is worth noting that the complex of subtilisin A to its biological receptor may be a suitable candidate for NMR studies. This complex of peptide and receptor may provide structural rigidity, resulting in less ambiguous

NMR data and affording concrete evidence of the stereochemistry of the thioether bridges present in subtilisin A.

Multiple approaches are being pursued in the effort to obtain a crystal structure of subtilisin A. Continued studies are needed to explore further methods which are amenable to the sensitive peptide, subtilisin A.

## **Chapter Four: Phenol-soluble Modulins.**

### **4.1 Introduction**

#### ***4.1.1 Biological Significance***

Phenol-soluble modulins are peptide virulence factors produced by staphylococci. These peptides elicit multiple immune responses from the host cell, contributing to the overall pathogenicity of these bacteria. The  $\beta$ -type PSMs are important in biofilm formation and detachment, whereas, the  $\alpha$ -type PSMs are cytolytic. Some  $\alpha$ -type PSMs are able to lyse important eukaryotic cells like erythrocytes, leukocytes, and neutrophils. Understanding the structure of these virulence factors will enable further structural studies, leading to a greater understanding of their biological impacts.

### **4.2 Results and Discussion**

#### ***4.2.1 Synthesis and Isolation of Phenol-soluble Modulins.***

PSM $\alpha$ 1, PSM $\alpha$ 3, and PSM $\beta$ 2 from *S. aureus* are virulence factors that are 21, 22, and 44 amino acids long, respectively. Solid phase peptide synthesis (SPPS) was used to synthesize PSM $\alpha$ 1 and PSM $\alpha$ 3. Briefly, each peptide was made on a Wang resin, at a 0.1 mmol scale. Deprotection of the amine-protecting group, fluorenylmethyloxycarbonyl (Fmoc), was achieved using a 20 % piperidine solution in DMF. Incoming amino acids were preactivated in a solution of DMF containing diisopropylethylamine (DIPEA) and 1-[bis(dimethylamino)methylene]-1*H*-1,2,3-triazolo[4,5-*b*]pyridinium 3-oxide hexafluorophosphate (HATU). As the peptide chain was extended on resin, the subsequent deprotections became less effective and the last 5 or 6 residues

were deprotected using a solution of 20 % piperidine in the magic mixture (1 % triton X-100 in a 1:1:1 DMF/NMP/DCM mixture at 60 °C) for PSM $\alpha$ 1 and PSM $\alpha$ 3, respectively.<sup>154</sup> Each peptide was cleaved from the resin using a mixture of 95:3:2 trifluoroacetic acid: water: triisopropyl silane and purified using a combination of dialysis and RP-HPLC. Yields of 0.88 mg and 0.99 mg were obtained for PSM $\alpha$ 1 and PSM $\alpha$ 3, respectively. Attempts to synthesize PSM $\beta$ 2 through the use of Fmoc-SPPS were unsuccessful. Briefly, despite using many different coupling reagents, along with elevated temperatures and microwave heat, the coupling efficiency of residues was quite low. This was thought to be due to agglomerations of hydrophobic residues during the synthesis. Insertion of pseudoproline at positions 19 and 25 was unsuccessful in reducing the agglomerations. Similarly, increased temperatures, the addition of chaotropic salts, and detergents were ineffective in reducing the agglomerations, and for this reason, a biological approach to the isolation of phenol-soluble modulin  $\beta$ 2 was adopted.

#### ***4.2.2 Heterologous Expression and Isolation of SUMO-PSM $\beta$ 2 Fusion Protein***

PSM $\beta$ 2 was overexpressed in *E. coli* BL21(DE3) as a His-tagged SUMO fusion protein and partially purified using Ni-NTA chromatography. The desired peptide was obtained by treatment of the fusion protein with SUMO protease. A second Ni-NTA column and RP-HPLC was used to purify the desired peptide from the SUMO protein and protease. Yields of 2–2.5 mg/L were obtained for PSM $\beta$ 2. Consistent with the natural peptides from *S. aureus*, the chemically synthesized PSM $\alpha$ 1 and PSM $\alpha$ 3 contained an N-terminal formylmethionine residue. PSM $\beta$ 2, produced through heterologous expression in *E. coli*, did not contain the

formylmethionine. While the formylmethionine may be important for the interaction of PSMs with some FPRs, it has also been shown that FPR2 also recognizes the unformylated PSMs.<sup>155</sup>

#### ***4.2.3 Circular Dichroism of Phenol-soluble Modulins.***

All three of these peptides were found to be insoluble in water and only sparingly soluble in 25 % d<sub>3</sub>-trifluoroethanol (TFE) in water. They were, however, soluble in 50% d<sub>3</sub>-TFE: water; hence, their solution structures in this solvent system were analyzed using CD spectroscopy. At room temperature, PSM $\alpha$ 1, PSM $\alpha$ 3, and PSM $\beta$ 2 were calculated to have moderate levels of  $\alpha$ -helicity (25.8, 37.5, and 22.2 %, respectively) in this structure-inducing solvent. Interestingly, while temperature seemed to have an effect on amide dispersion in the one-dimensional proton NMR, discussed below, the temperature did not greatly affect the level of  $\alpha$ -helicity observed in the CD (Figure). In PSM $\alpha$ 3 and PSM $\beta$ 2, the calculated percent  $\alpha$ -helicity was 39.5 % at 25 °C vs. 37.5 % at 37 °C and 25.9 % at 25 °C vs. 22.2 % at 40 °C, respectively. The amide region of the NMR spectra of PSM $\alpha$ 1 appeared to have sufficient separation of proton signals at 25 °C, but elevated temperatures (37 °C and 40 °C) were required to obtain sufficient separation of amide peaks for PSM $\alpha$ 3 and PSM $\beta$ 2, respectively.

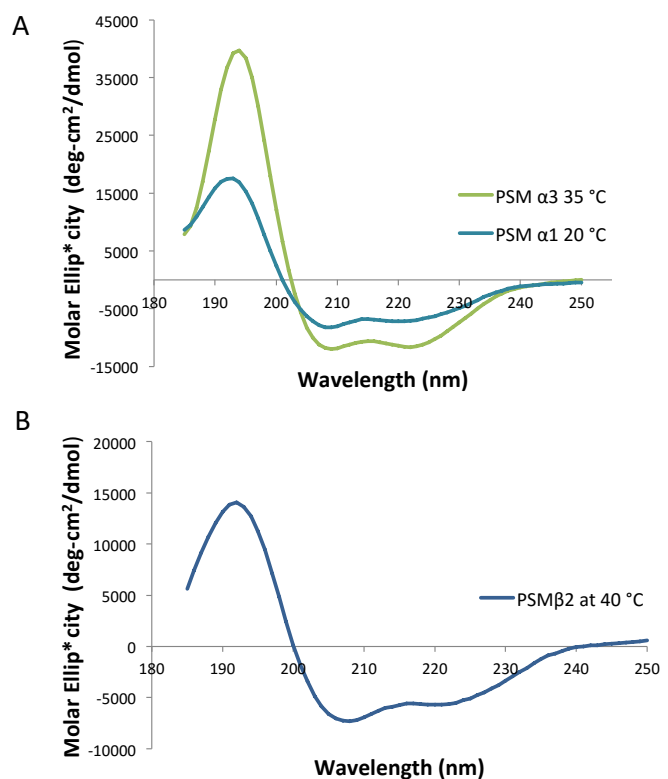


**Figure 23- CD spectra of A) PSM $\alpha$ 1 and PSM $\alpha$ 3 and B) PSM $\beta$ 2. Spectra were acquired in 50 % trifluoroethanol at 25, 37, and 40 °C, respectively.**

#### **4.2.4 PSM NMR Spectroscopy**

One-dimensional proton NMR studies of PSMs  $\alpha$ 1,  $\alpha$ 3 and  $\beta$ 2 revealed the peptides had a good dispersion of amide protons. Temperature scanning revealed greater dispersion of amide protons for PSM $\alpha$ 3 and PSM $\beta$ 2 at 37 °C and 40 °C, respectively. Analysis of the one-dimensional <sup>1</sup>H-NMR spectra indicated that the majority of side chain proton signals could be assigned without labeling the peptides. Subsequently, TOCSY and NOESY spectra were acquired for all three peptides at the aforementioned temperatures.

Evaluation of the TOCSY spectrum of PSM $\alpha$ 1 revealed no overlap between the signals of each spin system. The majority of spin systems in PSM $\alpha$ 3 had distinct signals, with only a few spin systems being indistinguishable due to spectral overlap. PSM $\beta$ 2 showed significantly more spectral overlap, which was not unexpected due to its length and its lower propensity to adopt  $\alpha$ -helicity as displayed by the circular dichroism spectrum. Chemical shift assignments of the side chain protons were made for all three peptides using the TOCSY spectrum. In the case of PSM $\alpha$ 1 and PSM $\alpha$ 3, the majority of protons were assigned. In the case of PSM $\beta$ 2, not all the protons could be assigned with the TOCSY spectra, with a complete assignment of approximately 75 %. In each peptide, the NOESY was used to order the amino acid residues from the C- to N-termini. Specifically, the signals common to  $\alpha$ - helices, NH-NH (i, i+1) and  $\alpha$ H-NH (i, i+3), were used to place the amino acids in order from the C- to N-termini.

#### ***4.2.5 Structure Calculation of PSM $\alpha$ 1, PSM $\alpha$ 3 and PSM $\beta$ 2***

Automated structure calculation of phenol-soluble modulin  $\alpha$ 1,  $\alpha$ 3 and  $\beta$ 2 was performed using CYANA 2.1.<sup>126</sup> NOE crosspeaks provided distance constraints, and the chemical shift assignments provided the basis for the CYANA calculation. The 20 lowest energy structures were generated in which the backbone overlap between the structures gave an overall RMSD of 0.77 Å, 0.64 Å and 0.80 Å for PSM  $\alpha$ 1,  $\alpha$ 3 and  $\beta$ 2, respectively. Complete structural statistics for PSM $\alpha$ 1, PSM $\alpha$ 3, and PSM $\beta$ 2 can be found in Table 2.1.

**Table 2.1-Summary of NMR Solution Structure Calculations of PSM $\alpha$ 1, PSM $\alpha$ 3, and PSM $\beta$ 2**

	<b>PSM<math>\alpha</math>1</b>	<b>PSM<math>\alpha</math>3</b>	<b>PSM<math>\beta</math>2</b>
total no. of NOE peak assignments	636	553	1320
short-range ( $ i - j  \leq 1$ )	538	452	1040
medium-range ( $1 <  i - j  < 5$ )	99	101	246
long-range ( $ i - j  \geq 5$ )	0	0	34
average target function value	$2.10 \times 10^{-3} \pm 2.66 \times 10^{-4}$	$0.00 \times 10^{-3} \pm 0.00 \times 10^{-4}$	$1.99 \times 10^{-2} \pm 5.66 \times 10^{-3}$
RMSD for full peptide			
backbone atoms (Å)	$0.77 \pm 0.17$	$0.64 \pm 0.19$	$0.80 \pm 0.21$
heavy atoms (Å)	$1.23 \pm 0.15$	$1.28 \pm 0.14$	$1.23 \pm 0.25$

#### ***4.2.6 Description of the Overall Structure of PSM $\alpha$ 1***

Despite the prediction of moderate levels of  $\alpha$ -helicity from the CD, PSM $\alpha$ 1 was found to be entirely  $\alpha$ -helical. The  $\alpha$ -helix is amphipathic and runs from residue 2 to 19 (Figure 24A). The presence of a salt bridge between Lys12 and Glu16 could be further stabilizing the formation of the  $\alpha$ -helix (Figure 25A). There is a slight bend in the helix that occurs at residue 6. The hydrophobicity map of the surface reveals that PSM $\alpha$ 1 has one hydrophobic and one hydrophilic face. The electrostatic potential surface map indicates a predominately cationic peptide with a strong anionic patch near the C-terminus of the hydrophilic face (Figure 24B/C).

#### ***4.2.7 Description of the Overall Structure of PSM $\alpha$ 3***

PSM $\alpha$ 3 was found to also be predominately  $\alpha$ -helical, though there was some variability in the C-terminus, resulting in the RMSD calculation to be between residues 1-20 only. The helix formed in PSM $\alpha$ 3 is amphipathic and runs from residue 2-20 (Figure 24D). A slight bend

in the helix is observed at residue 16. Two salt bridges are present between Glu2 and Lys6 and between residues Asp13 and Lys17 in the calculated structure for PSM $\alpha$ 3, potentially adding to the stability of this secondary structure (Figure 25B). Examination of the hydrophobic surface map reveals a hydrophobic face and a hydrophilic face. The electrostatic potential surface map indicates that there is a negative charge at the C-terminus on the hydrophilic face (Figure 24E/F).

#### ***4.2.8 Description of the Overall Structure of PSM $\beta$ 2***

PSM $\beta$ 2 contains three amphipathic helices that span residues 5-15, residues 17-23, and residues 25-43 (Figure 24G). The first helix has a slight bend and interacts with the third helix. Hydrophobic residues in  $\alpha$ -helix one and  $\alpha$ -helix three interact, forming a hydrophobic core. The hydrophobic surface maps of PSM $\beta$ 2 reveal a mostly hydrophilic surface with a few patches of hydrophobicity (Figure 24H). PSM $\beta$ 2 assumes a fold is primarily created by hydrophobic interactions between  $\alpha$ -helix 1 and  $\alpha$ -helix 3. Strong, long range, NOEs occur between the  $\gamma$ -protons of Ile8 and the entire side chain of Ile30. Additionally, a NOE signal is observed between the  $\gamma$ -protons of Ile8 and the amide of Val31. Multiple NOEs are present between the  $\alpha$ - and  $\beta$ -protons of Ile27 and the  $\gamma$ -protons of Ile8, further substantiating the interaction between  $\alpha$ -helix 1 and  $\alpha$ -helix 3. In the second helix, the  $\beta$ -protons of Ala15 interact with the  $\beta$ -protons of Ser20 in the third helix. Additionally, more NOEs occur between the  $\alpha$ -proton of Ala15 and the amide proton of Ser20. A salt bridge is present between Asp19 and Lys22 adding to the stability of the shortest  $\alpha$ -helix (Figure 25C). Surprisingly, even though this peptide has relatively few long-range NOEs, the large number of short- and medium-range NOEs result in a highly structured peptide as evidenced by the low RMSD and the overlay of the 20 lowest-energy

conformers. The electrostatic surface of PSM $\beta$ 2 reveals patches of cationic and anionic charge. Specifically, the N- and C-termini appear to be positively charged, and a patch of negative charge is found in the middle of the peptide (Figure 24I).

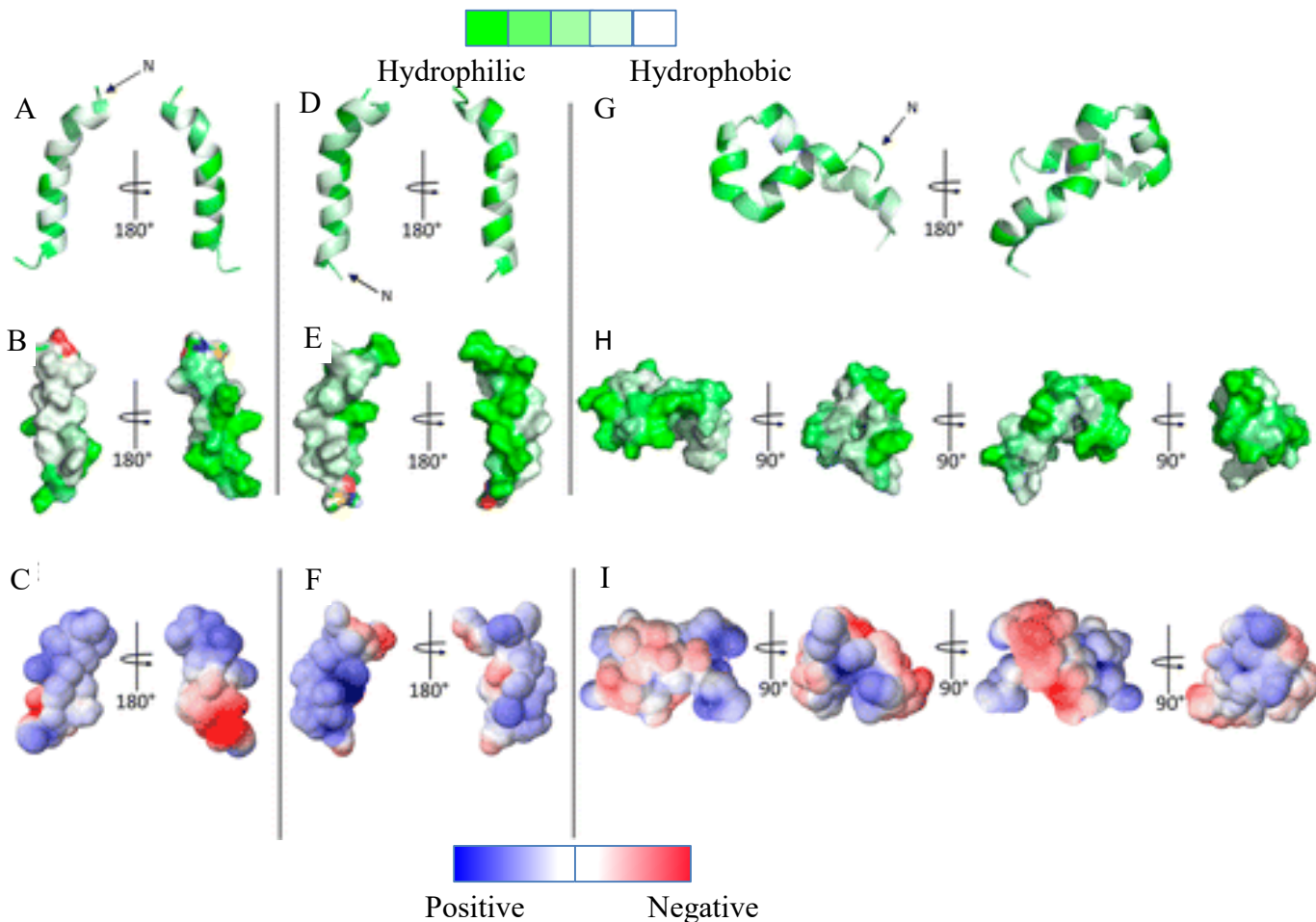


**Figure 24-** NMR solution structures depicting amphipathic helices of A) PSM $\alpha$ 1 D) PSM $\alpha$ 3 and G) PSM $\beta$ 2. Hydrophobic surface maps indicate a hydrophobic face and hydrophilic face in B) PSM $\alpha$ 1 and E) PSM $\alpha$ 3. The amphipathic helices in PSM $\beta$ 2 pack to give a hydrophobic core and hydrophilic outside as shown by the hydrophobicity surface map of

H) PSM $\beta$ 2. The formylmethionines of PSM $\alpha$ 1 and PSM $\alpha$ 3 are depicted in traditional coloring: nitrogen, blue; carboxyl, red; and sulfur, yellow. Hydrophobicity surface map representations of the PSMs were generated using PyMOL.<sup>156</sup> Electrostatic potential surface maps of C) PSM $\alpha$ 1, F) PSM $\alpha$ 3, and I) PSM $\beta$ 2. Electrostatic potential surface maps were generated using the APBS function of the PDB2PQR online pipeline.<sup>157</sup>

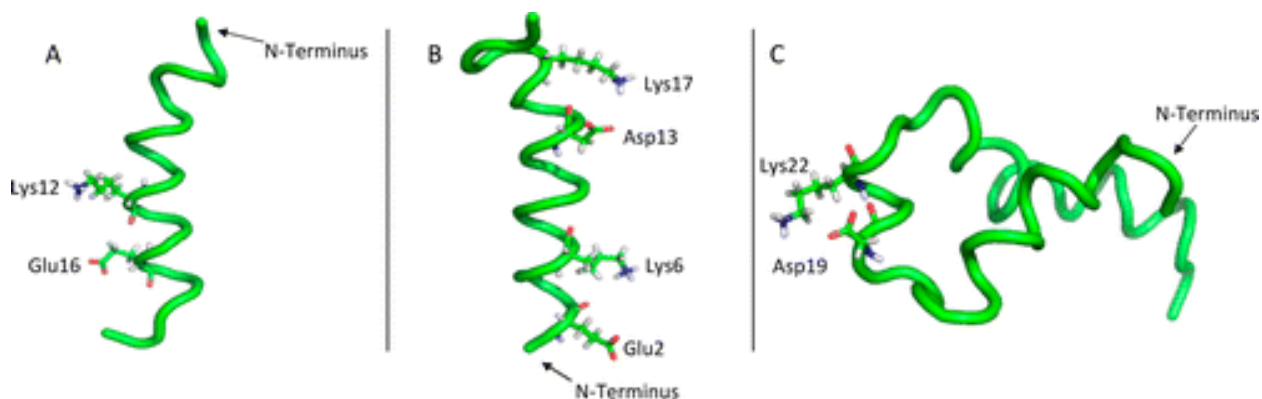


Figure 25- PyMOL<sup>156</sup> cartoon representation of (A) PSM $\alpha$ 1, (B) PSM $\alpha$ 3, and (C) PSM $\beta$ 2. Side chains that may be participating in salt bridges

#### 4.2.9 Comparison of PSM $\alpha$ 1 to PSM $\alpha$ 3

There are many similarities between PSM $\alpha$ 1 and PSM $\alpha$ 3. Both peptides form amphipathic helices that result in a predominately hydrophobic face and a predominately hydrophilic face. The electrostatic surfaces are cationic, and both peptides have an anionic charge near the C-termini. What is striking about these two peptides is the slight bend in the helix. In PSM $\alpha$ 1 the bend occurs near the N-terminus, at residue 6 whereas in PSM $\alpha$ 3 the bend in the helix occurs near the C-terminus at residue 16. The orientation of the peptides is such that

the backbone of the structures looks opposite to one another. The negative charge is near the straight part of the peptide in PSM $\alpha$ 1, and the negative charge is near the curved part of the peptide in PSM $\alpha$ 3. The biological implication of this remains a mystery and awaits further investigation. It is worth noting that PSM $\alpha$ 3 has significantly higher levels of cytotoxicity than that of PSM $\alpha$ 1, though whether this is related to their overall structures is unknown (Figure 21).

#### ***4.2.10 Tertiary Structure and its Influence on Biological Activity***

In a previous study,  $\delta$ -toxin has been used as a backbone scaffold to model the structure of PSM $\alpha$ 3. The amino acid sequence of PSM $\alpha$ 3 was superimposed on NMR solution structure of  $\delta$ -toxin.<sup>78</sup> There are subtle differences in the backbone structure of the model and the experimentally determined structure of PSM $\alpha$ 3. Namely, the positions of the amino acid side chains differ. A slight bend in the tertiary structure is present in the structure determined by NMR, whereas the modeled structure does not. The result is a subtle shift in the position of the amino acid side chains that have been determined to play an important role in cytolysis, biofilm formation, pro-inflammatory response, and antimicrobial activity. In the modeled structure, the hydrophilic side of the peptide is primarily responsible for the cytolytic properties and the hydrophobic side is primarily responsible for biofilm formation. Applying the biological function of individual amino acid residues as determined by the alanine scan published by Cheung et al.,<sup>78</sup> to the position of the amino acids according to our calculated structure, we found that the amino acids responsible for the cytolytic activity are actually located on both the hydrophobic and hydrophilic sides. Moreover, the residues important for biofilm formation, previously thought to be due to the hydrophobic side of the peptide, appear to be more evenly spread out throughout

the peptide and are on both the hydrophilic and hydrophobic sides. The amino acids responsible for antimicrobial activity are primarily located on the hydrophobic side as predicted. In the model structure of PSM $\alpha$ 3, the amino acids responsible for pro-inflammatory response were located primarily on the hydrophilic side of the peptide, which we find is in agreement with our calculated structure (Figure 26).

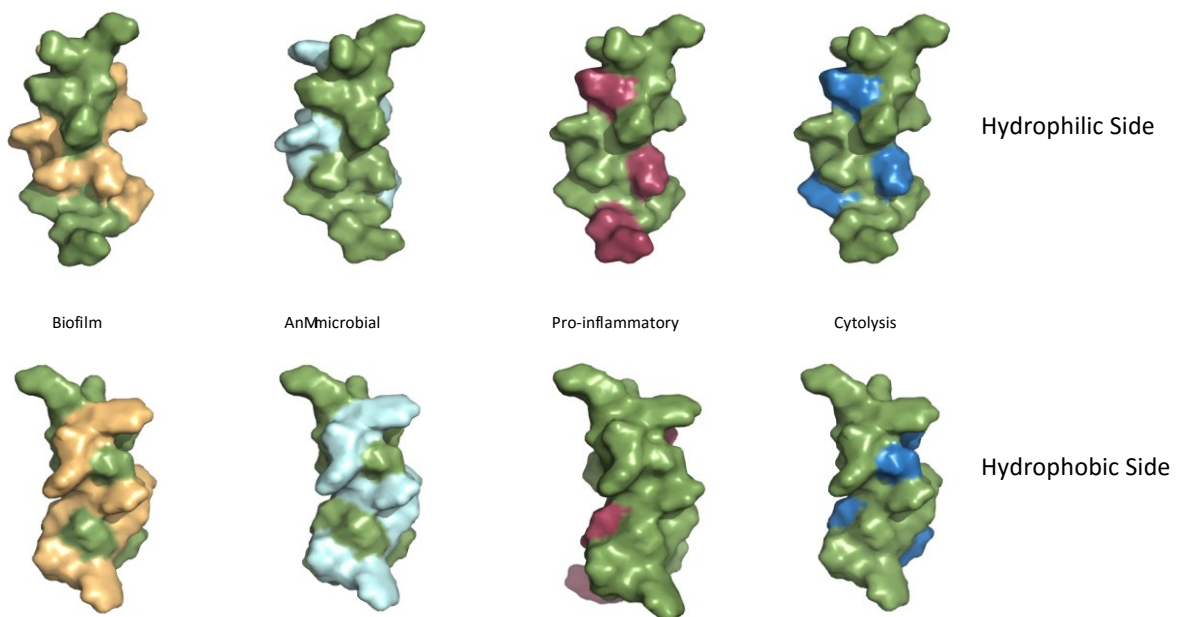


**Figure 26- Location of amino acids in PSM $\alpha$ 3 responsible for enacting a biological response, determined by Cheung and co-workers through an alanine scan. The top row reflects the hydrophilic side of PSM $\alpha$ 3, and the bottom row reflects the hydrophobic side. Amino acids not enacting any biological response are colored green. Amino acids contributing to biofilm formation and detachment are colored orange, those contributing to**

**antimicrobial activity light blue, those contributing to pro-inflammatory response red, and those contributing to cytolytic activity dark blue.**

#### ***4.2.11 Comparison of PSM $\beta$ 2 Structure to Leaderless Bacteriocins***

There are certain genetic determinants that are similar between PSMs and the leaderless bacteriocins.<sup>21,75</sup> Both are ribosomally synthesized, do not require post-translational modification, require no leader sequence for secretion, and are not co-transcribed with a dedicated immunity protein.<sup>21</sup> It was these genetic similarities that initially led us to investigate the structure of these toxins. As discussed in chapter 2, leaderless bacteriocins with broad-spectrum activity seem to adopt a similar overall fold, independent of the sequence homology. We hypothesized that regardless of the low degree of sequence similarity between PSM $\beta$ 2 and various leaderless bacteriocins, they may share a somewhat similar structural motif. While they both exhibit two  $\alpha$ -helices that form a “v-shape”, with a third  $\alpha$ -helix that runs perpendicular to one of the two “v-shape”  $\alpha$ -helices, the directionality of the helices is different between the leaderless bacteriocins and PSM $\beta$ 2. Additionally, PSM $\beta$ 2 and the leaderless bacteriocins are comprised of amphipathic helices, which fold in such a way to give a hydrophilic outer surface and hydrophobic core (Figure 27). However, there are key differences between  $\beta$ -type PSMs and leaderless bacteriocins. Primarily, the electrostatic potential surface maps reveal that PSM $\beta$ 2 is slightly anionic surface with a few patches of cationic character, whereas bacteriocins have a strongly cationic surface. The anionic surface of PSM $\beta$ 2 may explain why it does not exhibit antibacterial activity despite other similarities with the bacteriocins. Negatively charged phospholipid cell membranes in bacteria are proposed to attract bacteriocins through electrostatic

interactions with their cationic surface. A second noticeable difference between the bacteriocins and PSM $\beta$ 2 is the particular orientation, or directionality, of the  $\alpha$ -helices, as mentioned above. In the bacteriocins, the perpendicular helix is located at the C-terminus (e.g., helix 3 in the leaderless bacteriocin enterocin 7B), whereas in PSM $\beta$ 2, the perpendicular helix (i.e., helix 1) is located at the N-terminus. Furthermore, there are significantly less long range NOE's observed between the perpendicular helix and the two helices in the 'v-shape' in PSM $\beta$ 2 than in the case of leaderless bacteriocins. With less NOEs present in PSM $\beta$ 2 it may be that this peptide fold weaker in comparison to the interaction between the overlaying helix in the bacteriocins, resulting in a less compact structure overall.

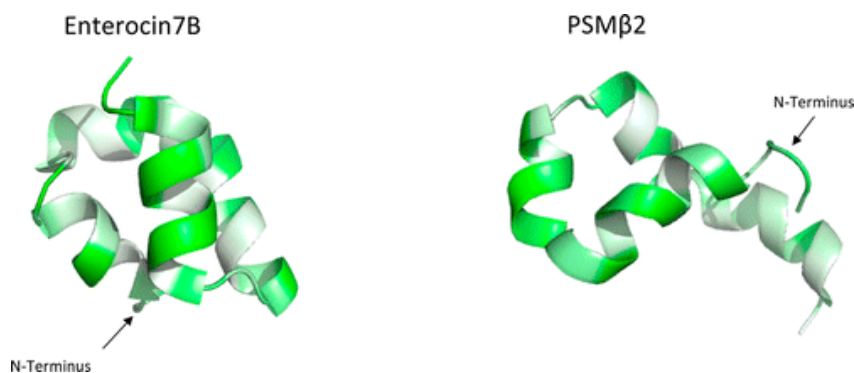


**Figure 27- Cartoon representation of amphipathic helices in leaderless bacteriocin enterocin 7B and peptide toxin PSM $\beta$ 2. Both peptides contain three  $\alpha$ -helices, two of which form a “v-shape” and a third perpendicular helix. In enterocin 7B, helix 1 and helix 2 form the “v- shape” and helix 3 is perpendicular to the curved helix 2. In PSM $\beta$ 2, helix 2 and helix 3 form the “v-shape” and helix 1 is perpendicular to the curved helix 3.**

### 4.3 Conclusions and Future Outlook

The solution structures of the staphylococcal virulence factors, PSMs  $\alpha 1$ ,  $\alpha 3$  and  $\beta 2$  were characterized using NMR spectroscopy. CYANA 2.1 was used as the structure calculation program. All three peptides appear to be highly structured and primarily  $\alpha$ -helical in the presence of 50 % trifluoroethanol. PSMs  $\alpha 1$  and  $\alpha 3$  each have a single amphipathic helix that has a slight bend near the N- and C-termini, respectively. PSM $\alpha 1$  and PSM $\alpha 3$  each contain a hydrophobic face and a hydrophilic face. In the midst of primarily cationic electrostatic surfaces, a strong anionic patch is located on the C-termini of each peptide. PSM $\beta 2$  is comprised of three amphipathic helices, which interact weakly with one another to give a hydrophobic core and a hydrophilic surface. Due to the size and genetic similarities between PSM $\beta 2$  and the leaderless bacteriocins it was proposed that they may share structural similarities. While there are a few similarities, there are more obvious differences, primarily the difference in electrostatic surface potential maps and the compact nature of the overall fold.

There remains much to be discovered with these virulence factors. One interesting aspect of these specific virulence factors is that each is exported with the same transport protein, the Pmt transporter, regardless of size or overall shape. This is particularly fascinating because there appears to be little structural similarity between the shorter  $\alpha$ -type PSMs and the longer  $\beta$ -type PSMs. Examination of the tertiary structure of each failed to illuminate structural, electrostatic or hydrophobic patterns, which could be responsible for recognition of the transport protein. Many in the scientific community believe that targeting the Pmt transporter would be the most effective treatment of the staphylococcus infection, particularly in light of the fact that

accumulation of these toxins within the cell lead to cell death. Investigation into the relationship between this transport protein and these virulence factors remains an attractive target.

These amyloid peptides contribute to biofilm formation through the formation of fibrils. After publication of our structural work on PSMs, crystallographic evidence has shown that the PSM $\alpha$ 3 form unusual tertiary and quaternary structures.<sup>158</sup> Typical fibril structures are made of cross- $\beta$  sheets, where the  $\beta$  sheet line up with the axis of the fibril.<sup>158,159</sup> PSM $\alpha$ 3 has been shown to form fibrils in a cross- $\alpha$  amyloid fashion (Figure 28).<sup>158</sup> The result is that the  $\alpha$ -helices are aligned head to tail and are horizontal to the axis of the fibril, this structural packing has never before been observed in eukaryotic amyloid structures.<sup>158</sup> These  $\alpha$ -cross fibrils share biological characteristics that are reminiscent of the  $\beta$ -cross fibrils.<sup>143</sup> With the crystal structure available of the amyloid network formed by PSM $\alpha$ 3, it may now be possible to disrupt the interaction of multiple PSM $\alpha$ 3 molecules with the development of a small molecule or small peptide inhibitor. Disruption of the fibril formation could lead to poorly structured biofilms in MRSA, resulting in reduced pathogenicity of this bacterial infection.

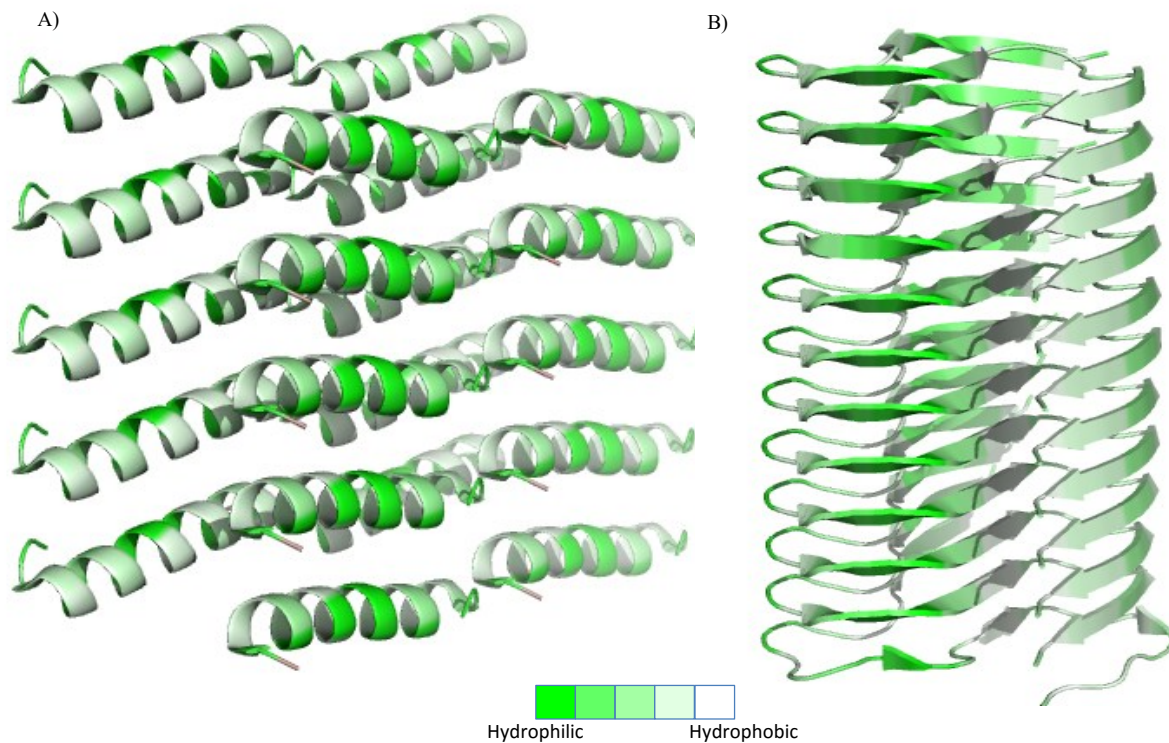


**Figure 28- Extended amyloid structure of A) PSM $\alpha$ 3 and B) a 42-residue  $\beta$ -amyloid formed in Alzheimer's disease. The fibril structure formed in the case of PSM $\alpha$ 3 is an atypical  $\alpha$ -cross amyloid structure whereas, the structure of the  $\beta$ -amyloid is a  $\beta$ -cross structure usually observed in fibril formation.**

## Chapter Five: Neopetrosiamide A and B

### 5.1 Introduction

Neopetrosiamide A and B were isolated from the marine sponge of the *Neopetrosia* sp. collected off the coast of Papua New Guinea.<sup>92</sup> As potent inhibitors of cancer cell invasion, these peptides show promising activity against cancer metastasis while remaining nonthreatening to non-cancerous cells.<sup>92</sup> A 28-amino acid peptide, neopetrosiamide A differs from neopetrosiamide B in the stereochemistry of the sulfoxide moiety at the methionine in position 24 of the peptides. Herein, the mixture of diastereomers will be referred to as neopetrosiamide. It is not clear if the sulfoxide moiety is the naturally produced species or if it is a product of the isolation and handling of this peptide. Interestingly, this peptide is rich in cysteines, and contains three disulfide bonds, which were initially reported to be between Cys3-26, Cys7-12, and Cys18-28.<sup>92</sup> The connectivity of the disulfides was later corrected by the Vederas group and determined to be between Cys3-26, Cys7-18, and Cys12-28.<sup>93</sup>

Short, disulfide-rich peptides represent a growing class of peptides that are produced across a wide-variety of life forms, including plants and mammals.<sup>160,161</sup> Many of these disulfide-rich peptides have interesting biological activities; cyclotides, isolated from plants, display anti-tumour, anti-HIV, and insecticidal activities.<sup>162</sup> The defensins ( $\alpha$ -,  $\beta$ - and  $\theta$ -) are mammalian antimicrobial peptides containing three disulfide bonds.<sup>163</sup>

Neopetrosiamide is unique in the sense that it was isolated from a marine sponge. Typical peptides isolated from other marine sponges contain one or no disulfide bonds whereas

neopetrosiamide contains three.<sup>92</sup> It is not known if neopetrosiamide is produced by the sponge itself or from a symbiotic bacterium present on the sponge surface.

### ***5.1.1 Biological Significance***

Cancer is a broad term used to describe a group of diseases that are characterized by the transformation of normal cells into tumour cells.<sup>164</sup> The progression of this phenomenon is a combination of a person's genetic make-up but is also heavily influenced by external carcinogens and, as such, cancer is one of the leading causes of morbidity and mortality worldwide.<sup>165</sup> In 2015, an estimated 8.8 million deaths were attributed to cancer worldwide. The economic impact of this disease is staggering. In 2010, the economic cost of cancer was estimated to be 1.16 trillion US dollars.<sup>165,166</sup> The incidence of new cancer diagnoses is expected to rise by 70 % over the next 2 decades.<sup>165</sup>

An underlying characteristic of cancer cells is the rapid reproduction of abnormal cells. The speed of cell creation leads to growth beyond the usual organ boundaries.<sup>165</sup> The ability to grow and spread into adjacent tissues is referred to as metastasis and is a major factor contributing to cancer related death.<sup>165</sup> Interestingly, many antimicrobial peptides have been shown to exhibit anti-tumour or anti-metastatic activity, inhibiting malignant cells from spreading to adjacent tissues.<sup>90,111,167</sup>

Neopetrosiamide has been found to inhibit the migration of cancer cells through the extracellular matrix (ECM).<sup>92</sup> The extracellular matrix is a complex mixture of proteins and polysaccharides that provide structural support of mammalian cells.<sup>92</sup> Attachment of cells to the ECM is mediated by integrins and receptors on the cells surface.<sup>92</sup> Cells can move through the

extracellular matrix in two distinct modes, mesenchymal migration and amoeboid migration. In mesenchymal migration the cells enzymatically degrade the ECM using proteases. In amoeboid migration the cells will adapt and change their shape to fit through the ECM.<sup>92</sup> To inhibit the migration of cancer cells through the ECM many cancer therapies rely on blocking the proteases present in mesenchymal migration.<sup>92</sup> Some types of cancer cells are able to evade these protease-blocking therapies by simply changing to amoeboid migration.<sup>92</sup> The transition between these types of migration makes it desirable to design cancer therapy drugs that inhibit both cancer migration pathways. Neopetrosiamide has been found to inhibit both of these pathways without affecting healthy, non-cancerous cells in the short term.<sup>92</sup>

## **5.2 Results and Discussion**

### ***5.2.1 Synthesis of residue 24 analogues of Neopetrosiamides A and B***

The presence of the diastereomeric center of the methionine sulfoxide poses purification challenges and as such, our group was interested in replacing this group with an amino acid residue unable to oxidize and form diastereomers. Previous work in our group has demonstrated that the methionine sulfoxide (M(O)24) at position 24 can be replaced with methionine (M(O)24M) and that the resulting neopetrosiamide retains full activity.<sup>93</sup> Furthermore, replacement of the methionine sulfoxide with norleucine (M(O)24Z) resulted in a neopetrosiamide with only slightly reduced activity.<sup>93</sup> Insertion of L-O-methylhomoserine (O-methyl HSE) at position 24, a conservative substitution relative to methionine, was synthesized to explore the peptides toleration to unnatural amino acids. To further explore the effect of

M(O)24 substitution in neopetrosiamides, eight non-oxidizable canonical amino acids were inserted at position 24 (Figure 29A).

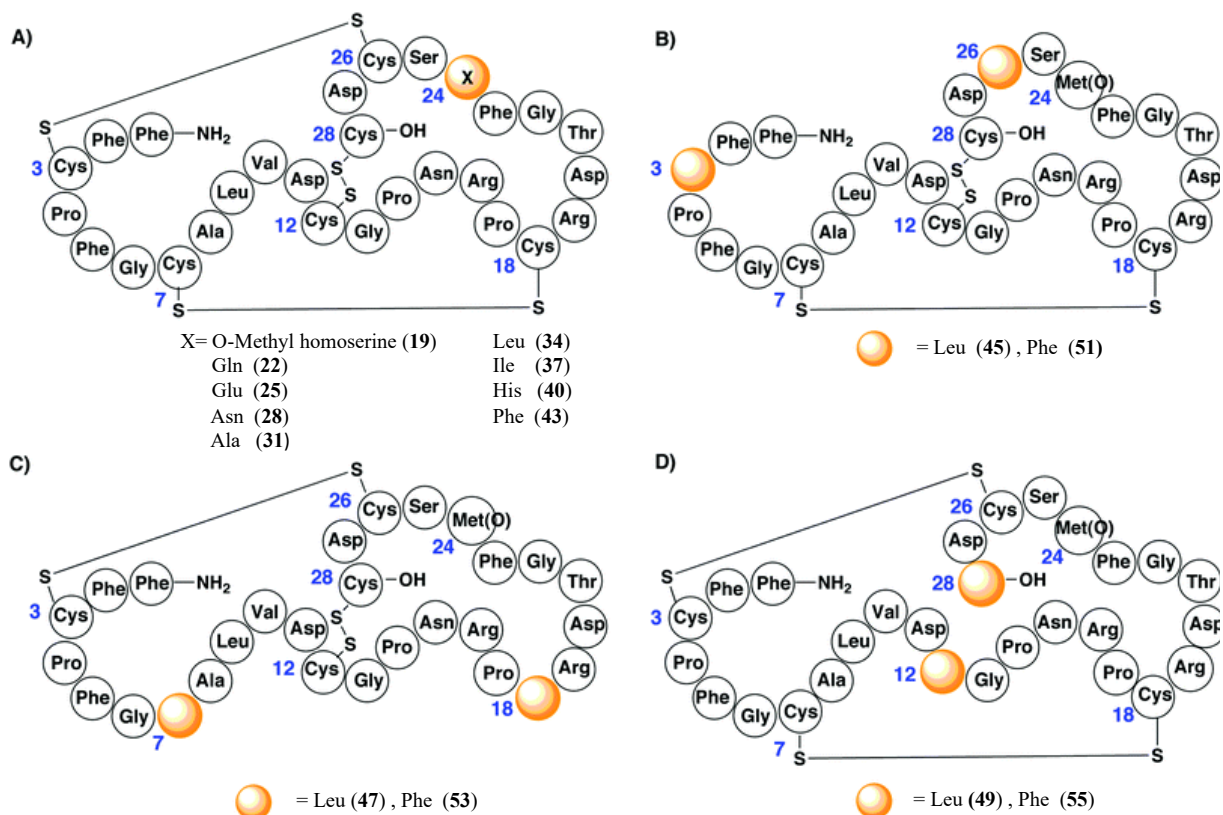
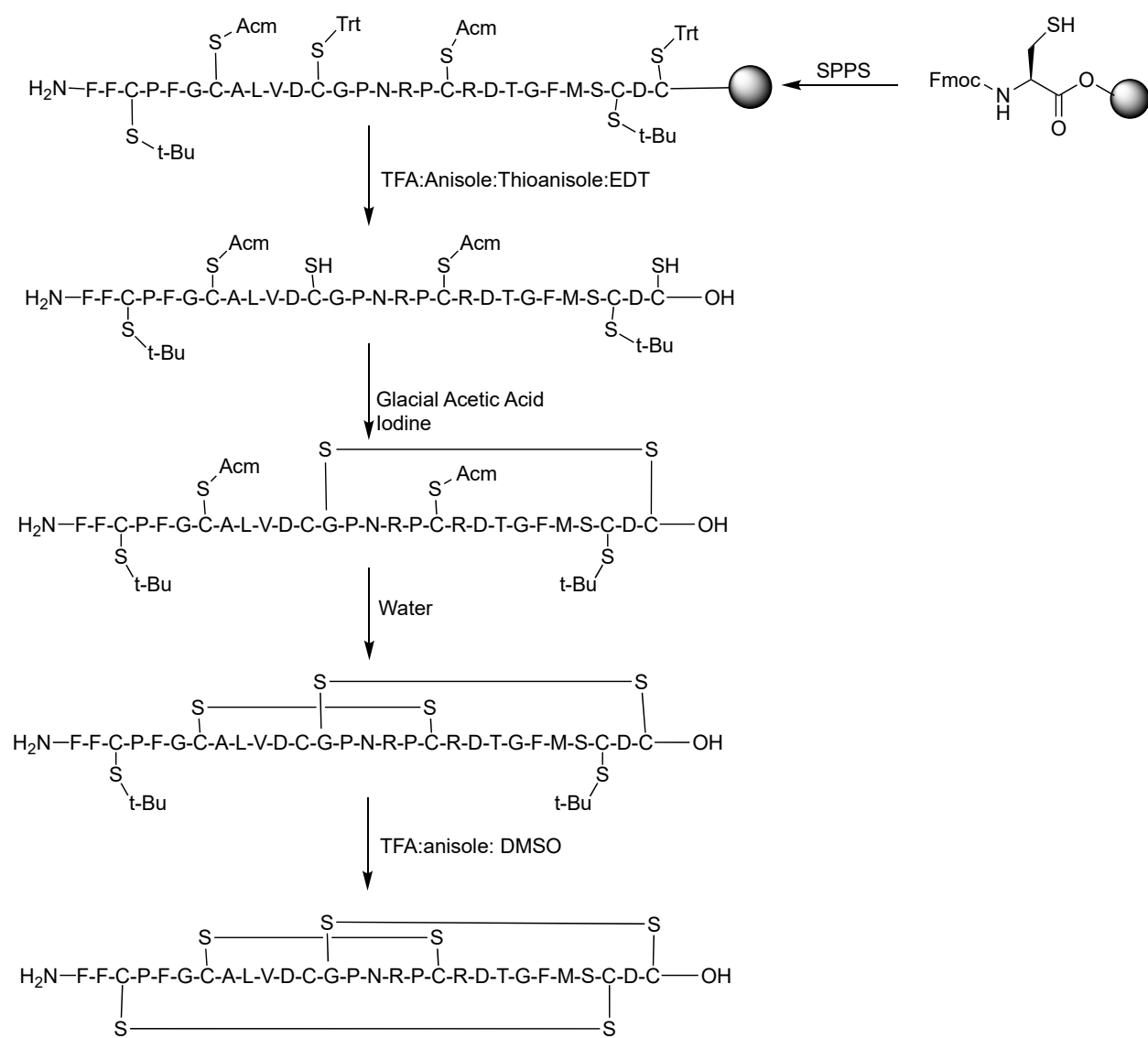


**Figure 29-** A) Cartoon representation of methionine sulfoxide substitution with various amino acids at position 24. B) Cartoon representation of the disulfide replacement of cysteine 3 and cysteine 26. C) Cartoon representation of disulfide replacement of cysteine 7 and cysteine 18. D) Cartoon representation of disulfide replacement of cysteine 12 and cysteine 28.

Each amino acid substitution was aimed at probing specific attributes of residue 24 in relation to methionine. M(O)24O-methyl HSE, similar in size and shape to methionine, was chosen to explore the importance on heteroatom electronegativity. Compounds **22** and **25** probed the importance of the length of the carbon side chain and the incorporation of terminal hydrogen-bond acceptor/donor capabilities. Closely related to **22**, compound **28** explored the effect of maintaining the hydrogen-bond acceptor/donor, but reduced the number of carbons in the side chain. Investigation of the tolerance to branched residues without hydrogen-bonding capabilities was achieved with compounds **31**, **34**, and **37**. Finally, tolerance to steric bulk was studied by incorporating aromatic rings at position 24 in compounds **40** and **43**.

Methodology previously developed by our group led to the synthesis of the residue 24 analogues of neopterosiamide. Briefly, Fmoc-protected amino acids were added sequentially to a preloaded 2-chlorotrityl resin containing trityl-protected cysteine. Following addition of the desired amino acids, treatment of the resin with a cocktail containing 90:5:3:2 TFA:thioanisole:EDT:anisole removes the desired peptide from the resin along with any acid labile protecting groups. The reaction time was limited to 1 h to prevent the cleavage of the *t*-butyl protected cysteine. Now resin free, the peptide was dissolved in glacial acetic acid containing dissolved iodine, which led to the oxidation of the free thiols of cysteine, affording the first disulfide bond. Addition of water to this reaction mixture led to the deprotection of the acetamidomethyl protected cysteines and remaining iodine in the solution facilitates the second disulfide bond. Upon purification of the bis-disulfide neopterosiamide the third disulfide was introduced by dissolving the peptide in trifluoroacetic acid, to remove the *t*-butyl protecting groups. DMSO in

solution enables the oxidation of remaining thiols to afford the third disulfide. The desired cysteine disulfide connectivity was as follows, Cys3-26, Cys7-18, and Cys12-28 (Scheme 5). To prevent intermolecular disulphide bond from forming the concentration of peptide was kept low, at 0.5 mg/mL. Some scrambling of disulfides is observed and the desired disulfide connectivity is determined by retention time in RP-HPLC.



**Scheme 5- Synthetic scheme of the sequential formation of disulfide bonds utilizing an orthogonal protection/deprotection strategy.**

### ***5.2.2 Synthesis of neopetrosiamide analogues with disulfide bonds substituted with hydrophobic pairs.***

Although correct connectivity of the disulfide bonds is critical for biological activity of neopetrosiamide, previous work by our group has demonstrated that some antimicrobial peptides

tolerate disulfide replacement with hydrophobic interactions.<sup>168,169</sup> Replacement of one of the three disulfides in neopetrosiamide would decrease the number of post-SPPS steps, also reducing the number of required HPLC purifications from two to one, thereby making neopetrosiamide more synthetically accessible. Our hypothesis was that two correct disulfide bonds could be sufficient to hold the peptide in the correct conformation and the third could be replaced with hydrophobic residues like phenylalanine or leucine. Phenylalanine is known to form  $\pi$ -stacking interactions or ring-locking interactions in peptides which could add stability in the place of the third disulfide bond.<sup>170,171</sup> Leucine-leucine interactions form a unique secondary structure in nature.<sup>172</sup> Multiple leucines, typically seven residues apart, interact to form a zipper like motif.<sup>172</sup> While nature usually relies on a network of leucines to create a leucine zipper, previous studies in our group have successfully replaced disulfide bonds in antimicrobial peptides with leucines and maintained antimicrobial activity.<sup>168,169,172</sup> In the same method described above, analogues of neopetrosiamide were synthesized where one of the three disulfide bonds was replaced with hydrophobic residues giving a total of six analogues (Figure 29B-D). Dr. Hongqiang Liu synthesized three analogues where each disulfide was sequentially replaced with phenylalanine. Next, the disulfide bonds were consecutively replaced with leucine residues in a combined effort of Dr. Chaytor and myself. The cysteine protecting groups were limited to trityl and acetamidomethyl, restricting the number of synthetic steps and purifications needed.<sup>122</sup>

### ***5.2.3 Activity Testing of the M(O)24 Neopetrosiamide Analogues and the Disulfide Replacement Analogues.***

To evaluate the biological activity of the residue 24 analogues, morphology of MDA-MB-231 cells were inspected before and after treatment with our M24X neopetrosiamides.

MDA-MB-231 is a highly metastatic, human breast cancer cell line that has the ability to invade adjacent tissues in a mesenchymal manner.<sup>91</sup> In our morphological studies, MDA-MB-231 cells are plated on matrigel, a protein mixture secreted from Engelbreth-Holm-Swarm (EHS) mouse sarcoma cells. This protein mixture mimics the basement membrane of the extracellular matrix that epithelially-derived breast tumour cells must first move through to initiate the metastatic cascade.<sup>173</sup> Matrigel is polymerized in a 96-well plate and the cells are placed on top in cell culture medium that contains the specified M24X derivative or a control compound. Upon overnight incubation at 37 °C, the morphology of the cells is analyzed. Active M24X compounds result in MDA-MB-231 cells that are unable to spread through the matrigel. The cells remain round and sit above the layer of matrigel (Figure 30A). Inactive M24X compounds result in cells that are able to invade the matrigel and the cells are oblong in shape (Figure 30C). Partially active compounds have a mixture of cells that remain round and on top of the matrigel and cells that have invaded the matrigel and are oblong in shape (Figure 30B). Naturally occurring neopetrosiamide isolated from the marine sponge or synthesized by the method described above acted as the positive control. The negative control is neopetrosiamide with the incorrect disulfide bond connection.

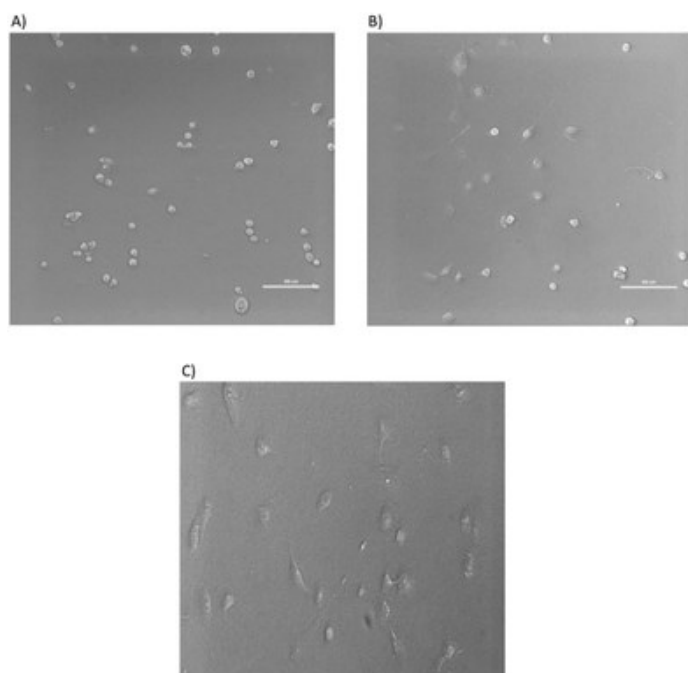


**Figure 30- Images of MDA-MB-231 breast cancer cells upon treatment with neopetrosiamide analogues. Scale bars on the bottom right corner of the pictures indicate 100  $\mu\text{m}$ . A) Example of MDA-MB-231 cells treated with an active neopetrosiamide analogue. Cells have rounded and detached from surface of matrigel. B) Representative picture of cells treated with a partially active analogue of neopetrosiamide. C) Picture of MDA-MB-231 cells that have been treated with an inactive neopetrosiamide analogue. Cells have invaded the matrigel and maintain their oblong shape.**

Of the fifteen analogues discussed above only three displayed partial activity, **25**, **31**, and **43** (Table 3.1). Previous studies have shown that the M(O)24M and M(O)24Nle analogues retained full activity even though M(O)24M is oxidatively unstable and M(O)24Nle contains a non-canonical amino acid.<sup>93</sup> The three compounds with activity reported in this study offer

increased oxidative stability and can potentially be made through site-directed mutagenesis. The lack of full activity of many of these analogues suggests that methionine sulfoxide is a structural ‘hot-spot’ for biological recognition of neopetrosiamides. Furthermore, all three disulfide bonds are required for biological activity. Substitution of any disulfide bond with hydrophobic residues resulted in an inactive peptide, suggesting a very specific and constrained structure is needed to inhibit cancer cell invasion. Similar results have been showing for other disulfide-rich biologically active peptides.<sup>173</sup>

**Table 3.1- Activity Against the Invasion of MDA-MB-231 Cells through Matrigel**

Compound	Analogue	50 $\mu\text{g mL}^{-1}$	20 $\mu\text{g mL}^{-1}$
	M(O)24M	+++	++
	M(O)24Nle	+++	++
(19)	M(O)24O-methyl HSE	–	–
(22)	M(O)24Q	–	–
(25)	M(O)24E	+++	+
(28)	M(O)24N	–	–
(31)	M(O)24A	+	–
(34)	M(O)24L	–	–
(37)	M(O)24I	–	–
(40)	M(O)24H	–	–
(43)	M(O)24F	+	–
(45)	C3L, C26L	–	–
(47)	C7L, C18L	–	–
(49)	C12L, C28L	–	–
(51)	C3F, C26F	–	–
(53)	C7F, C18F	–	–
(55)	C12F, C28F	–	–

+++, Fully active, no invasion of matrigel by cells. ++, Reduced activity, very few cells had invaded the matrigel. +, Partial activity, most cells had invaded the matrigel, few were rounded. –, No activity, all cells were able to invade the matrigel.

#### 5.2.4 Synthesis of Fluorescently Labeled Neopetrosiamide

The tertiary structure of neopetrosiamide reveals two distinct faces, hydrophobic and hydrophilic (Figure 31). As discussed above, replacement of the methionine sulfoxide at position 24 resulted in significant reductions or abolishment of activity. Located on the surface of the hydrophobic side of the peptide, we have proposed that this residue and non-polar face of the peptide plays an important role in the biological mode of action of these peptides.

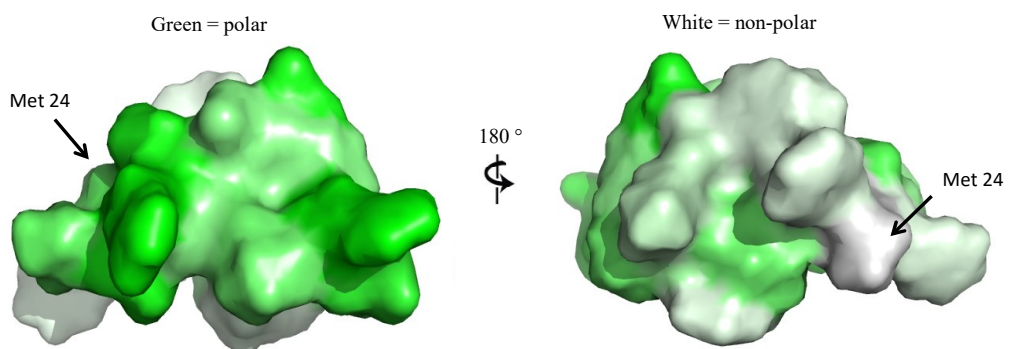
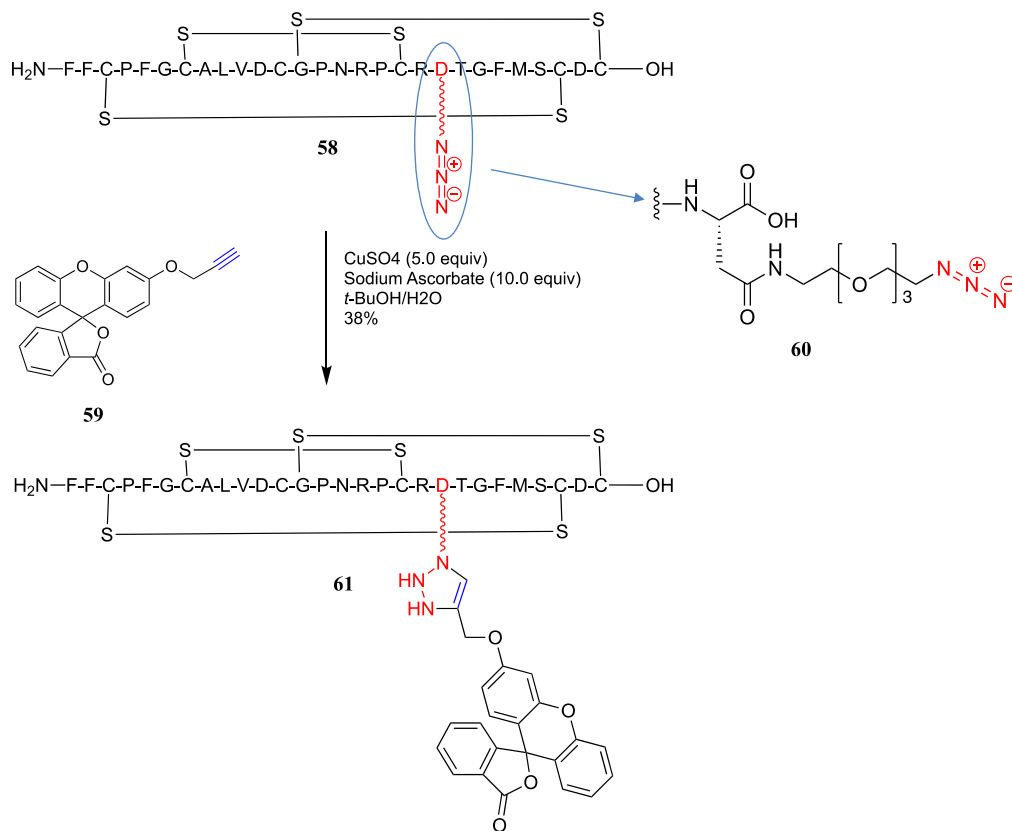


**Figure 31- Hydrophobic surface map of neopetrosiamide. One face of the peptide is hydrophilic and the other face of the peptide is hydrophobic.**

In order to gain a greater understanding of how neopetrosiamides are interacting within cancer cells, we were interested in visualizing neopetrosiamides within cells. To do this, neopetrosiamides were functionalized with an organic fluorescent dye through a covalent linker. Choosing the appropriate location to functionalize is essential, as some locations may actually result in disruption of the interactions between neopetrosiamide and its receptor responsible for eliciting the desired biological response. Due to the sensitivity of methionine sulfoxide at

position 24 on the hydrophobic face of the peptide, we chose to functionalize the hydrophilic side through the aspartate amino acid side chain.

Dr. Hongqiang Liu synthesized a derivative of aspartic acid, which contains a polyethylene glycol (PEG) linker functionalized with a terminal azide (**60**). Following incorporation of the pegylated aspartic acid to the linear neopetrosiamide by SPPS, the specific disulfides were formed following the methodology described above to give compound **58**. Activity testing of **58** revealed a fully active analogue of neopetrosiamide. Unfortunately upon “click” chemistry of the azide with an alkynylated fluorescein (**59**) the resultant neopetrosiamide analogue (**61**) was found to be inactive (Scheme 6).



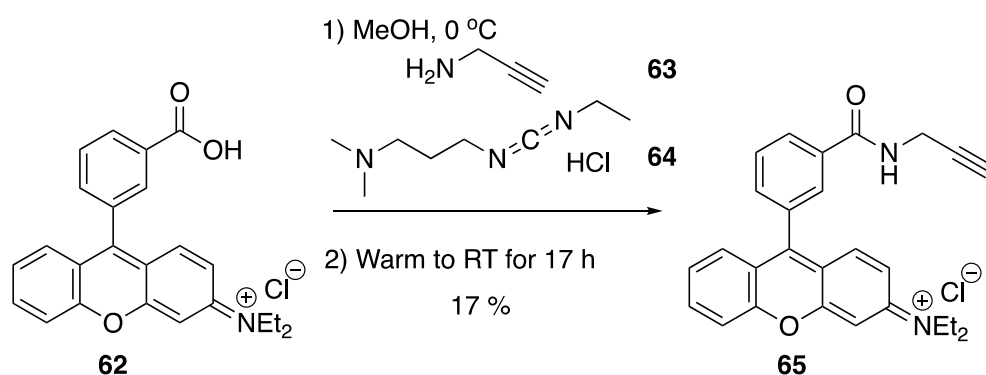
### Scheme 6- Synthesis of fluorescently labeled neoptrosiamide.

Two theories have been proposed to explain the loss of activity upon addition of the organic dye. The organic dye may be too sterically demanding or may interact with the surface of neoptrosiamide unfavourably, causing a deleterious effect on activity.<sup>174</sup> Secondly, if the length of the tether is not optimal, the large fluorescent organic dye could be hindering the mechanism of inhibition. A tether must be long and flexible enough to allow the active site of the neoptrosiamide to interact with the active site of the cellular target once the large dye is

attached. However, it must also be short enough that the PEG chain does not interfere with the tertiary structure of neopetrosiamides.

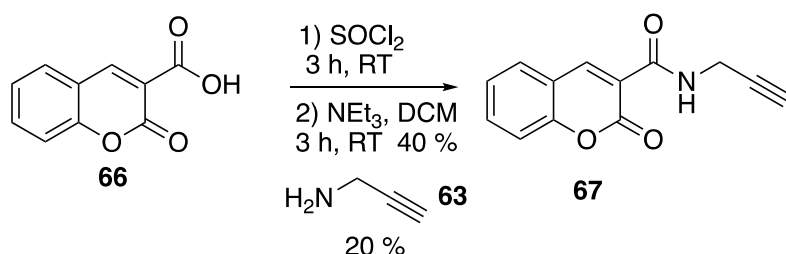
To test these theories, the length of the tether was varied and alternative fluorescent organic dyes were synthesized. Rhodamine, coumarin and BODIPY were each functionalized with an alkyne, which would allow for a [2+3] cycloaddition with the azide of the Asp20-PEG-3-azide.

Synthesis of the rhodamine B analogue containing an alkynyl linker was done in accordance to literature procedures and with yields consistent to literature reports.<sup>175</sup> Rhodamine B (**62**) was coupled to propargyl amine (**63**) in the presence of 1-(3-dimethylaminopropyl)-3-ethylcarbodiimide (EDC) hydrochloride (**64**). EDC is a coupling reagent, which forms a carbodiimide with the carboxylic acid of rhodamine B. This activated ester intermediate reacts with propargyl amine to form a new amide bond (**65**) in a 17 % yield (Scheme 7).



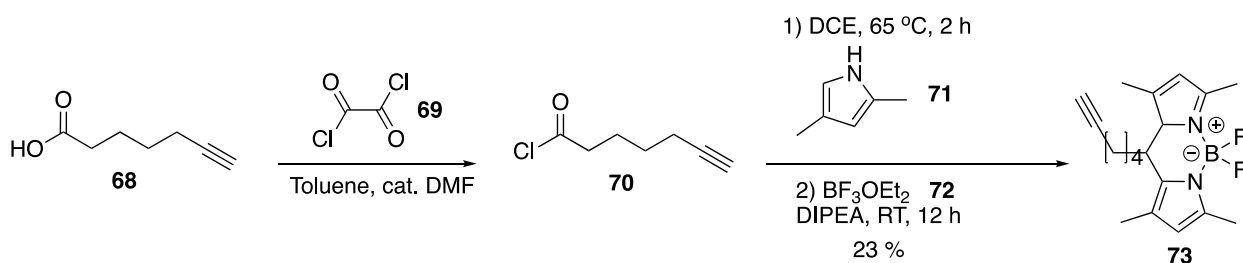
**Scheme 7- Functionalization of Rhodamine B with propargyl amine to form alkynyl functionalized Rhodamine B.**

Literature precedent for the formation of an alkyne functionalized coumarin derivative was followed.<sup>176</sup> Coumarin (**66**) was converted to an acyl chloride through reaction with thionyl chloride. The acyl chloride was then reacted with propargyl amine (**63**) to create a new amide bond and an alkyne functionalized coumarin dye (**67**) was obtained (Scheme 8).



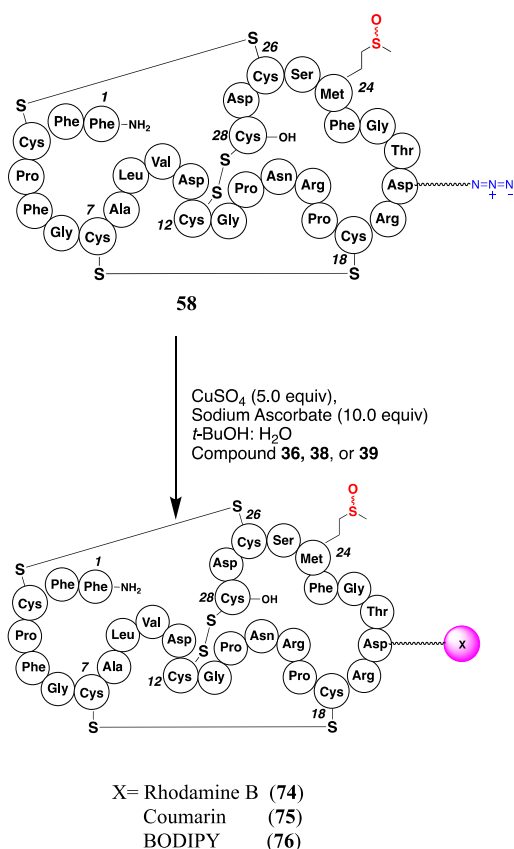
**Scheme 8- Formation of the alkyne functionalized coumarin dye through acylation and amide bond formation.**

To synthesize the alkyne functionalized BODIPY dye (**73**), 6-hexynoic acid (**68**) was converted to the acyl chloride using oxalyl chloride (**69**).<sup>177</sup> Condensation of the acyl chloride intermediate (**70**) with two equivalents of 2,4-methylpyrrole (**71**) and boron trifluoride diethyl etherate (**72**) afforded the desired compound **73** (Scheme 9). Compound **73** was obtained in 23 % yield.



**Scheme 9- Synthesis of alkyne functionalized BODIPY dye.**

Each fluorescent analogue, **65**, **68**, and **73**, was coupled to peptide **58** using a copper catalyzed [2+3] cycloaddition. The fluorescent labels, **65**, **68**, and **73**, were dissolved in 1:1 *t*-butyl alcohol:H<sub>2</sub>O with **58** in the presence of 5.0 equiv. of copper sulfate and 10 equiv. of sodium ascorbate leading to compounds **74**, **75**, and **76**, respectively (Scheme 10). Isolated yields of 0.5 mg, 0.7 mg and 0.3 mg were obtained for **74**, **75**, and **76**, respectively.

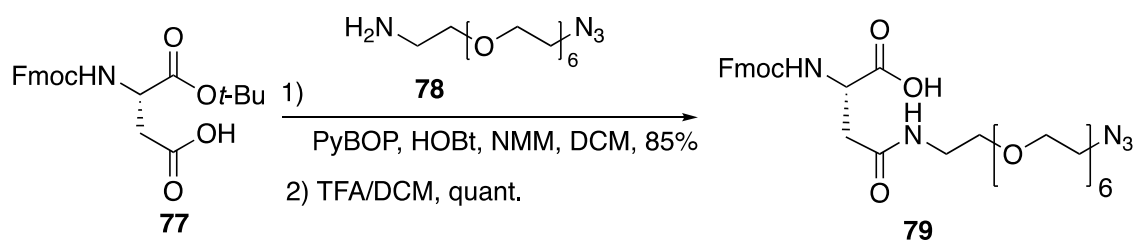


**Scheme 10-** Copper catalyzed ‘click’ reaction to afford fluorescently labeled neopetrosiamide analogues, **74**, **75**, and **76**.

Biological testing for activity of **74**, **75**, and **76** revealed that all three analogues are inactive against MDA-MB-231 cells. These results suggest that the PEG linker is too short, resulting in steric hinderance when neopetrosiamide approaches its biological target. Extending the length of the linker between the aspartic acid residue and the organic fluorescent dye could minimize the interference of the organic dye with the biological receptor.

### 5.2.5 Synthesis of Modified Aspartic Acid Derivative

To synthesize the modified aspartic acid residue, Fmoc-Asp-*Ot*-Bu (**77**) is coupled with the PEG<sub>6</sub> liker (**78**) in the presence of PyBOP (Scheme 11). Treatment of the pegylated aspartic acid with TFA removes the *t*-butyl backbone protecting group to afford compound **79**.



### Scheme 11- Synthesis of Pegylated Aspartic Acid Residue

Incorporation of the modified aspartic acid residue (**79**), at position 20, into the linear neopetrosiamide was achieved with Fmoc-SPPS. Subsequent disulfide formation was accomplished through the stepwise approach previously described to give **82** (Figure 32).

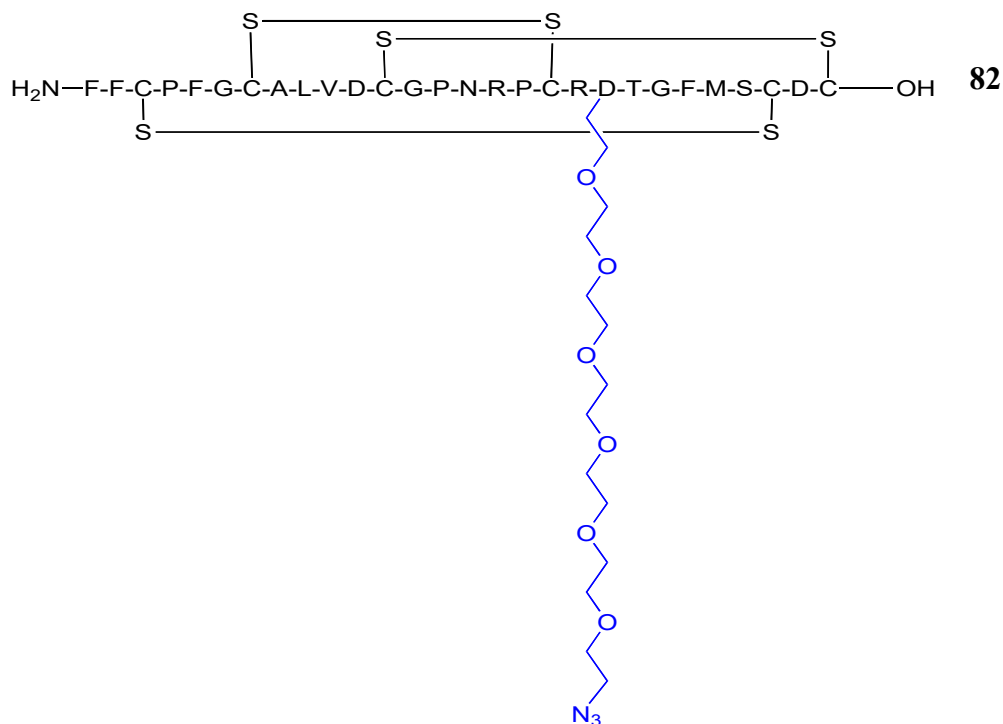


**Figure 32- Neopetrosiamide analogue containing a modified PEG<sub>6</sub> linker at the aspartic acid residue at position 20.**

Remarkably, when **82** was tested for activity, the MDA-MB-231 cells were unaffected, indicating this analogue is inactive. This was particularly unexpected due to the retained activity observed when a Asp20 is functionalized with a shorter PEG<sub>3</sub> linker. It is possible that the extended length of the linker results in a long, flexible unit and it may be able to disrupt the binding interactions between neopetrosiamide and its biological receptor. Examination of the surface structure of neopetrosiamide reveals that the spatial distance between Asp20 and Met24 is not as far as originally thought (Figure 33). The hydrophobic nature of the PEG<sub>6</sub> linker in addition to the length of the polyethylene glycol chain may allow for interaction between the chain and the predicted methionine ‘hot-spot’, critical for activity of the neopetrosiamide. Due to the limited

success of fluorescently labeling neopetrosiamide, an alternative method to identifying neopetrosiamides mode of action was adopted.

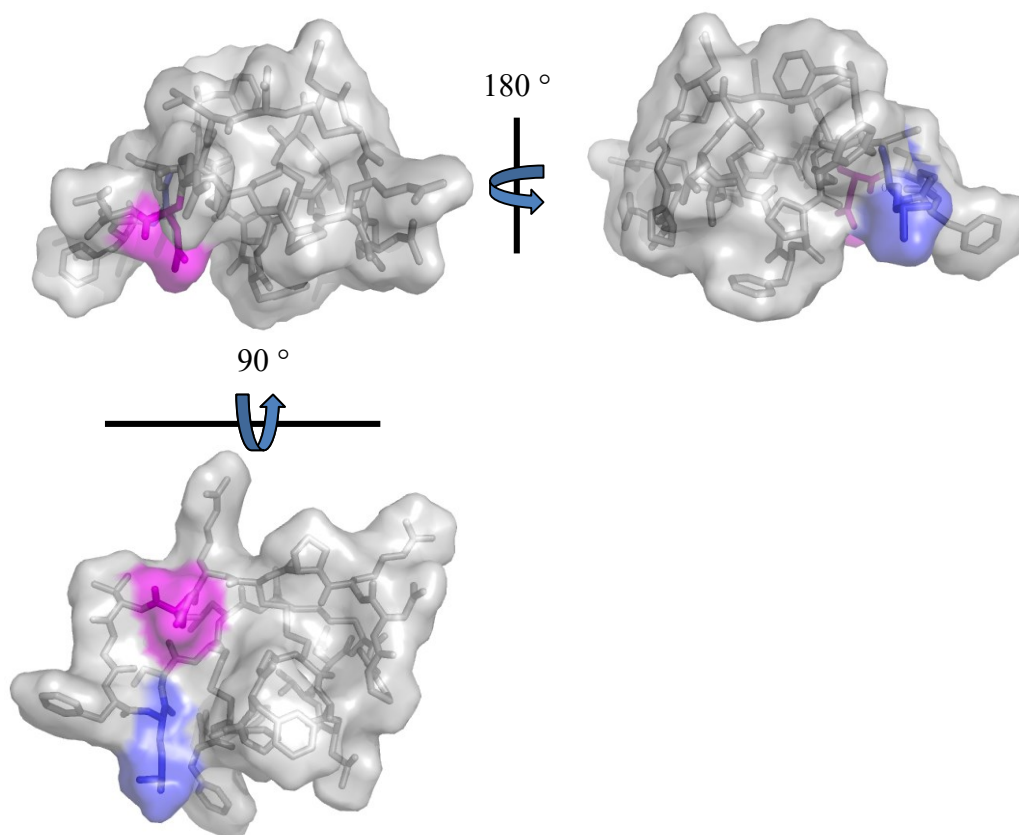


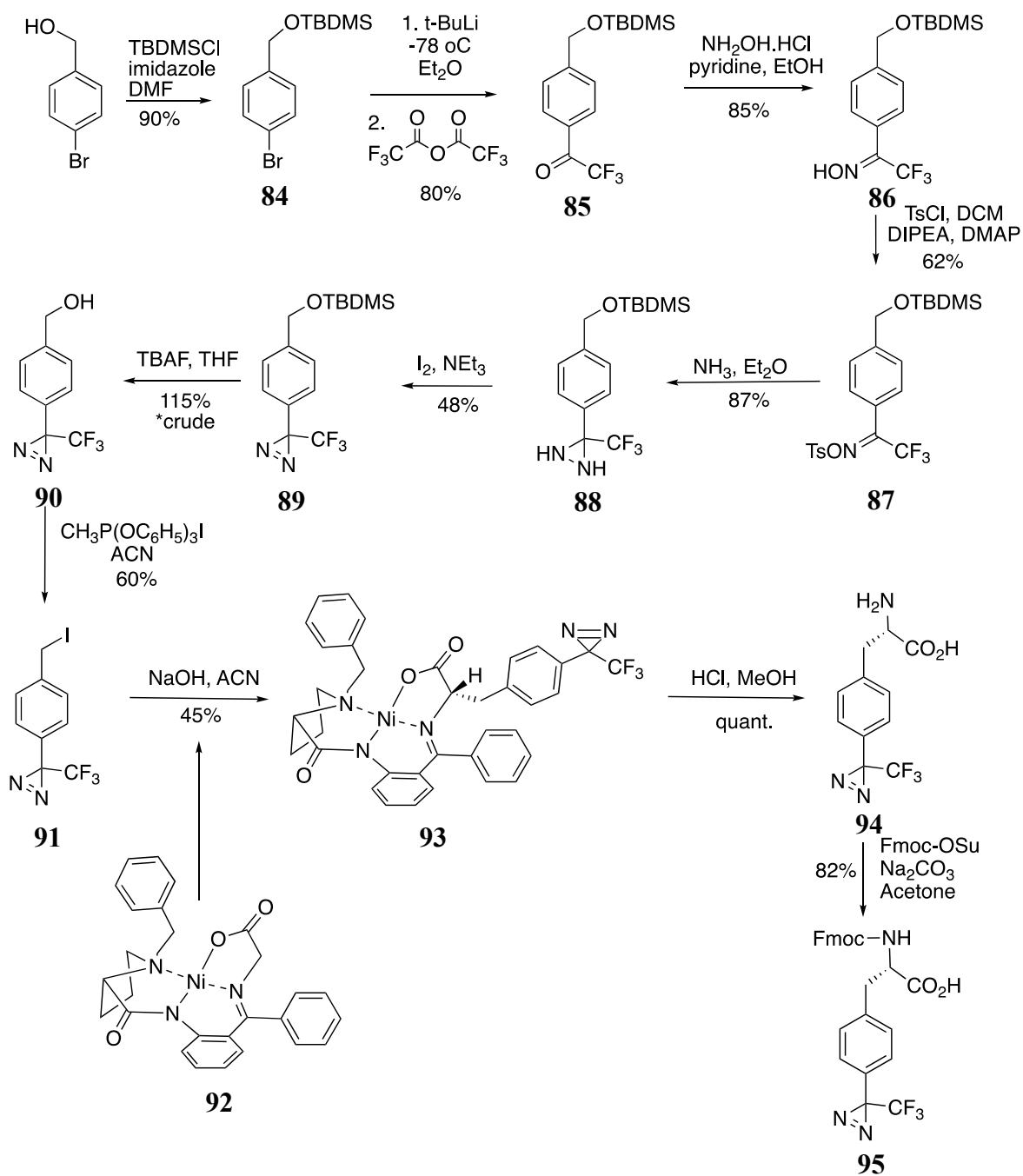
**Figure 33- PyMOL surface structure of neopetrosiamide. Aspartic acid 20 is shown in pink and methionine 24 is shown in blue. All other amino acid are colored grey. Aspartic acid 20 is located on the hydrophilic face and methionine 24 is located on the hydrophobic face. A 90 degree rotation of the peptide reveals the close spatial proximity of Asp20 to Met24.**

#### **5.2.6 Synthesis of a Photoaffinity Label.**

Photoaffinity labeling is a powerful tool employed to identify protein targets of interest. There are two potential drawbacks to photoaffinity labeling. First, the biological molecule or

peptide must retain its biological activity after functionalization with a photolinker. Previous studies have used benzophenone, a larger non-amino acid like photoaffinity linker. However, benzophenone is sterically large and may disrupt peptide structure due to its hydrophobic nature. Diazirine photoaffinity labels offer the advantage of being small and they can be installed on amino acid like backbones. Second, the molecule or peptide must contain a handle for fluorescent functionalization after the photoaffinity reaction takes place.

Substitution of the diastereotopic methionine sulfoxide was found to cause significant deleterious effects in the overall activity of neopetrosiamide, suggesting that this is a key residue in the mode of action of this peptide. To elucidate the biological receptor of neopetrosiamide, a strategy to incorporate a photoaffinity label was adopted. Due to the sensitivity of the methionine residue, it was desirable to incorporate the photoaffinity label in close proximity to this residue. Theoretically, if the methionine is indeed involved in the mode of action of these peptides, attachment of a photoaffinity linker close to this residue would maximize the chances of creating a covalent linkage between neopetrosiamide and its biological receptor and minimize non-specific binding. Phenylalanine at position 23 was chosen to be modified into a photo-labile phenylalanine. For this reason we chose to synthesize a photo-labile phenylalanine (**95**) (Scheme 12).



Scheme 12- Synthetic scheme of the synthesis of the diazerine derivative of phenylalanine.

Bromobenzyl alcohol (**83**) is protected with *tert*-butyldimethylsilyl chloride in good yield to give **84**. Reaction of **84** with *n*-butyllithium results in a lithium halogen exchange and subsequent reaction with trifluoroacetic anhydride gave **85** in moderate to good yield. The ketone on **85** is converted to an oxime through reaction with hydroxylamine hydrochloride in the presence of pyridine to give **86**. The resultant oxime alcohol is converted to a good leaving group by transformation into a tosylate through the reaction of tosyl chloride in the presence of DIPEA and DMAP to give **87**. A diaziridine ring is formed through the reaction of liquid ammonia to afford **88**. Conversion of the diaziridine to the corresponding diazine (**89**) was achieved through oxidation with iodine. The benzyl alcohol is deprotected with *tetra*-butylammonium fluoride to give **90**. Conversion of the alcohol of **90** to an iodide using methyltriphenoxyposphonium iodide. An anion was made at the glycine alpha-hydrogen of **92** by treatment with sodium hydroxide. Upon formation of the anion, **91** was introduced via an S<sub>N</sub>2 reaction to afford the chiral nickel complex (**93**). Acid hydrolysis of **93** resulted in the unprotected L-phenylalanine (**94**). Protection of the amino group with Fmoc was achieved through reaction with Fmoc-OSu to afford the desired Fmoc-L-phenylalanine (**95**).

To ensure that there was a handle available for fluorescent functionalization, four analogues of neopetrosiamide were prepared containing commercially available derivatives of phenylalanine at position one or position two (Figure 33).

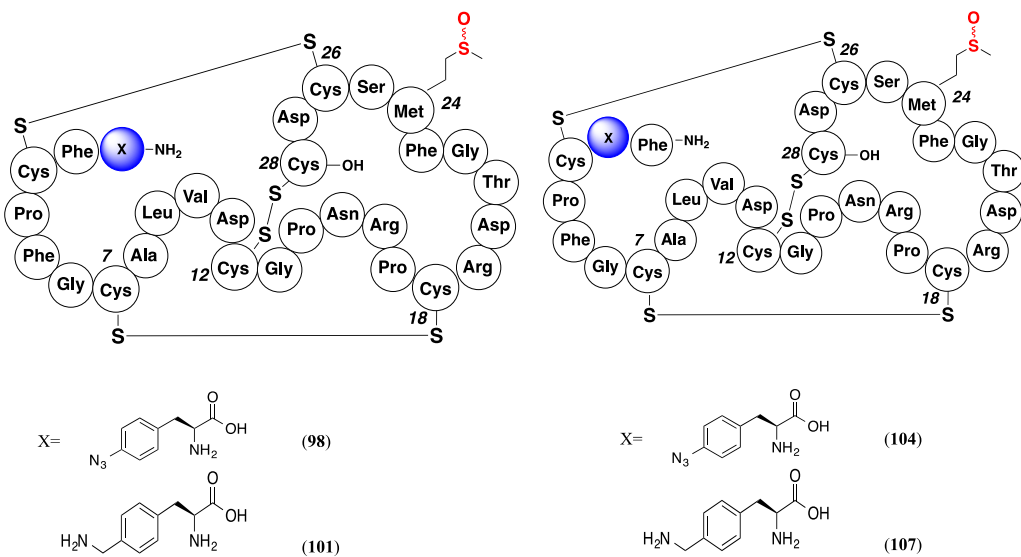


**Figure 34- Phenylalanine 1 and phenylalanine 2 analogues that provide a synthetic handle for fluorescent labeling of neoptrosiamide.**

Activity testing of compound **98**, **101**, **104** and **107** resulted in inhibition of MDA-MB-231 cells through the matrigel. Compound **98** displayed slightly reduced activity in comparison to **101**, **104**, and **107**. The activity observed is somewhat unexpected when the three dimensional structure of neopetrosiamide is inspected. Phe1 and Phe2 are spatially close to M(O)24 (Figure 34). Our previous hypothesis suggested that disruption of the hydrophobic face of the peptide, specifically of interference with the ability of methionine sulfoxide at position 24 to interact with its biological receptor, would lead to reduced activity. The amino acid side chains of the phenylalanine residues at position 1 and position 2 appear to be pointing away from the methionine sulfoxide, suggesting that despite the spatial proximity of these residues, little disruption in biological activity is observed.

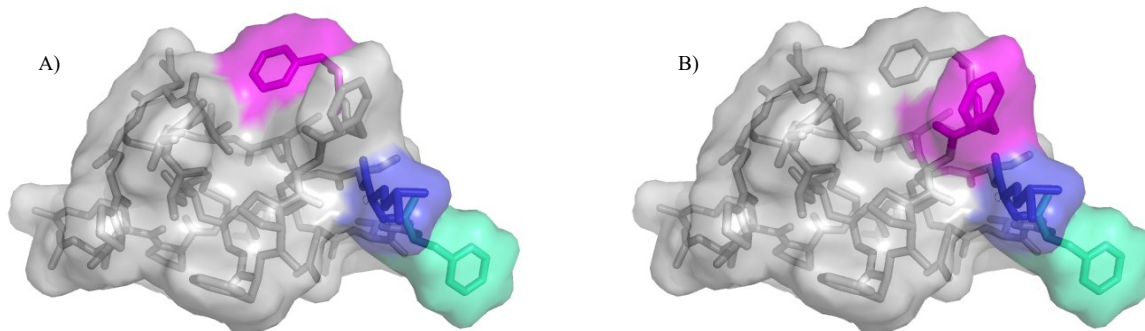


**Figure 35- Spatial orientation of A) Phe1, Met(O)24, and Phe23 and B) Phe2, Met(O)24, and Phe23. The backbone residues are color coded grey, amino acids of particular interest are colored explicitly as follows: A) Phe1, magenta; B) Phe2, magenta; Me(O)24, blue; and Phe23, teal.**

With active neopetrosiamide analogues in hand, **58**, **98**, **101**, **104**, and **107**, as well as the photoaffinity linker, **95**, analogues of neopetrosiamide containing modifications at Phe1/2 and

Phe23 can be made. Fmoc-SPPS of the linear peptide was underway, however, **95** proved problematic to couple to the solid phase resin. Further studies are needed to understand the forces behind the difficult incorporation of **95** during solid phase peptide synthesis.

### 5.2.7 Plasma Stability Assay of Neopetrosiamide

The stability of neopetrosiamide in mouse blood plasma was investigated to gain further insight on how these peptides might act in vivo. Natural neopetrosiamide was synthesized as described above. The synthetic neopetrosiamide was incubated in mouse blood plasma for 30 seconds. The sample was delipidated by running the sample through C8 resin from the SPE phenomenex cartridges. Following successive washes with water, to remove water soluble contaminants, the peptide was eluted with 60 % MeCN: H<sub>2</sub>O. The elution fraction was treated with TCEP to reduce the disulfide bonds and injected in LC-MS/MS to analyze fragmentation. Two fragments, a major cleavage product and minor cleavage product, of neopetrosiamide were found (Figure 35).

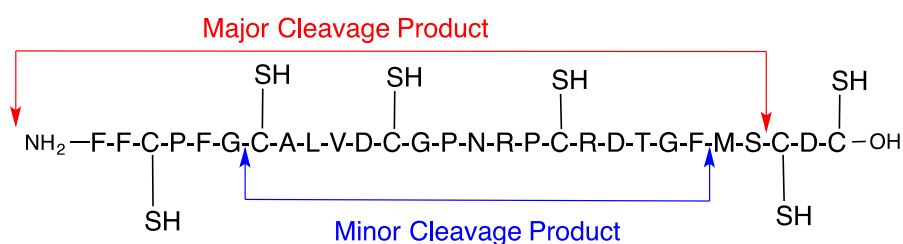


**Figure 36- Fragments observed by LC-MS of neopetrosiamide after incubation with mouse blood plasma.**

### ***5.2.8 Folding studies on Neopetrosiamide***

Protein folding is the physical process of a protein or peptide adopting a native 3-dimensional structure in a conformation that is biologically active. Hydrophobic interactions, hydrogen bonding, and van der Waals forces typically drive this spontaneous process. The process of protein and peptide folding can be described by the energy landscape theory. This theory describes a process in which proteins and peptides undergo rapid folding, unfolding and re-folding to obtain the lowest energy conformation. The lowest-energy state, often called the native state, is where proteins and peptides are most stable. Over time it has become apparent that some proteins and peptides require additional factors such as chaperone proteins, specific solvent environments like lipid bilayers, temperature, and correct pH ranges to assume the correct fold.

Our initial studies with synthetic neopetrosiamide A and B revealed that the predisposed disulfide connectivity between cysteine residues is not the correct disulfide pattern required for biological activity. Synthesis of neopetrosiamide A and B is exceedingly time consuming due to the need to use orthogonal protection/deprotection strategies to sequentially form disulfide bonds. It was proposed that performing global oxidation of the cysteine residues in the presence of a structure inducing solvent may lead to the correctly folded, biologically active peptide.

Linear, unprotected neopetrosiamide was dissolved in water, 1:1 mixtures of trifluoroethanol:water and 1:1 mixtures of methanol:water. To promote the formation of the disulfide bonds, a mixture of 1:8 of cysteine/cystine was added to the various solutions.

Reactions were monitored through HPLC and in each case, the undesired connections of disulfides were observed ( $t_R=11$  min).

Further literature investigation of other small disulphide rich peptides revealed that chaotropic salt concentration greatly aids in the folding of disulfide-rich peptides.<sup>178,179</sup> To test the effect of chaotropic salts to the overall disulfide formation in neopetrosiamide, four tandem experiments were set up with varying amounts of guanidinium hydrochloride. It was found that at 1 M guanidinium hydrochloride the ratio of correctly folded to incorrectly folded peptide was 1:1. This represents a major breakthrough in the synthesis of neopetrosiamides.

### **5.3 Conclusions and Future Outlook**

The synthesis of 15 neopetrosiamide analogues with substitutions at M(O)24 and sequential disulfide replacement analogues were prepared and tested for activity against the metastatic cancer cell line MDA-MB-231. Three of the analogues, **25**, **31**, and **43**, displayed partial activity, while the remaining 12 analogues resulted in complete abolishment of biological activity. These results suggest that the methionine sulfoxide at position 24 is critical for the inhibition of cancer cell migration, though the exact mode of action remains unknown. Furthermore, the three disulfide bonds present are essential for biological activity, indicating that neopetrosiamide has a highly compact and specific tertiary structure needed for biological activity.

Attempts to identify the biological receptor of neopetrosiamide have led to four additional active analogues with derivatives of phenylalanine located at position one or position

two. Attempts to incorporate the photoactive phenylalanine were unsuccessful and optimization of reaction conditions is required to incorporate this unnatural amino acid.

Neopetrosiamides are surprisingly unstable in mouse blood plasma, indicating that they could be unstable *in vivo*. Two degradation products were observed. The major cleavage product extended from the N-terminus to Ser25, indicating a cleavage site between Ser25 and Cys26. The minor degradation product was found to be a segment of neopetrosiamide between Cys7 and Phe23. The protease or proteases responsible have not yet been identified.

A major advancement in the synthesis of neopetrosiamide is the realization that biologically active peptide can be isolated from a global oxidation of all cysteine residues in the presence of guanidinium chloride, a chaotropic salt. This discovery opens new doors for further research into neopetrosiamides in that the material is more easily accessible.

There remain many unanswered questions about the mode of action of these peptides. The unique biological activity observed makes it desirable to further explore mode of action of neopetrosiamides. Furthermore, identification of the proteases responsible for degradation of neopetrosiamides could provide valuable insight into making neopetrosiamide more stable *in vivo*. The potent anti-metastatic activity observed upon the treatment of cells with neopetrosiamides has somewhat overshadowed the fact that neopetrosiamide may, in fact, be antimicrobial. It would be interesting to test this peptide against a suite of Gram-positive and Gram-negative bacterial strains to see what antimicrobial activity is present.

## **Chapter Six: Overview and Summary of Thesis Work**

Biologically active peptides are an important class of natural products in that they have a broad spectrum of activity ranging from antimicrobial to pathogenic to anti-metastatic properties. Understanding the structure of these peptides sheds light on potential modes-of-action and reveals privileged structural motifs favoured in nature. In this thesis, structural studies of antimicrobial peptides and peptide based virulence factors are discussed. In addition, synthetic modifications to the antimicrobial peptide, subtilisin A, are examined in relation to crystallographic studies. Finally, structure-activity-relationship studies on the anti-metastatic peptide, neopetrosiamide are explored and biological testing of the resulting analogues are discussed.

The structural characteristics of the leaderless bacteriocin, enterocin 7B, have been explored. Through this work, a connection between the structures of some leaderless and circular bacteriocins was discovered, leading to the hypothesis that these classes of bacteriocins may share a similar pore forming mode of action. Recent genomic studies have shown that garvicin ML, a circular bacteriocin, has a receptor on the bacterial membrane surface. Our attempts to grow bacterial mutants immune to enterocin 7 were unsuccessful. New methods of generating bacterial mutants are currently being explored.

The exact stereochemistry of the thioether bonds in subtilisin A remains uncertain as the calculated lowest energy NMR solution structures suggest that the LDD and DDD structure are

both close in energy. Attempts to link subtilisin A to a crystallizable protein through non-covalent interactions have been unsuccessful, and we are currently developing a method for covalent attachment of subtilisin A to carbonic anhydrase. Upon covalent attachment, the bioconjugate will be sent to collaborators for crystallography studies. Previously, subtilisin A has been found to degrade at pH > 5. While it is unknown what the exact structure of the degraded peptide is, the MALDI-TOF spectra indicates a net mass increase of +6. The degradation of the peptide has been reduced upon the addition of high concentrations of salt buffer, specifically phosphate buffer saline.

Phenol-soluble modulins are potent virulence factors produced by *Staphylococcus aureus*. Our work has shown that there are some limited structural similarities between the larger,  $\beta$ - type PSMs and the linear bacteriocins that were first predicted by Cintas and coworkers in 1998. The implication of this is not well understood at this time. The structural characterization of the  $\alpha$ -type PSMs has shown a similar tertiary structure. Our work has shown that previous models proposed for PSM $\alpha$ 3, which attributed physical characteristics to the hydrophobic and hydrophilic face of the peptide, were oversimplified and that the modes-of-action for cytolysis, biofilm formation, inflammation and antimicrobial activity are much more complicated than originally thought.

Neopetrosiamides are anti-metastatic peptides that were isolated from the marine sponge, *Neopetrosia* sp. These peptides have been shown to inhibit the amoeboid and mesenchymal migration of cancer cells through the basement membrane mimic, Matrigel. The mechanism-of-action remains unknown though we have shown that the secondary and tertiary structure is

highly sensitive to amino acid substitutions. We have investigated the sensitivity of amino acid substitution at the methionine sulfoxide at position 24 as well as the amenability of fluorescently labeling the peptide with various fluorescent labels. In the majority of the substitutions, the resultant analogues were inactive. We investigated the stability of this peptide in mouse plasma and found that it was degraded by unknown proteases quickly, despite the compact nature of the peptide due to the 3-disulfide bonds present. We were able to simplify the synthesis of the peptide by screening solvent conditions that favoured the correct disulfide formation during global oxidation reactions.

Structural studies on peptides remains an important area of research to gain a greater understanding of interactions of the individual peptides with their respective biological receptors. With greater understanding of the biological interactions taking place, synthetic chemistry can be used to improve peptide stability, bioavailability and enhance desirable biological activities. As demonstrated by this thesis, peptide chemistry is a growing area of interest for therapeutic applications.

## **Chapter Seven: Methods and Materials**

### **7.1 General Experimental Details**

#### ***7.1.1 Reagents and Solvents***

All commercially available reagents and solvents were purchased from the Aldrich Chemical Company Inc. (Madison, WI), Sigma Chemical Company (St. Louis, MO), Fisher Scientific Ltd. (Ottawa, ON) or Caledon (Georgetown, ON). All protected amino acids and SPPS resins were purchased from the Calbiochem-Novabiochem Corporation (San Diego, CA), Sigma-Aldrich Canada Ltd. (Oakville, ON), Chem Impex International Inc. (Wood Dale, IL) or VWR International (Mississauga, ON). All reagents and solvents were of American Chemical Society (ACS) grade and used without further purification. Reagents used in cell biology were purchased from Mediatech Inc. (Manassas, VA), ATCC (Manassas, VA) and GIBCO (Grand Island, NY).

#### ***7.1.2 General Techniques for Microbiological Work***

##### **7.1.2.1 Preparation of Media**

All media and media components were purchased from Becton Dickinson and Company (BD, Franklin Lakes, NJ, USA), unless otherwise indicated. Liquid media was prepared according to to manufacturers' instructions. Hard agar plates (1.5 % agar, w/v) were prepared by boiling the desired amount of agar in the applicable liquid media. The agar solution was autoclaved and aliquoted into 10 cm petri dishes (20 mL per plate) in a laminar flow hood and allowed to cool. The plates were stored at 4 - 8 °C until used. In the event that an antibiotic solution was added to the hard agar, the autoclaved agar solution was cooled to 55 °C prior to the addition of the antibiotic solution, the resultant plates were stored in the absence of light

(wrapped in aluminum foil) at 4 - 8 °C until used. Soft agar tubes (0.75 % agar, w/v) were prepared by boiling the desired amount of agar in the appropriate liquid media. The molten agar solution was aliquoted into 5 mL portions in screw-top tubes and autoclaved.

#### **7.1.2.2 Glycerol Stocks**

Glycerol stocks were used to maintain strains of bacteria. Glycerol (250 µL) was autoclaved in cryovials and the resulting sterile glycerol was mixed with a fresh bacterial culture (1000 µL) for a final concentration of 20 % glycerol. The stocks were stored at -80 °C and steps to minimize exposure to room temperature during subsequent inoculations were taken. Using aseptic technique, liquid cultures were inoculated by transferring a small amount of the frozen glycerol stock into the media using a sterile pipet tip.

#### **7.1.2.3 Antimicrobial Testing through Spot-on-Lawn Assays**

Soft agar (0.75 % agar, w/v) tubes in the appropriate liquid media were warmed in boiling water until a molten solution was obtained. The resultant molten agar was cooled to 55-60 °C and supplemented with fully-grown overnight liquid cultures of the indicator organism (100 µL). Subsequently, the solution was briefly vortexed and poured over a hard agar plate (20 mL; 1.5 % agar, w/v) of the same medium. Suspensions of the desired antibiotic/bacteriocin were pipetted onto the hardened surface (10 µL) and allowed to evaporate. Once samples had evaporated, the plates were capped and sealed with parafilm. Upon incubation overnight at an appropriate temperature for the indicator organism, the activity of the sample solution was judged based on the size and clarity of the zone of clearing.

#### **7.1.2.4 Cell Lysis**

##### **7.1.2.4.1 Cell Lysis with Cell Disrupter**

A TS series benchtop cell disrupter (Constant Systems Ltd, Low March, UK) was used to lyse bacterial cells. The cell disrupter was prepared by passing through 20 mL of the desired lysis buffer at 5 kpsi. Next, the bacterial cells were suspended in lysis buffer and passed through the system at 25 kpsi and the lysate was collected. The system was cleaned with 20 mL of lysis buffer which was passed through the disrupter at 25 kpsi and the flow through was collected and pooled with the lysate.

#### ***7.1.3 General Chromatographic Purification of Peptides and Proteins***

##### **7.1.3.1 Amberlite XAD-16 Hydrophobic Interactions Chromatography**

Amberlite XAD-16 resin (Sigma-Aldrich, St. Louis, MO, USA; usually 25- 40 g per liter of culture supernatant) was soaked in isopropanol for 15- 30 min. The resin slurry was poured into a glass column fitted at the base with Miracloth (EMD Millipore, Billerica, MA, USA), and the isopropanol was passed through the resin without letting the column run dry. The resin was then washed at 10 mL/min with 250 mL of 0.1 % trifluoroacetic acid (TFA) in water per 30 g resin. The column was stored under a volume of 0.1 % TFA until use. The solvent conditions and flow rates used are specific to the bacteriocin of interest and the solvent conditions and flow rates will be described below.

##### **7.1.3.2 C18 Solid-Phase Extraction Cartridges**

Both Strata C18-E (Phenomenex, Torrance, CA, USA) and Megabond C18 (Agilent, Santa Clara, CA, USA) solid-phase extraction (SPE) cartridges were used interchangeably.

These cartridges were pre-conditioned at 10 mL/min with 50 mL of methanol followed with 100 mL of Milli-Q water. Flow rates were controlled using a peristaltic pump.

#### **7.1.3.3 C8 Solid-Phase Extraction Cartridges**

Strata C8-E (Phenomenex, Torrance, CA, USA) cartridges were pre-conditioned at 10 mL/min with 50 mL of methanol followed with 100 mL of Milli-Q water. Flow rates were controlled using a peristaltic pump.

#### **7.1.3.4 HPLC**

All peptide compounds were purified to homogeneity using high-pressure liquid chromatography (HPLC). Separations were performed on Beckman System Gold chromatographs (analytical and preparative), a Varian Prostar Model 210 systems (analytical and preparative) and a Gilson system with a model 322 HPLC pump (preparative). A Millipore carbon filter removed small debris and dust from HPLC grade solvents prior to use. The solvents and gradients will be described below.

#### **7.1.3.5 Fluorescence Experiments**

Fluorescence of fluorescein was recorded on a 75 XE Photon Technology International (PTI) MP1 Fluorescence System. The excitation wavelength was set to 435 nm and the emission wavelength was set to 506 nm. All slits were open 1 mm and data was recorded every second. Data was recorded using Felix32 software and analyzed using Microsoft Excel.

## **7.1.4 Characterization of Proteins, Peptides and Small Molecules**

### **7.1.4.1 MALDI-TOF MS**

Matrix-assisted laser desorption ionization-time of flight mass spectrometry (MALDI-TOF MS) was performed on an AB Sciex Voyager Elite system (Foster City, CA, USA). Matrices 3,5- dimethoxy-4-hydroxycinnamic acid (sinapinic acid) and 4-hydroxy- $\alpha$ -cyanocinnamic acid (HCCA) were used with a two-layer sample preparation method. The AB Sciex Voyager Elite system was operated in positive reflection mode with delayed extraction or linear

### **7.1.4.2 LC- ESI MS**

Liquid Chromatography electrospray ionization mass spectrometry, (LC-ESI MS), was performed on an Agilent Technologies 1260 HPLC with G6130B MSD (Santa Clara, CA USA). Samples were ionized via ESI and monitored in positive mode.

### **7.1.4.3 HR-ESI MS**

High-resolution electrospray ionization mass spectrometry (HR-ESI MS) was performed on an Agilent Technologies 6220 oaTOF (Santa Clara, CA, USA). Samples were ionized via ESI and monitored in positive mode.

### **7.1.4.4 EI MS**

Electron impact mass spectrometry was performed on a Kratos MS50G Analytical (Dewsbury, West Yorkshire, UK). Samples were ionized via electron impact and monitored in positive mode.

#### **7.1.4.5 NMR Spectroscopy**

Spectral data were collected on several different nuclear magnetic resonance (NMR) spectrometers. At the University of Alberta Department of Chemistry, a Varian Inova 600 MHz spectrometer (equipped with a triple-resonance HCN cold probe) and a Varian VNMRS 700 MHz spectrometer (equipped with a triple-resonance HCN probe and Z-axis pulsed-field gradients) were used. Data were also acquired at the National High Field Nuclear Magnetic Resonance Centre (NANUC) on a Varian Inova 800 MHz spectrometer equipped with a triple-resonance HCN cold probe and Z-axis pulsed-field gradients.

#### **7.1.4.6 SDS-PAGE Gel Characterization**

The protein content in samples was analyzed using SDS-PAGE, either with a 10 % resolving gel topped with a 4 % stacking gel, or using a commercial 4 – 20 % Mini- PROTEAN TGX precast gel (Bio-Rad, Hercules, CA, USA). Protein samples were prepared in 2 X Laemmli Sample Buffer (Bio-Rad) and boiled at 100 °C for 10 min. Samples run on a PAGE gel containing a stacking gel were run at a voltage of 50 V for 30 min and then 180 V until the dye front reached the bottom of the gel. The 4 – 20 % commercial gels were run at 180 V until the dye front reached the bottom. Gels were rinsed for 3 x 5 min in fresh Milli-Q water, and then submerged and shaken in GelCode Blue Stain reagent (Pierce, Rockford, IL, USA) for 60 min. After decanting the stain, the gel was left in Milli-Q water overnight and scanned.

#### **7.1.4.7 Native PAGE Gel Characterization**

The protein content in the samples was analyzed using a native PAGE gel with a 10 % resolving gel and 6 % stacking gel. The stacking gel was prepared in the following manner; 2.0

mL of acrylamide/Bis-acrylamide (30 % / 0.8 %, w/v) was diluted in 7.89 mL of 0.375 M Tris-HCl (pH= 8.8). To induce cross-linking, 100  $\mu$ L of 10 % ammonium persulfate (w/v) and 10  $\mu$ L TEMED were mixed into the acrylamide solution. The resolving gel was prepared in the following manner; 3.4 mL of acrylamide/Bis-acrylamide (30 % / 0.8 %, w/v) was diluted in 6.49 mL of 0.375 M Tris-HCl (pH= 8.8). To induce cross-linking, 100  $\mu$ L of 10 % ammonium persulfate and 10  $\mu$ L TEMED were mixed into the acrylamide solution. Once the gel had been cast, the sample solutions were mixed 1:1 with 2x Sample buffer (62.5 mM Tris-HCl, pH= 6.8; 25 % v/v glycerol; 1 % bromophenol blue). Samples run on the PAGE gel were run at 80 V until dye had reached the bottom of the stacking layer and then at 120 V until the dye had reached the bottom of the resolving gel. Gels were rinsed for 3 x 5 min in fresh Milli-Q water, and then submerged and shaken in GelCode Blue Stain reagent (Pierce, Rockford, IL, USA) for 60 min. After decanting the stain, the gel was left in Milli-Q water overnight to destain and scanned for records.

### ***7.1.5 General Solid Phase Peptide Synthesis Conditions***

#### **7.1.5.1 General Procedure for Automated Solid Phase Peptide Synthesis (SPPS) using ABI 433A**

The peptide synthesis was completed on preloaded resin using an ABI-433A peptide synthesizer (Applied Biosystems) with UV monitoring capability (Perkin Elmer), detecting at 301 nm using standard *FastMoc* 0.1 mmol protocol. In the method employed, 10 equivalents of Fmoc amino acids were used with respect to the resin loading. Peptide couplings were done by mixing a solution of Fmoc-amino acid (in NMP) with a solution of HBTU, HOBt and DIPEA in DMF and pre-activated for 2.1 minutes. The activated solution was then transferred to the pre-

swelled resin and allowed to react for 9.3 minutes. End capping was performed with a solution of Ac<sub>2</sub>O, HOBt and DIPEA in NMP. Removal of the Fmoc group was done by using 22% piperidine in NMP and monitored by the absorption of dibenzofulvene-piperidine adduct at  $\lambda = 301$  nm on a UV-Vis spectrophotometer. The overall coupling cycle time for each amino acid was approximately 50 minutes. The following side chain protecting groups were employed for the peptide synthesis: Fmoc-Cys(Acm)-OH, Fmoc-Cys(Trt)-OH, Fmoc-Cys(*t*-Bu)-OH, Fmoc-Asp(*t*-Bu)-OH, Fmoc-Ser(*t*-Bu)-OH, Fmoc-Thr(*t*-Bu)-OH, Fmoc-Asn(Trt)-OH, Fmoc-Arg(Pmc)-OH. For cleavage, the resulting peptidyl resin was treated with a fresh mixture of TFA: Thioanisole: EDT: Anisole (90: 5: 3: 2, v/v/v/v, 10 mL/g peptidyl resin) for 1.5 – 2 h at room temperature. The solution was then filtered through a plug of cotton into cold diethyl ether. The white precipitate was collected by centrifugation and washed with cold ether. The crude peptide was then purified by RP-HPLC. Fractions containing the appropriate mass by MALDI-TOF MS were pooled, concentrated, lyophilized and re-purified to homogeneity.

## **7.2 Experimental Procedures for the Structural Characterization of Enterocin 7B, a Leaderless Bacteriocin.**

### **7.2.1 Isolation of Enterocin 7B (4)**

fM-G-A-I-A-K-L-V-A-K-F-G-W-P-F-I-K-K-F-Y-K-Q-I-M-Q-F-I-G-Q-G-W-T-I-D-Q-I-E-K-W-L-K-R-H

The purification of enterocin 7B was based on literature procedures with some modifications. *Enterococcus faecalis* 710C was grown in 100 mL of APT broth at 37 °C without shaking. This starter culture was used to inoculate (5 % inoculum, v/v) a 1 L batch of APT broth. Incubation of the resultant broth at 37 °C without shaking for 22 h lead to the production of

enterocin 7B. The cells were pelleted using a centrifuge (5,000 g, 10 min, 4 °C) and the supernatant was collected. SP Sepharose Fast Flow resin (20 mL) was loaded into a glass column and the base was fitted with Miracloth (EMD Millipore, Billerica, MA, USA). This resin was pre-equilibrated with 20 mM sodium phosphate, pH 6.9 and the resultant culture supernatant was passed, 1 mL/min, through the column. The column was washed with 100 mL of: (1) 20 mM sodium phosphate, pH 6.9, (2) 20 mM sodium phosphate, pH 6.9, with 0.2 M NaCl, and (3) 20 mM sodium phosphate, pH 6.9, with 1.0 M NaCl. The fraction containing 1.0 M NaCl was desalted using a preconditioned Bond Elut C18 solid-phase extraction cartridge (Agilent; 10 g, 60 mL). After passing the 1.0 M NaCl fraction through the cartridge at 5 mL/min, it was washed with 50 mL of: (1) 30 % ethanol, (2) 30 % acetonitrile, (3) 40 % isopropanol, and (4) 80 % isopropanol with 0.1 % TFA. The 80 % isopropanol with 0.1 % TFA fraction was concentrated on a rotary evaporator down to 10 mL. Enterocin 7B was purified to homogeneity using reverse-phase HPLC. A analytical C18 column was used (VYDAC 218TP54; 4.6 mm x 250 mm, 5 µm paritical size, 300 Å) with mobile phases A (water with 0.1 % TFA) and B (acetonitrile with 0.1 % TFA) at a flow rate of 1 mL/min, and detection at 220 nm. The solvent gradient started at 30 % B for 5 min, then increased to 71 % B over the course of 26 min. Enterocin 7B eluted after 25 min using this method. The identity of enterocin 7B was confirmed using MALDI –TOF spectrometry, [M+H]= 5206.

### ***7.2.2 Circular Dichroism***

An Olis DSM 17 CD spectrophotometer was used to acquire the CD spectra of enterocin 7B. Solutions of enterocin 7B were prepared (100 µL; 0.8 mg/mL) in unbuffered water, 20 mM

phosphate buffer (pH=7.0), and 50 % TFE in water. Each sample was analyzed in a 02 mm quartz cuvette. Enterocin 7B showed  $\alpha$ - helicity in each sample.

### 7.2.3 NMR Spectroscopy

A 0.8 mM solution of enterocin 7B was made by dissolving the peptide in 300  $\mu$ L of 90 % H<sub>2</sub>O and 10 % D<sub>2</sub>O. DSS was added to the sample to give a final concentration of 0.01 % and the final solution was transferred to a 5 mm Shegimi tube, with matched magnetic susceptibility to D<sub>2</sub>O. TOCSY, NOESY, DQF- COSY, <sup>13</sup>C-HSQC, and <sup>15</sup>N-HSQC data sets were acquired on a Varian VNMRS 700 MHz spectrometer at 27 °C. The water signal was suppressed using transmitter presaturation. Additional experimental details can be found in Table 6.1. All data sets were processed with NMRPipe and analyzed using NMRViewJ. Proton chemical shift assignments were assigned using the TOCSY, NOESY and DQF-COSY datasets (Table 6.2), all chemical shift assignments have been deposited in the BioMagResBank (accession number 19101).

**Table 6.1- Experiment Parameters of NMR Spectroscopic Data for Enterocin 7B**

<b>Ent7B</b>	<b>Sweep width (Hz) (t1, t2)<sup>a</sup></b>	<b>ni</b>	<b>np</b>	<b>nt</b>	<b>Mix time</b>
<b>dpgse- NOESY<sup>b</sup></b>	9765, 9765	448	8192	32	150 ms
<b>zTOCSY</b>	10000, 10000	448	8192	32	50 ms
<b><sup>15</sup>NHSQC</b>	9765, 2500	48	1640	512	
<b>gCOSY</b>	10000, 10000	512	20000	16	

<sup>a</sup> Directly and indirectly detected dimensions respectively. “ni” is the number of complex points collected for the indirectly detected dimension, while “np” is the number of real + imaginary points for the directly detected dimension. “nt” is the number of cumulative scans collected for each point of acquisition. The carrier position was empirically determined from the minimal residual HOD signal using a saturation effective field of ~ 80 Hz induced field strength and 2.5 seconds in length. The optimal 90° pulse width was determined using a nutation experiment.<sup>180</sup>

<sup>b</sup> 5 ms sinc shape pulses

**Table 6.2- Chemical Shift Assignment of Enterocin 7B**

		<b>HN</b>	<b>H<math>\alpha</math></b>	<b>H<math>\beta</math></b>
<b>Formyl</b>				8.24
<b>Met 1</b>	8.67	4.52	2.15, 2.09	$\gamma$ CH <sub>2</sub> 2.73, 2.62
<b>Gly 2</b>	8.84	4.01		
<b>Ala 3</b>	8.20	4.14	1.44	
<b>Ile 4</b>	7.96	3.81	2.21	$\gamma$ CH <sub>3</sub> 1.04, $\gamma$ CH <sub>2</sub> 1.64, 1.51, $\delta$ CH <sub>3</sub> 0.77
<b>Ala 5</b>	7.98	4.05	1.51	
<b>Lys 6</b>	7.77	4.11	2.03, 1.89	$\gamma$ CH <sub>2</sub> 1.72, 1.65, $\delta$ CH <sub>2</sub> 1.59, 1.44, $\epsilon$ CH <sub>2</sub> 2.95
<b>Leu 7</b>	8.15	4.31	2.29	$\gamma$ CH 2.13, $\delta$ CH <sub>3</sub> 1.58, 1.11
<b>Val 8</b>	9.01	3.38	2.05	$\gamma$ CH <sub>3</sub> 0.69, 0.72
<b>Ala 9</b>	7.84	4.13	1.52	
<b>Lys 10</b>	7.18	4.13	1.68, 1.51	$\gamma$ CH <sub>2</sub> 0.81, 0.65, $\delta$ CH <sub>2</sub> 1.42, 1.36, $\epsilon$ CH <sub>2</sub> 2.78, 2.69
<b>Phe 11</b>	8.43	4.56	3.32, 2.94	$\delta$ CH 7.35, $\epsilon$ CH 7.19, $\zeta$ CH 7.30
<b>Gly 12</b>	8.66	4.65, 4.04		

<b>Trp 13</b>	9.27	4.89	3.40	$\delta_1\text{CH}$ 7.30, $\varepsilon_1\text{NH}$ 10.17, $\zeta_2\text{CH}$ 7.42 $\eta_2\text{CH}$ 6.96, $\zeta_3\text{CH}$ 7.65, $\varepsilon_3\text{CH}$ 6.87
<b>Pro 14</b>			2.29, 2.04	$\gamma\text{CH}_2$ 2.35, 1.92, $\delta\text{CH}_2$ 4.06, 3.98
<b>Phe 15</b>	8.10	4.29	3.36, 3.01	$\delta\text{CH}$ 7.20, $\varepsilon\text{CH}$ 7.15, $\zeta\text{CH}_3$ 7.23
<b>Ile 16</b>	7.63	3.75	2.31	$\gamma\text{CH}_3$ 1.00
<b>Lys 17</b>	9.00	3.53	1.17, 0.95	$\gamma\text{CH}_2$ 1.44, 1.18
<b>Lys 18</b>	7.26	3.79	1.52, 1.42	$\gamma\text{CH}_2$ 1.01, 0.513, $\delta\text{CH}_2$ 1.36, $\varepsilon\text{CH}_2$ 2.73
<b>Phe 19</b>	7.16	5.04	2.93	$\delta\text{CH}$ 6.92, $\varepsilon\text{CH}$ 7.19, $\zeta\text{CH}$ 7.34
<b>Tyr 20</b>	7.39	3.76	3.37, 2.95	$\delta\text{CH}$ 6.98, $\varepsilon\text{CH}$ 6.86
<b>Lys 21</b>	8.43	3.74	1.79, 1.64	$\gamma\text{CH}_2$ 1.50, 1.30, $\varepsilon\text{CH}_2$ 2.95
<b>Gln 22</b>	7.91	3.33	1.89, 1.74	$\gamma\text{CH}_2$ 2.23, 1.14, $\varepsilon\text{NH}_2$ 7.17, 6.66
<b>Ile 23</b>	8.34	3.16	1.68	$\gamma\text{CH}_3$ 0.73, $\gamma\text{CH}_2$ 1.80, $\delta\text{CH}_3$ 0.97
<b>Met 24</b>	8.05	4.15	1.90, 1.76	$\gamma\text{CH}_2$ 2.33
<b>Gln 25</b>	7.42	3.85	1.98, 1.76	$\gamma\text{CH}_2$ 2.20, 1.64, $\varepsilon\text{NH}_2$ 6.94, 6.88
<b>Phe 26</b>	7.79	3.64	2.53, 2.23	$\delta\text{CH}$ 5.70, $\varepsilon\text{CH}$ 5.53, $\zeta\text{CH}$ 5.44
<b>Ile 27</b>	8.67	3.76	1.86	$\gamma\text{CH}_3$ 0.91, $\gamma\text{CH}_2$ 1.77, 0.78, $\delta\text{CH}_3$ 0.95
<b>Gly 28</b>	8.05	3.96		
<b>Gln 29</b>	7.63	4.45	2.10	$\gamma\text{CH}_2$ 2.48, $\varepsilon\text{NH}_2$ 7.03, 6.70
<b>Gly 30</b>	8.01	4.34, 3.92		
<b>Trp 31</b>	8.40	4.74	3.15, 2.63	$\delta_1\text{CH}$ 7.03, $\varepsilon_1\text{NH}$ 10.00, $\zeta_2\text{CH}$ 7.08, $\eta_2\text{CH}$ 6.44, $\zeta_3\text{CH}$ 5.87, $\varepsilon_3\text{CH}$ 6.49
<b>Thr 32</b>	8.51	4.52	1.39	
<b>Ile 33</b>	8.92	3.88	2.03	$\gamma\text{CH}_3$ 0.99, $\gamma\text{CH}_2$ 1.46, $\delta\text{CH}_3$ 0.98
<b>Asp 34</b>	8.23	4.41	2.60	
<b>Gln 34</b>	7.73	3.82	2.29	$\gamma\text{CH}_2$ 2.19, 1.99, $\varepsilon\text{NH}_2$ 6.69, 6.17
<b>Ile 36</b>	8.49	3.79	2.11	$\gamma\text{CH}_3$ 1.06, $\gamma\text{CH}_2$ 2.32, 0.95, $\delta\text{CH}_3$ 0.83
<b>Glu 37</b>	9.18	4.03	2.41, 2.28	$\gamma\text{CH}_2$ 2.99
<b>Lys 38</b>	8.05	3.97	1.90, 1.76	$\gamma\text{CH}_2$ 1.58, 1.44, $\delta\text{CH}_2$ 1.60, $\varepsilon\text{CH}_2$ 2.94
<b>Trp 39</b>	7.76	3.91	3.66, 3.39	$\delta_1\text{CH}$ 7.48, $\varepsilon_1\text{NH}$ 10.43, $\zeta_2\text{CH}$ 7.30 $\eta_2\text{CH}$ 6.80, $\zeta_3\text{CH}$ 6.19, $\varepsilon_3\text{CH}$ 7.02 $\delta\text{CH}_3$ 0.61, 0.98
<b>Leu 40</b>	9.11	3.67	1.94	$\delta\text{CH}_3$ 0.61, 0.98

<b>Lys 41</b>	7.98	4.23	2.10, 1.67	$\gamma\text{CH}_2$ 1.83,1.77
<b>Arg 42</b>	7.23	4.33	1.56	$\gamma\text{CH}_2$ 1.65, $\delta\text{CH}_2$ 3.09, $\epsilon\text{NH}$ 7.16
<b>His 43</b>	7.59	4.25	3.12, 2.24	$\delta_2\text{CH}$ 6.92, $\epsilon_1\text{CH}$ 6.19

### 7.2.4 Structure Calculations

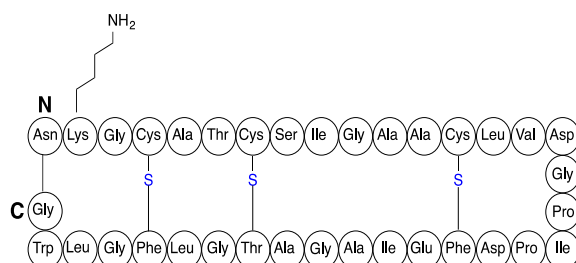
CYANA 2.1 was used for the structure calculations of enterocin 7B. Minimal manual NOE crosspeak assignments were made and automated NOE crosspeak assignment was completed by the CYANA program. NOE distance constraints were made by CYANA and based on signal intensity. CYANA employs an iterative structure calculation algorithm involving seven rounds of 10 000 steps per round. The final structure is an average of the 20 lowest energy structures calculated. The final structure calculation used 1005 NOE crosspeaks, of which 107 were long-range, 173 were medium-range and 355 were short-range. Coordinates for the final structure were deposited in the Protein Data Bank (accession number 22m60).

## 7.3 Experimental Procedures for Subtilosin A

### 7.3.1 General HPLC Method for Subtilosin A

Peptides were purified on a C18 column (VYDAC, 208TP1010 4.66 mm x 250 mm, 5  $\mu\text{m}$  particle size, 300  $\text{\AA}$ ) using a flow rate of 3.0 mL  $\text{min}^{-1}$  and UV detection at 220 and 254 nm. Briefly, starting with a 6:4 ratio of mobile phase A (water with 0.1 % TFA) to mobile phase B (MeCN with 0.1 % TFA), the column was equilibrated for 5 min. Mobile phase B was then increased to 60 % over 10 min, and then 80 % over 15 min. The organic phase was held at 80 % for 2 minutes and then decreased to 40 % over 2 min. Mobile phase B was held at 40 % for 5 min to allow for column re-equilibration.

### 7.3.1.1 Isolation of Subtilisin A (5)



Subtilisin A was isolated and purified according literature procedures with minor modifications. Briefly, a 10 mL tube of sterile LB media was inoculated with *B. subtilis* JH642. Culture was allowed to grow overnight (37 °C, 225 rpm). From this tube, a new tube of LB (10 mL) was inoculated by transferring 50 µL of fully grown culture to the fresh media. The culture was grown for 7 h at 37 °C, 225 rpm, and then was used to inoculate 1 L of NSM broth to give a 1 % inoculum, v/v. The resultant broth was grown for 16 h at 37 °C, 225 rpm. The NSM broth was made according to the following specifications. 8.0 g of nutrient broth was dissolved in 1 L of MilliQ water. To this base, 0.5 g of MgSO<sub>4</sub> 7H<sub>2</sub>O, and 2.0 g of KCl was added. This mixture was autoclaved and allowed to cool. Once cooled, the following salts were added to the media to give 1.0 mM Ca(NO<sub>3</sub>)<sub>2</sub> 4H<sub>2</sub>O, 0.1 mM MnCl<sub>2</sub> and 1 µM FeSO<sub>4</sub> 7H<sub>2</sub>O. Subtilisin A was extracted from the overnight culture by adding 250 mL (25 % v/v) of *n*-butanol to the cell culture. The mixture was agitated in the incubator at 225 rpm for 1 h. The resulting mixture was poured into a large separatory funnel and allowed to settle overnight. The butanol layer was collected and concentrated *in vacuo*. A brown residue was obtained that was dissolved in methanol and purified using the RP-HPLC method described above.  $t_R = 20.0$  min. Approximately 2.5- 5.0 mg of subtilisin A was obtained per liter of culture.

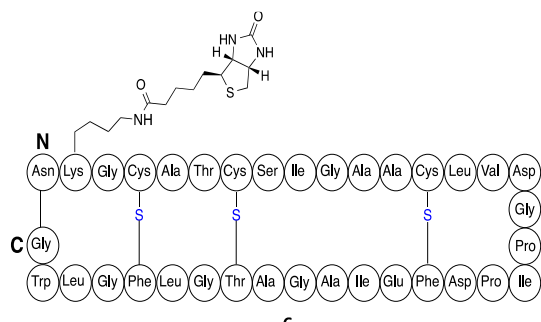
### 7.3.1.2 Capping with Cyclodextrin

Subtilosin A (**5**) (3.2 mg, 0.94  $\mu$ mole, 1 equiv.) was dissolved in a 1:1 mixture of MeCN:H<sub>2</sub>O.  $\alpha$ -cyclodextrin (4.5 mg, 4.7  $\mu$ mole, 5 equiv.) and  $\beta$ -cyclodextrin (5.3 mg, 4.7  $\mu$ mole, 5 equiv.) were added to the solution and the mixture was stirred overnight at room temperature. NMR analysis of the aqueous layer revealed a clean spectrum of  $\alpha$ -cyclodextrin and  $\beta$ -cyclodextrin but there was no discernible peaks attributed to subtilosin A.

### 7.3.1.3 Stability of Streptavidin to Various Organic Solvents

FITC-Streptavidin (5 mg, 83.3 nmole) was reconstituted in water (5 mL) to give a 1 mg mL<sup>-1</sup> stock solution. In 1.5 mL epindorfs, each organic solvent was added (450  $\mu$ L). To adjust the level of acidity of the organic solutions, trifluoroacetic acid was added and the pH was monitored using pH paper (Hydrion, Micro Essential Laboratory Inc. Brooklyn, NY, USA). Aliquots of Streptavidin (50  $\mu$ L) were added to each epindorf and incubated for 30 min. The fluorescence of each sample was taken using the general method for fluorescence detection described above. Following detection of initial fluorescence, each sample was inserted into a well of a 96-well plate coated with biotin. The solutions were incubated in the 96-well plate for an additional 15 min and the fluorescence recorded a second time.

### 7.3.1.4 Linkage of Subtilosin A with Biotin (7)



Subtilosin A (**5**) (3.2 mg, 1 equiv.) was dissolved in a 1:1 mixture of MeCN: PBS (30 mL) to give a final concentration of 0.1 mg mL<sup>-1</sup> at pH = 8. The NHS-ester of biotin (**6**) was added (0.4 mg, 1.4 equiv.) to the solution and the reaction mixture was stirred at 4 °C and monitored by MALDI-TOF spectroscopy. After 72 h, the reaction was determined to be 50 % done by MALDI-TOF. Compound (**7**) was purified using the general subtilosin A RP-HPLC method.  $t_R = 21.0$  min Calculated molecular weight for C<sub>137</sub>H<sub>201</sub>N<sub>36</sub>O<sub>39</sub>S<sub>6</sub> [M+H]<sup>+</sup> 3628 Found [M+H]<sup>+</sup> 3628.

### 7.3.1.5 Bioconjugation of Subtilosin A with Streptavidin

Compound (**7**) (7.8 mg, 2.14 μmole, 1equiv.) was dissolved in 1:1 MeCN : PBS (0.2 M, pH=8) Streptavidin (7.28 mg, 21.4 μmole, 10 equiv.) was added and the mixture was stirred at 4 °C and stirred for 96 h. Once the reaction was deemed to be complete by MALDI-TOF the pH of the solution was adjusted to 2 with 0.2 M HCl.

### 7.3.1.6 Purification of Subtilosin A Streptavidin Complex with HPLC

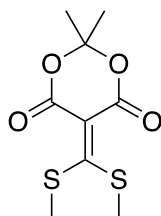
Using the general HPLC method described above the SubtilosinA-Biotin-Streptavidin complex was injected onto a C8 column. Multiple peaks present corresponding to Compound (**4**)

( $t_R = 20.0$  min), compound **(6)** ( $t_R = 21.0$  min), and unidentified fractions, and indicating decomposition of bioconjugate under RP-HPLC conditions.

#### 7.3.1.7 Purification of Subtilosin A using Amicon Tubes

An amicon tube (30 000 MWCO) was filled with 15 mL of 0.1 N NaOH and centrifuged for 20 min at 5000 x g. Remaining solution in the tube was decanted and the tube was filled with 15 mL MilliQ water. Centrifugation (5 000 x g, 20 min) afforded a tube with cleaned membrane, ready for sample purification. The crude mixture of compound **(6)** and streptavidin were concentrated *in vacuo* to remove acetonitrile present, and the resultant cloudy solution was diluted with fresh MilliQ water to a total volume of 15 mL. Following centrifugation (5 000 x g, 25 min), the resultant solution was given to collaborators to perform crystallization screens.

#### 7.3.1.8 Synthesis of Meldrum's Acid Derivative (8)



Meldrum's acid **(9)** (5.0 g, 35 mmol, 1 equiv.) was dissolved in 15 mL DMSO to afford a clear colorless solution. Triethylamine (7.08 g, 70 mmol, 2 equiv.) was added and the colorless solution turns bright yellow. Carbon disulphide (2.65 g, 35 mmol, 1 equiv.) is added and the reaction mixture is stirred for 2 h. Drop wise addition of the methyl iodide (9.93 g, 70 mmol, 2 equiv.) results in the reaction mixture becoming dark orange and eventually red. The reaction mixture is allowed to stir overnight. Ice is added to the reaction until a yellow precipitate is

formed. Vacuum filtration and subsequent recrystallization from methanol affords the title compound in 53 % yield (1.3 g). IR (CDCl<sub>3</sub>) 3000, 1728, 1680, 1410, 1310, 1280, 1040, 955 cm<sup>-1</sup>; <sup>1</sup>H-NMR (500 MHz, CDCl<sub>3</sub>) : 1.75 (s, 6H), 2.65 (s, 6H); <sup>13</sup>C-NMR (500 MHz, CDCl<sub>3</sub>): 21.3 (q), 26.6 (q), 102.9 (s), 103.0(s), 159.7(s), 192.3(8); EI-MS *m/z* 248 (17), 191 (15), 190 (17), 172 (35), 146 (29), 118 (29), 100 (27), 99 (98), 85 (21).

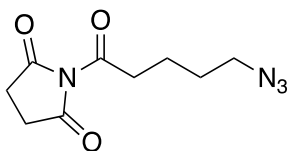
### 7.3.1.9 Linkage of Meldrums Acid Derivative to Subtilosin A and Carbonic Anhydrase (12)

5 mg of subtilosin A was dissolved in a 1:1 mixture of MeCN : PBS (0.2 M, pH= 7.2). Compound **8** was added portion wise ( 1 equiv. ) followed by addition of 1 equiv. of carbonic anhydrase. The reaction mixture was stirred over 72 h and monitored by HPLC. After 72 h, no reaction had taken place between subtilosin A and compound **8** as determined by HPLC and MALDI-TOF. The pH of the mixture was increased to 8 to see if the reaction could be driven forward, subtilosin A degraded ([M+H]<sup>+</sup>= 3406), and no detectable amounts of **12** was present.

### 7.3.1.10 Coupling of 5- Azido-2,5,-dioxo-1pyrrolidinyl Ester Linker to Subtilosin A (13)

8.6 mg of subtilosin A was dissolved in a 1:1 mixture of MeCN:PBS (0.2 M, pH=8). Crude mixture of compound (**14**) was added and the reaction mixture was stirred for 12 h. No reaction appeared to take place by MALDI-TOF. Expected [M+H]<sup>+</sup> = 4240 Found [M+H]<sup>+</sup> = 3406 *m/z*

### 7.3.1.11 Synthesis of 5- azido-2,5,-dioxo-1pyrrolidinyl ester (14).



To a solution of azidopentanoic acid (**15**) and *N*-hydroxysuccinamide (**16**) in DME at 0 °C, DCC was added and the reaction mixture was stirred at 0 °C for 1 h then placed at 4 °C for 12 h without stirring. The reaction mixture was filtered and concentrated in vacuo. The crude <sup>1</sup>H-NMR matched literature reports. DCU was difficult to remove and therefore crude linker was used in subsequent reactions without further purification.

## **7.4 Experimental Procedures for the Synthesis and Isolation of Phenol-soluble Modulins**

### **7.4.1 Synthesis of PSM $\alpha$ 1 and PSM $\alpha$ 3.**

#### **7.4.1.1 Manual Solid-phase Peptide synthesis of PSM $\alpha$ 1 and PSM $\alpha$ 3**

PSM $\alpha$ 1 and PSM $\alpha$ 3 were prepared through manual solid phase peptide synthesis (SPPS). The peptides were synthesized using a Wang resin on a 0.1 mmol scale utilizing a jacketed peptide synthesis reaction vessel. Coupling reactions were conducted using *N*-fluorenylmethyloxycarbonyl (Fmoc)-protected amino acids (5 equiv relative to resin loading) and activated with 1-[bis-(dimethylamino)methylene]-1*H*-1,2,3-triazolo[4,5-*b*]-pyridinium 3-oxide hexafluorophosphate (HATU) (4.9 equiv relative to resin loading) and diisopropylethylamine (DIPEA) (5 equiv relative to resin loading). Subsequent deprotection of the coupled amino acid was achieved using a 20 % piperidine solution in dimethylformamide (DMF). Because of ineffective deprotections of the last five and six residues (PSM $\alpha$ 1 and PSM $\alpha$ 3, respectively), deprotections were conducted using 20% piperidine in the “magic mixture” (1% Triton X-100 in a 1:1:1 DMF/NMP/DCM mixture at 60 °C). The coupling and deprotection reactions were monitored using the Kaiser test and matrix-assisted laser desorption ionization time-of-flight

mass spectrometry (MALDI-TOF MS). The peptides were cleaved from the resin using a 9.5:0.25:0.25 trifluoroacetic acid:triisopropylsilane:water (TFA:TIPS:H<sub>2</sub>O) ratio.

#### **7.4.1.2 Purification of PSM $\alpha$ 1 and PSM $\alpha$ 3**

Upon cleavage of the peptides from the resin, the crude peptide was dissolved in the minimum amount of dimethyl sulfoxide (DMSO) and diluted with water to give a volume:volume percent of 5 % DMSO in water. The solutions of crude peptide were partially purified through dialysis against water (20 h, 25 °C; molecular weight cutoff of 1000, Spectra/Por 7) followed by multiple iterations of reverse phase high-performance liquid chromatography (RP-HPLC) until the peptides were determined to be pure via MALDI-TOF MS. Briefly, for both PSM $\alpha$ 1 and PSM $\alpha$ 3, an analytical scale column (3.6  $\mu$ m particle size, 200 Å, 250 mm  $\times$  4.6 mm, Aeris Widepore C4, Phenomenex) was used with a 1 mL injection volume, a flow rate of 1.5 mL/min, and a detection wavelength set at 220 nm. A gradient of solvent A (0.1 % TFA in water) and solvent B (0.1 % TFA in isopropyl alcohol) was used. For PSM $\alpha$ 1, the level of solvent B was initially set to 40 % and held for 5 min. Over the next 20 min, the level of solvent B was increased to 95 % and held for an additional 5 min. For PSM $\alpha$ 3, the level of solvent B was initially set to 5 % and held for 5 min. Over the next 40 min, the level of solvent B was gradually increased to 60 % and then sharply increased to 95 % over 5 min. The level of solvent B was held at 95 % for 15 min. According to these gradients, PSM $\alpha$ 1 and PSM $\alpha$ 3 co-eluted with truncated peptides at 30 and 56 min, respectively. The peaks containing PSM $\alpha$ 1 and PSM $\alpha$ 3 were collected and injected for a second time using the same gradient as described above. Fractions of PSM $\alpha$ 1 determined to be pure through MALDI-TOF MS were

concentrated, lyophilized, and stored at  $-20\text{ }^{\circ}\text{C}$ . PSM $\alpha$ 3 was collected and injected for a third time following the same gradient as described above, and the fractions determined to be most pure by MALDI-TOF MS were concentrated under vacuum, lyophilized, and stored at  $-20\text{ }^{\circ}\text{C}$ . Yields of 0.88 and 0.99 mg were obtained for PSM $\alpha$ 1 and PSM $\alpha$ 3, respectively.

#### **7.4.1.3 Construction of Expression Vectors.**

A gene sequence encoding PSM $\beta$ 2 codon-optimized for *Escherichia coli* expression was purchased from BioBasic Inc. The gene was cloned into the pET SUMO (small ubiquitin-like modifier) expression vector according to the manufacturer's instructions (Invitrogen). Sequencing of the DNA construct confirmed that the sequence was correct and in frame with the His-tagged SUMO fusion protein. The resulting pET SUMO-PSM $\beta$ 2 plasmid was transformed into competent *E. coli* BL21(DE3) cells according to the manufacturer's instructions.

#### **7.4.1.4 Expression of His-Tagged SUMO-PSM $\beta$ 2.**

Protein expression in *E. coli* BL21(DE3) was performed in 1 L of Terrific Broth [12 g of tryptone, 24 g of yeast extract, 4 mL of glycerol, 2.31 g of potassium dihydrogen phosphate, and 12.64 g of potassium hydrogen phosphate (pH 7.4)]. Medium was inoculated [1 % (v/v)] with an overnight starter culture of *E. coli* BL21(DE3) (pET SUMO-PSM $\beta$ 2) and grown at  $37\text{ }^{\circ}\text{C}$  while being shaken at 225 rpm to an optical density (OD<sub>600</sub>) of 0.8–1.0. Kanamycin was used at a concentration of 50  $\mu\text{g}/\text{mL}$  for selective pressure. Protein expression was induced by adding isopropyl  $\beta$ -D-1-thiogalactopyranoside to a final concentration of 1 mM, and the culture was incubated at  $30\text{ }^{\circ}\text{C}$  for 24 h. The cells were then harvested (5000g for 15 min at  $4\text{ }^{\circ}\text{C}$ ), and the cell pellet was suspended in lysis buffer composed of 50 mM  $\text{NaH}_2\text{PO}_4$  (pH 8.0), 500 mM NaCl,

10 mM imidazole, and 1 % glycerol. The suspension was passed once through a Constant Systems Cell Disruptor, model TS (Constant Systems, Ltd.), operated at 25 kpsi. The lysate was centrifuged (15000 g for 30 min at 4 °C), and the supernatant, which contained the fusion protein, was collected for subsequent purification.

#### **7.4.1.5 Purification of Fusion Protein.**

The lysate supernatant was mixed with 2.0 mL of Ni-NTA agarose (Qiagen) resin and shaken for 1 h at 8 °C. It was then loaded onto a fritted column and allowed to flow by gravity. The resin was washed with 75 mL of buffer A [50 mM NaH<sub>2</sub>PO<sub>4</sub>, 500 mM NaCl, and 20 mM imidazole (pH 8.0)]. The fusion protein was eluted with 50 mL of buffer B [50 mM NaH<sub>2</sub>PO<sub>4</sub>, 500 mM NaCl, and 400 mM imidazole (pH 8.0)] and dialyzed for 3 h at 8 °C against a 20 mM Tris-HCl buffer (pH 8.0) with 150 mM NaCl. The purification was monitored by sodium dodecyl sulfate– polyacrylamide gel electrophoresis (SDS–PAGE).

#### **7.4.1.6 Cleavage of Fusion Protein.**

His-tagged SUMO protease (McLab, South San Francisco, CA) was used to cleave the SUMO tag from the fusion protein as suggested by the manufacturer. Briefly, a 200 µL cleavage cocktail contained 20 µg of fusion protein, 5 units of the His-tagged SUMO protease, 20 µL of 10 × SUMO protease buffer [500 mM Tris-HCl (pH 8.0), 2 % Igepal CA-360 (Sigma), and 10 mM dithiothreitol], and 150 mM NaCl. After cleavage (20 h, 25 °C), 1 mL of Ni- NTA agarose (Qiagen) resin was used to remove the His-tagged SUMO and SUMO protease. This reaction was scaled up as necessary. PSMβ2 was further purified by RP-HPLC using a preparative scale C18 column (5 µm particle size, 100 Å pore size, 21.2 mm × 250 mm, Luna AXIA). The

detector and flow rate were set at 220 nm and 8 mL/min, respectively. Ten milliliters of sample was injected per run. A gradient of solvent A (0.1 % TFA in water) and solvent B (0.1 % TFA in acetonitrile) was used. The level of solvent B was initially set at 30 % for 10 min, gradually increased to 95% for 30 min, and maintained at 95 % for 10 min. Fractions containing PSM $\beta$ 2, which co-eluted with impurities at 41 min, were combined and concentrated under vacuum, lyophilized, redissolved, and re-injected for a second round of RP-HPLC. The second round of RP-HPLC used a semipreparative C18 column (5  $\mu$ m particle size, 100 Å, 250 mm  $\times$  10 mm, Luna model no. 517180-1, Phenomenex). The flow rate and detector were set to 5 mL/min and 220 nm, respectively. Ten milliliters of sample was injected per run using the same gradient method described above. The fractions containing PSM $\beta$ 2, which eluted after 32 min, were collected, concentrated under vacuum, lyophilized, and stored at  $-20$  °C (Figure S3). Approximately 2–2.5 mg of peptide was obtained per liter of culture.

#### **7.4.1.7 NMR Spectroscopy.**

PSM $\alpha$ 1, PSM $\alpha$ 3, and PSM $\beta$ 2 were each dissolved in 500  $\mu$ L of 50 %  $d_3$ -TFE and 50% water to give final concentrations of 0.77, 0.75, and 1.9 mM, respectively. All samples were run using a standard 5 mm NMR tube, and with 4,4-dimethyl-4-silapentane-1-sulfonic acid [0.01% (w/v)] as a reference. One-dimensional  $^1\text{H}$  NMR and two-dimensional homonuclear  $^1\text{H}$ – $^1\text{H}$  TOCSY and NOESY spectra were acquired for PSM $\alpha$ 1, PSM $\alpha$ 3, and PSM $\beta$ 2. Briefly, the NMR spectra for PSM $\alpha$ 1 were recorded on a 600 MHz Varian VNMRS spectrometer equipped with a z-axis pulsed field gradient triple-resonance HCN probe. NMR spectra for PSM $\alpha$ 3 and PSM $\beta$ 2 were recorded on a 700 MHz Varian VNMRS spectrometer using a z-axis pulsed field gradient

triple- resonance HCN cold probe. The acquisition software was VNMRJ 4.2A on both spectrometers. As resonance overlap was observed in the amide region, temperature scans of PSM $\alpha$ 3 and PSM $\beta$ 2 revealed a greater dispersion of peaks at elevated temperatures. Therefore, the temperatures at which the NMR spectra were recorded were 25, 37, and 40 °C for PSM $\alpha$ 1, PSM $\alpha$ 3, and PSM $\beta$ 2, respectively. Water suppression was achieved by presaturation during the relaxation delay for the spectra of PSM $\alpha$ 1 and PSM $\alpha$ 3. Water suppression in the spectra of PSM $\beta$ 2 was achieved using excitation sculpting.<sup>181</sup> Experimental parameters are listed in Table 6.3. The spectra were analyzed using NMRPipe and NMRView, followed by manual assignment of chemical shifts as described below. Full chemical shift assignments can be found in Tables 6.4, 6.5, and 6.6 for PSM $\alpha$ 1, PSM $\alpha$ 3, and PSM $\beta$ 2, respectively.

**Table 6.3 NMR Experimental Parameters for PSM $\alpha$ 1, PSM $\alpha$ 3, and PSM $\beta$ 2**

<b>Experiment</b>	<b>Sweep width (Hz) (t2, t1)<sup>a</sup></b>	<b>ni</b>	<b>np</b>	<b>nt</b>	<b>Mix time (s)</b>
<b>PSM<math>\alpha</math>1</b>					
NOESY	6906.1, 6906.1	512	13812	64	0.200
TOCSY	6906.1, 6906.1	256	13812	32	0.100
<b>PSM<math>\alpha</math>3</b>					
NOESY	7716.0, 7716.0	512	15432	48	0.100
TOCSY	7716.0, 7716.0	512	15432	32	0.100
<b>PSM<math>\beta</math>2</b>					
NOESY ES	8389.3, 8389.3	512	8192	48	0.100
zTOCSY	8389.3, 8389.3	512	8192	32	0.080

<sup>a</sup> Directly and indirectly detected dimensions respectively. “ni” is the number of complex points collected for the indirectly detected dimension, while “np” is the number of real + imaginary points for the directly detected dimension. “nt” is the number of cumulative scans collected for each point of acquisition.

**Table 6.4- Chemical Shift Assignments of PSM $\alpha$ 1**

	<b>HN</b>	<b>H<math>\alpha</math></b>	<b>H<math>\beta</math></b>	<b>Others</b>
<b>FME1</b>	8.39	4.48	2.08, 2.15	$\gamma$ CH <sub>2</sub> 2.61, 2.66
<b>Gly2</b>	8.53	3.92		
<b>Ile3</b>	7.64	4.06	2.02	$\gamma$ CH <sub>2</sub> 1.29, 1.60, $\gamma$ CH <sub>3</sub> 0.98, $\delta$ CH <sub>3</sub> 0.94
<b>Ile4</b>	7.55	3.88	2.02	$\gamma$ CH <sub>2</sub> 1.34, 1.63, $\gamma$ CH <sub>3</sub> 0.98, $\delta$ CH <sub>3</sub> 0.91
<b>Ala5</b>	8.04	4.07	1.48	
<b>Gly6</b>	7.79	3.90		
<b>Ile7</b>	7.96	3.84	2.08	$\gamma$ CH <sub>2</sub> 1.17, 1.81, $\gamma$ CH <sub>3</sub> 0.97, $\delta$ CH <sub>3</sub> 0.88
<b>Ile8</b>	8.29	3.72	2.00	$\gamma$ CH <sub>2</sub> 1.27, 1.76, $\gamma$ CH <sub>2</sub> 0.95, $\delta$ CH <sub>3</sub> 0.85
<b>Lys9</b>	7.77	3.99	2.06	$\gamma$ CH <sub>2</sub> 1.46, 1.67, $\delta$ CH <sub>2</sub> 1.75, $\epsilon$ CH <sub>2</sub> 3.00
<b>Val10</b>	7.85	3.66	2.44	$\gamma$ CH <sub>3</sub> 0.98, 1.13
<b>Ile11</b>	8.60	3.70	2.01	$\gamma$ CH <sub>2</sub> 1.22, 1.81, $\gamma$ CH <sub>3</sub> 0.96, $\delta$ CH <sub>3</sub> 0.84
<b>Lys12</b>	8.87	3.96	1.90, 1.98	$\gamma$ CH <sub>2</sub> 1.43, $\delta$ CH <sub>2</sub> 1.70, $\epsilon$ CH <sub>2</sub> 2.95
<b>Ser13</b>	7.92	4.29	4.01, 4.24	
<b>Leu14</b>	8.42	4.11	1.55, 2.08	$\gamma$ CH 1.87, $\delta$ CH <sub>3</sub> 0.88
<b>Ile15</b>	8.61	3.77	2.01	$\gamma$ CH <sub>2</sub> 1.21, 1.88, $\gamma$ CH <sub>3</sub> 0.96, $\delta$ CH <sub>3</sub> 0.86
<b>Glu16</b>	8.35	4.09	2.12, 2.31	$\gamma$ CH <sub>2</sub> 2.50, 2.65
<b>Gln17</b>	8.05	4.10	2.18, 2.30	$\gamma$ CH <sub>2</sub> 2.09
<b>Phe18</b>	8.42	4.65	3.19, 3.31	$\delta$ CH 7.33
<b>Thr19</b>	8.10	4.48	4.38	$\gamma$ CH <sub>3</sub> 1.38
<b>Gly20</b>	8.09	4.02, 4.10		
<b>Lys21</b>	7.96	4.52	1.81	$\gamma$ CH <sub>2</sub> 1.47, 1.97, $\delta$ CH <sub>2</sub> 1.71, $\epsilon$ CH <sub>2</sub> 3.04

**Table 6.5-Chemical Shift Assignments of PSM $\alpha$ 3**

	<b>HN</b>	<b>H<math>\alpha</math></b>	<b>H<math>\beta</math></b>	<b>Others</b>
<b>FME1</b>	8.39	4.46	2.09, 2.13	$\gamma$ CH <sub>2</sub> 2.69, 2.62
<b>Glu2</b>	8.53	4.12	2.05	$\gamma$ CH <sub>2</sub> 2.42
<b>Phe3</b>	7.69	4.40	3.22	$\delta$ CH 7.25
<b>Val4</b>	7.53	3.59	2.14	$\gamma$ CH <sub>3</sub> 0.91
<b>Ala5</b>	8.02	4.12	1.52	
<b>Lys6</b>	7.65	4.06	2.01, 1.93	$\gamma$ CH <sub>2</sub> 1.47, $\delta$ CH <sub>2</sub> 1.74, 1.70, $\epsilon$ CH <sub>2</sub> 3.01
<b>Leu7</b>	7.92	4.13	1.69	$\gamma$ CH 1.57, $\delta$ CH <sub>3</sub> 0.89
<b>Phe8</b>	8.57	4.45	3.29, 3.23	$\delta$ CH 7.30, $\epsilon$ CH 7.27

<b>Lys9</b>	8.04	3.98	2.05	$\gamma\text{CH}_2$ 1.62, 1.52, $\delta\text{CH}_2$ 1.81, 1.73, $\epsilon\text{CH}_2$ 3.07
<b>Phe10</b>	8.07	4.36	3.31, 3.22	$\delta\text{CH}$ 7.01, $\epsilon\text{CH}$ 7.20, $\zeta\text{CH}$ 7.22
<b>Phe11</b>	8.58	4.23	3.18	$\delta\text{CH}$ 7.26, $\epsilon\text{CH}$ 7.33
<b>Lys12</b>	8.45	3.91	1.86	$\gamma\text{CH}_2$ 1.48, $\delta\text{CH}_2$ 1.67, $\epsilon\text{CH}_2$ 2.98
<b>Asp13</b>	8.25	4.47	3.03, 2.73	
<b>Leu14</b>	8.09	3.40	1.60	$\gamma\text{CH}$ 1.46, $\delta\text{CH}_3$ 0.83
<b>Leu15</b>	8.35	4.14	1.60	$\gamma\text{CH}$ 1.72, $\delta\text{CH}_3$ 0.89
<b>Gly16</b>	8.04	3.81, 3.92		
<b>Lys17</b>	7.76	4.19	1.90, 1.83	$\gamma\text{CH}_2$ 1.43, 1.38, $\delta\text{CH}_2$ 1.64, $\epsilon\text{CH}_2$ 2.96
<b>Phe18</b>	8.11	4.52	3.28, 3.17	$\delta\text{CH}$ 7.29
<b>Leu19</b>	8.27	4.35	1.82	$\gamma\text{CH}$ 1.65, $\delta\text{CH}_3$ 0.94
<b>Gly20</b>	7.79	3.99, 4.01		
<b>Asn21</b>	8.06	4.82	2.87, 2.74	
<b>Asn22</b>	8.05		2.77, 2.84	

**Table 6.6- Chemical Shift Assignments of PSM $\beta$ 2**

	<b>HN</b>	<b>H<math>\alpha</math></b>	<b>H<math>\beta</math></b>	<b>Others</b>
<b>Met1</b>		4.12	2.21	$\gamma\text{CH}_2$ 2.42
<b>Thr2</b>	8.30	4.56	4.33	$\gamma\text{CH}_3$ 1.32
<b>Gly3</b>	8.37	4.06		
<b>Leu4</b>	7.92	4.22	1.74	$\gamma\text{CH}$ 1.64, $\delta\text{CH}_3$ 0.99, 0.94
<b>Ala5</b>	7.94	4.07	1.50	
<b>Glu6</b>	7.69	4.10	2.15	$\gamma\text{CH}_2$ 2.54
<b>Ala7</b>	7.93	4.21	1.58	
<b>Ile8</b>	8.43	3.72	1.97	$\gamma\text{CH}_2$ 1.81, $\gamma\text{CH}_3$ 1.15, $\delta\text{CH}_3$ 0.93
<b>Ala9</b>	8.23	4.06	1.54	
<b>Asn10</b>	8.39	4.52	2.99, 2.82	$\delta\text{NH}_2$ 6.62, 7.34
<b>Thr11</b>	8.03	4.52	4.04	$\gamma\text{CH}_3$ 1.30
<b>Val12</b>	8.50	3.71	2.21	$\gamma\text{CH}_3$ 1.09, 0.98
<b>Gln13</b>	8.19	4.13	2.27, 2.22	$\gamma\text{CH}_2$ 2.58, 2.42 $\epsilon\text{NH}_2$ 6.54, 7.17
<b>Ala14</b>	8.05	4.21	1.60	
<b>Ala15</b>	8.33	4.16	1.60	
<b>Gln16</b>	8.22	4.18	2.21	$\gamma\text{CH}_2$ 2.43, 2.57, $\epsilon\text{NH}_2$ 6.55, 7.04
<b>Gln17</b>	8.35	4.16	2.30, 2.24	$\gamma\text{CH}_2$ 2.63, 2.47 $\epsilon\text{NH}_2$ 6.47, 6.91
<b>His18</b>	8.27	4.51	3.44, 3.38	$\delta\text{CH}$ 8.47, $\delta\text{NH}$ 7.39, $\epsilon\text{NH}$ 8.60, $\epsilon\text{CH}$ 8.27
<b>Asp19</b>	8.46	4.66	3.05, 2.98	

<b>Ser20</b>	8.18	4.35	4.08	
<b>Val21</b>	7.77	4.00	2.20	$\gamma\text{CH}_3$ 1.00
<b>Lys22</b>	7.95	4.20	1.96, 1.90	$\gamma\text{CH}_2$ 1.54, 1.48, $\delta\text{CH}_2$ 1.75, $\epsilon\text{CH}_2$ 3.03
<b>Leu23</b>	8.09	4.28	1.75	$\delta\text{CH}_3$ 0.96, 0.94
<b>Gly24</b>	8.29	3.93, 3.98		
<b>Thr25</b>	8.01	4.20	4.32	$\gamma\text{CH}_3$ 1.33
<b>Ser26</b>	7.92	4.48	4.18	
<b>Ile27</b>	7.97	3.99	2.03	$\gamma\text{CH}_2$ 1.30, 1.68, $\gamma\text{CH}_3$ 0.98, $\delta\text{CH}_3$ 0.91
<b>Val28</b>	7.70	3.69	2.14	$\gamma\text{CH}_3$ 1.08, 1.00
<b>Asp29</b>	7.85	4.49	3.09	
<b>Ile30</b>	7.88	3.86	2.14	$\gamma\text{CH}_2$ 1.22, $\gamma\text{CH}_3$ 0.98, $\delta\text{CH}_3$ 0.90
<b>Val31</b>	8.25	3.76	2.20	$\gamma\text{CH}_3$ 0.98, 1.08
<b>Ala32</b>	8.69	4.15	1.52	
<b>Asn33</b>	7.85	4.67	2.83, 2.94	$\delta\text{NH}_2$ 7.56, 6.58
<b>Gly34</b>	8.22	4.00		
<b>Val35</b>	8.24	3.94	2.24	$\gamma\text{CH}_3$ 1.03, 1.09
<b>Gly36</b>	8.12	3.94		
<b>Leu37</b>	7.84	4.24	1.79	$\gamma\text{CH}$ 1.72, $\delta\text{CH}_3$ 0.94, 0.97
<b>Leu38</b>	8.00	4.12	1.92, 1.85	$\gamma\text{CH}$ 1.66, $\delta\text{CH}_3$ 0.95, 0.98
<b>Gly39</b>	8.13	3.76	3.65	
<b>Lys40</b>	7.68	4.23	2.00, 1.95	$\gamma\text{CH}_2$ 1.59, 1.53, $\delta\text{CH}_2$ 1.73, $\epsilon\text{NH}_2$ 3.02
<b>Leu41</b>	7.99	4.11	1.59	$\gamma\text{CH}$ 1.16, $\delta\text{CH}_3$ 0.76
<b>Phe42</b>	7.86	4.71	3.33, 2.92	$\delta\text{CH}$ 7.32, $\epsilon\text{CH}$ 7.30
<b>Gly43</b>	7.73	4.09, 3.90		
<b>Phe44</b>	7.82	4.77	3.21, 3.08	$\delta\text{CH}$ 7.27, $\epsilon\text{CH}$ 7.32

#### 7.4.1.8 Circular Dichroism Spectroscopy.

PSM $\alpha$ 1, PSM $\alpha$ 3, and PSM $\beta$ 2 were dissolved in 50 % d3-TFE at concentrations of 0.88, 0.99, and 3.07 mg/mL respectively. Spectra were recorded on an OLIS DSM 17 (Olis) CD spectrophotometer at 25, 37, and 40 °C (for PSM $\alpha$ 1, PSM $\alpha$ 3, and PSM $\beta$ 2, respectively) in a 0.2 mm quartz cell. Samples were scanned five times from 250 to 185 nm. The percent  $\alpha$ -helicity was calculated as  $(3000 - \theta_{222})/39000 \times 100$ .

#### **7.4.1.9 Structure Calculations.**

The structures of PSM $\alpha$ 1, PSM $\alpha$ 3, and PSM $\beta$ 2 were calculated using CYANA 2.1.31. NOE cross-peaks were almost entirely automatically assigned by CYANA, and minimal manually assigned cross-peaks were provided. For PSM $\alpha$ 1, 636 cross-peak NOEs (0 long-range, 99 medium-range, and 538 short-range) were used in the final structure calculation. Chemical shift assignments for PSM $\alpha$ 1 were deposited in the Biological Magnetic Resonance Bank (BMRB) (accession number 30109), and coordinates for the structure were deposited in the Protein Data Bank (PDB) (accession number 5KHB). For PSM $\alpha$ 3, 553 cross-peak NOEs (0 long-range, 101 medium-range, and 452 short-range) were used in the final structure calculation. Chemical shift assignments for PSM $\alpha$ 3 were deposited in the BMRB (accession number 30106), and coordinates for the structure were deposited in the PDB (accession number 5KGY). PSM $\beta$ 2 had 1320 cross-peak NOEs (34 long-range, 246 medium-range, and 1040 short-range) that were used in the final structure calculation. Chemical shift assignments for PSM $\beta$ 2 were deposited in the BMRB (accession number 30107), and coordinates for the structure were deposited in the PDB (accession number 5KGZ).

### **7.5 Experimental Procedures for the Synthesis of Neopetrosiamide Analogues**

#### ***7.5.1 General Procedure for Stepwise Disulfide Formation***

##### **7.5.1.1 Formation of Bis-disulfide Bond Method A**

Iodine (10 equivalents) dissolved in methanol (< 5 mL) was added to the linear Cys protected peptide in acetic acid (0.5 mg mL<sup>-1</sup> solution), allowing the first disulfide to form. The reaction mixture was stirred at room temperature for 2 h. After 2 h water was added (20 % v/v)

to enable the deprotection of the acetamidomethyl protected cysteine and formation of the second disulfide bond. The reaction was monitored by MALDI-TOF MS. Once deemed complete, 0.1 M ascorbic acid was added until the solution became colorless. Following concentration *in vacuo*, the residue was purified using RP-HPLC. Fractions containing the desired product were pooled and lyophilized.

#### **7.5.1.2 Formation of Bis-disulfide Bond Method B**

Iodine (10 equivalents) dissolved in methanol (< 5 mL) was added to the linear Cys protected peptide in acetic acid (0.5 mg mL<sup>-1</sup> solution), allowing the first disulfide to form. The reaction mixture was stirred at room temperature for 2 h. After 2 h water was added (20 % v/v) to enable the deprotection of the acetamidomethyl protected cysteine and formation of the second disulfide bond. The reaction was monitored by MALDI-TOF MS. After the reaction was complete, the reaction mixture was poured into 6 to 9 volumes of cold ether, cooled in dry ice. The aqueous layer freezes and the ether is decanted off. The ether layer is washed with water three times. Aqueous fractions containing the desired peptide were pooled concentrated and lyophilized.

#### **7.5.1.3 Formation of Tris-disulfide Peptide.**

The oxidation solution was prepared at room temperature by dissolving DMSO (100 equiv.) and anisole (4 equiv.) in TFA. The bicyclic peptide with *t*-Bu protecting groups on the two remaining Cys residues was dissolved in the oxidizing reagent to give a concentration of 0.1 mg mL<sup>-1</sup>. The resulting mixture was stirred for 5 h at room temperature and then diluted with water. The solution was concentrated *in vacuo* and purified by RP-HPLC. Fractions containing

the desired product, as confirmed by RP-HPLC and MALDI-TOF MS, were pooled and lyophilized.

#### **7.5.1.4 General Method for the [2+3] Cycloaddition of Fluorescent Organic Dyes to the Azide Functionalized peptide**

The trisdisulfide peptide was dissolved in 1:1 (v/v) mixture of water and *t*-butanol. Once dissolved the fluorescent organic dye was added (3 equiv). A solution of 0.1N copper sulfate (5 equiv) and 0.2 N sodium ascorbate (10 equiv) was added. Reaction mixture was stirred in the absence of light for 24 h or until reaction was deemed complete by MALDI-TOF. Product was purified using the general RP-HPLC method.

#### **7.5.1.5 General Method for Purification of Peptides by HPLC**

Peptides were purified on a C8 column (VYDAC, 208TP1010 4.66 mm x 250 mm, 5  $\mu$ m particle size, 300 Å) using a flow rate of 3.0 mL min<sup>-1</sup> and UV detection at 220 and 254 nm. Briefly, starting with a 9:1 ratio of mobile phase A (water with 0.1 % TFA) to mobile phase B (MeCN with 0.1 % TFA), the column was equilibrated for 5 min. Mobile phase B was then increased to 30 % over 5 min, and then 60 % over 28 min. Following a brief increase of the organic phase to 80 % to clean the column, the organic phase was reduced to 10 % for 1 min and held at 10 % for an additional 1 min.

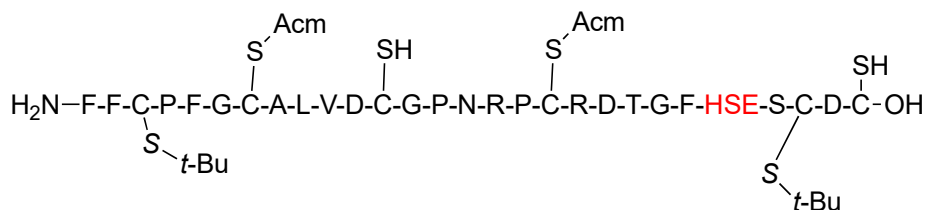
#### **7.5.1.6 General Cell Culture Protocols**

MDA-MB-231 cells were cultured in Alpha-Minimal Essential Medium (MEM) (Mediatech) supplemented with 10% fetal bovine serum (FBS) (ATCC) and 1 % penicillin–streptomycin (GIBCO). Cells were incubated under an atmosphere of 5% CO<sub>2</sub> at 37 °C. Cells were harvested using 0.05 % trypsin-EDTA solution in HBSS (Mediatech).

### 7.5.1.7 General Procedure for Invasion Assay of Analogues Against MDA-MB-231 Cells

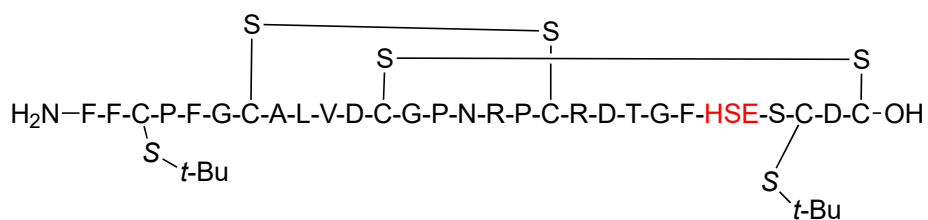
The matrigel (BD Sciences) was allowed to thaw overnight on ice at 4 °C. To maintain the fluidity of the matrigel, the 96 well serological plate, pipet tips and serological pipets were placed in the freezer overnight. Once thawed, the matrigel was diluted to a 1:1 mixture of matrigel to MEM at 4 °C. While on ice, 50  $\mu\text{L}$  of 1:1 matrigel:MEM is added to each well of the plate. The plate was placed in a 37 °C incubator overnight, dehydrating the matrigel and allowing for the matrigel to form a gel. Following incubation overnight the matrigel was re-hydrated by adding 50  $\mu\text{L}$  of MEM to each well followed by incubation at 37 °C for 30 min. Stock solutions of each analogue (5 mg  $\text{mL}^{-1}$ ) were made in 30 % acetonitrile in water. 2  $\mu\text{L}$  or 0.8  $\mu\text{L}$  aliquots of each solution in 50  $\mu\text{L}$  of MEM are added to the wells of re-hydrated matrigel. 100  $\mu\text{L}$  of freshly trypsinized MDA-MD-231 cells in MEM are added to each well to give a total of 200  $\mu\text{L}$  per well and final analogue concentrations of 50  $\mu\text{g mL}^{-1}$  or 20  $\mu\text{g mL}^{-1}$ . Each well has  $\sim 25\,000$  cells. The cells were allowed to incubate at 37 °C overnight to give sufficient time for cells to invade. Visualization of each well was achieved using a microscope with 20 x magnification.

### 7.5.1.8 Linear Peptide Formation of Residue 24 Substitution with *O*-Methyl Homoserine (M(O)24O-methyl HSE) (17)



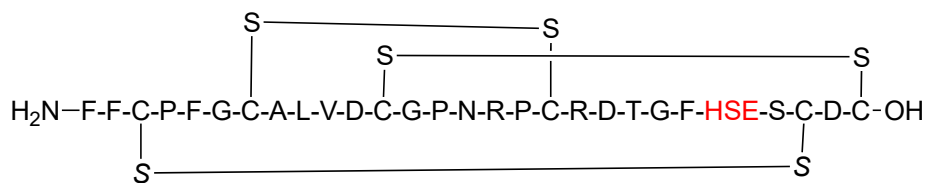
Linear peptide M(O)24O-methyl HSE was synthesized on a preloaded H<sub>2</sub>N-Cys(Trt)-2-ClTrt resin (0.62 mmol/g) on a 0.1 mmol scale using the automated peptide synthesizer according to the general method for solid phase peptide synthesis. Protection of the cysteine residues was Cys 3, 26-Acm; Cys 12, 28-Trt; Cys 7, 18- *t*-Bu. The crude peptide (150 mg 45.4 % relative to resin loading) was used in the next step without further purification. Calculated molecular weight for C<sub>143</sub>H<sub>216</sub>N<sub>37</sub>O<sub>41</sub>S<sub>6</sub> [M+H]<sup>+</sup> 3299.4 Found 3299.5 [M+H]<sup>+</sup>.

#### 7.5.1.9 Bis-disulfide Formation Residue 24 Substitution with *O*-Methyl Homoserine (M(O)24O-methyl HSE) (18)



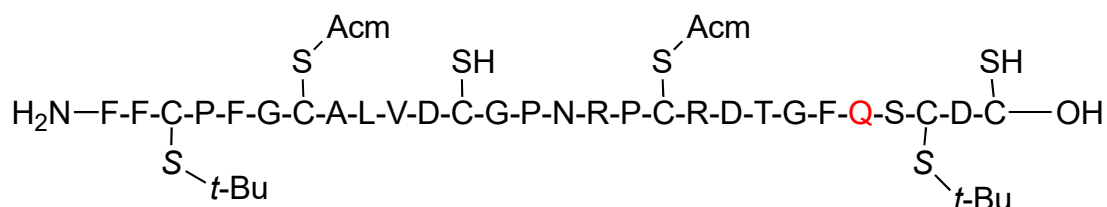
The bis-disulfide, M(O)24O-methyl HSE was synthesized according to the general method for bis-disulfide bond formation from the corresponding linear peptide. The crude peptide was purified by semi-prep RP-HPLC using the general method ( $t_R = 24.8$  min) to give bis-disulfide M(O)24O-methyl HSE as white powder (22 mg, 23.2% relative to 100 mg of crude linear peptide). Calculated molecular weight for C<sub>137</sub>H<sub>202</sub>N<sub>35</sub>O<sub>39</sub>S<sub>6</sub> [M+H]<sup>+</sup> 3153 Found [M+H]<sup>+</sup> 3153

#### 7.5.1.10 Tris-disulfide Formation of Residue 24 Substitution with *O*-Methyl Homoserine (M(O)24O-methyl HSE) (19)



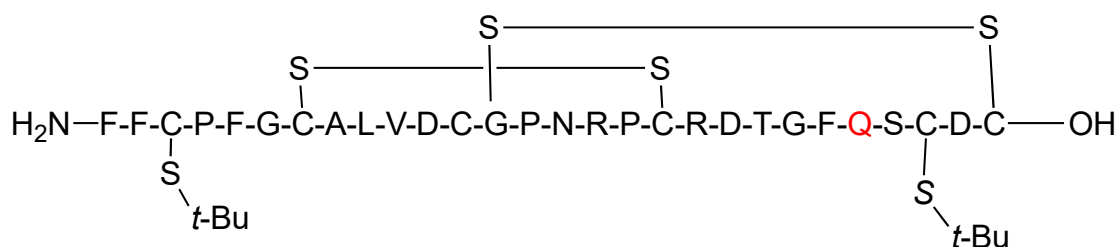
The introduction of the third disulfide bond was achieved by DMSO oxidation of the corresponding bicyclic peptide according to the general method for tris-disulfide bond formation. The crude peptide was purified by semi-preparative RP-HPLC using the general method ( $t_R = 24.9$  min, 1.0 mg, 26.3 % relative to 4 mg of bicyclic peptide purified). MALDI-TOF MS Calculated molecular weight for  $C_{129}H_{184}N_{35}O_{39}S_6$   $[M+H]^+$  3039 Found  $[M+H]^+$  3039.

#### 7.5.1.11 Linear Peptide Formation of Residue 24 Substitution with Glutamine (M(O)24Gln) (20)



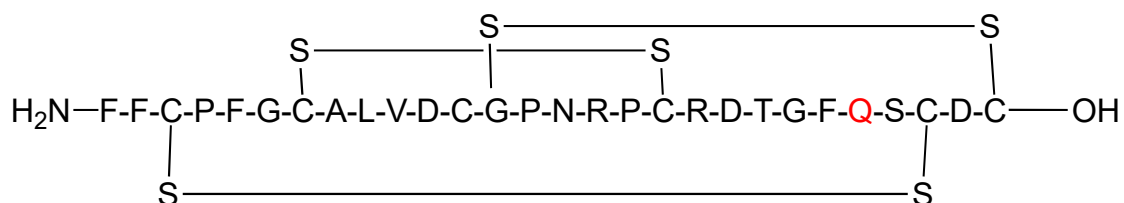
Linear peptide M(O)24Gln was synthesized on a preloaded  $H_2N$ -Cys(Trt)-2-ClTrt resin (0.62 mmol/g) on a 0.1 mmol scale using the automated peptide synthesizer according to the general method for solid phase peptide synthesis. Protection of the cysteine residues was Cys 3, 26-Acm; Cys 12, 28-Trt; Cys 7, 18- *t*-Bu. The crude peptide (160 mg, 48.3 % relative to resin loading) was used in the next step without further purification. MALDI-TOF MS calculated molecular weight for  $C_{143}H_{215}N_{38}O_{41}S_6$   $[M+H]^+$  3312 Found  $[M+H]^+$  3312.

#### 7.5.1.12 Bis-disulfide Formation of Residue 24 Substitution with Glutamine (M(O)24Gln) (21)



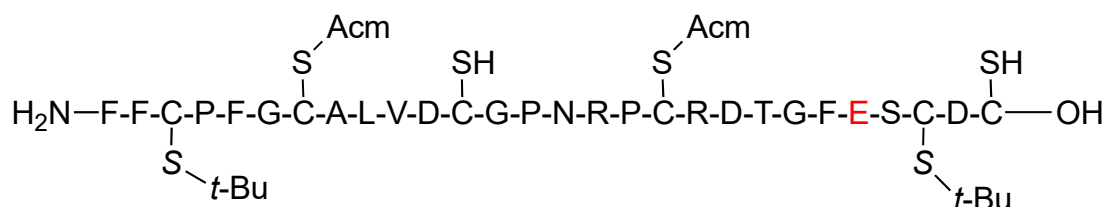
The bis-disulfide M(O)24Gln was synthesized according to general method A for bis-disulfide bond formation from the linear peptide. The crude peptide was purified by semi-prep RP-HPLC using the general method ( $t_R = 24.0$  min) to give the bis-disulfide M(O)24Gln as an off- white powder (7.6 mg, 5.3 % relative to 150 mg of crude linear peptide). Calculated molecular weight for  $C_{137}H_{201}N_{36}O_{39}S_6$   $[M+H]^+$  3166 Found  $[M+H]^+$  3166.

#### 7.5.1.13 Tris-disulfide Formation of Residue 24 Substitution with Glutamine (M(O)24Gln) (22)



The introduction of the third disulfide bond was achieved by DMSO oxidation of the bicyclic peptide according to the general method for tris-disulfide bond formation. The crude bis-disulfide M(O)24Gln was purified by semi-preparative RP-HPLC using the general method ( $t_R = 21.1$  min, 1.2mg, 27.0 % relative to 4.6 mg of bicyclic peptide purified). MALDI-TOF MS Calculated molecular weight for  $C_{129}H_{183}N_{36}O_{39}S_6$   $[M+H]^+$  3052.1 Found  $[M+H]^+$  3052.

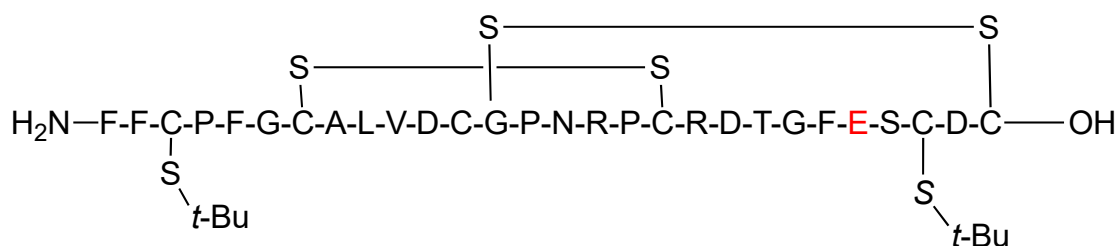
#### 7.5.1.14 Linear Peptide Formation of 24 Substitution with Glutamic Acid (M(O)24Glu) (23)



Linear peptide M(O)24Glu was synthesized on a preloaded  $H_2N$ -Cys(Trt)-2-ClTrt resin (0.62 mmol/g) on a 0.1 mmol scale using the automated peptide synthesizer according to the

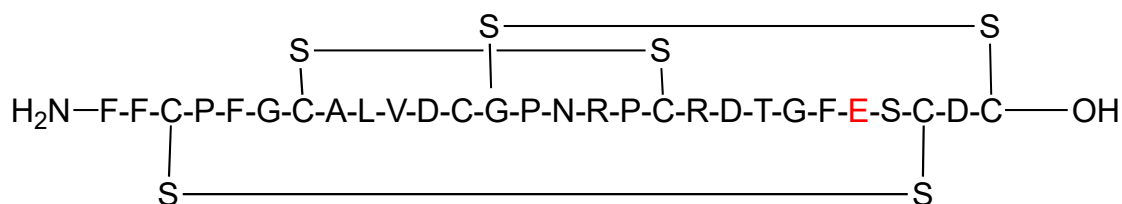
general method for solid phase peptide synthesis. Protection of the cysteine residues was Cys 3, 26-Acm; Cys 12, 28-Trt; Cys 7, 18- *t*-Bu. The crude peptide (152.9 mg, 45.9 % relative to resin loading) was used in the next step without further purification. MALDI-TOF MS calculated molecular weight for C<sub>143</sub>H<sub>213</sub>N<sub>37</sub>O<sub>42</sub>S<sub>6</sub> [M+H]<sup>+</sup> 3315 Found [M+H]<sup>+</sup> 3315.

#### 7.5.1.15 Bis-disulfide Formation of Residue 24 Substitution with Glutamic Acid (M(O)24Glu) (24)



The bis-disulfide of M(O)24Glu was synthesized according to general method A for bis-disulfide bond formation from the corresponding linear peptide. The crude peptide was purified by semi-prep RP-HPLC using the general method (*t<sub>R</sub>* = 24.0 min) to give the bis-disulfide M(O)24Glu as an off- white powder (12 mg, 24 % relative to 50 mg of crude linear peptide). Calculated molecular weight for C<sub>137</sub>H<sub>199</sub>N<sub>35</sub>O<sub>40</sub>S<sub>6</sub> [M+H]<sup>+</sup> 3169 Found [M+H]<sup>+</sup> 3169.

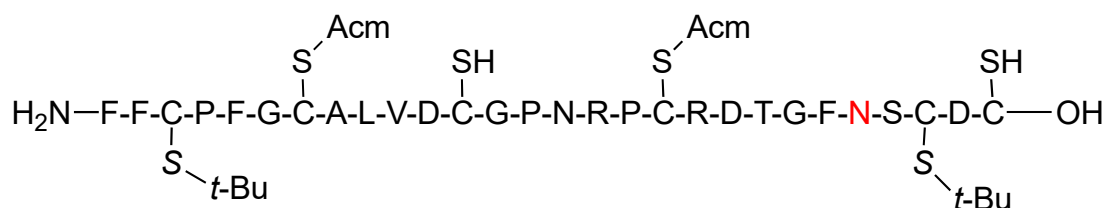
#### 7.5.1.16 Tris-disulfide Formation of Residue 24 Substitution with Glutamic Acid (M(O)24Glu) (25)



The introduction of the third disulfide bond was achieved by DMSO oxidation of the bicyclic peptide according to the general method for tris-disulfide bond formation. The crude

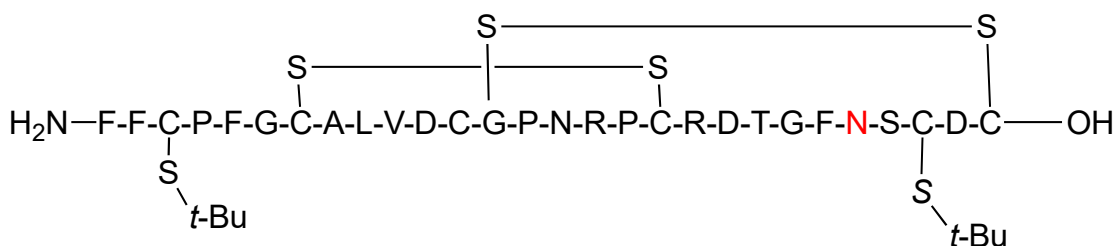
peptide was purified by semi-preparative RP-HPLC using the general method ( $t_R = 17.5$  min, 5.6 mg, 46.7% relative to 12 mg of bicyclic peptide purified). MALDI-TOF MS Calculated molecular weight for  $C_{129}H_{181}N_{35}O_{40}S_6$   $[M+H]^+$  3055 Found  $[M+H]^+$  3055.

#### 7.5.1.17 Linear Peptide Formation of Residue Asparagine (M(O)24Asn) (26)



Linear peptide M(O)24Asn was synthesized on a preloaded  $H_2N$ -Cys(Trt)-2-ClTrt resin (0.62 mmol/g) on a 0.1 mmol scale using the automated peptide synthesizer according to the general method for solid phase peptide synthesis. Protection of the cysteine residues was Cys 3, 26-Acm; Cys 12, 28-Trt; Cys 7, 18- *t*-Bu. The crude peptide (133 mg, 40.3 % relative to resin loading) was used in the next step without further purification. MALDI-TOF MS calculated molecular weight for  $C_{142}H_{212}N_{38}O_{41}S_6$   $[M+H]^+$  3300 Found  $[M+H]^+$  3300.

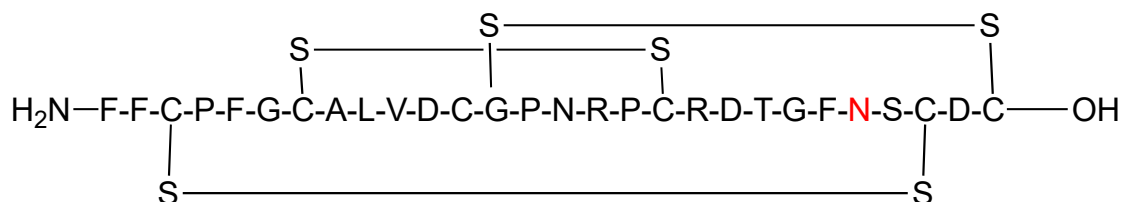
#### 7.5.1.18 Bis-disulfide formation of Residue 24 Substitution with Asparagine (M(O)24Asn) (27)



The bis-disulfide of M(O)24Asn was synthesized according to general method B for bis-disulfide bond formation from the corresponding linear peptide. The crude peptide was used without further purification giving an orange-yellow solid (8 mg, 40% relative to 20 mg of crude

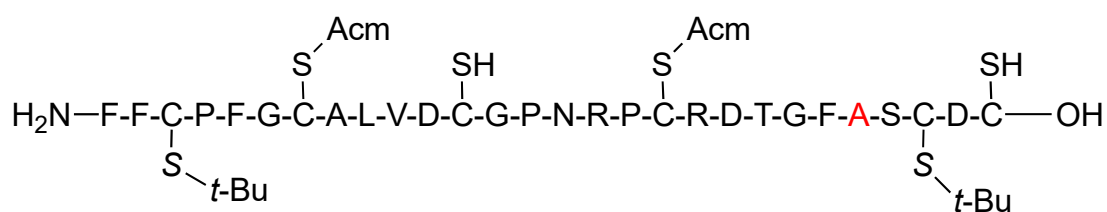
linear peptide). Calculated molecular weight for  $C_{136}H_{198}N_{36}O_{39}S_6$   $[M+H]^+$  3154 Found  $[M+H]^+$  3154.

#### 7.5.1.19 Tris-disulfide Formation of Residue 24 Substitution with Asparagine (M(O)24Asn) (28)



The introduction of the third disulfide bond was achieved by DMSO oxidation of the bicyclic peptide according to the general method for tris-disulfide bond formation. The crude peptide was purified by semi-preparative RP-HPLC using the general method ( $t_R = 18.7$  min, 2.1 mg, 26.3 % relative to 8 mg of crude bicyclic peptide). MALDI-TOF MS Calculated molecular weight for  $C_{128}H_{180}N_{36}O_{39}S_6$   $[M+H]^+$  3040 Found  $[M+H]^+$  3039.

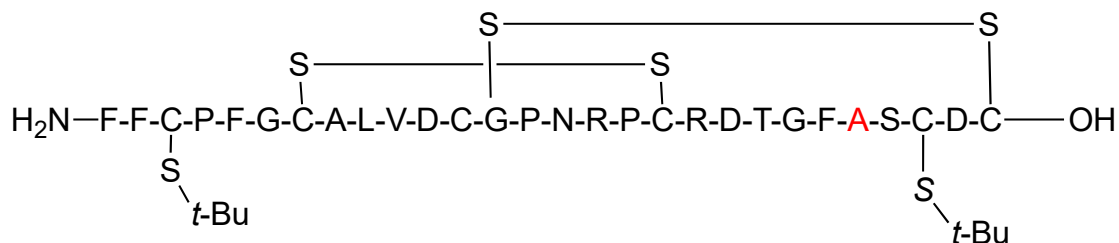
#### 7.5.1.20 Linear Peptide Formation of Residue 24 Substitution with Alanine (M(O)24Ala) (29)



Linear peptide M(O)24Ala was synthesized on a preloaded  $H_2N$ -Cys(Trt)-2-CITrt resin (0.62 mmol/g) on a 0.1 mmol scale using the automated peptide synthesizer according to the general method for solid phase peptide synthesis. Protection of the cysteine residues was Cys 3, 26-Acm; Cys 12, 28-Trt; Cys 7, 18- *t*-Bu. The crude peptide (50 mg, 15 % isolated yield relative

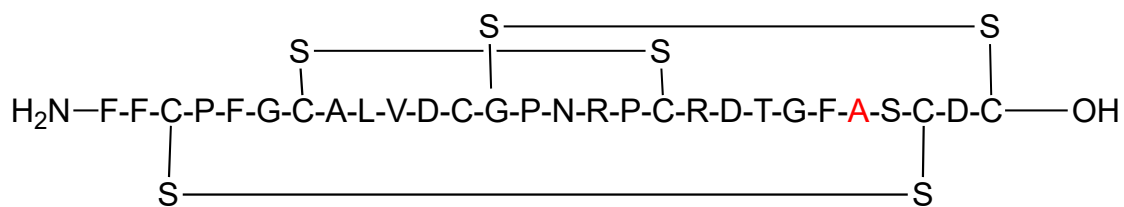
to resin loading) was used in the next step without further purification. MALDI-TOF MS calculated molecular weight for  $C_{140}H_{211}N_{37}O_{40}S_6$   $[M+H]^+$  3257 Found  $[M+H]^+$  3255.

#### 7.5.1.21 Bis-disulfide Formation of Residue 24 Substitution with Alanine (M(O)24Ala) (30)



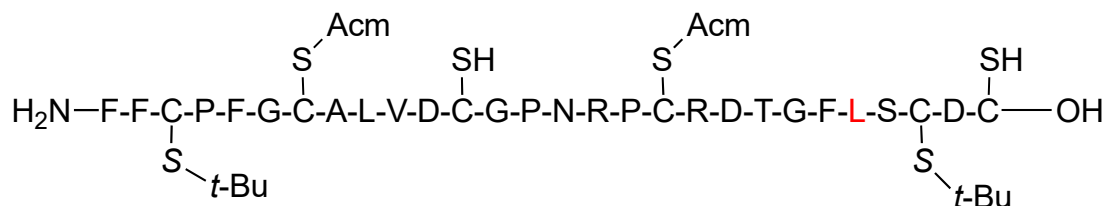
The bis-disulfide M(O)24Ala was synthesized according to general method B for bis-disulfide bond formation from the linear peptide. The crude peptide was used without further purification giving an orange-yellow solid (35 mg, 74 % relative to 50 mg of crude linear peptide). Calculated molecular weight for  $C_{135}H_{197}N_{35}O_{38}S_6$   $[M+H]^+$  3111 Found  $[M+H]^+$  3111.

#### 7.5.1.22 Tris-disulfide Formation of Residue 24 Substitution with Alanine (M(O)24Ala) (31)



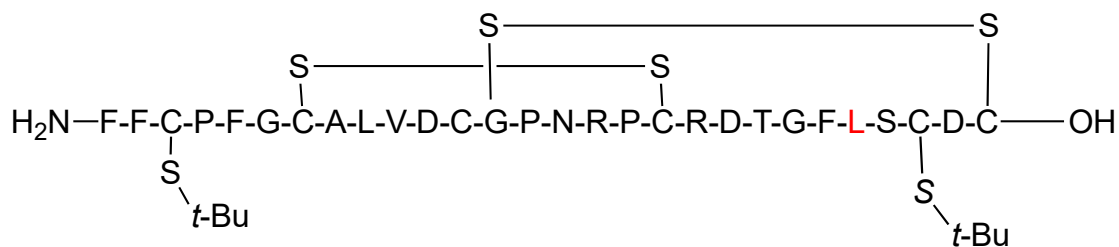
The introduction of the third disulfide bond was achieved by DMSO oxidation of the bicyclic peptide according to the general method for tris-disulfide bond formation. The crude peptide was purified by semi-preparative RP-HPLC using the general method ( $t_R = 23.2$  min, 1.47 mg, 4 % isolated yield relative to 35 mg of crude bicyclic peptide). MALDI-TOF MS Calculated molecular weight for  $C_{129}H_{130}N_{36}O_{39}S_6$   $[M+H]^+$  2998 Found  $[M+H]^+$  2997.

**7.5.1.23 Linear Peptide Formation of Residue 24 Substitution with Leucine (M(O)24Leu) (32)**



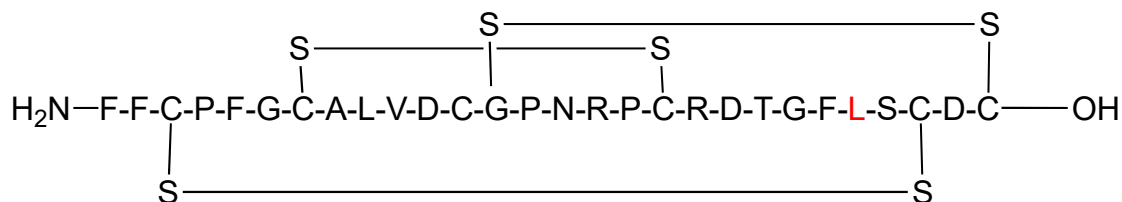
Linear peptide M(O)24Leu was synthesized on a preloaded H<sub>2</sub>N-Cys(Trt)-2-ClTrt resin (0.62 mmol/g) on a 0.1 mmol scale using the automated peptide synthesizer according to the general method for solid phase peptide synthesis. Protection of the cysteine residues was Cys 3, 26-Acm; Cys 12, 28-Trt; Cys 7, 18- *t*-Bu. The crude peptide (123 mg, 37.3 % relative to resin loading) was used in the next step without further purification. MALDI-TOF MS calculated molecular weight for C<sub>143</sub>H<sub>215</sub>N<sub>38</sub>O<sub>41</sub>S<sub>6</sub> [M+H]<sup>+</sup> 3299 Found [M+H]<sup>+</sup> 3299.

**7.5.1.24 Bis-disulfide Formation of Residue 24 Substitution with Leucine (M(O)24Leu) (33)**



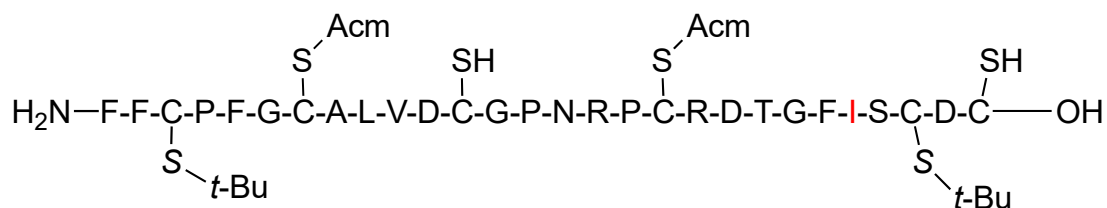
The bis-disulfide M(O)24Leu was synthesized according to general method B for bis-disulfide bond formation from the corresponding linear peptide. The crude peptide was used without further purification giving an orange-yellow solid (8 mg, 40% relative to 20 mg of crude linear peptide). Calculated molecular weight for C<sub>137</sub>H<sub>201</sub>N<sub>36</sub>O<sub>39</sub>S<sub>6</sub> [M+H]<sup>+</sup> 3153 Found [M+H]<sup>+</sup> 3153.

**7.5.1.25 Tris-disulfide Formation of Residue 24 Substitution with Leucine (M(O)24Leu) (34)**



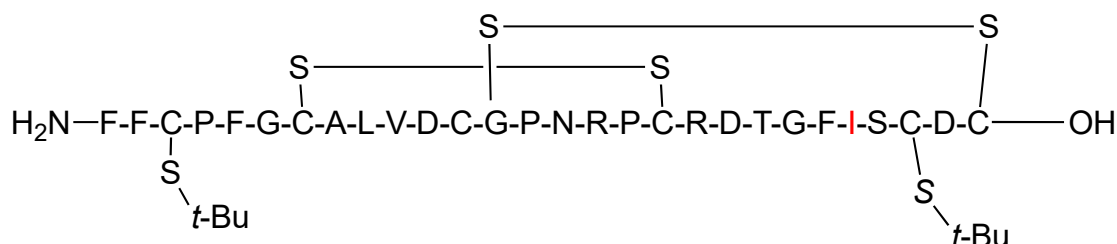
The introduction of the third disulfide bond was achieved by DMSO oxidation of the bicyclic peptide according to the general method for tris-disulfide bond formation. The crude peptide was purified by semi-preparative RP-HPLC using the general method ( $t_R = 24.9$  min, 2.1 mg, 26.3 % relative to 8 mg of crude bicyclic peptide). MALDI-TOF MS Calculated molecular weight for C<sub>129</sub>H<sub>185</sub>N<sub>36</sub>O<sub>39</sub>S<sub>6</sub> [M+H]<sup>+</sup> 3039 Found (M-2H)<sup>+</sup> 3037.

**7.5.1.26 Linear Peptide Formation of Residue 24 Substitution with Isoleucine (M(O)24Ile) (35)**



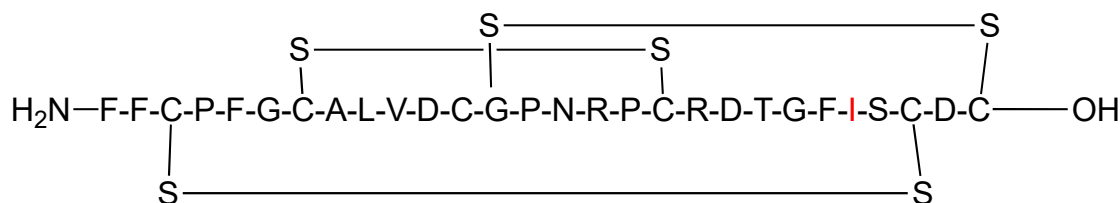
Linear peptide M(O)24Ile was synthesized on a preloaded H<sub>2</sub>N-Cys(Trt)-2-ClTrt resin (0.62 mmol/g) on a 0.1 mmol scale using the automated peptide synthesizer according to the general method for solid phase peptide synthesis. Protection of the cysteine residues was Cys 3, 26-Acm; Cys 12, 28-Trt; Cys 7, 18- *t*-Bu. The crude peptide (177 mg, 54 % relative to resin loading) was used in the next step without further purification. MALDI-TOF MS calculated molecular weight for C<sub>144</sub>H<sub>217</sub>N<sub>37</sub>O<sub>40</sub>S<sub>6</sub> [M+H]<sup>+</sup> 3299 Found [M+H]<sup>+</sup> 3299.

**7.5.1.27 Bis-disulfide Formation of Residue 24 Substitution with Isoleucine (M(O)24Ile) (36)**



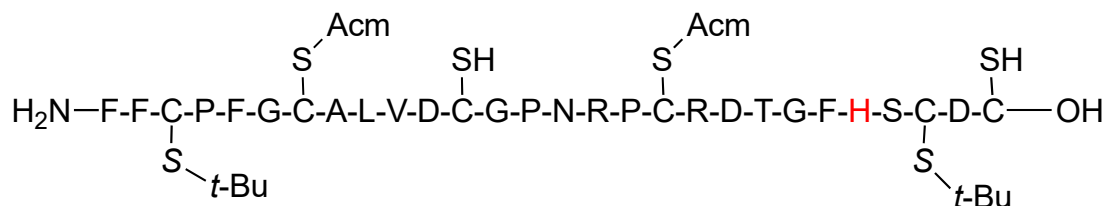
The bis-disulfide M(O)24Ile was synthesized according to general method B for bis-disulfide bond formation from the linear peptide. The crude peptide was used without further purification giving an orange-yellow solid (30 mg, 64 % isolated yield relative to 50 mg of crude. Calculated molecular weight for  $C_{138}H_{203}N_{35}O_{38}S_6$   $[M+H]^+$  3153 Found  $[M+H]^+$  3152.

**7.5.1.28 Tris-disulfide Formation of Residue 24 Substitution with Isoleucine (M(O)24Ile) (37)**



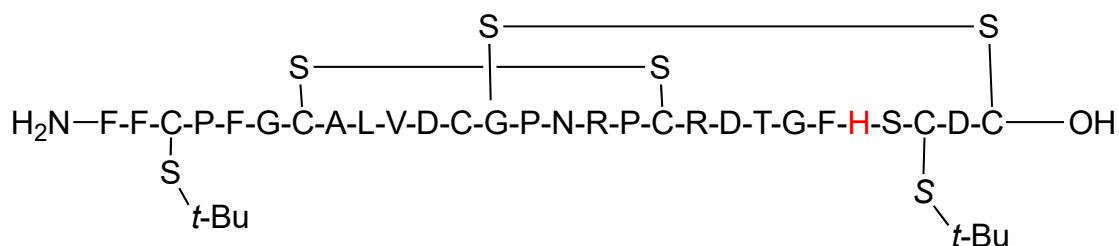
The introduction of the third disulfide bond was achieved by DMSO oxidation of the bicyclic peptide according to the general method for tris-disulfide bond formation. The crude peptide was purified by semi-preparative RP-HPLC using the general method ( $t_R = 20.6$  min, 1.94 mg, 7 % isolated yield relative to 30 mg of crude bicyclic peptide). MALDI-TOF MS Calculated molecular weight for  $C_{130}H_{185}N_{35}O_{38}S_6$   $[M+H]^+$  3039 Found  $(M + 2H)^+$  3040.

**7.5.1.29 Linear Peptide Formation of Residue 24 Substitution with Histidine (M(O)24His) (38)**



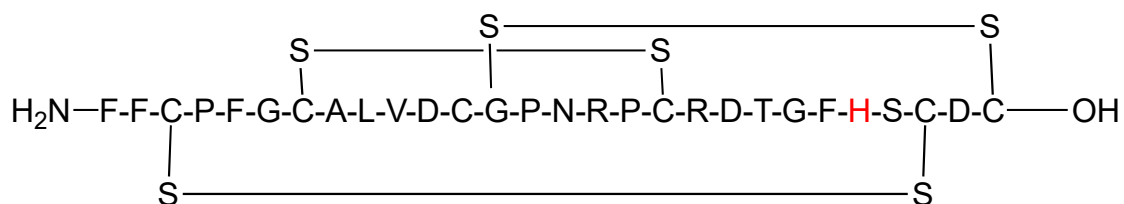
Linear peptide M(O)24His was synthesized on a preloaded H<sub>2</sub>N-Cys(Trt)-2-ClTrt resin (0.62 mmol/g) on a 0.1 mmol scale using the automated peptide synthesizer according to the general method for solid phase peptide synthesis. Protection of the cysteine residues was Cys 3, 26-Acm; Cys 12, 28-Trt; Cys 7, 18- *t*-Bu. The crude peptide (133 mg, 40 % relative to resin loading) was used in the next step without further purification. MALDI-TOF MS calculated molecular weight for C<sub>144</sub>H<sub>213</sub>N<sub>39</sub>O<sub>40</sub>S<sub>6</sub> [M+H]<sup>+</sup> 3323 Found [M+H]<sup>+</sup> 3323.

**7.5.1.30 Bis-disulfide Formation of Residue 24 Substitution with Histidine (M(O)24His) (39)**



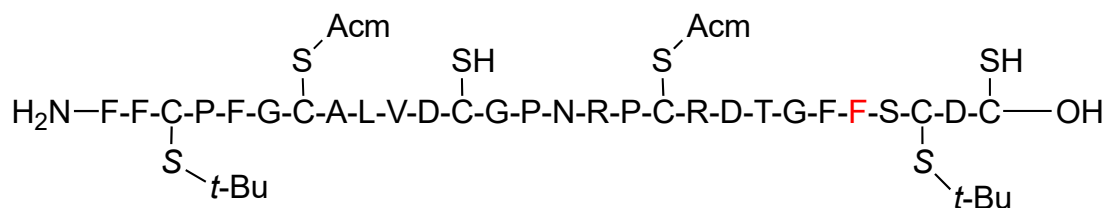
The bis-disulfide M(O)24His was synthesized according to general method B for bis-disulfide bond formation from the linear peptide. The crude peptide was used without further purification giving an orange-yellow solid (35 mg, 74 % isolated yield relative to 50 mg of crude linear peptide). Calculated molecular weight for C<sub>138</sub>H<sub>199</sub>N<sub>37</sub>O<sub>38</sub>S<sub>6</sub> [M+H]<sup>+</sup> 3177 Found [M+H]<sup>+</sup> 3177.

**7.5.1.31 Tris-disulfide Formation of Residue 24 Substitution with Histidine (M(O)24His) (40)**



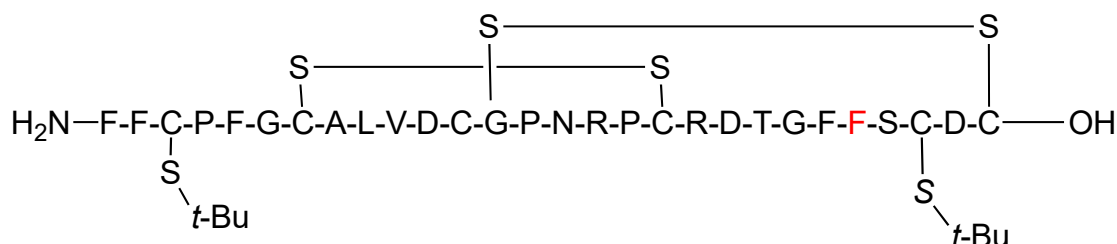
The introduction of the third disulfide bond was achieved by DMSO oxidation of the bicyclic peptide according to the general method for tris-disulfide bond formation. The crude peptide was purified by semi-preparative RP-HPLC using the general method ( $t_R = 23.7$  min, 2.91 mg, 8.8 % isolated yield relative to 35 mg of crude bicyclic peptide). MALDI-TOF MS Calculated molecular weight for C<sub>133</sub>H<sub>183</sub>N<sub>35</sub>O<sub>38</sub>S<sub>6</sub> [M+H]<sup>+</sup> 3063 Found (M)<sup>+</sup> 3062.

**7.5.1.32 Linear Peptide Formation of Residue 24 Substitution with Phenylalanine (M(O)24Phe) (41)**



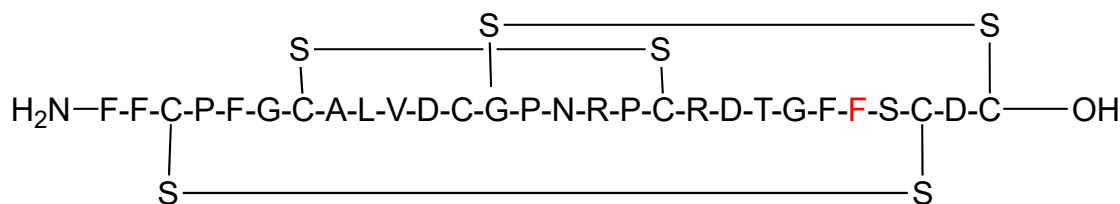
Linear peptide M(O)24Phe was synthesized on a preloaded H<sub>2</sub>N-Cys(Trt)-2-ClTrt resin (0.62 mmol/g) on a 0.1 mmol scale using the automated peptide synthesizer according to the general method for solid phase peptide synthesis. Protection of the cysteine residues was Cys 3, 26-Acm; Cys 12, 28-Trt; Cys 7, 18- *t*-Bu. The crude peptide (124 mg, 37 % relative to resin loading) was used in the next step without further purification. MALDI-TOF MS calculated molecular weight for C<sub>147</sub>H<sub>215</sub>N<sub>37</sub>O<sub>40</sub>S<sub>6</sub> [M+H]<sup>+</sup> 3331 Found [M+H]<sup>+</sup> 3335.

**7.5.1.33 Bis-disulfide Formation of Residue 24 Substitution with Phenylalanine (M(O)24Phe) (42)**



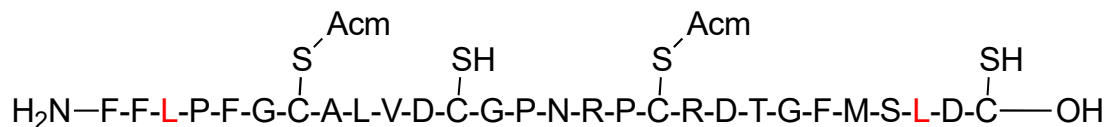
The bis-disulfide M(O)24Phe was synthesized according to general method B for bis-disulfide bond formation from the corresponding linear peptide. The crude peptide was used without further purification giving an orange-yellow solid (35 mg, 74 % isolated yield relative to 50 mg of crude linear peptide). Calculated molecular weight for  $C_{141}H_{201}N_{35}O_{38}S_6$   $[M+H]^+$  3187 Found  $[M+H]^+$  3186.

**7.5.1.34 Tris-disulfide Formation of Residue 24 Substitution with Phenylalanine (M(O)24Phe) (43)**



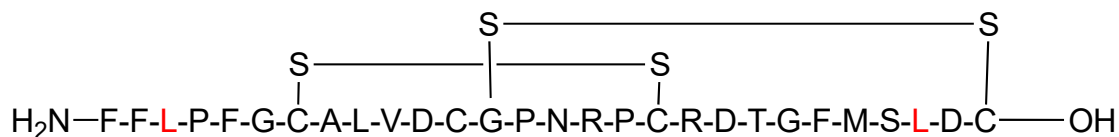
The introduction of the third disulfide bond was achieved by DMSO oxidation of the bicyclic peptide according to the general method for tris-disulfide bond formation. The crude peptide was purified by semi-preparative RP-HPLC using the general method ( $t_R = 15.6$  min, 1.96 mg isolated, 5.9 % isolated yield relative to 35 mg of crude bicyclic peptide). MALDI-TOF MS Calculated molecular weight for  $C_{133}H_{183}N_{35}O_{38}S_6$   $[M+H]^+$  3071 Found  $[M+H]^+$  3071.

### 7.5.1.35 Linear Peptide Formation of C3L, C26L (44)



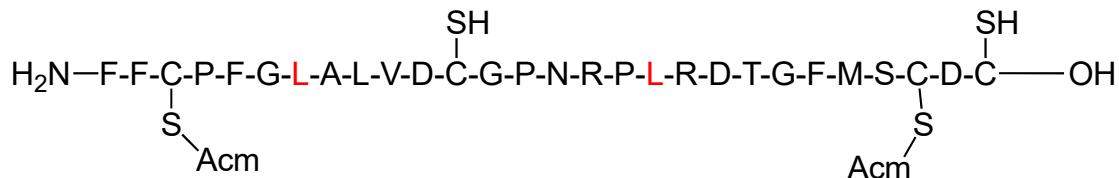
Linear peptide C3L, C26L was synthesized on a preloaded H<sub>2</sub>N-Cys(Acm)-2-ClTrt resin (0.62 mmol/g) on a 0.1 mmol scale using the automated peptide synthesizer according to the general method for solid phase peptide synthesis. Protection of the cysteine residues was Cys 7, 18-Trt, Cys 12, 28 -Acm. The crude peptide was used directly in the next reaction. MALDI-TOF MS calculated for C<sub>141</sub>H<sub>211</sub>N<sub>37</sub>O<sub>40</sub>S<sub>5</sub> [M+H]<sup>+</sup> 3223 Found [M+H]<sup>+</sup> 3323.

### 7.5.1.36 Bis-disulfide Peptide Formation of C3L, C26L (45)



The bis-disulfide of C3L, C26L was synthesized according to the general method A for bis-disulfide bond formation from the corresponding linear peptide. The crude peptide was purified by the semi-preparative RP-HPLC using the general method, t<sub>R</sub> = 23.8 min. MALDI-TOF MS calculated for C<sub>135</sub>H<sub>197</sub>N<sub>35</sub>O<sub>38</sub>S<sub>5</sub> [M+H]<sup>+</sup> 3077. Found [M+H]<sup>+</sup> 3077.

### 7.5.1.37 Linear Peptide Formation of C7L, C18L (46)



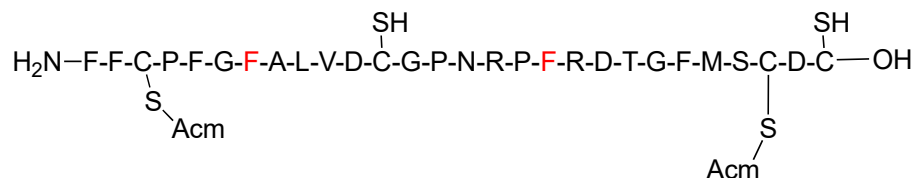
Linear peptide C7L, C18L was synthesized on a preloaded H<sub>2</sub>N-Cys(Trt)-2-ClTrt resin (0.62 mmol/g) on a 0.1 mmol scale using the automated peptide synthesizer according to the





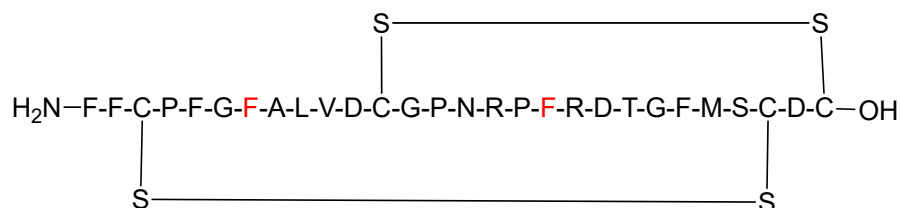
isolated yield relative to 30 mg of crude. MALDI-TOF MS calculated for  $C_{141}H_{194}N_{35}O_{38}S_5$   $[M+H]^+$  3145. Found  $(M + 2H)^+$  3146.

#### 7.5.1.43 Linear Peptide Formation of C7F, C18F (52)



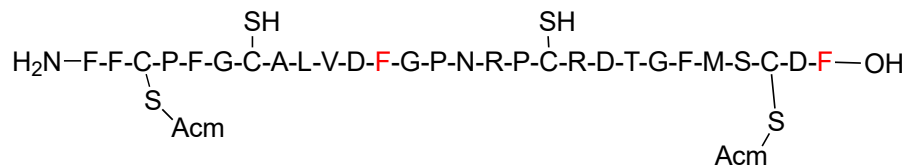
Linear peptide C7F, C18F was synthesized on a preloaded  $H_2N$ -Cys(Acm)-2-CITrt resin (0.32 mmol/g) on a 0.1 mmol scale using the automated peptide synthesizer according to the general method for solid phase peptide synthesis. Protection of the cysteine residues was Cys 12, 28-Acm, Cys 3, 26-Trt. The crude peptide was used directly in the next reaction. MALDI-TOF MS calculated for  $C_{147}H_{209}N_{37}O_{40}S_5$   $[M+H]^+$  3291. Found  $[M+H]^+$  3291.

#### 7.5.1.44 Bis-disulfide peptide formation of C7F, C18F (53)



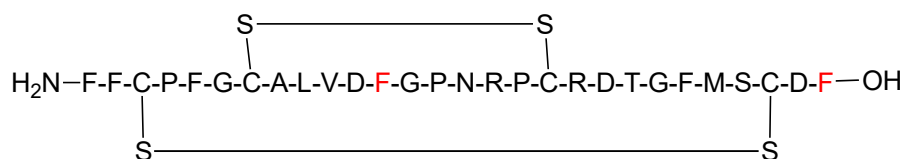
The bis-disulfide C7F, C18F was synthesized according to the general method for bis-disulfide bond formation from the corresponding linear peptide. The crude peptide was purified by the semi-preparative RP-HPLC using the general method,  $t_R = 25.6$  min (4.8 mg, 3.3 % isolated yield relative to 150 mg of crude linear peptide. MALDI-TOF MS calculated for  $C_{141}H_{194}N_{35}O_{38}S_5$   $[M+H]^+$  3145. Found  $(M + 2H)^+$  3146.

#### 7.5.1.45 Linear peptide formation of C12F, C28F (54)



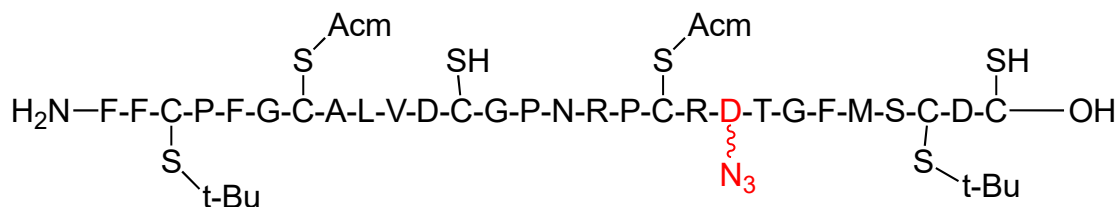
Linear peptide C12F, C28F was synthesized on a preloaded Fmoc-Phe-Wang resin (0.60 mmol/g) on a 0.1 mmol scale using the automated peptide synthesizer according to the general method for solid phase peptide synthesis. Protection of the cysteine residues was Cys 7, 18-Trt, Cys 3, 26-Acm. The crude peptide was used directly in the next reaction. MALDI-TOF MS calculated for  $\text{C}_{147}\text{H}_{209}\text{N}_{37}\text{O}_{40}\text{S}_5$   $[\text{M}+\text{H}]^+$  3291. Found  $[\text{M}+\text{H}]^+$  3291.

#### 7.5.1.46 Bis-disulfide peptide formation of C12F, C28F (55)



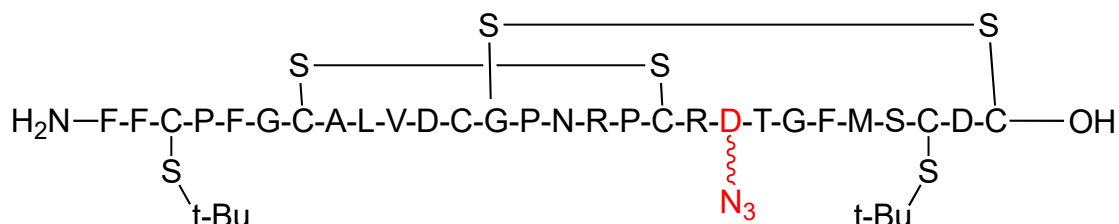
The bis-disulfide C12F, C28F was synthesized according to the general method for bis-disulfide bond formation from the corresponding linear peptide. The crude peptide was purified by the semi-preparative RP-HPLC using the general method,  $t_{\text{R}} = 29.6$  min (3.7 mg, 28.6 % isolated yield relative to 30 mg of crude linear peptide. MALDI-TOF MS calculated for  $\text{C}_{141}\text{H}_{194}\text{N}_{35}\text{O}_{38}\text{S}_5$   $[\text{M}+\text{H}]^+$  3145. Found  $(\text{M}+2\text{H})^+$  3146.

#### 7.5.1.47 Linear Peptide formation of Asp20-PEG-3-Azide-linear (56)



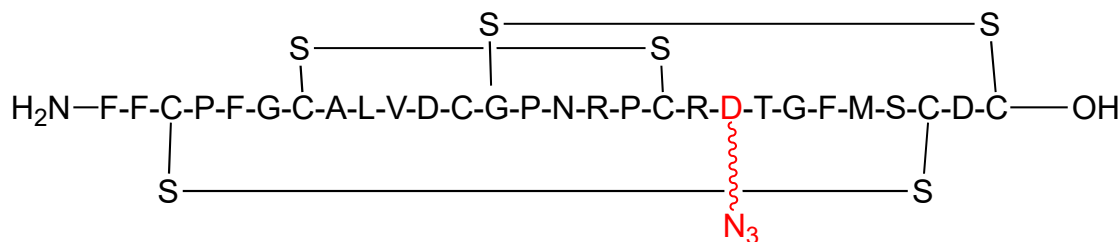
Linear peptide Asp20-PEG-3-Azide-linear was synthesized on a preloaded H<sub>2</sub>N-Cys(Acm)-2-ClTrt resin (0.62 mmol/g) on a 0.1 mmol scale using the automated peptide synthesizer according to the general method for solid phase peptide synthesis. Protection of the cysteine residues was Cys 3, 26-*t*-Bu; Cys 7, 18-Acm; Cys 12, 28-Trt. The crude peptide was used in the next step without further purification. Calculated molecular weight for C<sub>151</sub>H<sub>231</sub>N<sub>39</sub>O<sub>42</sub>S<sub>7</sub> [M+H]<sup>+</sup> 3489.1 Found [M+H]<sup>+</sup> 3490.5.

#### 7.5.1.48 Bis-disulfide formation of Asp20-PEG-3-Azide-Bisdisulfide (57)



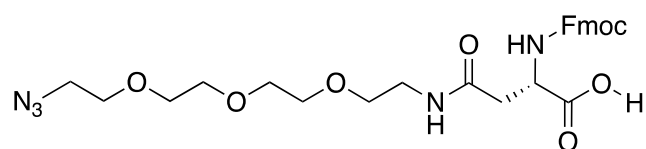
Peptide Asp20-PEG-3-Azide-bisdisulfide was synthesized according to the general method B for bis-disulfide bond formation from the linear peptide Asp20-PEG-3-Azide-linear. No further purification was performed. The crude peptide gave Asp20-PEG-3-Azide-bisdisulfide as an off- white powder. Calculated molecular weight for C<sub>142</sub>H<sub>217</sub>N<sub>37</sub>O<sub>40</sub>S<sub>7</sub> [M+H]<sup>+</sup> 3342.9 Found [M+H]<sup>+</sup> 3347.

#### 7.5.1.49 Tris-disulfide formation of Asp20-PEG-3-Azide-trisdisulfide (58)



The introduction of the third disulfide bond was achieved by DMSO oxidation of the bicyclic peptide Asp20-PEG-3-Azide-bisdisulfide according to the general method for trisulfide bond formation. The crude peptide was purified by semi-preparative RP-HPLC using the general method ( $t_R = 22$  min) to give Asp20-PEG-3-Azide-trisulfide as a white powder. Calculated molecular weight for  $C_{134}H_{199}N_{37}O_{40}S_7$   $[M+H]^+$  3256.7. Found  $[M+H]^+$  3255.

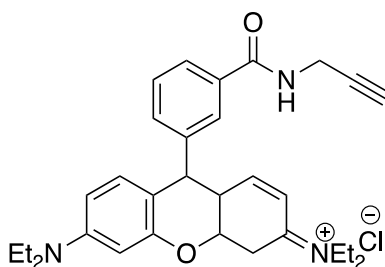
**7.5.1.50 Synthesis of PEG<sub>3</sub> Aspartic acid: (S)-15-(((9H-Fluoren-9-yl)methoxy)carbonylamino)-1-azido-13-oxo-3,6,9-trioxa-12-azahexadecan-16-oic acid (60)**



To a solution of Fmoc-Asp-*Ot*-Bu (1.036 g, 2.52 mmol) in DCM (20 mL) was added NMM (0.27 mL, 2.52 mmol) and HOBt (0.34 g, 2.52 mmol) followed by PyBOP (1.311 g, 2.52 mmol). Following a mixing period of 10 minutes, the 11-azido-3,6,9 trioxaundecan-1-amine (0.5 mL, 2.52 mmol) was added and the resulting mixture was stirred for 12 h. Removal of the solvent *in vacuo* gave an oily residue that was dissolved in EtOAc. The organic solution was washed with water then 10% citric acid. The organic layer was dried over sodium sulphate and concentrated *in vacuo*. The crude oil was purified via flash chromatography (10 % EtOAc in Hexanes) and the resulting oil was dissolved 20 mL of a 1:1 mixture of DCM:TFA. Upon stirring for 1 h, the solvent was removed and the product was used without further purification. Characterization conformed to literature reports:  $[\alpha]_D^{23.88^\circ}$  ( $c$  0.36,  $CHCl_3$ );  $^1H$  NMR ( $CDCl_3$ , 500MHz):  $\delta = 7.75$  (d, 2H,  $J = 7.5$  Hz, Fmoc-H), 7.60 (m, 2H, Fmoc-H), 7.39 (t, 2H,  $J = 5.0$  Hz,

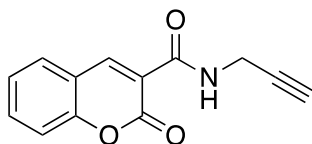
Fmoc-H), 7.30 (t, 2H,  $J = 7.5$  Hz, Fmoc-H), 6.94 (apparent s, 1H, NH), 6.31 (d, 1H,  $J = 7.5$  Hz, NH), 4.63 (m, 1H, H), 4.45-4.32 (m, 2H, Fmoc-CH<sub>2</sub>), 4.21 (t, 1H,  $J = 7.0$  Hz, Fmoc-CH), 3.66-3.34 (m, 16H, -CH<sub>2</sub>CH<sub>2</sub> & H), 2.94 (dd,  $J = 15.0, 4.0$  Hz, -CH<sub>2</sub>-CH<sub>2</sub>-N<sub>3</sub>), 2.81 (dd, 1H,  $J = 15.0, 6.0$  Hz). HRMS (ES): Calculated for C<sub>27</sub>H<sub>33</sub>N<sub>5</sub>O<sub>8</sub>Na 578.2221, found 578.2252.

#### 7.5.1.51 Formation of the alkyne functionalized Rhodamine B (65)



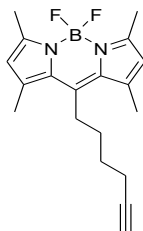
Propargylamine hydrochloride (6.0 mmol, 0.549 g) and rhodamine B (4.0 mmol, 1.92 g) were dissolved in anhydrous methanol (10.0 mL) and cooled to 0 °C. To this solution, triethylamine (6.0 mmol, 0.836 mL) was added. Addition of 1-[(3-dimethylamino)propyl]-3-ethycarbodiimide hydrochloride (6.0 mmol, 1.15 g) followed. The mixture was warmed to room temperature and stirred for 17 h. After 17 h, methanol was removed *in vacuo* and crude solids purified by column chromatography (1:3 EtOAc:Hexanes). Yield 17 % NMR analysis conformed to literature reports: <sup>1</sup>H NMR (400 MHz, CDCl<sub>3</sub>):  $\delta = 1.16$  (m, CH<sub>3</sub>, 12H), 1.77 (t,  $J = 2.4$  Hz, HC $\equiv$ C, 1H), 3.33 (m, NCH<sub>2</sub>CH<sub>3</sub>, 8H), 3.95 (d,  $J = 1.8$  Hz, H<sub>2</sub>C $\equiv$ C, 2H), 6.26–7.93 (m, aromatics, 10H).

#### 7.5.1.52 Formation of the Alkyne Functionalized Coumarin: N-(Prop-2-ynyl)-2-oxo-2H-chromene-3-carboxamide (68)



To a solution of thionyl chloride (10 mL), under an inert atmosphere of argon, coumarin-3-carboxylic acid (2.20 mmol, 0.4183 g) was added and the mixture was stirred for 3 h. The resulting slurry was filtered and the solids were carried forward immediately. The solids were dissolved in DCM (10 mL) and triethylamine (2.64 mmol, 0.2669 g) was added. Propargylamine (2.53 mmol, 0.134 g) in DCM (5 mL) was added dropwise to the mixture. The reaction mixture was stirred for 2 h and concentrated to dryness *in vacuo*. The resulting residue was dissolved in EtOAc and washed 3 x 2 M HC followed by a wash with saturated NaHCO<sub>3</sub>. The organic layer was dried with sodium sulfate, filtered and concentrated to dryness *in vacuo*. The solids were purified through column chromatography (1:3 EtOAc:Hexanes). Yield 46 % NMR analysis conformed to literature reports: <sup>1</sup>H NMR (400 MHz, CDCl<sub>3</sub>) δ = 2.27 (s, 1H, C≡CH), 4.26 (s, 2H, NHCH<sub>2</sub>), 7.38-7.43 (m, 2H, ArH); 7.67-7.71 (m, 2H, ArH), 8.96 (s, 1H, ArCH). ESI-MS m/z [MH<sup>+</sup>] 228.

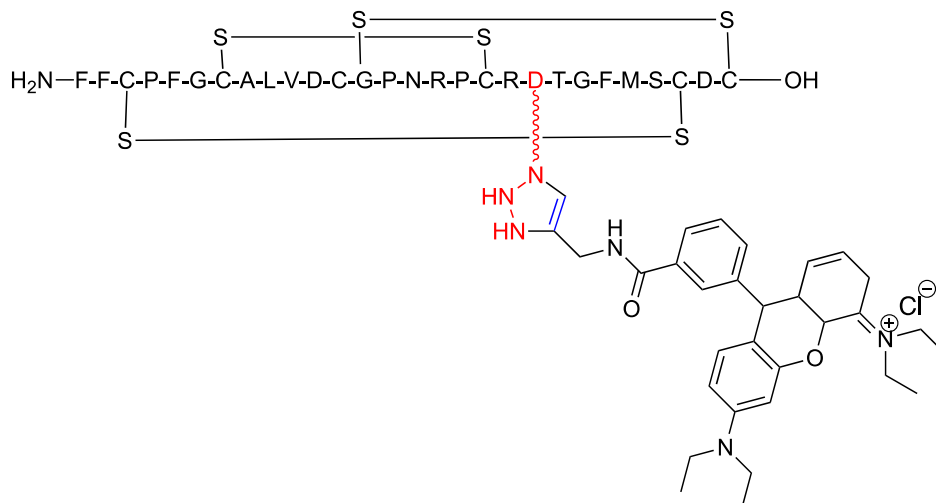
#### 7.5.1.53 Synthesis of 4,4-difluoro-8-(hept-6-yne)-1,3,5,7-tetramethyl-4-bora-3a,4a-diaza-s-indacene, the alkyne functionalized BODIPY (73)



Oxalyl chloride (14.74 mmol 1.8709 g) was added dropwise to a solution of hept-6-ynoic acid (9.83 mmol, 1.24 mL) in toluene (10 mL). A catalytic amount of DMF was added at room temperature and the reaction mixture was stirred for 3 h. After 3 h, oxalyl chloride was removed through co-evaporation with toluene. The reaction was then concentrated to dryness *in vacuo*. An oily brown residue was obtained.

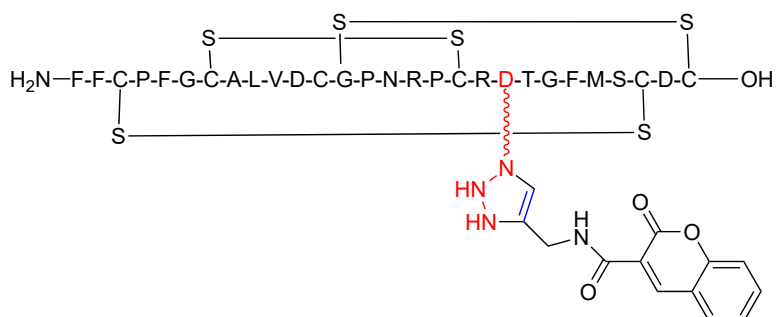
The oily residue was dissolved in DCE to give a 1M solution. 2-Dimethyl-1*H*-pyrrole was added slowly to the mixture and reaction was heated to 65 °C. After 2 h, the reaction was cooled to room temperature. Boron trifluoride etherate (5 eq) was added over 10 min followed by the drop-wise addition of DIPEA (4 eq). Reaction mixture was stirred for 12 h and filtered to obtain reddish brown solids. Yield 23 % NMR analysis conformed to literature reports: <sup>1</sup>H NMR (400 MHz, CDCl<sub>3</sub>): δ = 6.03 (s, 2H), 2.91-2.85 (m, 2H), 2.50 (s, 6H), 2.37 (s, 6H), 2.24 (dt, *J*<sub>1</sub> = 6.30 Hz, *J*<sub>2</sub> = 2.66 Hz, 2H), 1.95 (t, *J* = 2.64 Hz, 1H), 1.78-1.63 (m, 4H). <sup>13</sup>C NMR (100 MHz, CDCl<sub>3</sub>): δ = 153.70, 145.86, 140.30, 131.30, 121.52, 83.60, 68.94, 30.45, 28.79, 27.71, 18.05, 16.15, 14.31. ESI-MS: calculated for C<sub>19</sub>H<sub>23</sub>BF<sub>2</sub>N<sub>2</sub>H<sup>+</sup> 329.19951, found 329.19961

### 7.5.1.54 Formation of Asp20-PEG-3-Rhodamine (74)



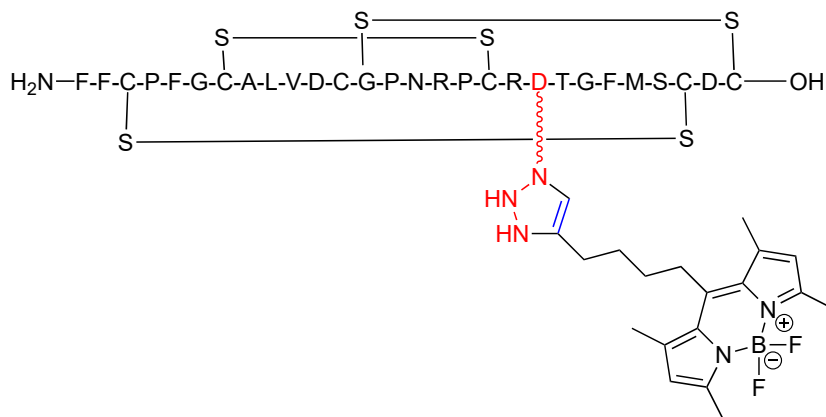
Peptide Asp20-PEG-3-Rhodamine (46) was synthesized according to the general method for the [2+3] cycloaddition from the purified trisdisulfide peptide Asp20-PEG-3-Azide-trisdisulfide (30). The crude peptide was purified using the general RP-HPLC method, to give Asp20-PEG-3-Rhodamine (46) as a bright-pink powder. Calculated molecular weight for  $C_{168}H_{233}N_{42}O_{42}S_7$   $[M+H]^+$  3737.5. Found  $[M+H]^+$  3739.

### 7.5.1.55 Formation of Asp20-PEG-3-Coumarin (75)



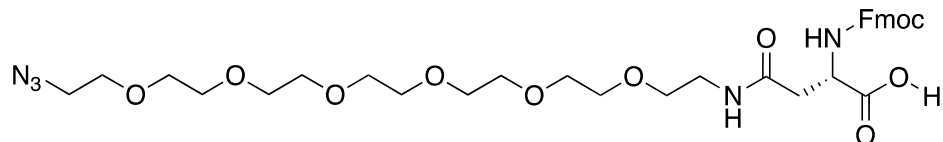
Peptide Asp20-PEG-3-Coumarin was synthesized according to the general method for the [2+3] cycloaddition from the purified trisdisulfide peptide Asp20-PEG-3-Azide-trisdisulfide. The crude peptide was purified using the general RP-HPLC method, to give Asp20-PEG-3-Coumarin as a pale beige powder. Calculated molecular weight for  $C_{138}H_{203}N_{35}O_{38}S_6$   $[M+H]^+$  3483.9. Found  $[M+H]^+$  3474. Calculated  $[M+H]^+$  was based on open ring 3-carboxycoumarin, found  $[M+H]^+$  determined that the coumarin was in a closed ring lactone.

#### 7.5.1.56 Formation of Asp20-PEG-3-BODIPY (76)



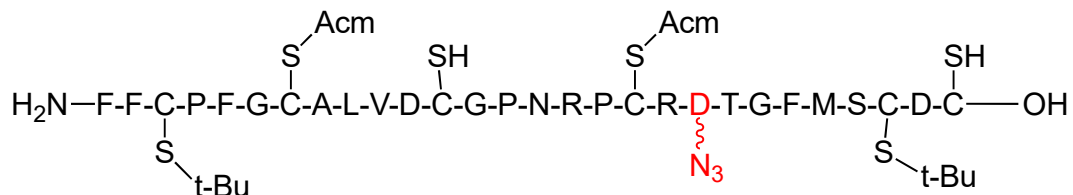
Peptide Asp20-PEG-3-BODIPY was synthesized according to the general method for the [2+3] cycloaddition from the purified trisdisulfide peptide Asp20-PEG-3-Azide-trisdisulfide (30). The crude peptide was purified using the general RP-HPLC method, to give Asp20-PEG-3-Rhodamine (46) as a bright-pink powder. Calculated molecular weight for  $C_{168}H_{233}N_{42}O_{42}S_7$   $[M+H]^+$  3584.5. Found  $[M+H]^+$  3585.

### 7.5.1.57 Synthesis of PEG<sub>6</sub> Linker (79)



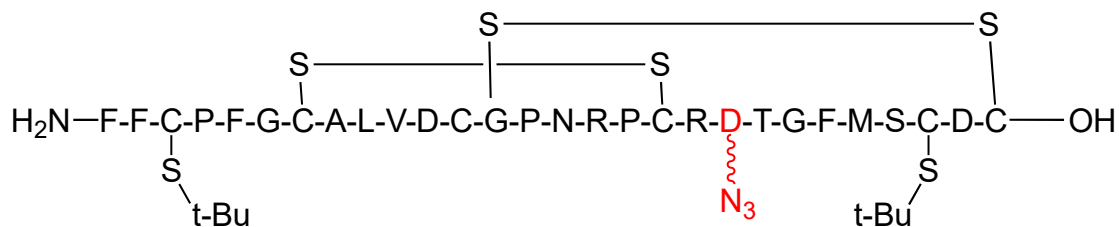
To a solution of Fmoc-Asp-*Ot*-Bu (1.036 g, 2.52 mmol) in DCM (20 mL) was added NMM (0.27 mL, 2.52 mmol) and HOBt (0.34 g, 2.52 mmol) followed by PyBOP (1.311 g, 2.52 mmol). Following a mixing period of 10 minutes, the *O*-(2-aminoethyl)-*O*-(2-azidoethyl)pentaethylene glycol (0.5 mL, 2.52 mmol) was added and the resulting mixture was stirred for 12 h. Removal of the solvent *in vacuo* gave an oily residue that was dissolved in EtOAc. The organic solution was washed with water and then 10 % citric acid. The organic layer was then dried over sodium sulphate, and concentrated *in vacuo*. The crude amino acid was purified on flash chromatography (10 % EtOAc in Hexanes) and concentrated *in vacuo*. The resultant oil was dissolved in 20 mL of a 1:1 mixture of DCM:TFA and allowed to stir for 1 h. The solvent was removed *in vacuo* and the product was used without further purification. <sup>1</sup>H NMR (CDCl<sub>3</sub>, 300MHz): δ = 7.75 (d, 2H, *J* = 7.5 Hz, Fmoc-H), 7.60 (m, 2H, Fmoc-H), 7.39 (t, 2H, *J* = 7.2 Hz, Fmoc-H), 7.30 (t, 2H, *J* = 7.5 Hz, Fmoc-H), 6.34 (apparent s, 1H, NH), 6.11 (d, 1H, *J* = 10.2 Hz, NH), 4.45-4.32 (m, 2H, Fmoc-CH<sub>2</sub>), 4.21 (t, 1H, *J* = 6.9 Hz, Fmoc-CH), 3.66-3.54 (m, 26H, -CH<sub>2</sub>CH<sub>2</sub>& CH<sub>2</sub>), 3.49 (s, 1H, H), 3.38 (t, 2H, *J* = 5.4 Hz, CH<sub>2</sub>) 2.94 (dd, 1H, *J* = 16.2, 4.0 Hz, -CH<sub>2</sub>-CH<sub>2</sub>-N<sub>3</sub>), 2.81 (dd, 1H, *J* = 16.2, 3.6 Hz).

### 7.5.1.58 Linear Peptide Formation of Asp20-PEG-6-Azide-Linear (80)



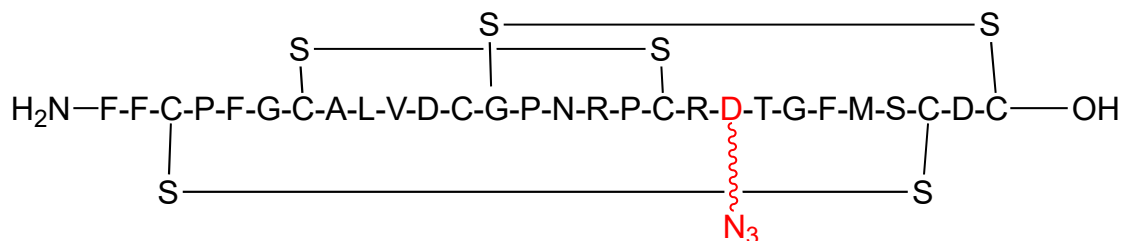
Linear peptide Asp20-PEG-6-Azide-linear was synthesized on a preloaded H<sub>2</sub>N-Cys(Acm)-2-ClTrt resin (0.62 mmol/g) on a 0.1 mmol scale using the automated peptide synthesizer according to the general method for solid phase peptide synthesis on the AB 433A synthesizer. Protection of the cysteine residues was Cys 3, 26-*t*-Bu; Cys 7, 18-Acm; Cys 12, 28-Acm. The crude peptide was purified by semi-prep RP-HPLC using the general method (*t<sub>R</sub>*=22 min). Calculated molecular weight for C<sub>144</sub>H<sub>217</sub>N<sub>37</sub>O<sub>40</sub>S<sub>6</sub> [M+H]<sup>+</sup> 3649. Found [M+H]<sup>+</sup> 3650.

### 7.5.1.59 Bis-disulfide Formation of Asp20-PEG-6-Azide-bisdisulfide (81)



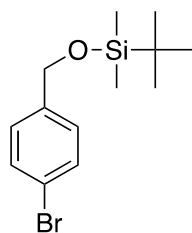
Peptide Asp20-PEG-6-Azide-bisdisulfide was synthesized according to general method B for bis-disulfide bond formation from the purified linear peptide Asp20-PEG-6-Azide-linear. The crude peptide was used without further purification to give Asp20-PEG-6-Azide-bisdisulfide as an off-white powder. Calculated molecular weight for C<sub>151</sub>H<sub>229</sub>N<sub>39</sub>O<sub>43</sub>S<sub>7</sub> [M+H]<sup>+</sup> 3503.1. Found [M+H]<sup>+</sup> 3504.1.

#### 7.5.1.60 Tris-disulfide Formation of Asp20-PEG-6-Azide-trisdisulfide (**82**)



The introduction of the third disulfide bond was achieved by DMSO oxidation of the bicyclic peptide Asp20-PEG-6-Azide-bisdisulfide according to the general method for trisdisulfide bond formation. The crude peptide was purified by semi-preparative RP-HPLC using the general method 1 ( $t_R = 22$  min) Calculated molecular weight for  $C_{143}H_{211}N_{39}O_{43}S_7$   $[M+H]^+$  3388.9 Found  $[M+H]^+$  3389.

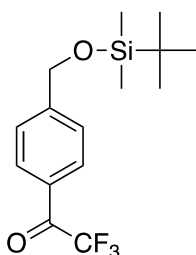
#### 7.5.1.61 4-Bromobenzyl Alcohol-*O*-(*tert*-Butyldimethylsilyl) Ether (**84**)



To a solution of 4-bromobenzylalcohol (**83**) (10.0 g, 53.0 mmol, 1.00 equiv.) in anhydrous DMF (40 mL), *tert*-butyldimethylsilyl chloride (8.74 g, 59.8 mmol, 1.10 equiv.) and imidazole (8.65 g, 127 mmol, 2.40 equiv.) were added under an atmosphere of argon. The mixture was heated to 40 °C and stirred for twenty-one hours. The reaction mixture was poured into ether (180 mL) and washed with water (3 x 50 mL), dried over magnesium sulphate, filtered and concentrated. Flash chromatography of the crude residue (30 g silica, 2 cm diameter in 5 % EtOAc: Hexane) resulted in pure product as a colorless liquid (16.0 g, 90 %). NMR analysis

conformed to literature reports.  $^1\text{H}$  NMR (400 MHz,  $\text{CDCl}_3$ ):  $\delta$  = 0.09 (6H, s, 2 x  $\text{CH}_3$ ), 0.93 (9H, s, 3 x  $\text{CH}_3$ ), 4.68 (2H, s,  $\text{CH}_2$ ), 7.19 (2H, d,  $J$  = 7.9 Hz, ArCH), 7.45 (2H, d,  $J$  = 8.2 Hz, ArCH);  $^{13}\text{C}$  NMR (100 MHz,  $\text{CDCl}_3$ )  $\delta$  = -4.84, 18.81, 26.35, 64.72, 120.98, 128.12, 131.68, 140.86.

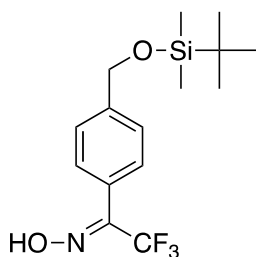
#### 7.5.1.62 4-[(*tert*-Butyldimethylsiloxy)methyl]-2,2,2-trifluoroacetophenone (85)



To a stirred solution of 4-bromobenzyl alcohol-*O*-(*tert*-butyldimethylsiloxy) ether (15.9 g, 53.0 mmol, 1.00 equiv.) in anhydrous ether (380 mL) was added *n*-butyl lithium (77.3 mmol, 45.00 mL, 1.7 M in hexanes) at -78 °C (acetone/dry ice) under an inert atmosphere of argon, over a period of ten minutes. The reaction mixture was allowed to stir under these conditions until a TLC on a mini-workup indicated good conversion to the aryl lithium (approximately two hours). Trifluoroacetic anhydride was added drop wise over 30 minutes and stirring continued for a further three hours. Saturated aqueous ammonium chloride (250 mL) was then added and the reaction mixture allowed to warm to room temperature. The reaction mixture was then diluted with ether (150 mL), and then separated and the organic layer washed with saturated aqueous ammonium chloride (2 x 125 mL) and water (2 x 75 mL). The combined aqueous layers were washed with ether (150 mL) and then the combined organics dried over magnesium sulphate, filtered and concentrated. Flash chromatography of the crude residue (70 g silica, 2 cm

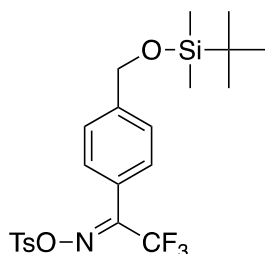
diameter in 5 % EtOAc: Hexane) resulted in pure product as a colorless liquid. (13.5 g, 80 %) as a colourless oil. NMR analysis conformed to literature reports.  $^1\text{H}$  NMR (400 MHz,  $\text{CDCl}_3$ ):  $\delta$  = 0.04 (6H, s, 2 x  $\text{CH}_3$ ) 0.87 (9H, s, 3 x  $\text{CH}_3$ ), 4.75 (2H, s,  $\text{CH}_2$ ), 7.50 (2H, d,  $J$  = 9.6 Hz, ArCH), 8.05 (2H, d,  $J$  = 8.4 Hz, ArCH).

#### 7.5.1.63 4-[(*tert*-Butyldimethylsiloxy)methyl]-2,2,2-trifluoroacetophenone oxime (86)



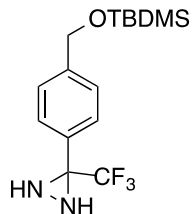
To a solution of 4-[(*tert*-butyldimethylsiloxy)methyl]-2,2,2-trifluoroacetophenone (13.0 g, 40.9 mmol, 1 equiv.) in anhydrous pyridine (100 mL) and anhydrous ethanol (47 mL) under an inert atmosphere of argon, hydroxylamine hydrochloride (3.12 g, 44.9 mmol, 1.10 equiv.) was added. The reaction mixture was brought to 80 °C and stirred overnight at this temperature. Once complete, the reaction mixture was cooled, concentrated, and suspended in ether (250 mL). The resulting organic layer was washed with water (4 x 100 mL), dried over magnesium sulphate, filtered and concentrated. The subsequent residue was purified by column chromatography (70 g silica, 2 cm diameter, dichloromethane) to yield the title compound (11.6 g, 85 %) as a colourless viscous liquid: NMR analysis conformed to literature reports.  $^1\text{H}$  NMR (400 MHz,  $\text{CDCl}_3$ ):  $\delta$  = 0.11 and 0.12 (6H, s, 2 x  $\text{CH}_3$ ), 0.95 and 0.96 (9H, s, 3 x  $\text{CH}_3$ ), 4.78 and 4.79 (2H, s,  $\text{CH}_2$ ), 7.40 (4H, m, ArCH);  $^{13}\text{C}$  NMR (100 MHz,  $\text{CDCl}_3$ ):  $\delta$  = -4.88, 18.84, 26.33, 64.89, 124.67, 126.29, 128.70, 129.01, 137.75, 144.15, 144.48, 149.15; (ESI-MS)  $m/z$  356  $[\text{M}+\text{Na}]^+$ .

**7.5.1.64 4-[(*tert*-Butyldimethylsiloxy)methyl]-2,2,2-trifluoroacetophenone-O-(4-toluenesulphonyl) oxime (87)**



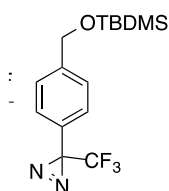
To a stirred solution of 4-[(*tert*-butyldimethylsiloxy)methyl]-2,2,2-trifluoroacetophenone oxime (10 g, 30.0 mmol, 1.00 equiv), anhydrous diisopropylethylamine (6.793 mL, 5.04 g, 39.0 mmol, 1.30 equiv) and 4-dimethylaminopyridine (0.367 g, 3.00 mmol, 0.1 equiv.) in anhydrous dichloromethane (50 mL) at 0 °C under an atmosphere of argon was added 4-toluenesulphonyl chloride (6.875 g, 36.0 mmol, 1.2 equiv.). The reaction was allowed to warm to room temperature and stirred for an additional two hours. The reaction mixture was then washed with water (3 x 25 mL), dried over magnesium sulphate, filtered and concentrated. The red oil was purified using column chromatography (70 g silica, 2 cm diameter, 3:4 dichloromethane:hexane) to afford the product (9.06 g, 62 %) as a pale green oil. NMR analysis conformed to literature reports. <sup>1</sup>H NMR (400 MHz, CDCl<sub>3</sub>): δ = 0.11 and 0.12 (6H, s, 2 x CH<sub>3</sub>), 0.95 and 0.96 (9H, s, 3 x CH<sub>3</sub>), 2.46 and 2.48 (3H, s, CH<sub>3</sub>), 4.77 and 4.78 (2H, s, CH<sub>2</sub>), 7.40 (6H, m, ArCH), 7.90 (2H, m, ArCH); (ESI-MS), m/z 510 [M+Na]<sup>+</sup>.

### 7.5.1.65 3-[ $\alpha$ -(*tert*-Butyldimethylsiloxy)-4-tolyl]-3-(trifluoromethyl)diaziridine (88)



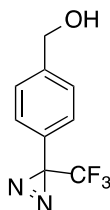
A three-neck flask was fit with a potassium carbonate drying tube and a acetone/dry ice condenser under an atmosphere of argon. A stirred solution of 4-[(*tert*-butyldimethylsiloxy)methyl]-2,2,2-trifluoroacetophenone-*O*-(4-toluenesulphonyl) oxime (5.00 g, 10.3 mmol, 1 equiv.) in anhydrous ether (30 mL) was cooled to -78 °C (acetone/dry-ice bath). Ammonia gas was bubbled through the solution until sufficient liquid ammonia had condensed (~80 mL). The reaction mixture was then allowed to stir at this temperature for a further three hours before being allowed to warm to room temperature over two hours. Upon warming to room temperature the ammonia gas evaporated and the reaction mixture was filtered and concentrated to give the title compound (2.96 g, 87 %) as a translucent paste that was used in subsequent transformations without further purification. NMR analysis conformed to literature reports. <sup>1</sup>H NMR (400 MHz, CDCl<sub>3</sub>):  $\delta$  = 0.10 (6H, s, 2 x CH<sub>3</sub>) 0.94 (9H, s, 3 x CH<sub>3</sub>), 2.20 (1H, d,  $J$  = 8.8 Hz, NH), 2.78 (1H, d,  $J$  = 8.4 Hz, NH), 4.76 (2H, s, CH<sub>2</sub>), 7.38 (2H, d,  $J$  = 8.4 Hz, ArCH), 7.58 (2H, d,  $J$  = 8.4 Hz, ArCH).

### 7.5.1.66 3-[ $\alpha$ -(*tert*-Butyldimethylsiloxy)-4-tolyl]-3-(trifluoromethyl)diazirine (89)



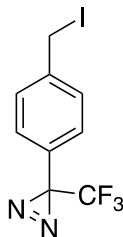
In a darkened fume hood, a stirred solution of 3-[ $\alpha$ -(*tert*-butyldimethylsiloxy)-4-tolyl]-3-trifluoromethyl diaziridine (2.500 g, 7.53 mmol 1.00 equiv.) and anhydrous triethylamine (1.745 mL, 1.267 g, 12.55 mmol, 1.67 equiv.) in anhydrous methanol (5 mL) was made. Iodine (1.594 g, 6.28 mmol, 1.20 equiv.) was added drop wise until a red/orange colour persisted. The reaction mixture was then allowed to stir for a further twenty minutes before being neutralised with 10 % aqueous citric acid solution and then quenched with a few drops of 5 % aqueous sodium metabisulphite solution. The reaction mixture was then poured in ether (150 mL) dried over sodium sulphate, filtered and concentrated. Column chromatography (70 g silica, 2 cm column, hexane:dichloromethane, 2:1 (column wrapped in aluminum foil) afforded the title compound (1.19 g, 48 %) as a light yellow oil. NMR analysis conformed to literature reports.  $^1\text{H}$  NMR (400 MHz,  $\text{CDCl}_3$ ):  $\delta$  = 0.09 (6H, s, 2 x  $\text{CH}_3$ ) 0.93 (9H, s, 3 x  $\text{CH}_3$ ), 4.74 (2H, s,  $\text{CH}_2$ ), 7.18 (2H, d,  $J$  = 8.0 Hz, ArCH), 7.38 (2H, d,  $J$  = 8.0 Hz, ArCH);  $^{13}\text{C}$  NMR (100 MHz,  $\text{CDCl}_3$ ):  $\delta$  = -4.94, 18.79, 26.30, 64.64, 120.79, 124.42, 126.64, 126.78, 127.98, 143.74.

### 7.5.1.67 4-[3-Trifluoromethyl-3*H*-diazirin-3-yl]benzyl alcohol (90)



In a darkened fume hood, a solution of tetrabutylammonium fluoride (4.32 mL, 1.00 M in THF, 1.20 equiv.) containing water (0.216 mL, 5 % v/v) was made. 3-[ $\alpha$ -(tert-butyl)dimethylsiloxy]-4-tolyl]-3-trifluoromethyl diazirine (1.19 g, 3.60 mmol, 1 equiv.) was added to this solution and the mixture was allowed to stir at room temperature for five hours. Upon completion the reaction mixture was diluted with ether (40 mL), washed with water (3 x 12 mL), dried over sodium sulphate, filtered and concentrated. The yellow oil was used without further purification (0.895 g, 115 %). NMR analysis conformed to literature reports.  $^1\text{H}$  NMR (400 MHz,  $\text{CDCl}_3$ ):  $\delta$  = 2.39 (1H, brs, OH), 4.66 (2H, s,  $\text{CH}_2$ ), 7.17 (2H, d,  $J$  = 8.0 Hz, ArCH), 7.35 (2H, d,  $J$  = 8.0 Hz, ArCH).

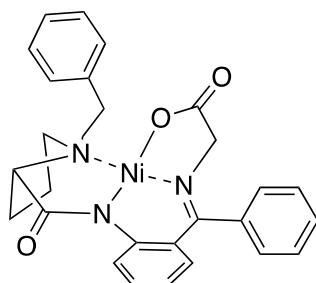
### 7.5.1.68 3-( $\alpha$ -Iodo-4-tolyl)-3-(trifluoromethyl)-3*H*-diazirine (91)



4-[3-Trifluoromethyl-3*H*-diazirin-3-yl]benzyl alcohol (0.895 g, 4.14 mmol, 1.00 equiv.) was dissolved in anhydrous acetonitrile (10 mL) under an inert atmosphere of argon, and

methyltriphenoxyphosphonium iodide (4.204 g, 8.28 mmol, 2.00 equiv.) was added. The reaction mixture was stirred for 24 hours. The mixture was diluted with ether (60 mL) and washed successively with sodium hydroxide (1 M, 2 x 40 mL) and water (2 x 50 mL). The organic layer was dried with magnesium sulphate, filtered and concentrated. Column chromatography (20 g silica, 2 cm column, ether:hexane, 1:2 (column wrapped in aluminum foil) of the crude red oil resulted in the title compound (0.812 g, 60 %) as a pale yellow solid. NMR analysis conformed to literature reports. <sup>1</sup>H NMR (500 MHz, CDCl<sub>3</sub>): δ = 4.42 (2H, s, CH<sub>2</sub>), 7.12 (2H, d, *J* = 8.5 Hz, ArCH), 7.40 (2H, d, *J* = 8.5 Hz, ArCH); (ESI-MS) *m/z* 327 [M+H]<sup>+</sup>.

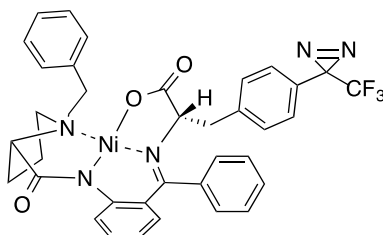
#### 7.5.1.69 Nickel Complexation of (*S*)-2-[*N*-(*N'*-benzylpropyl)amino]benzophenone and glycine (92)



In anhydrous methanol (16 mL), (*S*)-2-[*N*-(*N'*-benzylpropyl)amino]benzophenone (0.9635 g, 2.51 mmol), glycine (0.9410 g, 12.53 mmol) and nickel (II) nitrate hexahydrate (1.4721 g, 5.06 mmol) were added and the green solution was stirred at 55 °C for 10 minutes. Sodium methoxide (4.9 M in methanol, 4.35 mL, 21.30 mmol) was then added and the mixture was stirred at 55 °C at an additional one hour resulting in a brown solution. The reaction was quenched with acetic acid (1.7 mL) and the reaction mixture was diluted with water (80 mL). The resulting mixture was left in the fridge overnight. Red crystals were obtained upon filtration and the crude crystals

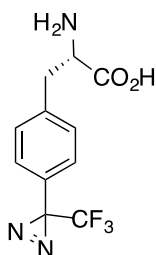
were purified by column chromatography (35 g silica, 1:3 EtOAc: Hexane) to give the title compound (0.794 g, 64%) as red crystals. NMR analysis conformed to literature reports.  $[\alpha]_D^{+2076.9^\circ}$  (c 0.60,  $\text{CH}_2\text{Cl}_2$ ); IR ( $\text{CHCl}_3$  cast) 3053, 2975, 1674, 1638  $\text{cm}^{-1}$ ;  $^1\text{H}$  NMR ( $\text{CDCl}_3$ , 400 MHz):  $\delta$  8.30 (d, 1H,  $J = 8.8$  Hz, Ar-H), 8.07(d, 2H,  $J = 7.1$  Hz, Ar-H), 7.58- 7.47 (m, 3H, Ar-H), 7.58-7.40 (m, 2H, Ar-H), 7.31 (dd, 1H,  $J = 7.4, 7.4$  Hz, Ar-H), 7.21 (dd, 1H, 7.2, 7.2 Hz, Ar-H), 7.10 (d, 1H,  $J = 7.2$  Hz, Ar-H), 7.20-6.95 (m, 1H, Ar-H), 6.80 (d, 1H,  $J = 7.0$  Hz, Ar-H), 6.75-6.68 (m, 1H, Ar-H), 4.49 (d, 1H,  $J = 12.7$  Hz, PhCHH), 3.83-3.64 (m, 4H, PhCHH, Pro-H $\delta$ , Gly-H $\alpha$ ), 3.52-3.42 (m, 1H, Pro-H $\alpha$ ), 3.42-3.28 (m, 1H, Pro-H $\delta$ ), 2.62-2.53 (m, 1H, Pro-H $\beta$ ), 2.36-2.50 (m, 1H, Pro-H $\beta$ ), 2.21-2.02 (m, 2H, Pro-H $\gamma$ );  $^{13}\text{C}$  NMR ( $\text{CDCl}_3$ , 100 MHz):  $\delta$  181.4, 177.3, 171.7, 142.6, 134.7, 133.3, 133.2, 132.2, 131.8, 129.8, 129.6, 129.4, 129.1, 128.9, 126.3, 125.7, 125.2, 124.3, 120.9, 69.9, 63.1, 61.3, 57.5, 30.8, 23.7; HR-MS (ESI) Calculated for  $\text{C}_{27}\text{H}_{25}\text{N}_3\text{O}_3\text{NaNi}$   $[\text{M}+\text{Na}]^+$  520.1142, found 520.1149.

#### 7.5.1.70 Alkylation of Nickel Complex with 3-( $\alpha$ -iodo-4-tolyl)-3-(trifluoromethyl)-3H-diazirine (93)



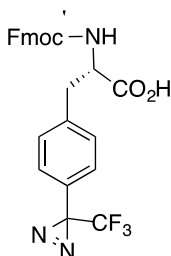
In a darkened fume hood, under an inert atmosphere of argon, the nickel complex (1.40 g, 2.82 mmol, 1.30 equiv.) and powdered sodium hydroxide (0.46 g, 11.92 mmol, 5.50 equiv.) were suspended in anhydrous acetonitrile (10 mL) and cooled to -10 °C (salt/ ice water bath). A solution of 3-( $\alpha$ -iodo-4-tolyl)-3-(trifluoromethyl)-3*H*-diazirine (0.706 g, 2.16 mmol, 1 equiv.) in anhydrous acetonitrile (5 mL) was added slowly. The mixture was warmed to room temperature and stirred for 20 h. The reaction mixture was diluted with dichloromethane (50 mL) and washed successively with aqueous acetic acid (0.2 M, 30 mL) and water (2 x 40 mL). The organic layer was then dried over magnesium sulphate, filtered and concentrated. Purification of the resulting red paste by column chromatography (35 g silica, 1.5 cm column, chloroform:acetone, 5:1 (column wrapped in aluminum foil)) afforded the product (0.678 g, 45 %) as a red glassy solid that was used in subsequent steps without further purification. NMR analysis conformed to literature reports. <sup>1</sup>H NMR (400MHz, CDCl<sub>3</sub>):  $\delta$  = 1.72 (1H, m, Pro CHH'), 1.88 (1H, m, Pro CHH'), 2.24 (2H, m, ProCH<sub>2</sub>), 2.37 (1H, m, Pro alkyl), 2.83 (1H, dd,  $J$  = 13.8 and 5.6, Phe CHH'), 3.06 (2H, m, Pro CH<sub>2</sub>), 3.33 (1H, dd,  $J$  = 10.2 and 6.1 Hz, Phe CHH'), 3.49, (1H, d,  $J$  = 12.8 Hz, Bzl CHH'), 4.29 (2H, m, Bzl CHH' and PheCH), 6.66 (2H, m, ArCH), 6.88 (1H, s, ArCH), 7.24 (9H, ArCH), 7.47 (1H, m, ArCH), 7.56 (2H, m, ArCH), 7.99 (2H, d,  $J$  = 7.2 Hz, ArCH), 8.22 (1H, d,  $J$  = 8.7 Hz, ArCH); <sup>13</sup>C NMR (100 MHz, CDCl<sub>3</sub>):  $\delta$  = 22.58, 28.25 (Q), 30.51, 38.98, 56.88, 63.19, 68.56, 70.10, 77.42, 116.51, 120.15, 120.55, 123.26, 123.79, 125.85, 126.66, 127.00, 127.43, 127.58, 128.30, 128.67, 128.83, 129.11, 129.80, 130.63, 120.86, 131.31, 131.56, 132.44, 133.11, 133.41, 133.97, 137.60, 142.76, 171.38, 178.00, 180.00; (ESI-MS),  $m/z$  697 [M+H]<sup>+</sup>.

### 7.5.1.71 (S)-3-[4-[3-(Trifluoromethyl)-3H-diazirin-3-yl]phenyl]alanine (94)



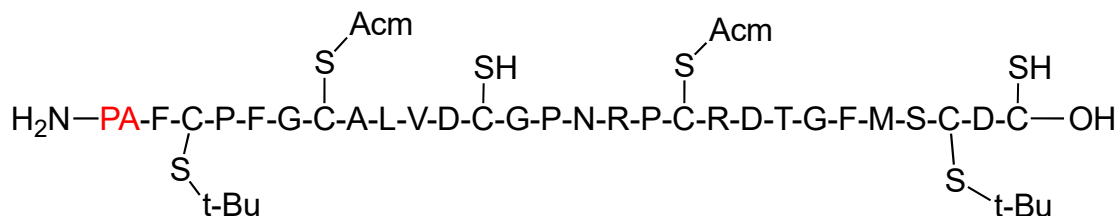
In a darkened fume hood, the alkylated nickel complex (0.500 g, 0.718 mmol) was dissolved in methanol (15 mL) and aqueous hydrochloric acid (1 N, 10 mL). The resulting red solution was heated at reflux for 15 min during which time the solution became a pale yellow color. The organic solvent was removed *in vacuo* and then the aqueous residue washed with dichloromethane (2 x 25 mL). The organic layers were combined and washed with water (2 x 15 mL). Aqueous layers were combined and brought to pH = 2.5 by addition of aqueous ammonia. Once at a pH of 2.5, the aqueous layers were absorbed onto Dowex50 (W2) H<sup>+</sup> exchange resin (30 g). The column was washed with water (100 mL), then methanol (80 mL) and then the product eluted with methanolic ammonia (2 M, 140 mL). Fractions were spotted on a TLC and tested with ninhydrin stain. Active fractions were concentrated and re-crystallised from the minimum amount of methanol/ water. (0.205 g, quantitative) as a white solid. NMR analysis conformed to literature reports. <sup>1</sup>H NMR (400 MHz, CF<sub>3</sub>CO<sub>2</sub>D), 3.43 (1H, m, CHH') 3.82 (1H, m CHH'), 4.60 (1H, m, CH), 7.19 (2H, m ArCH), 7.31 (2H, m, ArCH); (ESI-MS), m/z 285 [M+H]<sup>+</sup>; [α]<sub>D</sub> (c = 0.12, MeOH), -67.0 °C (lit. -70.1 °C).

**7.5.1.72 (S)-N-(9-Fluorenylmethoxycarbonyl)-[4-[3-(trifluoromethyl)-3H-diazirin-3-yl]phenyl]alanine (95)**



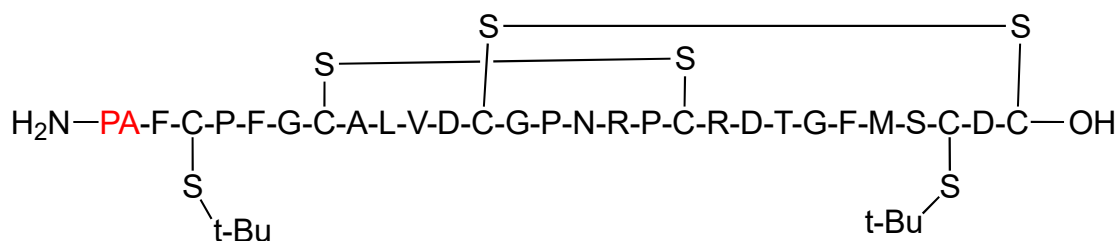
In a darkened fume hood, a suspension of (S)-3-[4-[3-(trifluoromethyl)-3H-diazirin-3-yl]phenyl]alanine (200 mg, 0.702 mmol) and sodium carbonate (220 mg, 2.12 mmol) in acetone (4 mL) and water (15 mL) was made. The mixture was brought to 0 °C, and N-(9-fluorenylmethoxycarbonyloxy) succinimide (245 mg, 0.702 mmol) was added in portions. The reaction mixture was warmed to room temperature and stirred for an additional 48 hours. The reaction mixture was brought to pH 1.0 by addition of aqueous hydrochloric acid (1.0 M). The aqueous layer was extracted with ethyl acetate (15 mL). The organic layer was washed successively with aqueous hydrochloric acid (1.0 M; 10 mL) and water (2 x 10 mL). The organic layer was dried over magnesium sulphate and concentrated. Column chromatography (methanol:dichloromethane, 5:95) on the crude solid gave the title compound (287 mg, 82 %) as a off-white solid. NMR analysis conformed to literature reports. <sup>1</sup>H NMR(400 MHz, CDCl<sub>3</sub>): δ = 3.12 (1H,dd, *J* = 5.7 and 13 .5, CHH' ), 3.21 (1H, dd, *J* = 5.1 and 13.8, CHH' ), 4.20 (1H, t, *J* = 6.5 CH Fmoc), 4.40 (1H, m, CHH Fmoc ), 4.50 (1H, m, CHH), 4.70 (1H, m, CH), 5.19 (1H, d, *J* = 7.7, NH), 7.09 (2H, d, *J* = 7.9, Ar Phe), 7.13 (2H, d, *J* = 7.9, Ar Phe), 7.30 – 7.33 (2H, m, Ar Fmoc), 7.41 (2H, t, *J* = 7.4, Ar Fmoc), 7.54-7.59 (2H, m, Ar Fmoc), 7.78 (2H, d, *J* = 7.3, Ar Fmoc); (ESI-MS), *m/z* 494 [M+H]<sup>+</sup>.

### 7.5.1.73 Linear Peptide Formation of F1PA (96)



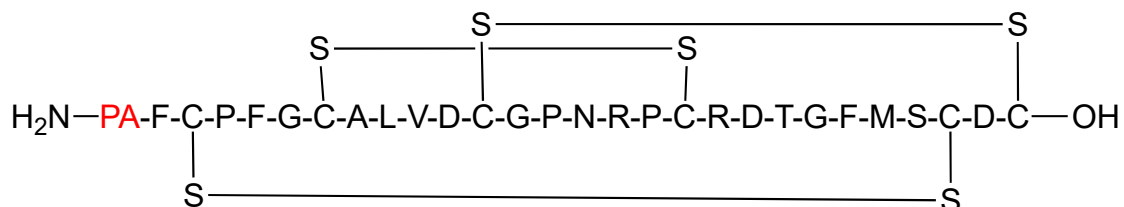
Linear peptide F1PA was synthesized on a preloaded H<sub>2</sub>N-Cys(Trt)-2-ClTrt resin (0.62 mmol/g) on a 0.1 mmol scale using the automated peptide synthesizer according to the general method for solid phase peptide synthesis. Protection of the cysteine residues was Cys 3, 26-Acm; Cys 12, 28-Trt; Cys 7, 18- t-Bu. The crude peptide (124 mg, 37 % relative to resin loading) was used in the next step without further purification. MALDI-TOF MS calculated molecular weight for C<sub>143</sub>H<sub>214</sub>N<sub>40</sub>O<sub>40</sub>S<sub>7</sub> [M+H]<sup>+</sup> 3357 Found [M+H]<sup>+</sup> 3358.

### 7.5.1.74 Bis-disulfide Formation of F1PA (97)



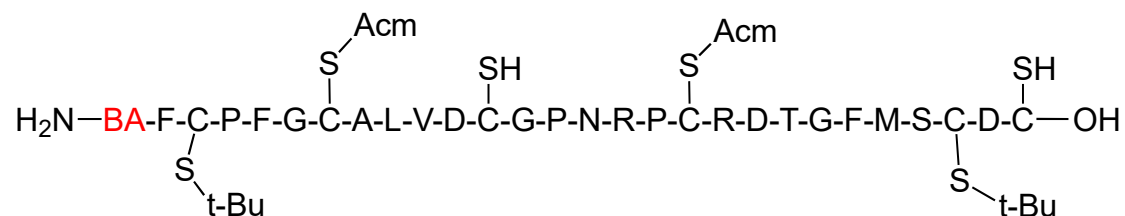
The bis-disulfide F1PA was synthesized according to the general method B for bis-disulfide bond formation from the corresponding linear peptide. The crude peptide was used without further purification giving an orange-yellow solid (35 mg, 74 % isolated yield relative to 50 mg of crude linear peptide). Calculated molecular weight for C<sub>137</sub>H<sub>202</sub>N<sub>38</sub>O<sub>38</sub>S<sub>7</sub> [M+H]<sup>+</sup> 3215 Found [M+H]<sup>+</sup> 3216.

### 7.5.1.75 Tris-disulfide Formation of Residue 1 Substitution with Phenylazide F1PA (98)



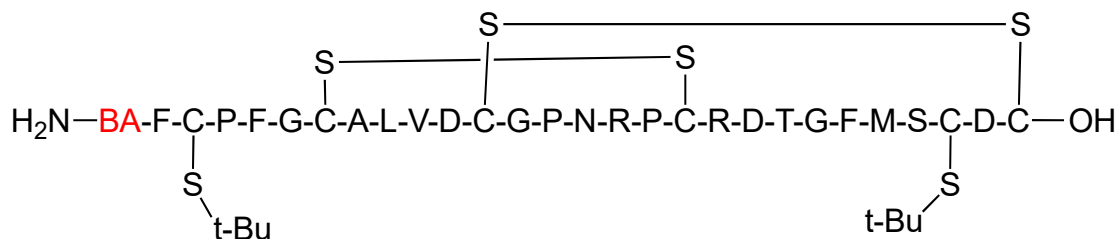
The introduction of the third disulfide bond was achieved by DMSO oxidation of the bicyclic peptide according to the general method for tris-disulfide bond formation. The crude peptide (9) was purified by semi-preparative RP-HPLC using the general method ( $t_R = 15.6$  min, 1.96 mg isolated, 5.9 % isolated yield relative to 35 mg of crude bicyclic peptide). MALDI-TOF MS Calculated molecular weight for  $C_{129}H_{188}N_{38}O_{38}S_7$   $[M+H]^+$  3101 Found  $[M+H]^+$  3102.

### 7.5.1.76 Linear Peptide Formation of F1BA (99)



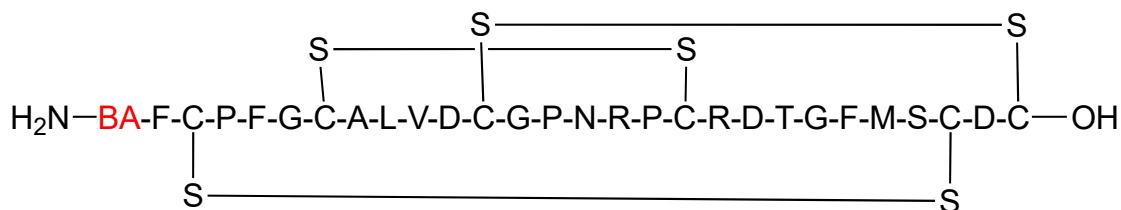
Linear peptide F1PA was synthesized on a preloaded  $H_2N$ -Cys(Trt)-2-ClTrt resin (0.62 mmol/g) on a 0.1 mmol scale using the automated peptide synthesizer according to the general method for solid phase peptide synthesis. Protection of the cysteine residues was Cys 3, 26-Acm; Cys 12, 28-Trt; Cys 7, 18- *t*-Bu. The crude peptide (124 mg, 37 % relative to resin loading) was used in the next step without further purification. MALDI-TOF MS calculated molecular weight for  $C_{144}H_{218}N_{38}O_{40}S_7$   $[M+H]^+$  3345 Found  $[M+H]^+$  3346.

### 7.5.1.77 Bis-disulfide Formation of F1BA (100)



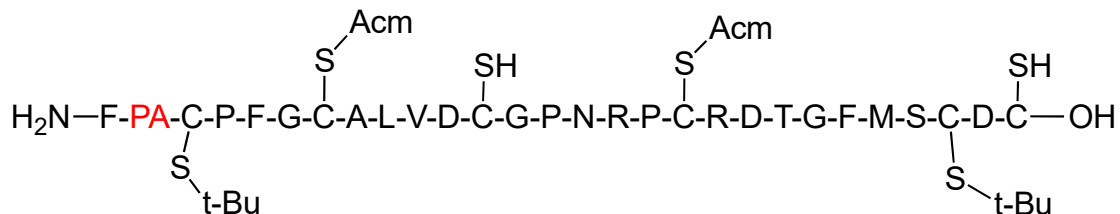
The bis-disulfide F1BA was synthesized according to the general method B for bis-disulfide bond formation from the corresponding linear peptide. The crude peptide was used without further purification giving an orange-yellow solid (35 mg, 74 % isolated yield relative to 50 mg of crude linear peptide). Calculated molecular weight for C<sub>138</sub>H<sub>204</sub>N<sub>36</sub>O<sub>38</sub>S<sub>7</sub> [M+H]<sup>+</sup> 3199 Found [M+H]<sup>+</sup> 3200

### 7.5.1.78 Tris-disulfide Formation of Residue 1 Substitution with Benzylamine F1BA (101)



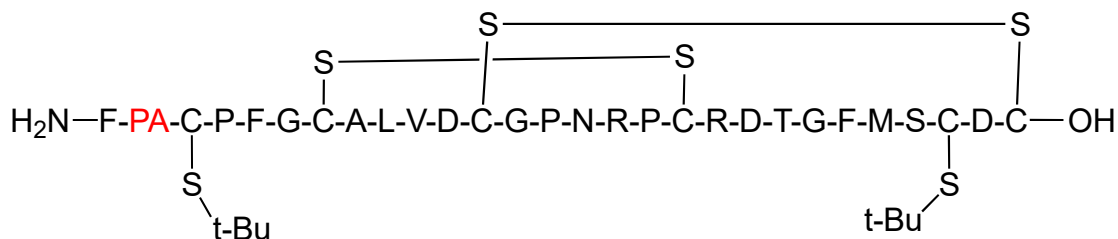
The introduction of the third disulfide bond was achieved by DMSO oxidation of the bicyclic peptide according to the general method for tris-disulfide bond formation. The crude peptide was purified by semi-preparative RP-HPLC using the general method (*t<sub>R</sub>* = 15.6 min, 1.96 mg isolated, 5.9 % isolated yield relative to 35 mg of crude bicyclic peptide). MALDI-TOF MS Calculated molecular weight for C<sub>130</sub>H<sub>184</sub>N<sub>36</sub>O<sub>38</sub>S<sub>7</sub> [M+H]<sup>+</sup> 3087 Found [M+H]<sup>+</sup> 3088.

### 7.5.1.79 Linear Peptide Formation of F2PA (102)



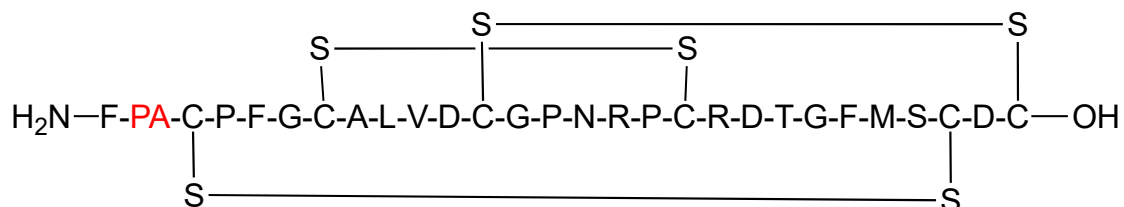
Linear peptide F1PA was synthesized on a preloaded  $\text{H}_2\text{N}-\text{Cys}(\text{Trt})-2-\text{ClTrt}$  resin (0.62 mmol/g) on a 0.1 mmol scale using the automated peptide synthesizer according to the general method for solid phase peptide synthesis. Protection of the cysteine residues was Cys 3, 26-Acm; Cys 12, 28-Trt; Cys 7, 18- *t*-Bu. The crude peptide (124 mg, 37 % relative to resin loading) was used in the next step without further purification. MALDI-TOF MS calculated molecular weight for  $\text{C}_{143}\text{H}_{214}\text{N}_{40}\text{O}_{40}\text{S}_7$   $[\text{M}+\text{H}]^+$  3357 Found  $[\text{M}+\text{H}]^+$  3358.

### 7.5.1.80 Bis-disulfide Formation of F2PA (103)



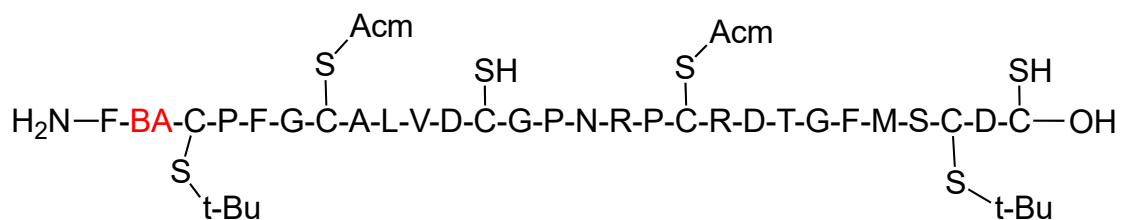
The bis-disulfide F2PA was synthesized according to the general method B for bis-disulfide bond formation from the corresponding linear peptide. The crude peptide was used without further purification giving an orange-yellow solid (35 mg, 74 % isolated yield relative to 50 mg of crude linear peptide). Calculated molecular weight for  $\text{C}_{137}\text{H}_{202}\text{N}_{38}\text{O}_{38}\text{S}_7$   $[\text{M}+\text{H}]^+$  3215 Found  $[\text{M}+\text{H}]^+$  3216.

### 7.5.1.81 Tris-disulfide Formation of Residue 1 Substitution with Phenylazide F2PA (104)



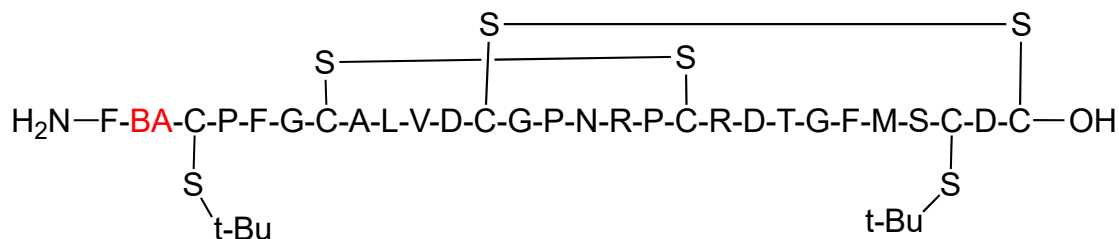
The introduction of the third disulfide bond was achieved by DMSO oxidation of the bicyclic peptide (33) according to the general method for tris-disulfide bond formation. The crude peptide (9) was purified by semi-preparative RP-HPLC using the general method ( $t_R = 15.6$  min, 1.96 mg isolated, 5.9 % isolated yield relative to 35 mg of crude bicyclic peptide). MALDI-TOF MS Calculated molecular weight for  $C_{129}H_{188}N_{38}O_{38}S_7$   $[M+H]^+$  3101 Found  $[M+H]^+$  3102.

### 7.5.1.82 Linear Peptide Formation of F2BA (105)



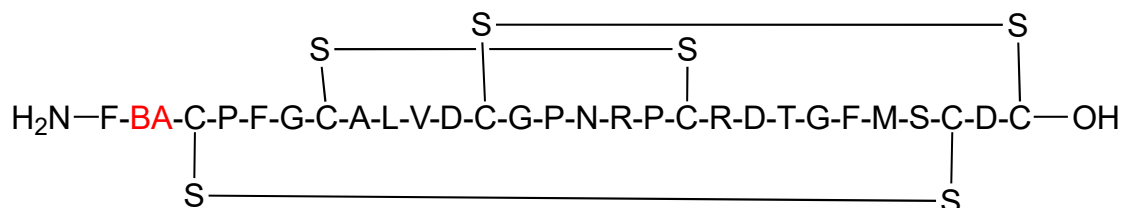
Linear peptide F1PA was synthesized on a preloaded  $H_2N-Cys(Trt)-2-ClTrt$  resin (0.62 mmol/g) on a 0.1 mmol scale using the automated peptide synthesizer according to the general method for solid phase peptide synthesis. Protection of the cysteine residues was Cys 3, 26-Acm; Cys 12, 28-Trt; Cys 7, 18- *t*-Bu. The crude peptide (124 mg, 37 % relative to resin loading) was used in the next step without further purification. MALDI-TOF MS calculated molecular weight for  $C_{144}H_{218}N_{38}O_{40}S_7$   $[M+H]^+$  3345 Found  $[M+H]^+$  3347.

### 7.5.1.83 Bis-disulfide Formation of F2BA (106)



The bis-disulfide peptide was synthesized according to the general method B for bis-disulfide bond formation from the corresponding linear peptide. The crude peptide was used without further purification giving an orange-yellow solid (35 mg, 74 % isolated yield relative to 50 mg of crude linear peptide). Calculated molecular weight for C<sub>138</sub>H<sub>204</sub>N<sub>36</sub>O<sub>38</sub>S<sub>7</sub> [M+H]<sup>+</sup> 3199 Found [M+H]<sup>+</sup> 3200

### 7.5.1.84 Tris-disulfide Formation of Residue 1 Substitution with Phenylazide F2BA (107)



The introduction of the third disulfide bond was achieved by DMSO oxidation of the bicyclic peptide according to the general method for tris-disulfide bond formation. The crude peptide (was purified by semi-preparative RP-HPLC using the general method (t<sub>R</sub> = 15.6 min, 1.96 mg isolated, 5.9 % isolated yield relative to 35 mg of crude bicyclic peptide. MALDI-TOF MS Calculated molecular weight for C<sub>130</sub>H<sub>184</sub>N<sub>36</sub>O<sub>38</sub>S<sub>7</sub> [M+H]<sup>+</sup> 3087 Found [M+H]<sup>+</sup> 3088.

### **7.5.1.85 Linear Formation of Phenylalanine 23 Substitute with Photophenylalanine (PP) (F23PP) (108)**

Linear peptide F1PA was synthesized on a preloaded H<sub>2</sub>N-Cys(Trt)-2-ClTrt resin (0.62 mmol/g) on a 0.1 mmol scale using the automated peptide synthesizer according to the general method for solid phase peptide synthesis. Protection of the cysteine residues was Cys 3, 26-Acm; Cys 12, 28-Trt; Cys 7, 18- *t*-Bu. After coupling the unnatural photophenylalanine the subsequent deprotection reaction was monitored with UV. The lack of a significant UV signal indicated that the coupling reaction was unsuccessful.

## References

- (1) Dias, D. A.; Urban, S.; Roessner, U. A Historical Overview of Natural Products in Drug Discovery. *Metabolites* **2012**, *2* (2), 303–336.
- (2) Li, J. W.-H.; Vederas, J. C. Drug Discovery and Natural Products: End of an Era or an Endless Frontier? *Science* **2009**, *325* (5937), 161.
- (3) Bérdy, J. Thoughts and Facts about Antibiotics: Where We Are Now and Where We Are Heading. *J. Antibiot. (Tokyo)* **2012**, *65* (8), 385–395.
- (4) Demain, A. L.; Sanchez, S. Microbial Drug Discovery: 80 Years of Progress. *J. Antibiot. (Tokyo)* **2009**, *62* (1), 5–16.
- (5) Walsh, C. T.; Wencewicz, T. A. Prospects for New Antibiotics: A Molecule-Centered Perspective. *J. Antibiot. (Tokyo)* **2014**, *67* (1), 7–22.
- (6) Gupta, S. K.; Nayak, R. P. Dry Antibiotic Pipeline: Regulatory Bottlenecks and Regulatory Reforms. *J. Pharmacol. Pharmacother.* **2014**, *5* (1), 4–7.
- (7) O’Niel, J. *Tackling Drug-Resistant Infections Globally: Final Report and Recommendations*; 2016; pp 1–14.
- (8) Diep, D. B.; Nes, I. F. Ribosomally Synthesized Antibacterial Peptides in Gram Positive Bacteria. *Curr. Drug Targets* **2002**, *3* (2), 107–122.
- (9) Nissen-Meyer, J.; Nes, I. F. Ribosomally Synthesized Antimicrobial Peptides: Their Function, Structure, Biogenesis, and Mechanism of Action. *Arch. Microbiol.* **1997**, *167* (2–3), 67–77.
- (10) Arnison, P. G.; Bibb, M. J.; Bierbaum, G.; Bowers, A. A.; Bugni, T. S.; Bulaj, G.; Camarero, J. A.; Campopiano, D. J.; Challis, G. L.; Clardy, J.; Cotter, P. D.; Craik, D. J.; Dawson, M.; Dittmann, E.; Donadio, S.; Dorrestein, P. C.; Entian, K.-D.; Fischbach, M. A.; Garavelli, J. S.; Goeransson, U.; Gruber, C. W.; Haft, D. H.; Hemscheidt, T. K.; Hertweck, C.; Hill, C.; Horswill, A. R.; Jaspars, M.; Kelly, W. L.; Klinman, J. P.; Kuipers, O. P.; Link, A. J.; Liu, W.; Marahiel, M. A.; Mitchell, D. A.; Moll, G. N.; Moore, B. S.; Mueller, R.; Nair, S. K.; Nes, I. F.; Norris, G. E.; Olivera, B. M.; Onaka, H.; Patchett, M. L.; Piel, J.; Reaney, M. J. T.; Rebuffat, S.; Ross, R. P.; Sahl, H.-G.; Schmidt, E. W.; Selsted, M. E.; Severinov, K.; Shen, B.; Sivonen, K.; Smith, L.; Stein, T.; Suessmuth, R. D.; Tagg, J. R.; Tang, G.-L.; Truman, A. W.; Vederas, J. C.; Walsh, C. T.; Walton, J. D.; Wenzel, S. C.; Willey, J. M.; van der Donk, W. A. Ribosomally Synthesized and Post-Translationally Modified Peptide Natural Products: Overview and Recommendations for a Universal Nomenclature. *Nat. Prod. Rep.* **2013**, *30* (1), 108–160.
- (11) Cotter, P. D.; Ross, R. P.; Hill, C. Bacteriocins - a Viable Alternative to Antibiotics? *Nat. Rev. Microbiol.* **2013**, *11* (2), 95–105.
- (12) Grande Burgos, M. J.; Pulido, R. P.; Del Carmen Lopez Aguayo, M.; Galvez, A.; Lucas, R. The Cyclic Antibacterial Peptide Enterocin AS-48: Isolation, Mode of Action, and Possible Food Applications. *Int. J. Mol. Sci.* **2014**, *15* (12), 22706–22727.
- (13) Mathur, H.; O’Connor, P. M.; Cotter, P. D.; Hill, C.; Ross, R. P. Heterologous Expression of Thuricin CD Immunity Genes in *Listeria Monocytogenes*. *Antimicrob. Agents Chemother.* **2014**, *58* (6), 3421–3428.

- (14) Shelburne, C. E.; An, F. Y.; Dholpe, V.; Ramamoorthy, A.; Lopatin, D. E.; Lantz, M. S. The Spectrum of Antimicrobial Activity of the Bacteriocin Subtilosin A. *J. Antimicrob. Chemother.* **2007**, *59* (2), 297–300.
- (15) Ramu, R.; Shirahatti, P. S.; Devi, A. T.; Prasad, A.; J, K.; M S, L.; F, Z.; B L, D.; M N, N. P. Bacteriocins and Their Applications in Food Preservation. *Crit. Rev. Food Sci. Nutr.* **2015**, *0*.
- (16) Klaenhammer, T. R. Genetics of Bacteriocins Produced by Lactic Acid Bacteria. *FEMS Microbiol. Rev.* **1993**, *12* (1–3), 39–85.
- (17) Yang, S.-C.; Lin, C.-H.; Sung, C. T.; Fang, J.-Y. Antibacterial Activities of Bacteriocins: Application in Foods and Pharmaceuticals. *Front. Microbiol.* **2014**, *5*.
- (18) Pettit, R. K. Small-molecule Elicitation of Microbial Secondary Metabolites. *Microb. Biotechnol.* **2011**, *4* (4), 471–478.
- (19) Monciardini, P.; Iorio, M.; Maffioli, S.; Sosio, M.; Donadio, S. Discovering New Bioactive Molecules from Microbial Sources. *Microb. Biotechnol.* **2014**, *7* (3), 209–220.
- (20) David, B.; Wolfender, J.-L.; Dias, D. A. The Pharmaceutical Industry and Natural Products: Historical Status and New Trends. *Phytochem. Rev.* **2015**, *14* (2), 299–315.
- (21) Cintas, L. M.; Casaus, P.; Holo, H.; Hernandez, P. E.; Nes, I. F.; Havarstein, L. S. Enterocins L50A and L50B, Two Novel Bacteriocins from *Enterococcus Faecium* L50, Are Related to Staphylococcal Hemolysins. *J. Bacteriol.* **1998**, *180* (8), 1988–1994.
- (22) Patton, G. C.; Paul, M.; Cooper, L. E.; Chatterjee, C.; van der Donk, W. A. The Importance of the Leader Sequence for Directing Lanthionine Formation in Lactacin 481. *Biochemistry (Mosc.)* **2008**, *47* (28), 7342–7351.
- (23) Oman, T. J.; van der Donk, W. A. Follow the Leader: The Use of Leader Peptides to Guide Natural Product Biosynthesis. *Nat. Chem. Biol.* **2010**, *6* (1), 9–18.
- (24) Flühe, L.; Knappe, T. A.; Gattner, M. J.; Schäfer, A.; Burghaus, O.; Linne, U.; Marahiel, M. A. The Radical SAM Enzyme AlbA Catalyzes Thioether Bond Formation in Subtilosin A. *Nat. Chem. Biol.* **2012**, *8* (4), 350–357.
- (25) van Belkum, M. J.; Worobo, R. W.; Stiles, M. E. Double-Glycine-Type Leader Peptides Direct Secretion of Bacteriocins by ABC Transporters: Colicin V Secretion in *Lactococcus Lactis*. *Mol. Microbiol.* **1997**, *23* (6), 1293–1301.
- (26) Alvarez-Sieiro, P.; Montalban-Lopez, M.; Mu, D.; Kuipers, O. P. Bacteriocins of Lactic Acid Bacteria: Extending the Family. *Appl. Microbiol. Biotechnol.* **2016**, *100* (7), 2939–2951.
- (27) Towle, K. M.; Vederas, J. C. Structural Features of Many Circular and Leaderless Bacteriocins Are Similar to Those in Saposins and Saposin-like Peptides. *MedChemComm* **2017**, *8* (2), 276–285.
- (28) Ovchinnikov, K. V. A Study of Leaderless Bacteriocins, with Focus on Structure- Function and Receptor Characterization, Norwegian University of Life Sciences: As, Norway, 2016.
- (29) Uzelac, G.; Kojic, M.; Lozo, J.; Aleksandrak-Piekarczyk, T.; Gabrielsen, C.; Kristensen, T.; Nes, I. F.; Diep, D. B.; Topisirovic, L. A Zn-Dependent Metallopeptidase Is

- Responsible for Sensitivity to LsbB, a Class II Leaderless Bacteriocin of *Lactococcus Lactis* Subsp *Lactis* BGMN1-5. *J. Bacteriol.* **2013**, *195* (24), 5614–5621.
- (30) Acedo, J. Z.; van Belkum, M. J.; Lohans, C. T.; Towle, K. M.; Miskolzie, M.; Vederas, J. C. Nuclear Magnetic Resonance Solution Structures of Lacticin Q and Aureocin A53 Reveal a Structural Motif Conserved among Leaderless Bacteriocins with Broad-Spectrum Activity. *Biochemistry (Mosc.)* **2016**, *55* (4), 733.
- (31) Ovchinnikov, K. V.; Kristiansen, P. E.; Uzelac, G.; Topisirovic, L.; Kojic, M.; Nissen-Meyer, J.; Nes, I. F.; Diep, D. B. Defining the Structure and Receptor Binding Domain of the Leaderless Bacteriocin LsbB. *J. Biol. Chem.* **2014**, *289* (34), 23838–23845.
- (32) Lohans, C. T.; Towle, K. M.; Miskolzie, M.; McKay, R. T.; van Belkum, M. J.; McMullen, L. M.; Vederas, J. C. Solution Structures of the Linear Leaderless Bacteriocins Enterocin 7A and 7B Resemble Carnocyclin A, a Circular Antimicrobial Peptide. *Biochemistry (Mosc.)* **2013**, *52* (23), 3987–3994.
- (33) Sievers, F.; Wilm, A.; Dineen, D.; Gibson, T. J.; Karplus, K.; Li, W.; Lopez, R.; McWilliam, H.; Remmert, M.; Söding, J.; Thompson, J. D.; Higgins, D. G. Fast, Scalable Generation of High-Quality Protein Multiple Sequence Alignments Using Clustal Omega. *Mol. Syst. Biol.* **2011**, *7*, 539.
- (34) Hyink, O.; Balakrishnan, M.; Tagg, J. R. *Streptococcus Rattus* Strain BHT Produces Both a Class I Two-Component Lantibiotic and a Class II Bacteriocin. *FEMS Microbiol. Lett.* **2005**, *252* (2), 235–241.
- (35) Netz, D. J.; Pohl, R.; Beck-Sickinger, A. G.; Selmer, T.; Pierik, A. J.; Bastos Mdo, C.; Sahl, H. G. Biochemical Characterisation and Genetic Analysis of Aureocin A53, a New, Atypical Bacteriocin from *Staphylococcus Aureus*. *J. Mol. Biol.* **2002**, *319* (3), 745–756.
- (36) Iwatani, S.; Yoneyama, F.; Miyashita, S.; Zendo, T.; Nakayama, J.; Sonomoto, K. Identification of the Genes Involved in the Secretion and Self-Immunity of Lacticin Q, an Unmodified Leaderless Bacteriocin from *Lactococcus Lactis* QU 5. *Microbiology* **2012**, *158*, 2927–2935.
- (37) Iwatani, S.; Zendo, T.; Yoneyama, F.; Nakayama, J.; Sonomoto, K. Characterization and Structure Analysis of a Novel Bacteriocin, Lacticin Z, Produced by *Lactococcus Lactis* QU 14. *Biosci. Biotechnol. Biochem.* **2007**, *71* (8), 1984–1992.
- (38) Sandiford, S.; Upton, M. Identification, Characterization, and Recombinant Expression of Epidermicin NI01, a Novel Unmodified Bacteriocin Produced by *Staphylococcus Epidermidis* That Displays Potent Activity against Staphylococci. *Antimicrob. Agents Chemother.* **2012**, *56* (3), 1539–1547.
- (39) Gajic, O.; Buist, G.; Kojic, M.; Topisirovic, L.; Kuipers, O. P.; Kok, J. Novel Mechanism of Bacteriocin Secretion and Immunity Carried Out by Lactococcal Multidrug Resistance Proteins. *J. Biol. Chem.* **2003**, *278* (36), 34291–34298.
- (40) Iwatani, S.; Horikiri, Y.; Zendo, T.; Nakayama, J.; Sonomoto, K. Bifunctional Gene Cluster InqBCDEF Mediates Bacteriocin Production and Immunity with Differential Genetic Requirements. *Appl. Environ. Microbiol.* **2013**, *79*, 2446–2449.
- (41) Moll, G. N.; Konings, W. N.; Driessen, A. J. M. Bacteriocins: Mechanism of Membrane Insertion and Pore Formation. *Antonie Van Leeuwenhoek* **1999**, *76* (1–4), 185–198.

- (42) de Planque, M. R.; Bonev, B. B.; Demmers, J. A.; Greathouse, D. V.; Koeppe, R. E.; Separovic, F.; Watts, A.; Killian, J. A. Interfacial Anchor Properties of Tryptophan Residues in Transmembrane Peptides Can Dominate over Hydrophobic Matching Effects in Peptide-Lipid Interactions. *Biochemistry (Mosc.)* **2003**, *42* (18), 5341–5348.
- (43) Gleason, N. J.; Vostrikov, V. V.; Greathouse, D. V.; Grant, C. V.; Opella, S. J.; Koeppe, R. E. Tyrosine Replacing Tryptophan as an Anchor in GWALP Peptides. *Biochemistry (Mosc.)* **2012**, *51* (10), 2044–2053.
- (44) Yoneyama, F.; Imura, Y.; Ichimasa, S.; Fujita, K.; Zendo, T.; Nakayama, J.; Matsuzaki, K.; Sonomoto, K. Lacticin Q, a Lactococcal Bacteriocin, Causes High-Level Membrane Permeability in the Absence of Specific Receptors. *Appl. Environ. Microbiol.* **2009**, *75* (2), 538–541.
- (45) Yoneyama, F.; Imura, Y.; Ohno, K.; Zendo, T.; Nakayama, J.; Matsuzaki, K.; Sonomoto, K. Peptide-Lipid Huge Toroidal Pore, a New Antimicrobial Mechanism Mediated by a Lactococcal Bacteriocin, Lacticin Q. *Antimicrob. Agents Chemother.* **2009**, *53* (8), 3211–3217.
- (46) Netz, D. J. A.; Bastos, M. do C. de F.; Sahl, H.-G. Mode of Action of the Antimicrobial Peptide Aureocin A53 from *Staphylococcus Aureus*. *Appl. Environ. Microbiol.* **2002**, *68* (11), 5274–5280.
- (47) Gabrielsen, C.; Brede, D. A.; Hernandez, P. E.; Nes, I. F.; Diep, D. B. The Maltose ABC Transporter in *Lactococcus Lactis* Facilitates High-Level Sensitivity to the Circular Bacteriocin Garvicin ML. *Antimicrob. Agents Chemother.* **2012**, *56* (6), 2908–2915.
- (48) Kjos, M.; Oppegard, C.; Diep, D. B.; Nes, I. F.; Veening, J.-W.; Nissen-Meyer, J.; Kristensen, T. Sensitivity to the Two-Peptide Bacteriocin Lactococcin G Is Dependent on UppP, an Enzyme Involved in Cell-Wall Synthesis. *Mol. Microbiol.* **2014**, *92* (6), 1177–1187.
- (49) Oppegård, C.; Kjos, M.; Veening, J.-W.; Nissen-Meyer, J.; Kristensen, T. A Putative Amino Acid Transporter Determines Sensitivity to the Two-Peptide Bacteriocin Plantaricin JK. *MicrobiologyOpen* **2016**, *5* (4), 700–708.
- (50) Babasaki, K.; Takao, T.; Shimonishi, Y.; Kurahashi, K. Subtilosin A, A New Antibiotic Peptide Produced by *Bacillus Subtilis* 168- Isolation, Structural-Analysis and Biogenesis. *J. Biochem. (Tokyo)* **1985**, *98* (3), 585–603.
- (51) Rea, M. C.; Sit, C. S.; Clayton, E.; O'Connor, P. M.; Whittall, R. M.; Zheng, J.; Vederas, J. C.; Ross, R. P.; Hill, C. Thuricin CD, a Posttranslationally Modified Bacteriocin with a Narrow Spectrum of Activity against *Clostridium Difficile*. *Proc. Natl. Acad. Sci. U. S. A.* **2010**, *107* (20), 9352–9357.
- (52) Lee, H.; Churey, J. J.; Worobo, R. W. Biosynthesis and Transcriptional Analysis of Thurincin H, a Tandem Repeated Bacteriocin Genetic Locus, Produced by *Bacillus Thuringiensis* SF361. *Fems Microbiol. Lett.* **2009**, *299* (2), 205–213.
- (53) Huang, T.; Geng, H.; Miyapuram, V. R.; Sit, C. S.; Vederas, J. C.; Nakano, M. M. Isolation of a Variant of Subtilosin A with Hemolytic Activity. *J. Bacteriol.* **2009**, *191* (18), 5690–5696.

- (54) Fontecave, M.; Atta, M.; Mulliez, E. S-Adenosylmethionine: Nothing Goes to Waste. *Trends Biochem. Sci.* **2004**, *29* (5), 243–249.
- (55) Jarrett, J. T. The Generation of 5'-Deoxyadenosyl Radicals by Adenosylmethionine-Dependent Radical Enzymes. *Curr. Opin. Chem. Biol.* **2003**, *7* (2), 174–182.
- (56) Grove, T. L.; Himes, P. M.; Hwang, S.; Yumerefendi, H.; Bonanno, J. B.; Kuhlman, B.; Almo, S. C.; Bowers, A. A. Structural Insights into Thioether Bond Formation in the Biosynthesis of Sactipeptides. *J. Am. Chem. Soc.* **2017**.
- (57) Zheng, G. L.; Hehn, R.; Zuber, P. Mutational Analysis of the Sbo-Alb Locus of *Bacillus Subtilis*: Identification of Genes Required for Subtilosin Production and Immunity. *J. Bacteriol.* **2000**, *182* (11), 3266–3273.
- (58) Zheng, G. L.; Yan, L. Z.; Vederas, J. C.; Zuber, P. Genes of the Sbo-Alb Locus of *Bacillus Subtilis* Are Required for Production of the Antilisterial Bacteriocin Subtilosin. *J. Bacteriol.* **1999**, *181* (23), 7346–7355.
- (59) Sit, C. S.; van Belkum, M. J.; McKay, R. T.; Worobo, R. W.; Vederas, J. C. The 3D Solution Structure of Thurincin H, a Bacteriocin with Four Sulfur to Alpha-Carbon Crosslinks. *Angew. Chem.-Int. Ed.* **2011**, *50* (37), 8718–8721.
- (60) Wang, G.; Manns, D. C.; Churey, J. J.; Worobo, R. W. Short Communication: Naturally Sensitive *Bacillus Thuringiensis* EG10368 Produces Thurincin H and Acquires Immunity after Heterologous Expression of the One-Step-Amplified Thurincin H Gene Cluster. *J. Dairy Sci.* **2014**, *97* (7), 4115–4119.
- (61) Rea, M. C.; Clayton, E.; O'Connor, P. M.; Shanahan, F.; Kiely, B.; Ross, R. P.; Hill, C. Antimicrobial Activity of Lacticin 3147 against Clinical *Clostridium Difficile* Strains. *J. Med. Microbiol.* **2007**, *56* (7), 940–946.
- (62) Wang, G.; Feng, G.; Snyder, A. B.; Manns, D. C.; Churey, J. J.; Worobo, R. W. Bactericidal Thurincin H Causes Unique Morphological Changes in *Bacillus Cereus* F4552 without Affecting Membrane Permeability. *Fems Microbiol. Lett.* **2014**, *357* (1), 69–76.
- (63) Mathur, H.; Rea, M. C.; Cotter, P. D.; Hill, C.; Ross, R. P. The Sactibiotic Subclass of Bacteriocins: An Update. *Curr. Protein Pept. Sci.* **16** (6), 549–558.
- (64) Noll, K. S.; Prichard, M. N.; Khaykin, A.; Sinko, P. J.; Chikindas, M. L. The Natural Antimicrobial Peptide Subtilosin Acts Synergistically with Glycerol Monolaurate, Lauric Arginate, and Epsilon-Poly-L-Lysine against Bacterial Vaginosis-Associated Pathogens but Not Human Lactobacilli. *Antimicrob. Agents Chemother.* **2012**, *56* (4), 1756–1761.
- (65) Noll, K. S.; Sinko, P. J.; Chikindas, M. L. Elucidation of the Molecular Mechanisms of Action of the Natural Antimicrobial Peptide Subtilosin Against the Bacterial Vaginosis-Associated Pathogen *Gardnerella Vaginalis*. *Probiotics Antimicrob. Proteins* **2011**, *3* (1), 41–47.
- (66) Thennarasu, S.; Lee, D. K.; Poon, A.; Kawulka, K. E.; Vederas, J. C.; Ramamoorthy, A. Membrane Permeabilization, Orientation, and Antimicrobial Mechanism of Subtilosin A. *Chem. Phys. Lipids* **2005**, *137* (1–2), 38–51.
- (67) Clatworthy, A. E.; Pierson, E.; Hung, D. T. Targeting Virulence: A New Paradigm for Antimicrobial Therapy. *Nat. Chem. Biol.* **2007**, *3* (9), 541–548.

- (68) Spellberg, B.; Bartlett, J. G.; Gilbert, D. N. The Future of Antibiotics and Resistance. *N. Engl. J. Med.* **2013**, *368* (4), 299–302.
- (69) Lowy, F. D. Staphylococcus Aureus Infections. *N Engl J Med* **1998**, *339* (8), 520–532.
- (70) Tong, S. Y. C.; Davis, J. S.; Eichenberger, E.; Holland, T. L.; Fowler, V. G. J. Staphylococcus Aureus Infections: Epidemiology, Pathophysiology, Clinical Manifestations, and Management. *Clin Microbiol Rev* **2015**, *28*, 603.
- (71) Otto, M. Staphylococcus Aureus Toxins. *Curr. Opin. Microbiol.* **2014**, *17*, 32–37.
- (72) Cheung, G. Y. C.; Joo, H.-S.; Chatterjee, S. S.; Otto, M. Phenol-Soluble Modulins - Critical Determinants of Staphylococcal Virulence. *FEMS Microbiol. Rev.* **2014**, *38* (4), 698–719.
- (73) Gonzalez, D. J.; Okumura, C. Y.; Hollands, A.; Kersten, R.; Akong-Moore, K.; Pence, M. A.; Malone, C. L.; Derieux, J.; Moore, B. S.; Horswill, A. R.; Dixon, J. E.; Dorrestein, P. C.; Nizet, V. Novel Phenol-Soluble Modulins in Community-Associated Methicillin-Resistant Staphylococcus Aureus Identified through Imaging Mass Spectrometry. *J. Biol. Chem.* **2012**, *287* (17), 13889–13898.
- (74) Li, S.; Huang, H.; Rao, X.; Chen, W.; Wang, Z.; Hu, X. Phenol-Soluble Modulins: Novel Virulence-Associated Peptides of Staphylococci. *Future Microbiol.* **2014**, *9* (2), 203–216.
- (75) Peschel, A.; Otto, M. Phenol-Soluble Modulins and Staphylococcal Infection. *Nat. Rev. Microbiol.* **2013**, *11* (10), 667–673.
- (76) Tsompanidou, E.; Denham, E. L.; van Dijl, J. M. Phenol-Soluble Modulins, Hellhounds from the Staphylococcal Virulence-Factor Pandemonium. *Trends Microbiol.* **2013**, *21* (7), 313–315.
- (77) Laabei, M.; Jamieson, W. D.; Yang, Y.; van den Elsen, J.; Jenkins, A. T. A. Investigating the Lytic Activity and Structural Properties of Staphylococcus Aureus Phenol Soluble Modulins (PSM) Peptide Toxins. *Biochim. Biophys. Acta BBA - Biomembr.* **2014**, *1838* (12), 3153–3161.
- (78) Cheung, G. Y. C.; Kretschmer, D.; Queck, S. Y.; Joo, H.-S.; Wang, R.; Duong, A. C.; Nguyen, T. H.; Bach, T.-H. L.; Porter, A. R.; DeLeo, F. R.; Peschel, A.; Otto, M. Insight into Structure-Function Relationship in Phenol-Soluble Modulins Using an Alanine Screen of the Phenol-Soluble Modulins (PSM) Alpha 3 Peptide. *Faseb J.* **2014**, *28* (1), 153–161.
- (79) Wang, R.; Braughton, K. R.; Kretschmer, D.; Bach, T. H. L.; Queck, S. Y.; Li, M.; Kennedy, A. D.; Dorward, D. W.; Klebanoff, S. J.; Peschel, A.; DeLeo, F. R.; Otto, M. Identification of Novel Cytolytic Peptides as Key Virulence Determinants for Community-Associated MRSA. *Nat. Med.* **2007**, *13* (12), 1510–1514.
- (80) Novick, R. P.; Ross, H. F.; Projan, S. J.; Kornblum, J.; Kreiswirth, B.; Moghazeh, S. Synthesis of Staphylococcal Virulence Factors Is Controlled by a Regulatory RNA Molecule. *EMBO J.* **1993**, *12* (10), 3967–3975.
- (81) Chatterjee, S. S.; Joo, H. S.; Duong, A. C.; Dieringer, T. D.; Tan, V. Y.; Song, Y.; Fischer, E. R.; Cheung, G. Y.; Li, M.; Otto, M. Essential Staphylococcus Aureus Toxin Export System. *Nat. Med.* **2013**, *19* (3), 364–367.

- (82) Molloy, S. Biofilms: Biofilms Take Shape. *Nat. Rev. Microbiol.* **2012**, *10* (3), 162–162.
- (83) Periasamy, S.; Joo, H. S.; Duong, A. C.; Bach, T. H.; Tan, V. Y.; Chatterjee, S. S.; Cheung, G. Y.; Otto, M. How Staphylococcus Aureus Biofilms Develop Their Characteristic Structure. *Proc. Natl. Acad. Sci. U. S. A.* **2012**, *109* (4), 1281–1286.
- (84) Schwartz, K.; Syed, A. K.; Stephenson, R. E.; Rickard, A. H.; Boles, B. R. Functional Amyloids Composed of Phenol Soluble Modulins Stabilize Staphylococcus Aureus Biofilms. *PLOS Pathog.* **2012**, *8* (6), e1002744.
- (85) Costerton, J. W. Bacterial Biofilms: A Common Cause of Persistent Infections. *Science* **1999**, *284* (5418), 1318–1322.
- (86) Flemming, H.-C.; Wingender, J. The Biofilm Matrix. *Nat. Rev. Microbiol.* **2010**, *8* (9), 623–633.
- (87) Pokorny, A.; Birkbeck, T. H.; Almeida, P. F. F. Mechanism and Kinetics of Delta-Lysin Interaction with Phospholipid Vesicles. *Biochemistry (Mosc.)* **2002**, *41* (36), 11044–11056.
- (88) Duong, A. C.; Cheung, G. Y. C.; Otto, M. Interaction of Phenol-Soluble Modulins with Phosphatidylcholine Vesicles. *Pathog. Basel Switz.* **2012**, *1* (1), 3–11.
- (89) Schweizer, F. Cationic Amphiphilic Peptides with Cancer-Selective Toxicity. *Eur. J. Pharmacol.* **2009**, *625* (1–3), 190–194.
- (90) Gaspar, D.; Veiga, A. S.; Castanho, M. A. R. B. From Antimicrobial to Anticancer Peptides. A Review. *Front. Microbiol.* **2013**, *4*.
- (91) Austin, P.; Heller, M.; Williams, D. E.; McIntosh, L. P.; Vogl, A. W.; Foster, L. J.; Andersen, R. J.; Roberge, M.; Roskelley, C. D. Release of Membrane-Bound Vesicles and Inhibition of Tumor Cell Adhesion by the Peptide Neopetrosiamide A. *Plos One* **2010**, *5* (5), e10836.
- (92) Williams, D. E.; Austin, P.; Diaz-Marrero, A. R.; Van Soest, R.; Matainaho, T.; Roskelley, C. D.; Roberge, M.; Andersen, R. J. Neopetrosiamides, Peptides from the Marine Sponge Neopetrosia Sp That Inhibit Amoeboid Invasion by Human Tumor Cells. *Org. Lett.* **2005**, *7* (19), 4173–4176.
- (93) Liu, H.; Boudreau, M. A.; Zheng, J.; Whittal, R. M.; Austin, P.; Roskelley, C. D.; Roberge, M.; Andersen, R. J.; Vederas, J. C. Chemical Synthesis and Biological Activity of the Neopetrosiamides and Their Analogues: Revision of Disulfide Bond Connectivity. *J. Am. Chem. Soc.* **2010**, *132* (5), 1486–+.
- (94) Haastert, P. J. M. V. Amoeboid Cells Use Protrusions for Walking, Gliding and Swimming. *PLOS ONE* **2011**, *6* (11), e27532.
- (95) Paňková, K.; Rösel, D.; Novotný, M.; Brábek, J. The Molecular Mechanisms of Transition between Mesenchymal and Amoeboid Invasiveness in Tumor Cells. *Cell. Mol. Life Sci.* **2010**, *67* (1), 63–71.
- (96) Ruoslahti, E.; Pierschbacher, M. D. Arg-Gly-Asp: A Versatile Cell Recognition Signal. *Cell* **1986**, *44* (4), 517–518.
- (97) Dunehoo, A. L.; Anderson, M.; Majumdar, S.; Kobayashi, N.; Berkland, C.; Siahaan, T. J. Cell Adhesion Molecules for Targeted Drug Delivery. *J. Pharm. Sci.* **2006**, *95* (9), 1856–1872.

- (98) Mills, S.; Stanton, C.; Hill, C.; Ross, R. P. New Developments and Applications of Bacteriocins and Peptides in Foods. *Annu. Rev. Food Sci. Technol.* **2011**, *2* (1), 299–329.
- (99) Lucera, A.; Costa, C.; Conte, A.; Del Nobile, M. A. Food Applications of Natural Antimicrobial Compounds. *Front. Microbiol.* **2012**, *3*.
- (100) Bhunia, A. K.; Johnson, M. C.; Ray, B. Purification, Characterization and Antimicrobial Spectrum of a Bacteriocin Produced by *Pediococcus Acidilactici*. *J. Appl. Bacteriol.* **1988**, *65* (4), 261–268.
- (101) Piper, C.; Cotter, P. D.; Ross, R. P.; Hill, C. Discovery of Medically Significant Lantibiotics. *Curr. Drug Discov. Technol.* **2009**, *6* (1), 1–18.
- (102) Drider, D.; Fimland, G.; Héchard, Y.; McMullen, L. M.; Prévost, H. The Continuing Story of Class IIa Bacteriocins. *Microbiol. Mol. Biol. Rev.* **2006**, *70* (2), 564–582.
- (103) Eijsink, V. G.; Skeie, M.; Middelhoven, P. H.; Brurberg, M. B.; Nes, I. F. Comparative Studies of Class IIa Bacteriocins of Lactic Acid Bacteria. *Appl. Environ. Microbiol.* **1998**, *64* (9), 3275–3281.
- (104) Lohans, C. T.; Vederas, J. C. Development of Class IIa Bacteriocins as Therapeutic Agents. *Int. J. Microbiol.* **2011**, *2012*, e386410.
- (105) Goldstein, B. P.; Wei, J.; Greenberg, K.; Novick, R. Activity of Nisin against *Streptococcus Pneumoniae*, in Vitro, and in a Mouse Infection Model. *J. Antimicrob. Chemother.* **1998**, *42* (2), 277–278.
- (106) De Kwaadsteniet, M.; Doeschate, K. T.; Dicks, L. M. T. Nisin F in the Treatment of Respiratory Tract Infections Caused by *Staphylococcus Aureus*. *Lett. Appl. Microbiol.* **2009**, *48* (1), 65–70.
- (107) Brand, A. M.; de Kwaadsteniet, M.; Dicks, L. M. T. The Ability of Nisin F to Control *Staphylococcus Aureus* Infection in the Peritoneal Cavity, as Studied in Mice. *Lett. Appl. Microbiol.* **2010**, *51* (6), 645–649.
- (108) Kruszewska, D.; Sahl, H.-G.; Bierbaum, G.; Pag, U.; Hynes, S. O.; Ljungh, Å. Mersacidin Eradicates Methicillin-Resistant *Staphylococcus Aureus* (MRSA) in a Mouse Rhinitis Model. *J. Antimicrob. Chemother.* **2004**, *54* (3), 648–653.
- (109) Mullane, K.; Lee, C.; Bressler, A.; Buitrago, M.; Weiss, K.; Dabovic, K.; Praestgaard, J.; Leeds, J. A.; Blais, J.; Pertel, P. Multicenter, Randomized Clinical Trial to Compare the Safety and Efficacy of LFF571 and Vancomycin for *Clostridium Difficile* Infections. *Antimicrob. Agents Chemother.* **2015**, *59* (3), 1435–1440.
- (110) Khusro, A.; Aarti, C.; Agastian, P. Anti-Tubercular Peptides: A Quest of Future Therapeutic Weapon to Combat Tuberculosis. *Asian Pac. J. Trop. Med.* **2016**, *9* (11), 1023–1034.
- (111) Kaur, S.; Kaur, S. Bacteriocins as Potential Anticancer Agents. *Front. Pharmacol.* **2015**, *6*.
- (112) Bhunia, A. K.; Johnson, M. C.; Ray, B.; Belden, E. L. Antigenic Property of Pediocin AcH Produced by *Pediococcus Acidilactici* H. *J. Appl. Bacteriol.* **1990**, *69* (2), 211–215.
- (113) Chumchalová, J.; Smarda, J. Human Tumor Cells Are Selectively Inhibited by Colicins. *Folia Microbiol. (Praha)* **2003**, *48* (1), 111–115.

- (114) Fuska, J.; Fusková, A.; Smarda, J.; Mach, J. Effect of Colicin E3 on Leukemia Cells P388 in Vitro. *Experientia* **1979**, *35* (3), 406–407.
- (115) Smarda, J.; Obdržálek, V.; Táborský, I.; Mach, J. The Cytotoxic and Cytocidal Effect of Colicin E3 on Mammalian Tissue Cells. *Folia Microbiol. (Praha)* **1978**, *23* (4), 272–277.
- (116) Hetz, C.; Bono, M. R.; Barros, L. F.; Lagos, R. Microcin E492, a Channel-Forming Bacteriocin from *Klebsiella Pneumoniae*, Induces Apoptosis in Some Human Cell Lines. *Proc. Natl. Acad. Sci. U. S. A.* **2002**, *99* (5), 2696–2701.
- (117) Lagos, R.; Tello, M.; Mercado, G.; García, V.; Monasterio, O. Antibacterial and Antitumorogenic Properties of Microcin E492, a Pore-Forming Bacteriocin. *Curr. Pharm. Biotechnol.* **2009**, *10* (1), 74–85.
- (118) Joo, N. E.; Ritchie, K.; Kamarajan, P.; Miao, D.; Kapila, Y. L. Nisin, an Apoptogenic Bacteriocin and Food Preservative, Attenuates HNSCC Tumorigenesis via CHAC1. *Cancer Med.* **2012**, *1* (3), 295–305.
- (119) Sand, S. L.; Nissen-Meyer, J.; Sand, O.; Haug, T. M. Plantaricin A, a Cationic Peptide Produced by *Lactobacillus Plantarum*, Permeabilizes Eukaryotic Cell Membranes by a Mechanism Dependent on Negative Surface Charge Linked to Glycosylated Membrane Proteins. *Biochim. Biophys. Acta* **2013**, *1828* (2), 249–259.
- (120) Martín, R.; Escobedo, S.; Martín, C.; Crespo, A.; Quiros, L. M.; Suarez, J. E. Surface Glycosaminoglycans Protect Eukaryotic Cells against Membrane-Driven Peptide Bacteriocins. *Antimicrob. Agents Chemother.* **2015**, *59* (1), 677–681.
- (121) Towle, K. M.; Lohans, C. T.; Miskolzie, M.; Acedo, J. Z.; van Belkum, M. J.; Vederas, J. C. Solution Structures of Phenol-Soluble Modulins  $\alpha 1$ ,  $\alpha 3$ , and  $\beta 2$ , Virulence Factors from *Staphylococcus Aureus*. *Biochemistry (Mosc.)* **2016**, *55* (34), 4798–4806.
- (122) Towle, K. M.; Chaytor, J. L.; Liu, H.; Austin, P.; Roberge, M.; Roskelley, C. D.; Vederas, J. C. Synthesis and Biological Studies of Neopetrosiamides as Inhibitors of Cancer Cell Invasion. *Org. Biomol. Chem.* **2013**, *11* (9), 1476–1481.
- (123) Liu, X.; Vederas, J. C.; Whittal, R. M.; Zheng, J.; Stiles, M. E.; Carlson, D.; Franz, C. M. A. P.; McMullen, L. M.; van Belkum, M. J. Identification of an N-Terminal Formylated, Two-Peptide Bacteriocin from *Enterococcus Faecalis* 710C. *J. Agric. Food Chem.* **2011**, *59* (10), 5602–5608.
- (124) Luo, P.; Baldwin, R. L. Mechanism of Helix Induction by Trifluoroethanol: A Framework for Extrapolating the Helix-Forming Properties of Peptides from Trifluoroethanol/Water Mixtures Back to Water. *Biochemistry (Mosc.)* **1997**, *36* (27), 8413–8421.
- (125) Rohl, C. A.; Baldwin, R. L. Comparison of NH Exchange and Circular Dichroism as Techniques for Measuring the Parameters of the Helix–Coil Transition in Peptides. *Biochemistry (Mosc.)* **1997**, *36* (28), 8435–8442.
- (126) Güntert, P.; Mumenthaler, C.; Wüthrich, K. Torsion Angle Dynamics for NMR Structure Calculation with the New Program Dyanal. *J. Mol. Biol.* **1997**, *273* (1), 283–298.
- (127) Cebrian, R.; Martinez-Bueno, M.; Valdivia, E.; Albert, A.; Maqueda, M.; Sanchez-Barrena, M. J. The Bacteriocin AS-48 Requires Dimer Dissociation Followed by

- Hydrophobic Interactions with the Membrane for Antibacterial Activity. *J. Struct. Biol.* **2015**, *190* (2), 162–172.
- (128) Bahar, A. A.; Ren, D. Antimicrobial Peptides. *Pharmaceuticals* **2013**, *6* (12), 1543–1575.
- (129) Hechard, Y.; Pelletier, C.; Cenatiempo, Y.; Frere, J. Analysis of sigma(54)-Dependent Genes in *Enterococcus Faecalis*: A Mannose PTS Permease (EIIMan) Is Involved in Sensitivity to a Bacteriocin, Mesentericin Y105. *Microbiol.-Sgm* **2001**, *147*, 1575–1580.
- (130) Lohans, C. T. Structural Characterization of Bacterial Antimicrobial Peptides. Doctor of Philosophy, University of Alberta: Edmonton, AB, 2014.
- (131) Martin-Visscher, L. A.; Gong, X.; Duszyk, M.; Vederas, J. C. The Three-Dimensional Structure of Carnocyclin A Reveals That Many Circular Bacteriocins Share a Common Structural Motif. *J. Biol. Chem.* **2009**, *284* (42), 28674–28681.
- (132) Gong, X.; Martin-Visscher, L. A.; Nahirney, D.; Vederas, J. C.; Duszyk, M. The Circular Bacteriocin, Carnocyclin A, Forms Anion-Selective Channels in Lipid Bilayers. *Biochim. Biophys. Acta* **2009**, *1788* (9), 1797–1803.
- (133) Martin-Visscher, L. A.; Yoganathan, S.; Sit, C. S.; Lohans, C. T.; Vederas, J. C. The Activity of Bacteriocins from *Carnobacterium Maltaromaticum* UAL307 against Gram-Negative Bacteria in Combination with EDTA Treatment. *FEMS Microbiol. Lett.* **2011**, *317* (2), 152–159.
- (134) Silkin, L.; Hamza, S.; Kaufman, S.; Cobb, S. L.; Vederas, J. C. Spermicidal Bacteriocins: Lacticin 3147 and Subtilosin A. *Bioorg. Med. Chem. Lett.* **2008**, *18* (10), 3103–3106.
- (135) Marx, R.; Stein, T.; Entian, K.-D.; Glaser, S. J. Structure of the *Bacillus Subtilis* Peptide Antibiotic Subtilosin A Determined by 1H-NMR and Matrix Assisted Laser Desorption/Ionization Time-of-Flight Mass Spectrometry. *J. Protein Chem.* **2001**, *20* (6), 501–506.
- (136) Kawulka, K.; Sprules, T.; McKay, R. T.; Mercier, P.; Diaper, C. M.; Zuber, P.; Vederas, J. C. Structure of Subtilosin A, an Antimicrobial Peptide from *Bacillus Subtilis* with Unusual Posttranslational Modifications Linking Cysteine Sulfurs to Alpha-Carbons of Phenylalanine and Threonine. *J. Am. Chem. Soc.* **2003**, *125* (16), 4726–4727.
- (137) Kawulka, K. E.; Sprules, T.; Diaper, C. M.; Whittall, R. M.; McKay, R. T.; Mercier, P.; Zuber, P.; Vederas, J. C. Structure of Subtilosin A, a Cyclic Antimicrobial Peptide from *Bacillus Subtilis* with Unusual Sulfur to Alpha-Carbon Cross-Links: Formation and Reduction of Alpha-Thio-Alpha-Amino Acid Derivatives. *Biochemistry (Mosc.)* **2004**, *43* (12), 3385–3395.
- (138) Sit, C. S.; McKay, R. T.; Hill, C.; Ross, R. P.; Vederas, J. C. The 3D Structure of Thuricin CD, a Two-Component Bacteriocin with Cysteine Sulfur to Alpha-Carbon Cross-Links. *J. Am. Chem. Soc.* **2011**, *133* (20), 7680–7683.
- (139) Yeates, T. O.; Kent, S. B. H. Racemic Protein Crystallography. *Annu. Rev. Biophys.* **2012**, *41* (1), 41–61.
- (140) Warke, A.; Momany, C. Addressing the Protein Crystallization Bottleneck By Cocrystallization. *Cryst. Growth Des.* **2007**, *7* (11), 2219–2225.

- (141) Thomas, E. W.; McKelvy, J. F.; Sharon, N. Specific and Irreversible Inhibition of Lysozyme by 2[prime],3[prime]-Epoxypropyl [Beta]-Glycosides of N-Acetyl-D-Glucosamine Oligomers. *Nature* **1969**, 222 (5192), 485–486.
- (142) Fan, C. Structural and Inhibitory Studies of LL-Diaminopimelate Aminotransferase and Investigation of Methods for Small Peptide Crystallization. Doctor of Philosophy, University of Alberta: Edmonton, AB, 2012.
- (143) Wimmer, R.; Larsen, K. L.; Otzen, D. E.; Aachmann, F. L. Structural Background of Cyclodextrin-Protein Interactions. *Protein Eng.* **2013**, 16 (12), 905–912.
- (144) Tiwari, G.; Tiwari, R.; Rai, A. K. Cyclodextrins in Delivery Systems: Applications. *J. Pharm. Bioallied Sci.* **2010**, 2 (2), 72–79.
- (145) Aachmann, F. L.; Larsen, K. L.; Wimmer, R. Interactions of Cyclodextrins with Aromatic Amino Acids: A Basis for Protein Interactions. *J. Incl. Phenom. Macrocycl. Chem.* **2012**, 73 (1–4), 349–357.
- (146) SANO, T.; Vajda, S.; Cantor, C. R. Genetic Engineering of Streptavidin, a Versatile Affinity Tag. *J. Chromatogr. B* **715**, 85–91.
- (147) Schwartz, B. L.; Bruce, J. E.; Anderson, G. A.; Hofstadler, S. A.; Rockwood, A. L.; Smith, R. D.; Chilkoti, A.; Stayton, P. S. Dissociation of Tetrameric Ions of Noncovalent Streptavidin Complexes Formed by Electrospray Ionization. *J. Am. Soc. Mass Spectrom.* **1995**, 6 (6), 459–465.
- (148) Zehl, M.; Allmaier, G. Instrumental Parameters in the MALDI-TOF Mass Spectrometric Analysis of Quaternary Protein Structures. *Anal. Chem.* **2005**, 77 (1), 103–110.
- (149) Humbert, N.; Zocchi, A.; Ward, T. R. Electrophoretic Behavior of Streptavidin Complexed to a Biotinylated Probe: A Functional Screening Assay for Biotin-Binding Proteins. *ELECTROPHORESIS* **2005**, 26 (1), 47–52.
- (150) Song, J.; Li, Y.; Ji, C.; Zhang, J. Z. H. Functional Loop Dynamics of the Streptavidin-Biotin Complex. *Sci. Rep.* **2015**, 5.
- (151) Diehl, K. L.; Kolesnichenko, I. V.; Robotham, S. A.; Bachman, J. L.; Zhong, Y.; Brodbelt, J. S.; Anslyn, E. V. Click and Chemically Triggered Declick Reactions through Reversible Amine and Thiol Coupling via a Conjugate Acceptor. *Nat. Chem.* **2016**, 8 (10), 968–973.
- (152) Ben Cheikh, A.; Chucho, J.; Manisse, N.; Pommelet, J. C.; Netsch, K. P.; Lorenca, P.; Wentrup, C. Synthesis of .alpha.-Cyano Carbonyl Compounds by Flash Vacuum Thermolysis of (Alkylamino)methylene Derivatives of Meldrum's Acid. Evidence for Facile 1,3-Shifts of Alkylamino and Alkylthio Groups in Imidoylketene Intermediates. *J. Org. Chem.* **1991**, 56 (3), 970–975.
- (153) Rempel, B. P.; Withers, S. G. Covalent Inhibitors of Glycosidases and Their Applications in Biochemistry and Biology. *Glycobiology* **2008**, 18 (8), 570–586.
- (154) Zhang, L.; Goldammer, C.; Henkel, B.; Zuhl, F.; Panhaus, G.; Jung, G.; Bayer, E. *Innovation and Perspectives in Solid Phase Synthesis. Peptides, Proteins and Nucleic Acids. Biological and Biomedical Applications*; Mayflower Worldwide: Birmingham, UK, 1994.

- (155) Kretschmer, D.; Gleske, A.-K.; Rautenberg, M.; Wang, R.; Köberle, M.; Bohn, E.; Schöneberg, T.; Rabiet, M.-J.; Boulay, F.; Klebanoff, S. J.; van Kessel, K. A.; van Strijp, J. A.; Otto, M.; Peschel, A. Human Formyl Peptide Receptor 2 Senses Highly Pathogenic *Staphylococcus Aureus*. *Cell Host Microbe* **2010**, *7* (6), 463–473.
- (156) Schrödinger, L. The PyMOL Molecular Graphics System, Version 1.8. **2015**.
- (157) Dolinsky, T. J.; Nielsen, J. E.; McCammon, J. A.; Baker, N. A. PDB2PQR: An Automated Pipeline for the Setup of Poisson-Boltzmann Electrostatics Calculations. *Nucleic Acids Res.* **2004**, *32* (Web Server issue), 665.
- (158) Tayeb-Fligelman, E.; Tabachnikov, O.; Moshe, A.; Goldshmidt-Tran, O.; Sawaya, M. R.; Coquelle, N.; Colletier, J.-P.; Landau, M. The Cytotoxic *Staphylococcus Aureus* PSM $\alpha$ 3 Reveals a Cross- $\alpha$  Amyloid-like Fibril. *Science* **2017**, *355* (6327), 831–833.
- (159) Rambaran, R. N.; Serpell, L. C. Amyloid Fibrils. *Prion* **2008**, *2* (3), 112–117.
- (160) Bulaj, G. Formation of Disulfide Bonds in Proteins and Peptides. *Biotechnol. Adv.* **2005**, *23* (1), 87–92.
- (161) Patil, N. A.; Tailhades, J.; Hughes, R. A.; Separovic, F.; Wade, J. D.; Hossain, M. A. Cellular Disulfide Bond Formation in Bioactive Peptides and Proteins. *Int. J. Mol. Sci.* **2015**, *16* (1), 1791–1805.
- (162) Park, S.; Strömstedt, A. A.; Göransson, U. Cyclotide Structure–Activity Relationships: Qualitative and Quantitative Approaches Linking Cytotoxic and Anthelmintic Activity to the Clustering of Physicochemical Forces. *PLoS ONE* **2014**, *9* (3).
- (163) Ganz, T. Defensins: Antimicrobial Peptides of Innate Immunity. *Nat. Rev. Immunol.* **2003**, *3* (9), 710–720.
- (164) Jemal, A.; Siegel, R.; Ward, E.; Murray, T.; Xu, J.; Smigal, C.; Thun, M. J. Cancer Statistics, 2006. *CA. Cancer J. Clin.* **2006**, *56* (2), 106–130.
- (165) Stewart, B. and W. World Cancer Report 2014 [http://www.thehealthwell.info/search-results/world-cancer-report-2014?source=relatedblock&content=resource&member=572160&catalogue=none&collection=Conditions,Chronic%20Conditions,Cancer&tokens\\_complete=true](http://www.thehealthwell.info/search-results/world-cancer-report-2014?source=relatedblock&content=resource&member=572160&catalogue=none&collection=Conditions,Chronic%20Conditions,Cancer&tokens_complete=true) (accessed Apr 12, 2017).
- (166) WHO | Cancer <http://www.who.int/mediacentre/factsheets/fs297/en/> (accessed Apr 12, 2017).
- (167) Hoskin, D. W.; Ramamoorthy, A. Studies on Anticancer Activities of Antimicrobial Peptides. *Biochim. Biophys. Acta* **2008**, *1778* (2), 357–375.
- (168) Derksen, D. J.; Boudreau, M. A.; Vederas, J. C. Hydrophobic Interactions as Substitutes for a Conserved Disulfide Linkage in the Type IIa Bacteriocins, Leucocin A and Pediocin PA-1. *Chembiochem* **2008**, *9* (12), 1898–1901.
- (169) Sit, C. S.; Lohans, C. T.; van Belkum, M. J.; Campbell, C. D.; Miskolzie, M.; Vederas, J. C. Substitution of a Conserved Disulfide in the Type IIa Bacteriocin, Leucocin A, with L-Leucine and L-Serine Residues: Effects on Activity and Three-Dimensional Structure. *ChemBioChem* **2012**, *13* (1), 35–38.
- (170) McGaughey, G. B.; Gagné, M.; Rappé, A. K.  $\pi$ -Stacking Interactions Alive and Well in Proteins. *J. Biol. Chem.* **1998**, *273* (25), 15458–15463.

- (171) Anjana, R.; Vaishnavi, M. K.; Sherlin, D.; Kumar, S. P.; Naveen, K.; Kanth, P. S.; Sekar, K. Aromatic-Aromatic Interactions in Structures of Proteins and Protein-DNA Complexes: A Study Based on Orientation and Distance. *Bioinformation* **2012**, *8* (24), 1220–1224.
- (172) Landschulz, W.; Johnson, P.; McKnight, S. The Leucine Zipper- A Hypothetical Structure Common to a New Class of DNA-Binding Proteins. *Science* **1988**, *240* (4860), 1759–1764.
- (173) Alewood, D.; Nielsen, K.; Alewood, P. F.; Craik, D. J.; Andrews, P.; Nerrie, M.; White, S.; Domagala, T.; Walker, F.; Rothacker, J.; Burgess, A. W.; Nice, E. C. The Role of Disulfide Bonds in the Structure and Function of Murine Epidermal Growth Factor (mEGF). *Growth Factors* **2005**, *23* (2), 97–110.
- (174) Corson, T. W.; Aberle, N.; Crews, C. M. Design and Applications of Bifunctional Small Molecules: Why Two Heads Are Better Than One. *ACS Chem. Biol.* **2008**, *3* (11), 677–692.
- (175) Suenaga, M.; Kaneko, Y.; Kadokawa, J.; Nishikawa, T.; Mori, H.; Tabata, M. Amphiphilic Poly(N-Propargylamide) with Galactose and Lauryloyl Groups: Synthesis and Properties. *Macromol. Biosci.* **2006**, *6* (12), 1009–1018.
- (176) Chimenti, F.; Secci, D.; Bolasco, A.; Chimenti, P.; Bizzarri, B.; Granese, A.; Carradori, S.; Yáñez, M.; Orallo, F.; Ortuso, F.; Alcaro, S. Synthesis, Molecular Modeling, and Selective Inhibitory Activity against Human Monoamine Oxidases of 3-Carboxamido-7-Substituted Coumarins†. *J. Med. Chem.* **2009**.
- (177) Verdoes, M.; Hillaert, U.; Florea, B. I.; Sae-Heng, M.; Risseeuw, M. D. P.; Filippov, D. V.; van der Marel, G. A.; Overkleeft, H. S. Acetylene Functionalized BODIPY Dyes and Their Application in the Synthesis of Activity Based Proteasome Probes. *Bioorg. Med. Chem. Lett.* **2007**, *17* (22), 6169–6171.
- (178) Bang, D.; Chopra, N.; Kent, S. B. H. Total Chemical Synthesis of Crambin. *J. Am. Chem. Soc.* **2004**, *126* (5), 1377–1383.
- (179) Bang, D.; Kent, S. B. H. A One-Pot Total Synthesis of Crambin. *Angew. Chem. Int. Ed.* **2004**, *43* (19), 2534–2538.
- (180) Wu, P. S. C.; Otting, G. Rapid Pulse Length Determination in High-Resolution NMR. *J. Magn. Reson. San Diego Calif 1997* **2005**, *176* (1), 115–119.
- (181) Hwang, T. L.; Shaka, A. J. Water Suppression That Works. Excitation Sculpting Using Arbitrary Wave-Forms and Pulsed-Field Gradients. *J. Magn. Reson. A* **1995**, *112* (2), 275–279.